Architecture and evolution of the continental crust of East Greenland from integrated geophysical studies

Aufbau und Entwicklungsgeschichte der kontinentalen Kruste Ostgrönlands aus integrierten geophysikalischen Untersuchungen

---

Vera Schlindwein

Ber. Polarforsch. 270 (1998)
ISSN 0176 - 5027

Vera Schlindwein

Alfred-Wegener-Institut für Polar- und Meeresforschung
Sektion Geophysik
Columbusstraße
D-27568 Bremerhaven

Die vorliegende Arbeit ist die inhaltlich unveränderte Fassung einer Dissertation, die 1998 dem Fachbereich Geowissenschaften der Universität Bremen vorgelegt wurde.

Table of contents

Abstract

East Greenland shares with Scandinavia the traces of the Arctic Caledonian orogen, its collapse and the break-up of the North-Atlantic. In contrast to Scandinavia, the structure of the continental crust of East Greenland remains relatively unknown. The Alfred Wegener Institute for Polar and Marine Research undertook an extensive geophysical programme to investigate the crustal structure of East Greenland. The integrated interpretation of these data together with geological information yielded a model for the architecture and evolution of the continental crust of East Greenland.

The data of a reconnaissance-type aeromagnetic survey of North-East Greenland were compiled in a regional magnetic anomaly map at 3700 m altitude. The accuracy of the map is limited to about 14 nT due to imperfect removal of transient variations of the Earth's magnetic field. However, the data set allows studies of large-scale structures like the Caledonian orogen of East Greenland. The survey area was divided into provinces with distinct magnetic signatures. The interpretation of the magnetic signatures is based on comparison with exposed geological structures and is locally supported by in situ measurements of magnetic susceptibilities. The Caledonian fold belt of East Greenland could be subdivided into a northern non-magnetic part, where pervasive Caledonian reworking probably demagnetised the crust, and a southern area, where isolated provinces with positive anomalies occur. Magnetite survived Caledonian metamorphism in these areas. The sensitivity of magnetite to Caledonian metamorphism was recognised in several places in the Caledonides of East Greenland. This observation might be useful in determining the much-debated degree of Caledonian reworking of the crystalline complexes of East Greenland.

Combined land-sea seismic refraction studies were carried out in the fjord region of East Greenland. Despite non-ideal survey conditions like curved profile geometry, the seismic data yielded a first insight in the crustal structure of the fjord region of East Greenland and the neighbouring areas to the north and south. The crust beneath the Caledonian mountain range is fairly homogeneous without marked reflectivity. Its thickness exceeds 43 km. The Moho rises eastwards in two slopes separated by a plateau at about 30 km depth beneath the Devonian basins in the fjord region of East Greenland. North of the fjord region, the plateau is only weakly developed and it is entirely absent south of the fjord region. On all profiles, a pronounced westward dipping reflector is detected in the lower crust. Another striking feature of the crustal architecture is encountered only north of Kong Oscar Fjord. Beneath the Mesozoic sedimentary basins, a high velocity layer is situated in the lowermost crust between 16 and 22 km depth. Its location coincides with a pronounced negative magnetic anomaly, which could be related to Tertiary magmatism. The high velocity layer was therefore interpreted as a Tertiary magmatic underplate.

By combining gravity and seismic data, a regional picture of the topography of the Moho was gained which allowed correlation of Moho topography and surface geology. A model for crustal evolution of East Greenland was derived which is discussed in the geological framework of the North-Atlantic region.

The Caledonian orogen collapsed in Devonian times along a major west-dipping shear zone represented by the reflector in the lower crust. By simple shear mechanism extension, the crustal thickness was reduced from originally more than 55 km to a more stable 40 to 30 km. At least the area between 69°N and 75°N, which corresponds to the magnetically defined southern part of the Caledonides, experienced this type of extensional collapse. Post-Devonian extension further divides this southern area into two differently developing parts. A marked contrast exists in the Late Jurassic - Early Cretaceous rifting north and south of Kong Oscar Fjord. North of Kong Oscar Fjord, considerable tectonic activity accompanied the formation of new extensional structures and the second Moho slope east of the Devonian structures. In contrast, in the southern area, the same crustal block as in Devonian times was continuously further thinned without evoking much tectonic activity. These differences in crustal evolution critically governed Tertiary magmatism. Under the influence of the Iceland hotspot, melts formed beneath the entire rift. The crust north of Kong Oscar Fjord trapped these melts at its base, whereas south of Kong Oscar Fjord, the melts easily ascended through the crust to the surface and erupted. However, on the basis of the presented data set, it was not possible to determine the parameters of crustal architecture which control the behaviour of the crust towards melts at its base.

Zusammenfassung

Ostgrönland und Skandinavien tragen die Spuren des Arktischen Kaledonischen Gebirges, dessen Kollaps und des Aufbruchs des Nordatlantik. Die Struktur der Erdkruste Ostgrönlands ist im Gegensatz zu Skandinavien noch relativ unbekannt. Das Alfred-Wegener-Institut für Polar- und Meeresforschung führte ein umfangreiches geophysikalisches Meßprogramm zur Untersuchung der Erdkruste Ostgrönlands durch. Die integrierte Interpretation dieser Daten gemeinsam mit geologischen Informationen lieferte ein Modell für den Aufbau und die Entwicklungsgeschichte der kontinentalen Kruste Ostgrönlands.

Die Daten einer aeromagnetischen Erkundungsbefliegung Nordostgrönlands wurden zu einer regionalen Karte magnetischer Anomalien in 3700 m Höhe verarbeitet. Die Genauigkeit der Karte ist auf ungefähr 14 nT begrenzt, weil zeitliche Variationen des Erdmagnetfeldes nicht vollständig aus den Meßdaten entfernt werden konnten. Der Datensatz erlaubt jedoch die Analyse großräumiger Strukturen wie des Kaledonischen Gebirges Ostgrönlands. Das Meßgebiet wurde in Provinzen mit charakteristischen magnetischen Signaturen unterteilt. Die Interpretation dieser magnetischen Kennzeichen beruht auf dem Vergleich mit bekannten geologischen Strukturen und wird an einigen Stellen durch in situ Messungen magnetischer Gesteinssuszeptibilitäten unterstützt. Das Kaledonische Gebirge Ostgrönlands läßt sich in einen nördlichen, unmagnetischen Teil und einen südlichen Teil mit vereinzelten Vorkommen starker positiver Anomalien aufteilen. Während die Kruste im nördlichen Teil im Zuge tiefgreifender kaledonischer Überprägung seine magnetischen Minerale verloren hat, überlebte Magnetit in den Gegenden positiver Anomalien im südlichen Teil die kaledonische Metamorphose. Die empfindliche Reaktion von Magnetit auf kaledonische Metamorphose wurde an mehreren Stellen des Kaledonischen Gebirges Ostgrönlands erkannt. Diese Beobachtung könnte dazu benutzt werden, den umstrittenen Grad kaledonischer Überprägung der kristallinen Komplexe Ostgrönlands zu bestimmen.

Kombinierte Land-See-Refraktionsseismik wurde in der Fjordregion Ostgrönlands durchgeführt. Trotz wenig idealer Meßbedingungen, wie zum Beispiel kurvigen Profilverlaufs, lieferten die seismischen Daten einen ersten Einblick in die Struktur der Erdkruste in der Fjordregion Ostgrönlands und den nördlich und südlich angrenzenden Gebieten. Die Kruste unter dem Kaledonischen Gebirge erscheint relativ homogen und ohne ausgeprägte Reflektivität. Sie erreicht eine Mächtigkeit von mehr als 43 km. Die Moho steigt nach Osten hin in zwei Hängen an, die von einem Plateau in ungefähr 30 km Tiefe unterhalb der Devonischen Sedimentbecken der Fjordregion Ostgrönlands getrennt weden. Dieses Plateau ist nördlich der Fjordregion kaum ausgeprägt und fehlt südlich davon gänzlich. Alle seismischen Profile zeigen einen markanten, westwärts einfallenden Reflektor in der unteren Kruste. Eine weitere auffällige Struktur kommt lediglich nördlich des Kong Oscar Fjords vor. Unter den Mesozoischen Sedimentbecken befindet sich in 16 bis 22 km Teife eine seismische Hochgeschwindigkeitsschicht. Ihre Position deckt sich mit einer ausgeprägten negativen magnetischen Anomalie, die in Zusammenhang mit tertiärem Vulkanismus gebracht werden konnte. Die Hochgeschwindigkeitsschicht wurde deshalb als magmatische Unterplattung der Kruste interpretiert.

Aus der Kombination von seismischen und gravimetrischen Daten konnte ein regionales Bild der Mohotopographie gewonnen werden, das die Korrelation von Mohotopographie und Oberflächengeologie ermöglicht. Daraus konnte ein Modell für die Entwicklung der Erdkruste Ostgrönlands abgeleitet werden und im geologischen Rahmen der Nordatlantikregion diskutiert werden.

Das Kaledonische Gebirge kollabierte im Devon entlang einer großen westwärts einfallenden Abscherungszone, die sich in Form des Reflektors in der Unterkruste äußert. Durch "simple shear" Extension wurde die Mächtigkeit der Kruste von ursprünglich mehr als 55 km auf stabilere 30 bis 40 km reduziert. Zumindest das Gebiet zwischen 69°N und 75°N, entsprechend dem südlichen Teil der Kaledoniden, wie er aus den magnetischen Daten definiert wurde, erfuhr diese Art von Extensionskollaps. Die Post-Devonische Dehnung führt zu einer weiteren Aufteilung dieses südlichen Gebiets in zwei sich unterschiedlich entwickelnde Regionen. Rifting im späten Jura und der frühen Kreide gestaltet sich nördlich und südlich des Kong Oscar Fjord auf sehr verschiedene Weise. Nördlich des Kong Oscar Fjord begleitet starke tektonische Aktivität die Bildung neuer Extensionsstrukturen und des zweiten Mohoabhangs östlich der Devonischen Strukturen. Südlich des Kong Oscar Fjord hingegen wird derselbe Krustenblock wie im Devon kontinuierlich weiter ausgedünnt, ohne viel tektonische Aktivität hervorzurufen. Diese Unterschiede in der Krustenentwicklung haben entscheidenden Einfluß auf den Tertiären Magmatismus. Begünstigt durch den Island "hotspot" bilden sich unter dem gesamten Rift Schmelzen. Die Kruste nördlich des Kong Oscar Fjord hielt diese Schmelzen an ihrer Unterseite gefangen, während die Schmelzen südlich des Kong Oscar Fjord leicht durch die Kruste an die Oberfläche dringen und eruptieren. Welche Parameter des Krustenaufbaus dieses unterschiedliche Verhalten gegenüber Schmelzen an der Unterseite der Kruste steuern, konnte an Hand dieses Datensatzes nicht geklärt werden.

"I have sought to bring East Greenland before the eyes of the specialist and of all interested persons, and to do so in a form that reflects both the beauty of the region and its scientific importance."

Louise A. Boyd (1935)

1 Introduction

The beauty of East Greenland and its scientific importance have enthralled explorers and geologists since the early 19th century. Spectacular outcrops document East Greenland's long and eventful geological history from Archaean times to the present day. The stunning landscape and the harsh climate, however, severely limit any geophysical work. Clavering's expedition in 1823, for example, in its endeavour to measure the Earth's acceleration as close to the North Pole as possible had to stop at 74.5°N, when sea-ice prevented further northward progress. The Pendulum Islands (Fig. 1.1) were named after these first gravity measurements in East Greenland (Wright, 1935).

Even in modern times, the geophysical exploration of the continental crust of East Greenland is limited and does not do justice to its scientific importance. East Greenland shares with Scandinavia and Britain the traces of the Caledonian orogeny, its extensional collapse and the break-up of the North Atlantic. Whereas the structure of the Scandinavian and British crust is well studied, the architecture and evolution of East Greenland's continental crust remains a major relatively unknown part of the jigsaw puzzle of the continents around the North Atlantic. Exploring the development of the continental crust of East Greenland therefore contributes to a deeper understanding of the geological framework of the North Atlantic region.

This study attempts to integrate and interpret newly acquired geophysical data from East Greenland in this geological framework.

Outline of the field studies

In 1990, the Alfred Wegener Institute for Polar and Marine Research (AWI) started a geophysical programme to investigate the crustal structure of East Greenland. The morphology and harsh climate of East Greenland impose constraints on such a task.

Seismic refraction data can most conveniently be acquired where major fjords provide natural transects through the survey area. Along these fjords, seismic energy is generated by shipborne airguns and is recorded on land. The seismic refraction data are restricted to the fjord systems between Scoresby Sund (70°N) and Bredefjord (75°N) (Fig. 1.1). This study focuses on the area between Kong Oscar Fjord (72°N) and Kejser Franz Fjord (73°N). As the area partly belongs to the provinces of North-East Greenland and Central East Greenland, it will, for convenience, be referred to as the "fjord region" of East Greenland.

North of about 75° N, extensive E-W trending fjords are lacking, and the inland ice extends almost to the coast. Offshore, the area is blocked with sea-ice all year round. Seismic refraction data could not be collected. However, a large scale aeromagnetic survey covers East Greenland north of 70°N and has at its aim to provide a regional overview over the magnetic properties of the crust. Together with gravity data, this data set forms the only basis for deep crustal studies north of 75°N.

In situ measurements of magnetic susceptibilities were carried out in the Caledonian crystalline complexes of East Greenland between about 72°N and 73°N (Fig. 1.1). These data provide ground information on the magnetic properties of the exposed rocks and thereby aid in the interpretation of the aeromagnetic data.

In the fjord region of East Greenland, the good coverage with seismic refraction and potential field data enables a joint interpretation of all data sets together with geological information. On the basis of the regional potential field data and surface geology, the results from the detailed investigation of the fjord region can be evaluated in a regional context.

Outline of the thesis

During this study, a large and valuable geophysical data set was acquired, processed and compiled, and will be presented here for the first time. Great emphasis was laid on a detailed documentation of the data set, its processing, estimates of the accuracy of the results and their reliability for geological interpretation. In particular, in the chapter on in situ magnetic susceptibility studies, this necessarily involved a detailed description of rock types and local geology. As this chapter is to be understood as a documentation of raw data, which are mainly of value to geologists, I deliberately did not include the explanations of geological terminology which a geophysicist might wish to find. However, these ground studies led to a deeper understanding of the investigated aeromagnetic anomalies. Therefore, the key results are included or referred to in the chapter on geological interpretation of the aeromagnetic anomaly map.

An integrated geoscientific analysis requires the simultaneous consideration of all available results and information. As this kind of thinking is difficult to present in a logically progressing account of the work, the anticipation of some results could not be avoided.

The geological framework of the study area and previous geophysical investigations will be introduced in chapter 2. It contains a simplified overview over the geological history of East Greenland. More detailed accounts of local geology are given in the text where relevant for the geological interpretation of geophysical data. In order not to separate the interpretation of individual data sets from the presentation of the data set, chapters 3 and 4 each present data, their processing and modelling or interpretation. Chapter 3 includes the magnetic data and their interpretation. Chapter 4 is dedicated to the gravity and seismic data and the joint modelling of potential field and seismic

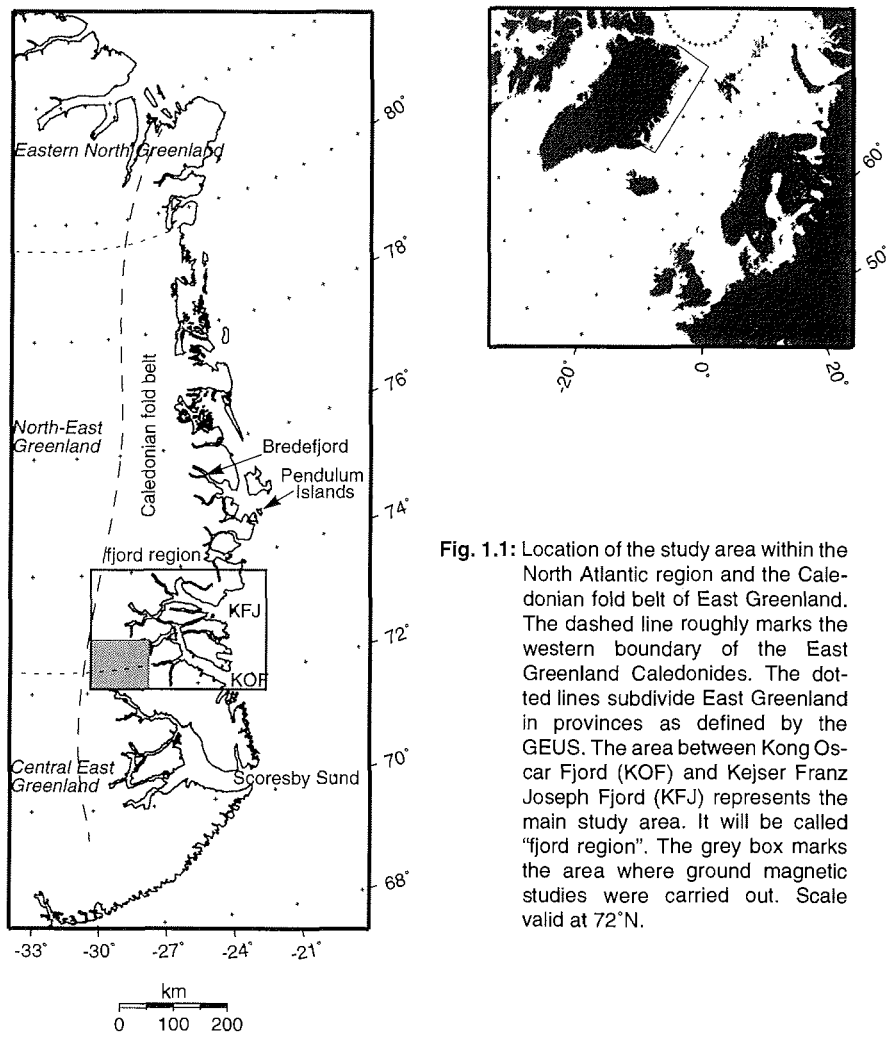

Fig. 1.1: Location of the study area within the North Atlantic region and the Caledonian fold belt of East Greenland. The dashed line roughly marks the western boundary of the East Greenland Caledonides. The dotted lines subdivide East Greenland in provinces as defined by the GEUS. The area between Kong Oscar Fjord (KOF) and Kejser Franz Joseph Fjord (KFJ) represents the main study area. It will be called "fjord region". The grey box marks the area where ground magnetic studies were carried out. Scale valid at 72°N.

data. Each of these data chapters concludes with a short summary of the key results which should help the reader to understand the model for the crustal evolution of East Greenland without having to read through the details of data processing. This model for the crustal evolution of East Greenland was derived from the integrated interpretation of all data sets. It is presented and discussed in a regional geological framework in chapter 5. A number of problems remained unsolved and new questions were raised by this hypothesis for crustal evolution. They are addressed in the concluding chapter 6 and proposals for future work are made.

2 Geological and geophysical background

2.1 Geology of East Greenland

The beginning of geological exploration of East Greenland dates back to the years 1869/70. The Second German North Pole expedition led by Karl Koldewey discovered and partially explored Kejser Franz Joseph Fjord and the coastal area of East Greenland as far north as 77°N (Fig. 2.1). A first geological description and a sketch map of the region between 73°N and 76°N were published (Hochstetter et al., 1874). In 1926, Lauge Koch tackled the enormous task of systematic geological mapping of East Greenland. His series of expeditions from 1926 to 1958 resulted in detailed geological maps from the area between 72°N and 76°N (Koch & Haller, 1971; Haller, 1971). Recent regional mapping is now undertaken by the Geological Survey of Denmark and Greenland (GEUS), until 1995 the Geological Survey of Greenland (GGU). Their activities have included mapping projects in North Greenland in 1978-80 and 1984-85 (Henriksen & Higgins, 1991), in North-East Greenland in 1988-90 (Henriksen, 1994a) and in eastern North Greenland in 1993-95 (Henriksen, 1994b) (see Fig. 1.1). Currently, the area between 72°N and 75°N is the focus of the regional geological mapping of GEUS in East Greenland.

The N-S trending Caledonian orogen dominates the geology of East Greenland (Fig. 2.1). It extends parallel to the coast from the Scoresby Sund area (70°N) to Kronprins Christian Land (81°N). Detailed accounts of the geology of the East Greenland Caledonides have been given by Haller (1971), Henriksen & Higgins (1976) and Henriksen (1985). The following description of the geology of East Greenland is based on the summary by Henriksen (1994a). Fig. 2.2 summarizes the history of geological events in East Greenland.

Caledonian foreland

The western margin of the Caledonian fold belt is exposed in Kronprins Christian Land (79°30'-81°30'N); elsewhere it is only intermittently exposed along the margin of the inland ice in windows in the Scoresby Sund region (70°-72°N) and in Dronning Louise Land (76°-77°30'N). It is characterized by westward thrusts which, in Kronprins Christian Land, involved the foreland Lower Palaeozoic sedimentary rocks only superficially, whereas crystalline complexes were also affected farther south. The Caledonian foreland in eastern North Greenland consists of thick sequences of sedimentary rocks deposited between Middle Proterozoic (Independence Fjord Group) and Silurian times (Hagen Fjord Group, Franklinian Basin). A major volcanic event in Middle Proterozoic times at about 1230 Ma produced the Zig-Zag Dal Basalts and intruded the Independence Fjord Group sandstones with dolerites (Midsommersø Dolerites) (Surlyk, 1991). Equivalents of these rocks are also found in the foreland in Dronning Louise Land. The western margin of the East Greenland Caledonides is assumed to continue southwards from Dronning Louise Land beneath the inland ice. In the Scoresby Sund area, for example in Charcot Land and Gåseland, tectonic windows offer a view of Caledonian foreland rocks, which here are mainly of crystalline nature.

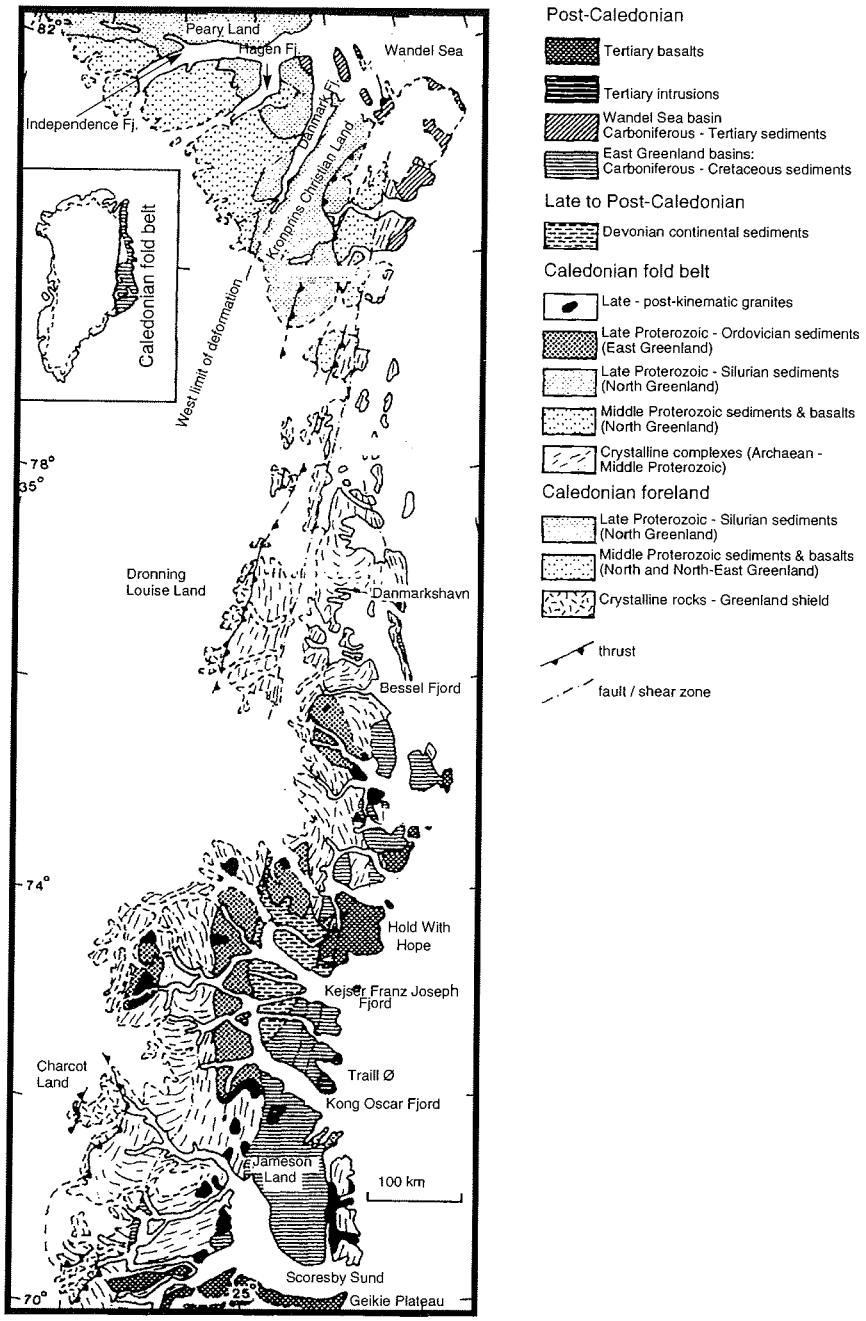

Fig. 2.1: Simplified geological map of East Greenland (adapted from Henriksen, 1994a). The map covers the Caledonian fold belt of East Greenland and the adjacent post-Caledonian units.The description in the text follows the structure of the legend. An overview over the timing of geological events is given in Fig. 2.2.

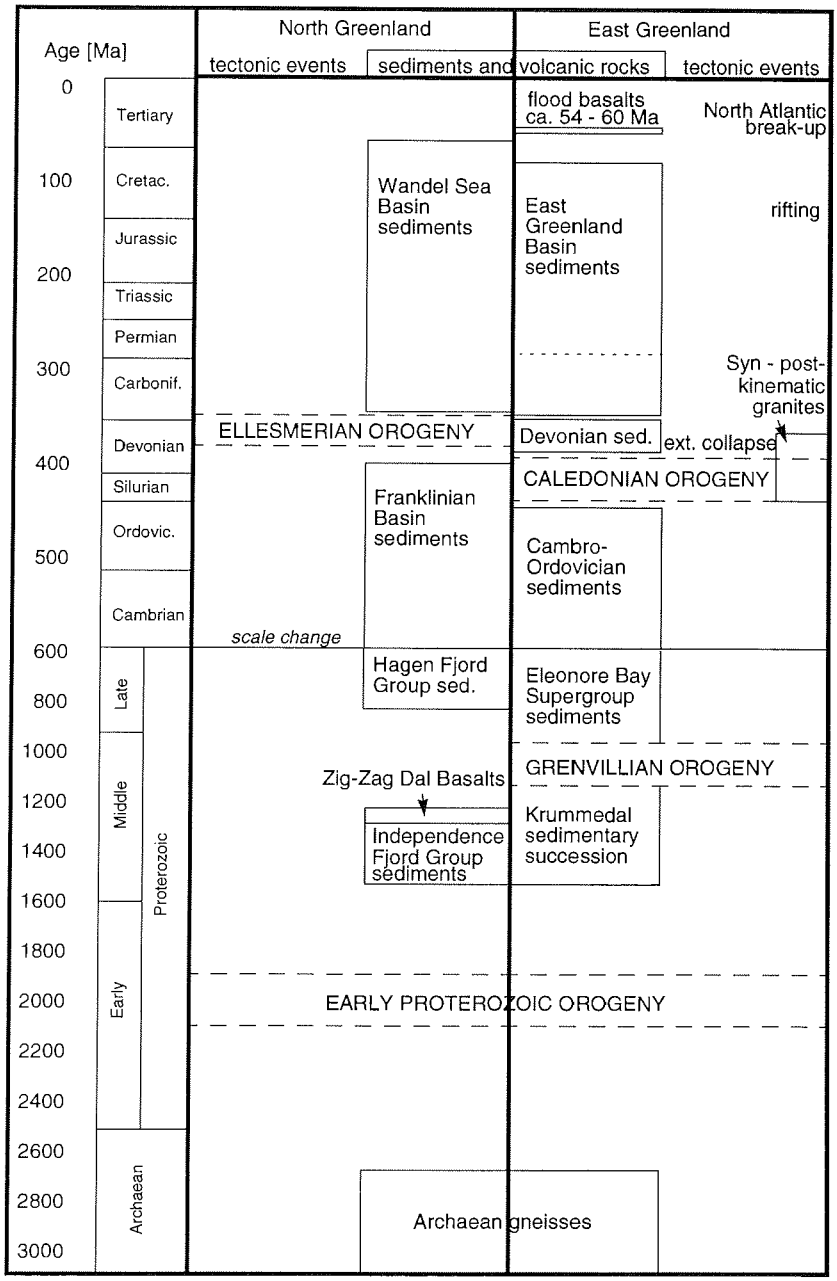

Fig. 2.2: Simplified overview over the main geological events in East and North Greenland (adapted from Escher & Pulvertaft, 1995, and Henriksen, 1994a).

Caledonian fold belt

The Caledonian fold belt is dominated by Archaean to Middle Proterozoic basement rocks which are overlain in some areas by Late Proterozoic to Ordovician sedimentary sequences. Both basement and cover were deformed during the Caledonian orogeny which affected the area in Latest Ordovician to Early Devonian (ca. 445 - 385 Ma) times (Fig. 2.2) (e.g. Dallmeyer et al., 1994).

Crystalline basement. The crystalline basement includes infracrustal rocks, such as gneisses, migmatites or granites, and supracrustal units, for example the Krummedal metasedimentary rocks. Among the infracrustal complexes are units which have yielded Archaean and Lower Proterozoic protolith ages (Kalsbeek et al., 1993). The Caledonian crystalline complexes witness to several metamorphic events including Early Proterozoic (ca. 1900 Ma) and Grenvillian (ca. 1100 Ma) orogenies. The latter has not been proven north of about 76°N. A long-standing problem of Caledonian orogeny is the degree of Caledonian reworking, as Archaean and Proterozoic elements within the crystalline complexes have survived Caledonian deformation and metamorphism. In contrast, Caledonian eclogites testify to high-pressure metamorphism in coastal areas from Danmarkshavn and northwards (Gilotti, 1993, 1994; Brueckner & Gilotti, 1993).

Cover sequences. The crystalline basement is overlain in eastern North Greenland by Middle Proterozoic to Silurian sedimentary sequences, exposed both in the foreland and in the Caledonian nappes of Kronprins Christian Land. Between 72°N and 76°N, the cover sequences consist of the Late Proterozoic Eleonore Bay Supergroup sedimentary sequence and Cambrian to Ordovician successions. Their composite thickness may be as much as 17 km. These sequences experienced Caledonian folding but only low-grade metamorphism which increases towards the base of the sequence.

Caledonian intrusives. Intermediate to acid plutonic activity accompanied the Caledonian orogeny and the subsequent extensional collapse. Granite intrusions are widespread in the Caledonian fold belt south of Bessel Fjord (76°N), and are particularly abundant along the contact between the crystalline basement and the Eleonore Bay Supergroup. North of 76°N, Caledonian granite intrusions are absent.

Post-Caledonian deposits

Devonian extensional collapse. Caledonian orogenic shortening was succeeded by extensional tectonics in Devonian time. West-directed Caledonian thrusts bordering the Eleonore Bay Supergroup units, for example, were reactivated as extensional faults with top-to-the-east displacement (e.g. Hartz & Andresen, 1995; Strachan, 1994). Intra-montane molasse-type basins formed south of about 74.5°N. These fault-bounded basins accumulated some 8 km of Devonian continental sediments. The faulting activity terminated in Early Carboniferous time.

East Greenland basins. Continental deposition continued throughout Lower Permian time and a Late Palaeozoic sequence formed which overlies the Devonian deposits unconformably. A new tectonic regime was initiated in Lower Permian time (dotted line in Fig. 2.2). It is characterized by a series of extensional events which persisted throughout the Mesozoic. The most prominent rifting event took place in the Late Jurassic-Early Cretaceous (Surlyk, 1990). A thick sequence of mainly marine sediments was deposited during Mesozoic time. In Jameson Land, this sequence conceals the Devonian sediments, whereas in the region north of Kong Oscar Fjord, the Mesozoic basins are separated by a fault zone from the Devonian basins to the west.

Tertiary magmatism

Rifting culminated in the opening of the North Atlantic in Tertiary times at about 54 Ma (e.g. Larsen & Watt, 1985; Saunders et al., 1997). Influenced by the Iceland hotspot, large amounts of melts formed which extruded as tholeiitic basalts. The southern continuation of the Caledonian fold belt in the Scoresby Sund area is concealed beneath the up to 3 km thick sequence of flood basalts of the Geikie Plateau. Intrusive activity accompanied the volcanism and led to major dyke and sill complexes within the Mesozoic East Greenland basins (e.g. Larsen & Marcussen, 1992). North of Kong Oscar Fjord, minor amounts of flood basalts largely equivalent to those of the Geikie Plateau are exposed along the coast, especially on Hold With Hope (e.g. Upton et al., 1995). A late magmatic event at about 30 Ma accompanied the separation of the Jan Mayen Ridge, which was once situated off East Greenland south of 72°N (e.g. Larsen, 1990). Tertiary intrusives on Traill Ø and southern Kong Oscar Fjord witness to this event.

North Greenland

The major E-W trending Franklinian basin of North Greenland extends from Peary Land to the north coast of Greenland. A northern part with deep water sediments can be distinguished from a southern shelf area with shallow water sedimentation (e.g. Surlyk, 1991). The northern part of the Franklinian Basin was involved in the Ellesmerian orogeny in Devonian times. In Late Palaeozoic times, a rifting event affected the far end of North-East Greenland (e.g. Surlyk, 1991), and the Wandel Sea basin developed in this tectonic regime. A change in tectonic style took place in Mesozoic times when a prominent NW-SE trending strike-slip belt formed reflecting rifting between North Greenland and Svalbard. Sediments accumulated in the Wandel Sea basin from Upper Carboniferous times throughout the Mesozoic into Tertiary times, and conceal the northern continuation of the Caledonian fold belt.

2.2 Previous geophysical studies of East Greenland

Earlier geophysical studies of the continental crust of East Greenland have mainly concentrated on the post-Caledonian basins, in particular the Jameson Land Basin; these areas have been the focus of prospecting for hydrocarbons. High quality seismic reflection profiles reveal the crustal structure. Larsen & Marcussen (1992) give an account of the work in the Jameson Land Basin, and present a model for the architecture of the crust with emphasis on the sedimentary sequences and the Tertiary intrusives within the Jameson Land Basin. The geophysical exploration of the shelf offshore East Greenland has been summarized by Larsen (1990). In addition, some academic geophysical research has been aimed at the structure of the shelf and continental margin offshore East Greenland. Hinz et al. (1993) compare the characteristics of the East Greenland volcanic margin between about 72°N and 78°N with the conjugate Vøring margin off the coast of Norway. Farther north, only sparse seismic reflection data exist (e.g. Hinz et al., 1991). A recent cruise of RV Polarstern in summer 1997 (Arktis XIII/3) was dedicated to the acquisition of seismic reflection data off Kronprins Christian Land and across the Fram Strait. The continent-ocean transition was crossed by six profiles between 78.5°N and 81°N (Jokat et al., 1998, in preparation).

Deep seismic sounding studies of the continental shelf and the continent-ocean transition off East Greenland between 70°N and 72°N were carried out during cruise

Arktis V/3b of RV Polarstern in summer 1988. The results are presented by Weigel et al. (1995). The profiles shot during this expedition extend into the Scoresby Sund and into the mouth of Kong Oscar Fjord where they form a seaward continuation of the seismic refraction profile KOF which is presented here.

The first seismic refraction studies to investigate the crustal structure of the Caledonian fold belt were carried out by AWI in summer 1990 during the cruise Arktis VII/3 of RV Polarstern (Jokat et al., 1996). Mandler (1995) modelled and interpreted the seismic refraction data and combined them with gravity data. He found a thick continental crust beneath the Caledonian fold belt of up to 48 km thickness. In addition, there were indications of high seismic velocities in the lowermost crust west of the Jameson Land Basin. Mandler (1995) related this structure to the Tertiary magmatic event. A detailed study of the crustal structure in the western part of the Jameson Land Basin was also undertaken during this cruise (Fechner & Jokat, 1996). The indication of a thick Caledonian crust was an unexpected result, because the Caledonian fold belts of Norway and Scotland show shallow Moho depths (see chapter 5.2.1). In order to better constrain the maximum crustal thickness beneath the Caledonides of East Greenland and to verify the magmatic underplating in the Scoresby Sund area, the seismic refraction profiles in this area were extended during the cruise Arktis X/2 of RV Polarstern in summer 1994. In addition, new seismic refraction data across the Caledonian fold belt were acquired between 72°N and 75°N. These data are presented here.

Apart from the seismic data, a set of potential field data exists for East Greenland. The National Survey and Cadastre (KMS), Denmark, is continuously enlarging its data base consisting of land and marine gravity measurements (e.g. Forsberg,1991; see chapter 4.1.1). GEUS has carried out an aeromagnetic survey in East Greenland mainly covering the shelf area (e.g. Larsen, 1977). A part of this data set was compiled and published as aeromagnetic anomaly map (Thorning, 1988). The aeromagnetic surveys by AWI supplements this data set by covering onshore East Greenland.

3 Aeromagnetic study of East Greenland

3.1 Aeromagnetic data

3.1.1 Data acquisition

Survey setup

The aeromagnetic surveys of the AWI were designed to supplement the seismic refraction studies by providing a regional overview over the magnetic anomalies of East and North Greenland north of 70°N. The aeromagnetic data were acquired during 4 survey campaigns, called AEROMAG93-96, which were flown in the summers of 1993 through 1996. With line spacings between 10-40 km and survey altitudes up to 3700 m, the surveys have only reconnaissance character. The limited range of the aircraft and large distances between suitable airfields imposed logistic constraints on the scientific program. Fig. 3.1 shows the total of about 55 500 km of aeromagnetic profiles which were acquired during AEROMAG93-96.

The southern area was covered from Constable Pynt (CNP) as base of operation (AEROMAG93/96), the northern part from Station Nord (NOR) (AEROMAG94/95/96). The surveys were connected by overlapping lines and a survey flight from CNP to NOR and back during AEROMAG96. For logistic reasons, the N-S tielines could not be flown independently from the E-W profile lines during magnetically quiet times, but had to be incorporated in the regular survey flights.

The survey was flown at constant barometric altitude. The flight levels varied between 600 ft (183 m) offshore North Greenland and from 8000 ft (2438 m) to 12000 ft (3658 m) onshore depending on terrain elevation and weather conditions. In addition, three low level flights at 4000 ft (1219 m) elevation were flown along the seismic refraction profiles through the Kong Oscar Fjord, the Dickson Fjord and the Kejser Franz Joseph Fjord.

Transient variations of the Earth's magnetic field were recorded at 10 s intervals at the base of operation by a proton precession magnetometer. The term transient variation is used here to describe time variations of the Earth's external field as suggested by Barton (1995). The term "diurnal variation" often used in this context is ambiguous and could also denote a 24-h periodic variation or the solar quiet daily variation Sq. Recording the transient variations of the magnetic field at the bases of operation was vital for both correcting the survey data for the transient variations and for identifying magnetically quiet periods of the day for the survey flights. For AEROMAG96, CNP and NOR were too far away from the survey area. Therefore, a second reference magnetometer was deployed at Zackenberg (ZAC).

The AWI's Dornier Do 228 aircraft "POLAR2" is equipped with a gradiometer system of optically pumped Geometrics G833 He4 magnetometers, which record the total intensity of the magnetic field. The sensors are mounted in stingers on the nose and the wingtips. The magnetometer data together with navigation and system related parameters are logged at a sample rate of 20 Hz (AEROMAG93: 10 Hz) onboard. Data at

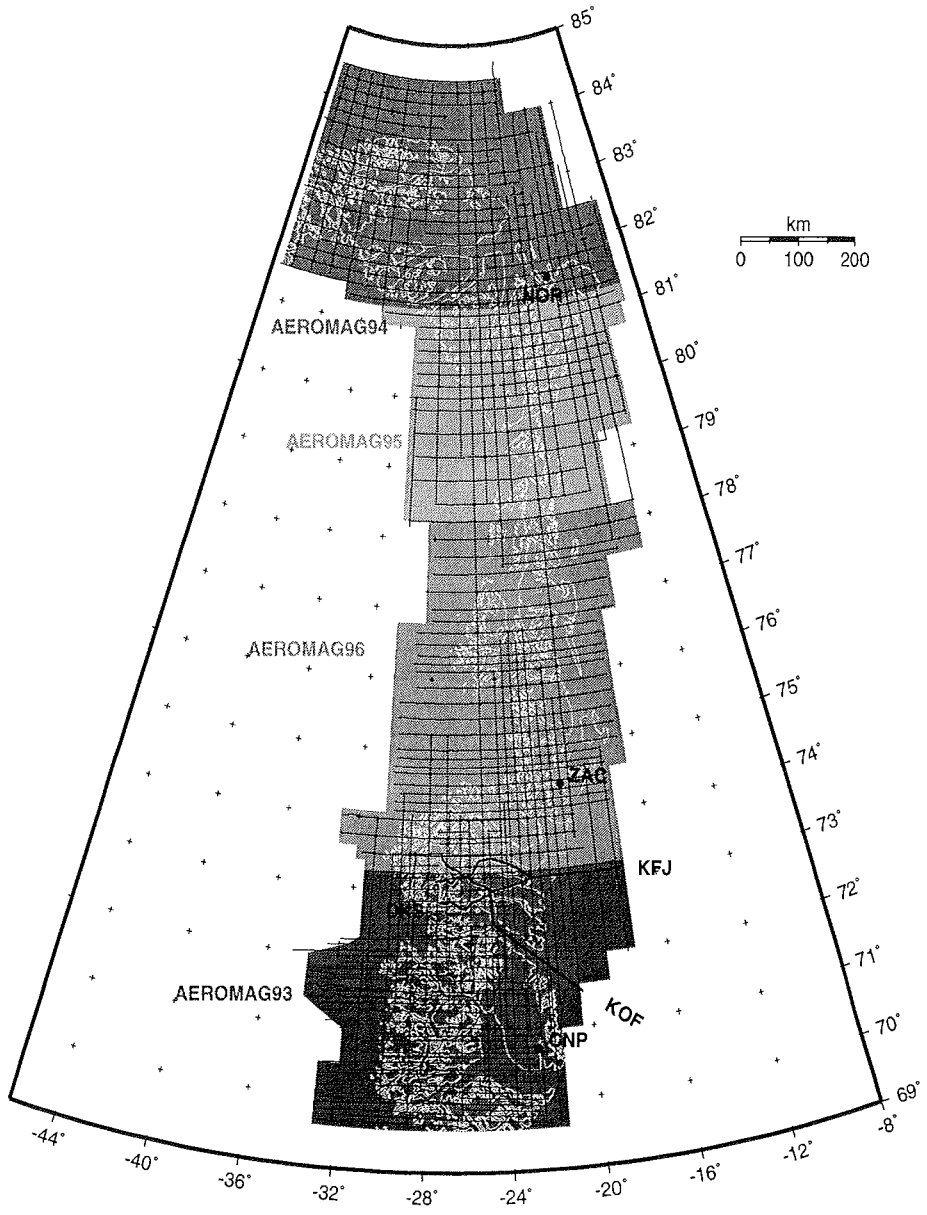

Fig. 3.1: Aeromagnetic survey lines acquired during AEROMAG93-96. Dots mark the location of the reference magnetometers: CNP: Constable Pynt, ZAC: Zackenberg, NOR: Station Nord. Bold lines show the low level profiles over seismic refraction lines: KFJ: Kejser Franz Joseph Fjord, KOF: Kong Oscar Fjord, DKS: Dickson Fjord. The grey shaded areas show the extent of the gridded aeromagnetic anomaly map. All map projections in the following are UTM. Scale valid at 76°N.

10 Hz intervals are output to tape as raw data for processing. For compilation of the aeromagnetic anomaly maps data are reduced to 1 Hz intervals. This corresponds to a spatial sample distance of 74-93 m depending on the ground speed of the aircraft, which varied between 144 kts (267 km/h) and 180 kts (333 km/h).

Compensation

Airborne magnetic surveys with magnetometers mounted on the aircraft require a sophisticated procedure of compensation. Permanent, induced and eddy current fields are produced by the aircraft as moving ferromagnetic substance and interfere with the measurements of the magnetic field of the Earth. These interference fields need to be eliminated at the location of the magnetometers. The following compensation procedure was applied to compensate the gradiometer system on POLAR2:

Large permanent fields are constructively compensated by a fixed installation of correction magnets (AEROMAG93/94). The remaining permanent fields are suppressed by triple compensation coils, which produce magnetic fields in the longitudinal, transversal and vertical direction at the location of each sensor. These fields need to be adjusted in the survey area at the start of each campaign. The so-called static compensation is flown at 10000 ft (3041 m) altitude over a compensation point in the survey area with small magnetic gradients and during magnetically quiet times. For the compensation of longitudinal interference fields, the compensation point is overflown heading magnetic north and after a fast turn heading magnetic south. The procedure is repeated and the coil currents are iteratively adjusted until the difference between the sensor readings at the compensation point in north and south direction is ideally reduced to zero. The same procedure flying east and west is used to correct for transversal field components. The currents in the vertical compensation coils are adjusted after flying eastwards over the compensation point and taking sensor readings while roll positions of about +15° and -15° immediately before and after the compensation point are assumed. The entire procedure is repeated until a satisfactory minimum of the permanent interference field is reached.

The quality of the compensation depends critically upon the temporal stability of the ambient field. The manoeuvre between 2 readings to be compared takes about 90-120 s for the horizontal components and 20-30 s for the vertical component. Fast temporal changes of the Earth's magnetic field at high latitudes can reach the magnitude of the interference field to be compensated and therefore disturb the static compensation. Fig. 3.2 lists the remaining differences after static compensation in quiet day conditions during AEROMAG96.

Interference field component	Left wing sensor	Right wing sensor	Nose boom sensor
Longitudinal	0.2 nT	2.3 nT	0.3 nT
Transversal	1.0 nT	1.8 nT	2.3 nT
Vertical	3.5 nT	1.1 nT	2.5 nT

Fig. 3.2: Remaining differences between sensor readings at opposite aircraft headings (horizontal components) and +15°/-15° roll angles (vertical component) after static compensation during AEROMAG96.

The remaining interference field consists of a small permanent field, an induced and an eddy current field produced by the movement of the aircraft as conducting surface with respect to the flux of the ambient field. The purpose of the dynamic compensation is to provide a model for these fields at the location of each sensor. The total field recorded by the sensors is expressed as the sum of the ambient field and the above interference field (Leliak, 1961). The equation can be linearized and solved numerically for the coefficients of the interference field (Mertikas, 1993).

Special measurements are carried out to provide input data for the numerical solution: The compensation point is crossed subsequently in 8 directions (magnetic N, NE, E, etc.) while sinuosoidal movements with respect to each of the aircraft's axes are performed. The effect of these roll, yaw and pitch manoeuvres in all 8 directions on the magnetic readings is recorded together with the aircraft's attitude and additional parameters like control positions. The obtained model for the interference field is used to correct the survey data. Applying this model to the dynamic compensation data reduces the effect of the aircraft's movements on the sensor recordings by 80% from amplitudes of 30 nT to 6 nT. The absolute size of the corrections made to the survey data, which are flown along straight lines with insignificant movements of the aircraft, are of the order of 1 nT.

For some unexplained reason, the compensated sensors do not yield the same total field values, but show large offsets, which varied from campaign to campaign. Therefore, an additional calibration was necessary to obtain correct absolute values. During AEROMAG96, each survey flight ended with flying at about 10 m height over the ground reference station. The simultaneous recordings of the ground station and the sensors were compared and an average offset for the calibration of each sensor calculated. The procedure proved very useful as it also yields an estimate of how reproducible the measurements are. The results are listed below.

Flight No.	Reference station - left wing sensor [nT]	Reference station - right wing sensor [nT]	Reference station - nose boom sensor [nT]
1	-65.7	-12.9	178.9
2	-69.6	-5.4	187.8
3	-67.8	-3.4	194.0
4	-69.9	-5.1	180.9
5	-68.5	2.8	179.8
6	-69.3	-4.2	197.4
7	-66.6	-2.6	196.7
8	-65.1	-2.3	199.4
Average	-67.8	-4.1	189.4
Standard deviation	1.8	4.4	8.6

Fig. 3.3: Differences between the reference station and the sensor readings for 8 calibration flights over the reference station at CNP.

Using the gradiometer system to measure gradients of the Earth's magnetic field instead of absolute values is especially desirable in high latitudes as gradiometer surveys are independent of transient variations. Typical gradients of the magnetic field of the Earth's crust at the survey altitude of 3700 m are smaller than 0.5 nT per 16.96 m distance between left and right wing sensor. Accurately measuring these differences requires a compensation of interference fields to at least 0.1 nT.

The compensation of AEROMAG96 was good enough to detect the largest gradients in the survey area (1 nT /16.96 m). However, the first survey, AEROMAG93, suffered from frequent failures of the right wing and nose boom sensors and less successful compensation. For these reasons, only the data of the left wing sensor were used for all surveys, because this sensor proved to be the most stable during all campaigns (c.f. Fig. 3.3).

3.1.2 Data processing

The recordings of the total intensity of the magnetic field of the left wing sensor were processed in the following way to obtain aeromagnetic anomalies.

- **Editing**
  The raw data were inspected, and the profile and tie lines extracted from the survey flights. Data disturbed, for example, by radio transmission or occasional de-icing of the aircraft and spikes in the navigation data were removed. A low pass filter (1 Hz corner frequency) was applied to the 10 Hz raw data. The data were then corrected for magnetic interference fields using the model of the dynamic compensation of each campaign, respectively, and resampled to 1 Hz.
- **IGRF correction**
  Magnetic anomalies were obtained by removing the International Geomagnetic Reference Field (IGRF) from the data. The IGRF for the epoch 1990-1995 (IAGA, 1991) was used for the entire survey and calculated forward to the period of each survey.
- **Correction for transient variations of the Earth's magnetic field**
  Correcting transient variations of the Earth's external magnetic field in polar regions is a difficult task. The ionosphere within the auroral oval exhibits a large variety of different phenomena which greatly influence ground magnetic recordings at high latitudes (e.g. Kertz, 1989). As an example, Fig. 3.4 shows a sketch of the ionospheric current system of an auroral electrojet, which is one of the dominant manifestations of magnetospheric substorms (Kamide & Kokubun, 1996). The currents vary strongly with time and latitude. A maximum of the westward auroral electrojet is on average between 2 and 4 magnetic local time and at about 67°N invariant latitude. The AEROMAG survey area extends between 72° and 82°N invariant latitude in this inhomogeneous current system. Fig. 3.5 compares magnetograms from 4 different observation sites in East Greenland and Iceland. In general, the 4 magnetograms are clearly related. The nights are disturbed with variations of up to 200 nT in amplitude, whereas all locations recorded magnetically more quiet day times. The disturbances at Leirvogur have different polarity from the others suggesting that in this case the auroral electrojet might be located between Leirvogur and Constable Pynt. Studying magnetograms of several days, it can be observed that generally the disturbances occur simultaneously or with phase shifts at the observation sites. The frequency content of the variations within a given time window is comparable at all

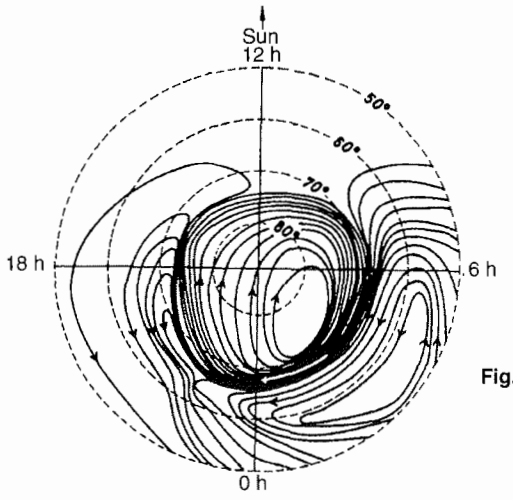

Fig. 3.4: Ionospheric current system of an auroral electrojet (after Kertz, 1969). The currents flow in 100 to 120 km altitude. Times are magnetic local time, latitudes are invariant latitudes.

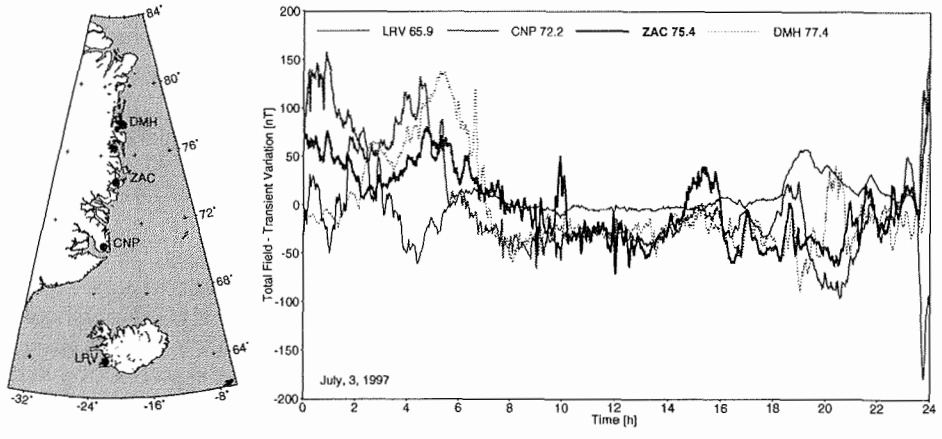

Fig. 3.5: Transient variations of the Earth's magnetic field at 4 magnetometer sites in Iceland and Greenland. LRV: Leirvogur, CNP: Constable Pynt, ZAC: Zackenberg, DMH: Danmarkshavn. The numbers behind the station index indicate the station position in terms of invariant latitude.

locations. However, the shape of the curves may differ significantly, which can lead to differences between the recordings of several hundred nT. It is important to note these difficulties involved in correcting data of a large scale aeromagnetic survey at high latitudes for transient variations of the external field.

For the calculation of transient variations the average value of a quiet day within the survey period was subtracted from the total field recordings of each base station. It was assumed, that long-period disturbances have a more regional extent, while

short-period variations occur locally. With distances of up to 500 km between the survey profiles and the base station it was not attempted to correct for these short-period variations. After several tests, the long-period component of the variations, with periods longer than 30 min, was extracted by lowpass filtering and subtracted from the survey data. For AEROMAG93, CNP was used as reference, ZAC for the main part of AEROMAG96 and NOR for the remaining data set. The result of the correction was carefully assessed by comparing parallel lines as well as analysing misfits at line intersections. Heavily disturbed data were removed.

Fig. 3.6 illustrates the effect of the correction for transient variations using a statistics of misfits at line intersections as an example. A subset of the AEROMAG96 data was chosen with 43 intersecting lines flown roughly at the same altitude (10000-12000 ft). The absolute misfit between intersecting lines before and after correction was calculated for all intersections. The uncorrected data exhibit a broad distribution of absolute intersection misfits. After the correction, 90% of the data concentrate at misfits less than 50 nT, with the majority of the intersections having misfits less than 20 nT.

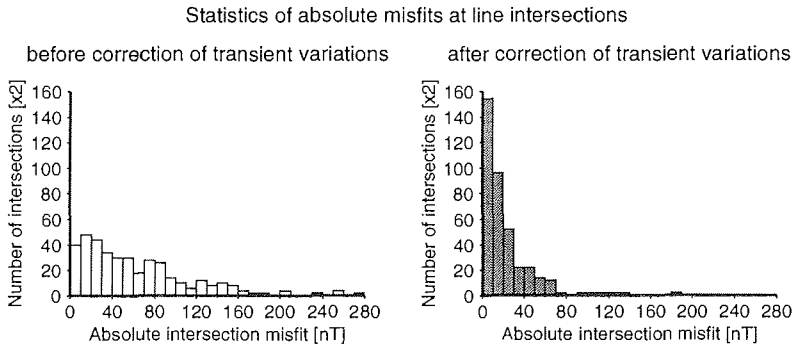

Fig. 3.6: Effect of the correction for transient variations. A total of 193 line intersections of 43 AEROMAG96 lines between 73°-77°N and 17.5°-25.5°W were selected for the statistics. Each intersection appears twice in the statistics.

- **Upward continuation**

  Prior to merging the data sets from AEROMAG93-96, the data were upward continued to a common altitude level of 3700 m. Two different algorithms were used for upward continuation. An equivalent source algorithm for continuation of potential fields between arbitrary surfaces (Hansen & Miyazaki, 1984) was applied to AEROMAG93-95. It also allowed to upward continue parts of the AEROMAG93 survey with flight level changes of up to 2000 ft during survey lines. In order to remove edge effects, the survey lines were trimmed by about 2 km at each end after the upward continuation. AEROMAG96 data were continued to 3700 m by level-to-level continuation in the Fourier domain (e.g. Blakely, 1995). The different processing methods are merely a consequence of using different software packages for the data processing. There is no difference in the results.

- **Merging the data sets**

  Before the data sets from AEROMAG93-96 were merged, overlapping survey lines were analysed and offsets between the surveys determined. The AEROMAG96 data had been calibrated using the base station recordings at CNP as absolute reference. Overlapping lines with AEROMAG93 and 95 were examined and constant shifts applied to both surveys. AEROMAG94 was shifted to fit the AEROMAG95 data at common lines.

  The entire data set was then adjusted to minimize the misfit at the line intersections in the following way: In order to manipulate the survey data as little as possible, only constant shifts were applied to the survey lines. All lines and intersections were treated equally, no lines were held fixed. This results from the fact, that tie lines were not flown independently on magnetically quiet days to link the profile lines of the entire survey and can therefore not be used as reference lines. A least squares algorithm minimized the misfits at the intersections, such that the mean misfit per line is approximately zero. Gridded anomaly maps of both unadjusted and adjusted data sets were compared to check the effects of the adjustment procedure. The adjustment procedure reduced the average absolute misfit of all 1126 line intersections from 21 nT with a standard deviation of 29 nT to 14 nT with a standard deviation of 18 nT. The histograms in Fig. 3.7 show a tightening of the distribution of absolute misfits after the line adjustment. 90% of the data now have misfits smaller than 30 nT instead of 50 nT, the majority of the intersections fits better than 15 nT. For comparison, Thorning (1984) could reduce the average intersection misfit of a comparable survey in West Greenland to 16.9 nT.

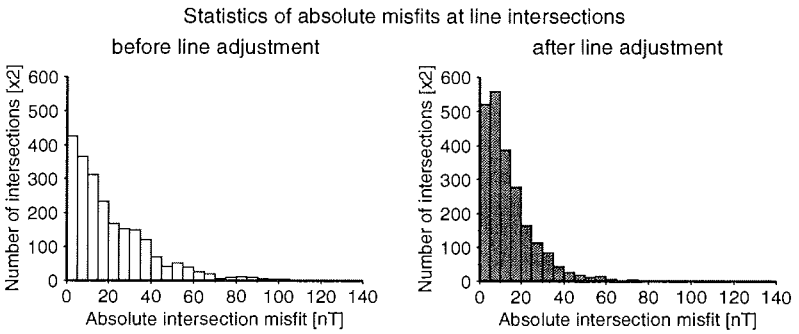

Fig. 3.7: Effect of the line adjustment. The statistics represents the entire data set of AEROMAG93-96 with 280 lines intersecting at 1126 points. Each intersection appears twice in the statistics.

- **Assessment of accuracy**

  The line intersection statistics yields a rough estimate of the accuracy of the aeromagnetic survey and the resulting aeromagnetic anomaly maps. The average misfit of 14 nT has to be considered in relation to the size of the observed anomalies which reach maximum amplitudes of 1450 nT.

Uncompensated interference fields of the aircraft are one order of magnitude smaller than this misfit. Therefore, the quality of the compensation does not play a critical role in this survey. The remaining misfit can be mainly attributed to imperfect removal of transient variations. Rapid changes of the Earth's external field of this order of magnitude are common in high latitudes. They cannot be corrected for and can often not be distinguished from geologically produced anomalies in the survey data. This must be kept in mind when interpreting the aeromagnetic anomaly maps.

3.1.3 Aeromagnetic anomaly maps

For map display, the aeromagnetic data were interpolated onto a regular grid. A grid cell size of 0.05° longitude and 0.042° latitude, or 1.5 km x 4.7 km at 75°N latitude, was chosen. Prior to gridding, the data were averaged if more than a single value came to lie within one grid cell. Smith & Wessel (1990) suggested a continuous curvature algorithm for gridding. They use splines in tension to avoid unwanted oscillations or extraneous inflection points of the calculated surface, which are commonly produced by minimum curvature approaches with natural bicubic spline interpolation. The continuous curvature algorithm, implemented in the Generic Mapping Tools (Wessel & Smith, 1991, 1995), was applied.

The sample interval of aeromagnetic data in the flight direction is about 80 m, whereas normal to the profile lines the nearest data point may be as far as 40 km away. Gridding averages data along the flight tracks and interpolates values into the data gaps between flight lines. It is therefore advantageous to display the data also along flight lines in so-called "wiggle plots". Details of the anomalies are not lost by averaging and the data coverage is honestly reflected. However, it is more difficult to gain a regional overview over magnetic trends and structures due to the large line spacing. In addition, E-W profile and N-S tie lines cannot be clearly displayed simultaneously in one map. Therefore, both types of display methods are used in this study. The gridded aeromagnetic anomaly data are shown as colour map in Fig. 3.15. A wiggle plot of all E-W profile lines is shown in Fig. 3.8.

The low level flights through Kejser Franz Joseph, Kong Oscar and Dickson Fjord (see Fig. 3.1) were processed in the same way as the high altitude survey data, except for upward continuation and line adjustment, which were not performed. The data are shown below as wiggle plot (Fig. 3.9).

3.1.4 Key results

Aeromagnetic data from 4 surveys were compiled into a regional aeromagnetic anomaly map of East Greenland at 3700 m altitude. Vigorous short-period transient variations of the Earth's magnetic field limit the accuracy of the data set to about 14 nT. This has to be compared to the range of magnetic anomalies from a minimum of -460 nT to a maximum of +1150 nT. Typical anomalies have amplitudes in excess of 100 nT and are therefore well resolved in terms of the accuracy of the data set.

Fig. 3.8 gives an overview over the different magnetic pattern in East Greenland. Magnetic provinces can be distinguished not only on the basis of different amplitudes of the anomalies. The wavelength of the anomalies plays an equally important role. For example, the "high frequency - high amplitude" anomalies at 70°N contrast to the magnetically "flat" area between 78°N and 79°N. In North Greenland, west of about 32°W, a change from short-wavelength anomalies to long wave-length anomalies with com-

parable amplitudes can be observed from 82°N to 83°N. Another typical feature of the anomaly map are isolated, pronounced maxima. Their geological significance has been verified by an increased coverage with flight lines. For example, the exactly N-S trending anomaly at 27°W between 73° and 72°N has been investigated in some detail to exclude artefacts.

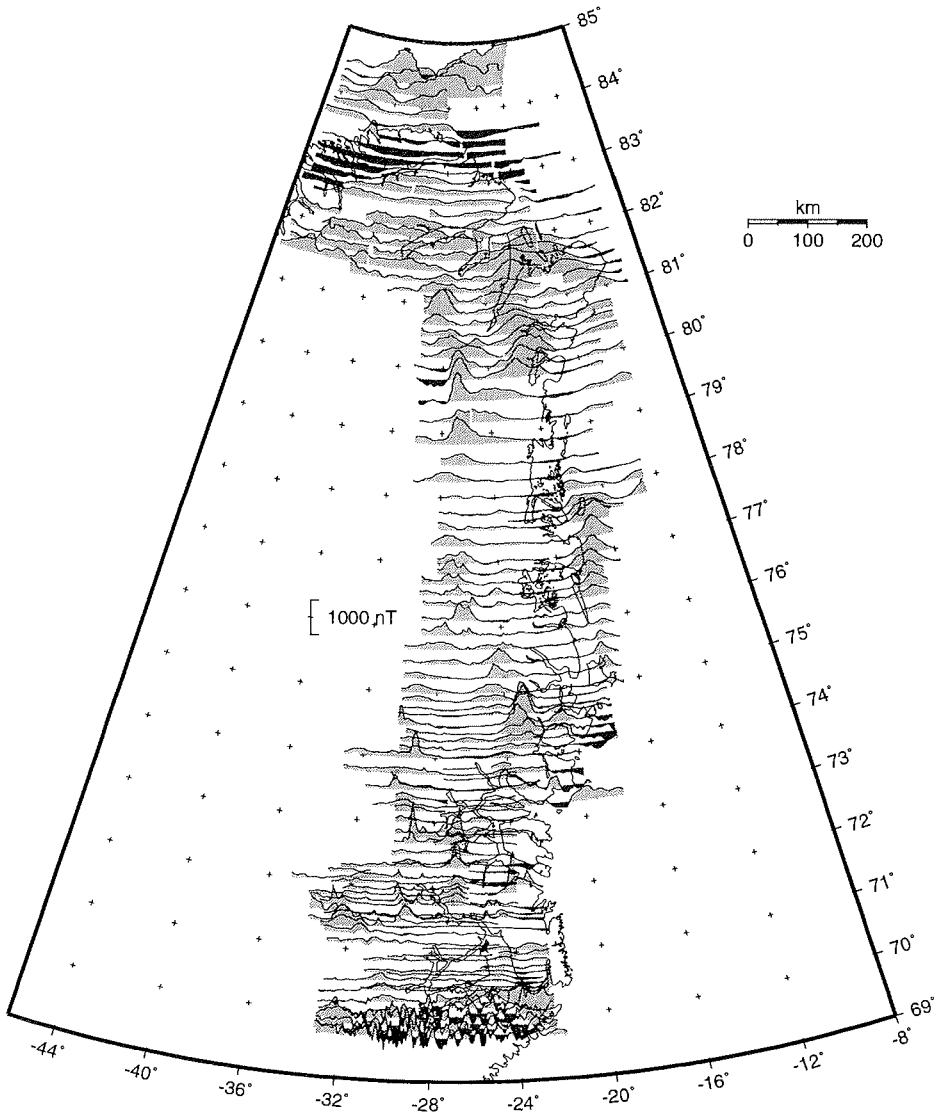

Fig. 3.8: Aeromagnetic anomalies along E-W flight tracks. Survey altitude 3700 m. Positive anomalies in light grey, negative anomalies in dark grey. Scale valid at 76°N.

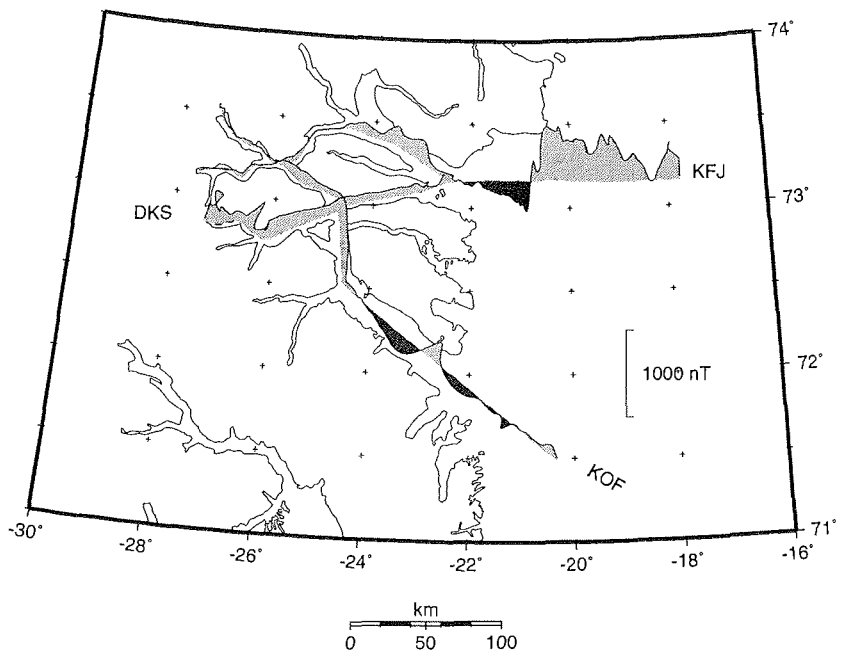

Fig. 3.9: Aeromagnetic anomalies along the flight tracks KJF, KOF, DKS. Survey altitude 1219 m. Positive anomalies in light grey, negative anomalies in dark grey. Scale valid at 72°N.

3.2 Magnetic susceptibility data

Following the AEROMAG campaigns, the 1997-1998 geological mapping project of East Greenland between 72°N and 75°N undertaken by the GEUS provided the logistic and scientific basis for detailed ground studies of magnetically anomalous areas. Of special interest were the high amplitude anomalies of Gletscherland and the extended area of flat anomalies centred along 26° 50'W in Nathorst Land (Fig. 3.10). Reconnaissance flights to the western nunataks and a detailed study of the anomalies associated with the Charcot Land window provided additional data outside this area. In order to detect possible sources of magnetic anomalies, the magnetic properties of the surface rocks needed to be measured. In this study, the measurements were confined to determining the magnetic susceptibility of the exposed rocks.

The magnetic susceptibility χ of a material describes its response to an external magnetic field. It is defined as the proportionality factor between this external magnetic field H and the resulting induced magnetisation M of the material.

$$M = \chi H$$

H and M are measured in A/m. Hence, χ is dimensionless. The system of SI units is used here throughout.

3.2.1 Data acquisition and processing

The fieldwork consisted of collecting in situ susceptibility data together with geological observations of the studied rock types, their extent and relation to other rocks. This information was obtained in close cooperation with the GEUS mapping project.

102 localities were visited from 7 different field camps by walking, during helicopter reconnaissance and rubberboat trips along the shores of Furesø (Fig. 3.10). The position of the localities was determined using portable GPS receivers and barometric altimeters. The magnetic susceptibilities were measured with an Exploranium KT-9 kappameter designed for field use. It determines the magnetic susceptibility by registering the response to a defined external field applied to the rock using an induction coil. The instrument can detect susceptibilities in the range between $0.01 \cdot 10^{-3}$ and $999 \cdot 10^{-3}$ SI units.

In order to acquire a statistically significant database, between 10 and 150 susceptibility readings were taken per locality, depending for example upon the homogeneity of the exposed rocks or the size of the outcrop. In total, 3330 susceptibility values were recorded. The data were either collected randomly at about 1 m intervals in outcrops of homogeneous rock types or along profiles perpendicular to the strike direction of strongly layered or banded rocks. In a few cases, bands of potentially magnetite-bearing rocks were over-represented in the measurements at a locality. The relative proportion of these rocks in the examined outcrop was estimated and the data were weighted accordingly for the calculation of site mean values.

The susceptibility data were classified in several groups according to lithology and geological provinces. The classification is based on field observations and, especially in the Charcot Land window, on the geological maps by Koch & Haller (1971) and the former GGU (Higgins, 1982).

Site means were calculated for all localities taking weighting factors into account. The results are shown in the logarithmic bar plots below and in detail in Appendix 1.

3.2.2 Magnetic minerals

The magnetic susceptibility of a rock is determined by the contributions of its ferrimagnetic, paramagnetic and diamagnetic minerals. Diamagnetic minerals like quartz or plagioclase making up the bulk of the felsic composition do not produce a significant susceptibility compared to the paramagnetic minerals like biotite, amphibole, pyroxene or olivine dominating the mafic composition. Henkel (1991) found from analysis of 30000 samples of crystalline rocks from northern Scandinavia a typical range susceptibilities of paramagnetic minerals from $0.75 \cdot 10^{-3}$ SI units to $3 \cdot 10^{-3}$ SI units. Ferrimagnetic minerals yield the largest contribution to the magnetic susceptibility of a rock. Magnetite (Fe_3O_4) and its solid solution with ulvospinel (Fe_2TiO_4) are considered to be the dominant ferrimagnetic phases for magnetic studies of crustal rocks (Blakely & Connard, 1989). The volume fraction f of magnetite in a rock sample can be estimated from its magnetic susceptibility k by the approximate relation (see Shive et al., 1992, for references):

$$f \approx \frac{5}{4\pi} k$$

Within one outcrop the susceptibilities can vary substantially reflecting the inhomogeneous mineralogy. The histograms of Fig. 3.11 illustrate two contrasting examples. A

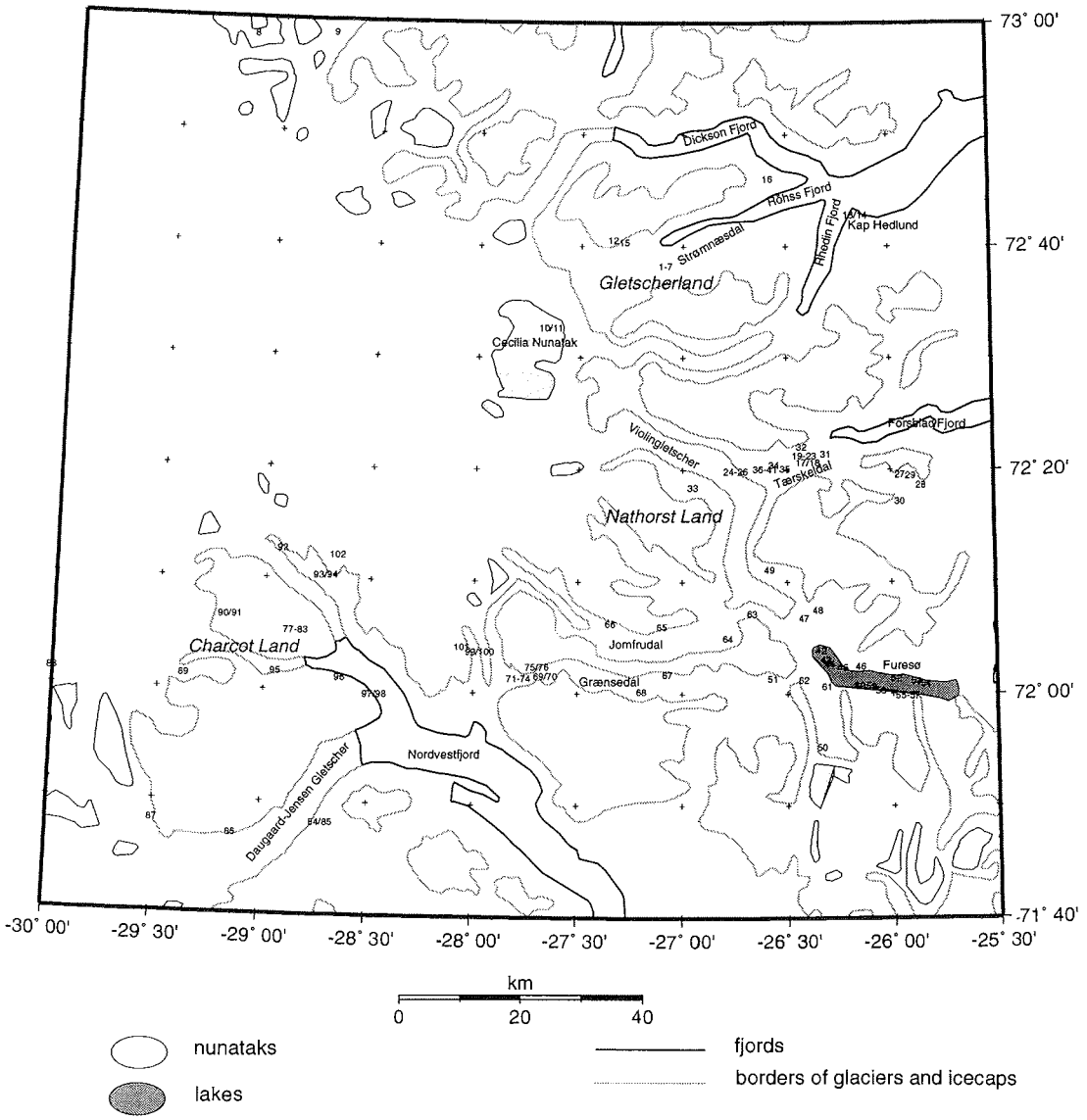

Fig. 3.10: Localities of susceptibility measurements. The positions of the localities are indicated by their numbers. For clarity, closely spaced localities were grouped (e.g. 36-41 in Tærskeldal). Scale valid at 72°N.

magnetite-bearing granitic gneiss was found at 3 localities up to 100 km apart. The rocks at all 3 localities were very similar which is also reflected by the susceptibilities clustering around 30 to 40 · 10^{-3} SI units. Hence, a fairly homogeneous magnetite content can be expected for this rock type. In contrast, the 120 m thick sequence of amphibolitic rocks with intercalated metasedimentary layers which are partly retrogressed is predominantly weakly magnetic. However, magnetite occurs in different layers (mica-chlorite-schist, garnet-amphibolite) in very varying concentrations as reflected by the broad distribution of susceptibility readings between about 10 and 130 · 10^{-3} SI units without any preference for a certain susceptibility.

3.2.3 Susceptibilities and geological observations

Basement rocks. In Fig. 3.12 basement lithologies are displayed. Following Higgins et al. (1981) the terminology "basement" is used here to describe infracrustal gneiss complexes, especially the Gletscherland complex (Fig. 3.10).

- The basement gneisses include a variety of well banded, often veined, grey hornblende, biotite and granitic gneisses. They testify to high deformation during several orogenic events (Henriksen, 1985). The variety of the gneisses is reflected by the site mean susceptibilities. About a third of the site mean susceptibilities concentrates at low values of typically 0.3 · 10^{-3} SI units, which may reflect mainly the susceptibility of the paramagnetic minerals included in the gneiss. In addition, a range of site means between 1 and 20 · 10^{-3} SI units is observed which probably witness to a corresponding range of magnetite concentrations of 0.4‰ to 8‰. At localities 3, 5 and 65, magnetite was seen in hand specimen.

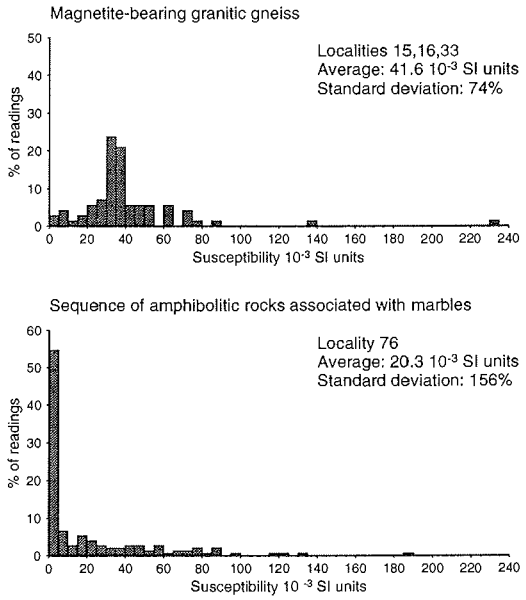

Fig. 3.11: Histograms showing the distribution of susceptibility readings at different localities.

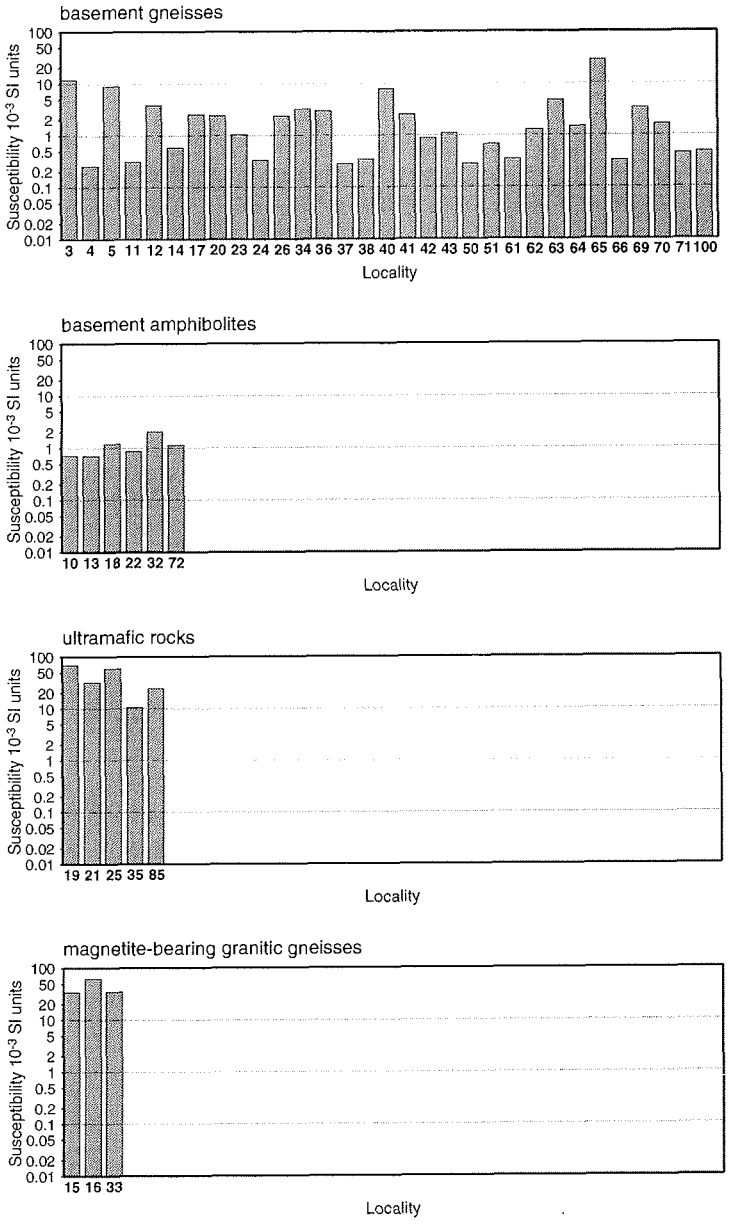

Fig. 3.12: Site mean susceptibilities for different lithologies of the infracrustal gneiss complexes. The positions of the localities are shown in Fig. 3.10. The lithologies are described in the text.

- Dark amphibolitic bands and lenses are plentiful within the basement complex. They are concordant and deformed together with the basement gneisses. The thickness of the bands may vary from centimetre size to several tens of metres. The measurements listed in this group stem from bands of at least metre size, whereas measurements from thin bands within the gneisses were incorporated into the class of basement gneisses. Magnetically, the amphibolites are characterized by fairly uniform site means of about $1 \cdot 10^{-3}$ SI units, reflecting the typical susceptibility of its mafic, paramagnetic mineralogy as observed by Henkel (1991).
- A chain of ultramafic bodies ranging in size between 2 m x 5 m and about 50 m x 500 m are embedded in the gneisses of Tærskeldal (localities 19, 21, 25, 35). They are partly heavily altered and show a great variety of mineral assemblages including olivine, clinopyroxene, amphibole, hornblende and bronzite. This is matched by a varying content of ferrimagnetic minerals as reflected by the range of site mean susceptibilities between 10 and $70 \cdot 10^{-3}$ SI units. The ultramafic body encountered at locality 85 east of Daugaard-Jensen Gletscher fits into this picture.
- Localities 15,16 and 33 were identified on the aeromagnetic map as centres of major positive anomalies. At all 3 localities a light grey to pinkish, medium grained homogeneous magnetite-bearing granitic gneiss was found. It consists mainly of quartz, feldspar and biotite. Garnet is absent. Compared to the basement gneisses the granitic gneiss is weakly deformed and foliated, with leucocratic veins and pockets cross-cutting the gneissosity. The presence of oxides can be detected from the appearance of the weathered surfaces. At locality 16, dark schlieren of pure magnetite were seen, making up roughly 50% of some boulders. Apart from these bands, the rock type is magnetically fairly homogeneous with high average susceptibilities of about $40 \cdot 10^{-3}$ SI units at all localities. The outcrops each have roughly km size. At locality 33, SW of Violingletscher, the contact to the surrounding gneisses is beautifully exposed showing clearly that the granitic gneiss cross-cuts older structures of the basement gneisses.

Supracrustal rocks. A variety of supracrustal rocks was examined in the field. The resulting site mean susceptibilities are shown in Fig. 3.13.

- Included in the basement complex are metasedimentary rock units, notably marble-amphibolite associations and rusty red weathering metasediments. Their character is similar to the Krummedal supracrustal sequence defined in the area between 70° and 72°N, however their relationship is not firmly established (Henriksen, 1985). The rock type is weakly magnetic showing typically susceptibilities of about $0.4 \cdot 10^{-3}$ SI units. However, two exceptions occur, showing one order of magnitude higher susceptibilities. At locality 7 in Strømnæsdal, a thin mafic band making up less than 10% of the outcrop of metasedimentary rocks yielded a susceptibility of about $23 \cdot 10^{-3}$ SI units, giving rise to the increased site mean value. Locality 73 in Grænsedal consists of a very weathered mica-garnet-schist which is adjacent to a prominent magnetic amphibolitic band (localities 74 and 76).
- The association of amphibolites with marbles in the supracrustal sequences is very common in the entire region. However, confined to the area around Jomfrudal and Grænsedal strikingly magnetic varieties of the amphibolitic rocks were found. They form part of often flat lying metasedimentary sequences, up to a few 100 m thick, which are intercalated frequently in the basement gneisses. The rock type is characterized as a garnetiferous amphibolite, showing varying degrees of alteration. The

site mean susceptibilities are divided in two classes and demonstrate that this rock type is not necessarily magnetite-bearing. The lower values between 1 and 4 · 10^{-3} SI units are typical values for amphibolites comparable to those of the basement amphibolites (Fig. 3.12). However, an increased content of magnetite is necessary to produce values of 17 · 10^{-3} SI units, observed at the other localities. The susceptibilities at each of these localities vary considerably (Fig. 3.11), testifying to a very inhomogeneous distribution of magnetite, which is not only confined to the amphibolites but also encountered in thin metasedimentary layers (mica-chlorite-schist, locality 76).

- The migmatite zone bordering the Gletscherland complex to the west (Henriksen, 1985) has been studied along the shores of Furesø. The migmatisation increases towards the Stauning Alper granites to the east. The susceptibilities are fairly homogeneous and only vary between 0.1 and 0.4 · 10^{-3} SI units. The outlier at locality 57 with 0.01 · 10^{-3} SI units is produced by a band of clean, recrystallized quartzites included in the sequence. Decreasing susceptibility with increasing proportion of leucosome could be observed in some cases, but could not be confirmed in all cases.
- During two reconnaissance flights, Eleonore Bay Supergroup (EBSG) metasedimentary rocks were visited. Localities 8 and 9 are situated in the western nunatak zone. At locality 9, a quartzitic rock, occurring in the lower part of the Petermann Series, which has been correlated with the EBSG (Sønderholm & Tirsgaard, 1993), was examined. Localities 28 and 29 lie in Schaffhauserdal close to the boundary to the migmatite complex described above. At all localities essentially non-magnetic rock types were found as illustrated by the low site mean susceptibilities.

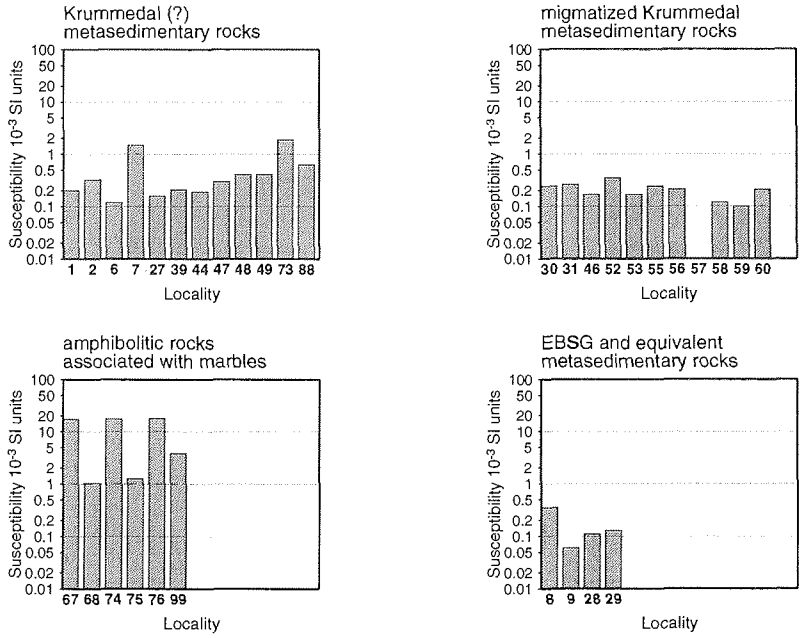

Fig. 3.13: Site mean susceptibilities for different supracrustal lithologies. The positions of the localities are shown in Fig. 3.10. The lithologies are described in the text.

Charcot Land. The Charcot Land tectonic window (Fig. 3.10) exposes infracrustal rocks of probably Archaean-Early Proterozoic age which are overlain by the Charcot Land supracrustal sequence. Both were affected by a metamorphic event predating the emplacement of a granitic intrusion at about 1840 Ma (Hansen et al., 1981). The degree of metamorphism within the Charcot Land window increases towards the north. Susceptibility measurements of the infracrustal rocks and the supracrustal sequence, consisting of metasedimentary rocks and basic extrusives and intrusives (Higgins, 1982), were made (Fig. 3.14).

- The site means of basement gneiss localities are displayed along with the values obtained from the muscovite-granite intrusion (localities 79, 91, 95). The gneisses are veined, homogeneous, grey gneisses, strongly foliated, but they show weak folding. Concordant amphibolites are intercalated in the gneisses. In the roof zone of the granite intrusion, the gneisses are cut by numerous pegmatite dykes making up large proportions of the rocks close to the batholith. The susceptibilities of about $0.3 \cdot 10^{-3}$ SI units for both rock types reflect their mainly felsic nature combined with the absence of ferrimagnetic minerals.
- Amphibolites were also encountered within the Charcot Land supracrustal sequence, often in association with marbles. However, measurements were only taken at 2 localities, which does not allow any general conclusions regarding their magnetic properties. Locality 83 shows a typical amphibolite susceptibility, whereas clearly increased values ($7 \cdot 10^{-3}$ SI units) are observed for the outcrop of amphibolites at locality 98, which is adjacent to the small lens of highly magnetic garnet-mica-schist of locality 97.

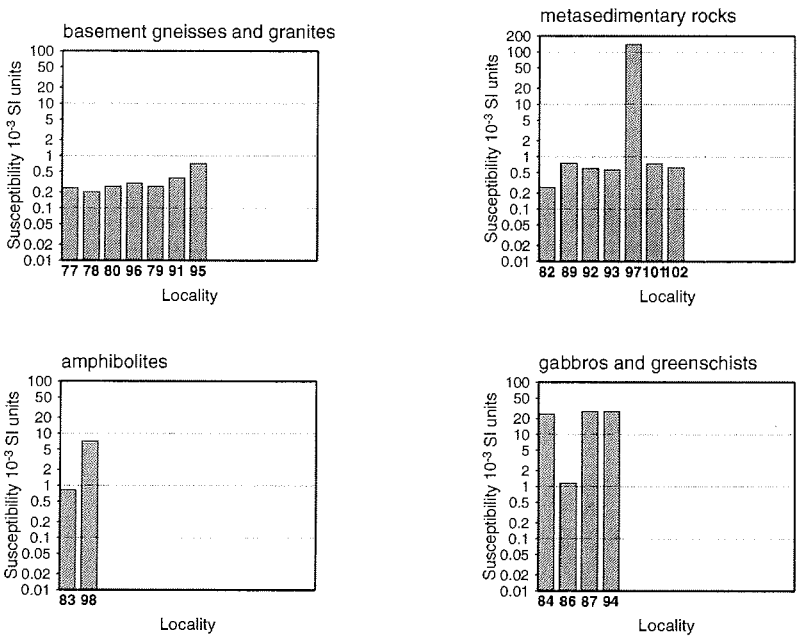

Fig. 3.14: Site mean susceptibilities for different lithologies of the Charcot Land window. The positions of the localities are shown in Fig. 3.10. The lithologies are described in the text.

- The metasedimentary rocks studied comprise metapelitic to metapsammitic units, marbles (locality 82) and a garnet-mica-schist (locality 97). The metapelitic to metapsammitic rocks show typical susceptibilities of $0.5 \cdot 10^{-3}$ SI units at all localities. The marbles are even less magnetic. The garnet-mica-schist of locality 97 has unusual magnetic properties. It shows the largest site mean susceptibility of all localities ($138 \cdot 10^{-3}$ SI units). Apart from > 5 cm large garnet crystals in a matrix of mica the rock must comprise on average 5.5% magnetite. This highly magnetic garnet-mica-schist was confined to an outcrop of about 10 m x 50 m surrounded by amphibolitic rocks (locality 98).
- The basic intrusives and extrusives occur in different metamorphic grades increasing towards the north. Greenschists were studied at the south side of Daugaard-Jensen Gletscher. They represent the low-grade equivalent of lavas and tuffs. Remains of pillow structures were found locally (Higgins, 1982). At locality 84, the greenschists are exposed close to the thrust forming the eastern boundary of the Charcot Land window. The magnetisation increased rapidly away from the thrust towards the less sheared parts of the about 50 m thick band of greenschists. Two outcrops of hornblende gabbro (Higgins, 1982) yielded very different susceptibilities. Whereas the hornblende gabbro at locality 86 is clearly foliated and weakly magnetic, the gabbro at locality 87 exhibits no foliation, although the mineral assemblage testifies to metamorphic overprint (J. D. Friderichsen, pers. comm., 1997). A site mean value of about $27 \cdot 10^{-3}$ SI units is attributed to this locality. Finally, a dark amphibole-garnet-hornblende rock at locality 94 could represent an amphibolite facies version of the basic extrusives and intrusives. However, it could as well be classified as amphibolites, although, in contrast to the amphibolites of localities 83 and 88, it was not associated with marbles at this locality. A susceptibility of $29 \cdot 10^{-3}$ SI units was measured.

Finally, a striking feature of the Charcot Land area are a small number of distinct Tertiary doleritic dykes of about 10 m width which cut straight across all older structures. Susceptibilities were measured at two localities yielding an average value of $17 \cdot 10^{-3}$ SI units.

3.2.4 Key results

Susceptibility measurements were carried out at 102 localities in the crystalline complexes of Gletscherland, Nathorst Land and Charcot Land (Fig. 3.10). Basement rocks exhibit generally low susceptibilities reflecting their mainly paramagnetic mineralogy. A prominent exception is a magnetite-bearing granitic gneiss encountered at three localities in Gletscherland. This granitic gneiss cross-cuts older structures but has experienced deformation itself. Ultramafic bodies included in the basement complexes have varying susceptibilities depending on the degree of alteration and their mineral assemblage. Metasedimentary rocks within the basement complexes have low susceptibilities. However, a common feature, studied in Nathorst Land, are amphibolitic rocks in association with marbles and metasedimentary sequences. In this succession, the amphibolitic rocks and metasedimentary rocks with low-grade alteration may be highly magnetic. The Charcot Land window exposes a non-magnetic basement complex which is covered by a supracrustal sequence with metamorphic overprint increasing towards the north. Magmatic rocks within this sequence show high susceptibilities if no significant metamorphic overprint is seen.

3.3 Crustal structure in the light of aeromagnetic data

For a geological interpretation, the aeromagnetic anomaly map of East Greenland has been divided into 26 provinces with distinct magnetic signatures. These areas have been identified using both the aeromagnetic anomaly map as shown in Fig. 3.15 and detailed wiggle plots of selected areas (Fig. 3.16 - Fig. 3.20). Fig. 3.15 gives an overview over these magnetic provinces marked by numbers which are referred to in the text. The individual areas are analysed in context with surface geology and available geophysical data in order to define possible sources for the magnetic anomaly pattern. This link between aeromagnetic measurements and magnetic properties of crustal rocks is greatly enhanced by susceptibility measurements of exposed rocks in Central East Greenland. Emphasis is placed on the interpretation and discussion of the magnetic anomalies of the Caledonian fold belt.

No attempt has been made to model the magnetic anomalies and to present models for source bodies. Due to the large survey altitude the shape and width of the anomalies are deceptive and tend to suggest too deep sources. This is very instructively shown by comparing for example the anomaly over Gletscherland with the detailed aeromagnetic survey by Larsen (1977) which was flown in this area at 1850 m constant barometric altitude. His data show an assemblage of narrow anomalies following magnetic lineaments and giving hints to several source bodies. These structures could not be resolved at 3700 m survey altitude. Hence, modelling the high altitude reconnaissance type data without additional constraints and information cannot yield source models which are reasonably close to geological reality. However, rough forward modelling was performed in order to estimate source dimension necessary to produce the amplitude of individual anomalies when the magnetic susceptibilities of the source rocks were known from ground measurements.

3.3.1 North Greenland

North Greenland is magnetically very well structured and shows 6 regional-scale magnetic provinces which correlate to geological provinces.

(1) Morris Jesup Plateau (Fig. 3.15)

Offshore North Greenland lies an about 200 km broad marginal plateau that extends towards the north-east (Dawes,1990). Its magnetic signature had been investigated previously by Ostenso & Wold (1971) and Riddihough et al. (1973). The area is characterized by a large positive magnetic anomaly with amplitudes up to 850 nT. Low-level aeromagnetic surveys reveal a complex anomaly pattern (e.g. Dawes, 1990, his Fig. 4A) which can only be guessed from this survey. The positive magnetic anomaly is attributed to the predominantly oceanic nature of the Morris Jesup plateau, consisting probably of Fe-Ti-rich basalts (Dawes, 1990). However, the detailed structure of the Morris Jesup Plateau and the sources for the complex magnetic character are subject to speculation (see Dawes, 1990, for a review).

Fig. 3.15 (overleaf): Aeromagnetic anomalies over East Greenland at 3700 m altitude. The numbers refer to magnetic provinces which are explained in the text. Scale valid at 76°N.

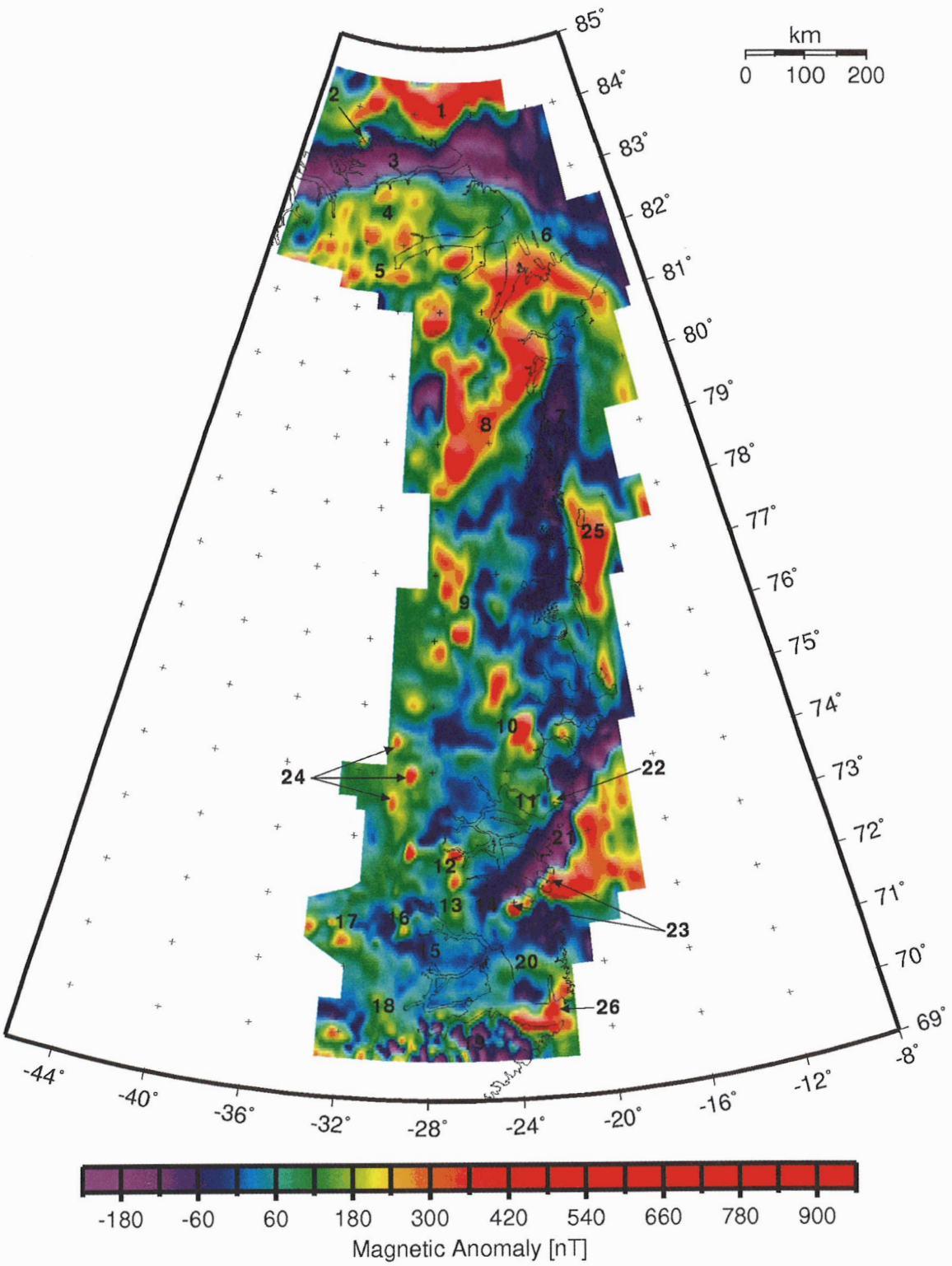
km
0 100 200
85°
84°
83°
82°
81°
80°
79°
78°
77°
76°
75°
74°
73°
72°
71°
70°
69°
-8°
-12°
-16°
-20°
-24°
-28°
-32°
-36°
-40°
-44°
1
2
3
4
5
6
7
8
9
10
11
12
13
16
17
18
20
21
22
23
24
25
26
-180 -60 60 180 300 420 540 660 780 900
Magnetic Anomaly [nT]

(2) Kap Washington Group volcanics (Fig. 3.16)
An isolated positive magnetic anomaly of about 380 nT amplitude is situated on the north coast of Peary Land. It coincides with exposures of the Kap Washington Group consisting of sedimentary units and per-alkaline volcanics (Surlyk, 1991). They formed during Late Cretaceous rifting of the Eurasian basin. Apart from more acid volcanic products, the sequence contains basic lavas which could be responsible for the magnetic anomaly. The "within-plate" chemistry of the volcanics suggests that the area was underlain essentially by continental crust at that stage (Dawes, 1990).

(3) Franklinian basin,
(4) Franklinian shelf,
(5) Independence Fjord Group and Midsommersø Dolerites (Fig. 3.16)
North Greenland is dominated by a characteristic sequence of three magnetic anomaly patterns. It consists to the south of an area of positive anomalies with a distinct short-wavelength pattern (5). Adjacent to the north, these positive anomalies are flat long-wavelength features (4). This pattern ends abruptly and is replaced to the north by a trough of negative anomalies (3).

Anomaly (5). The magnetic signature (5) is encountered where rocks of the Independence Fjord Group (IFG) are exposed (Escher & Pulvertaft, 1995). The short-wavelength character of the anomalies correlates to some extent with the topographic relief suggesting a shallow or outcropping magnetic source.

The IFG consists mainly of sandstones deposited in Middle Proterozoic times on Archaean basement (Surlyk, 1991; Higgins, 1986). Both basement and the Independence Fjord sandstones were heavily intruded during a major volcanic event at about 1230 Ma producing large volumes of basic magmas (Kalsbeek & Jepsen, 1983). The resulting Midsommersø Dolerite Formation frequently forms flat-lying sheets of dolerites which can sometimes be followed for tens of kilometres. They range in thickness from a few metres to several hundreds of metres (Sønderholm & Jepsen, 1991). I suggest that these dolerites cause the magnetic signature (5). They occur in sufficient volumes in the entire area of (5). Susceptibility measurements of two single hand specimen yielded a value of about $10 \cdot 10^{-3}$ SI units for a sample of the dolerites and about $0.1 \cdot 10^{-3}$ SI units for a sample of the sandstones. The samples were picked randomly and may not be representative, but the measured values would support the hypothesis of the dolerites as source for the magnetic anomalies.

The magnetic anomaly pattern (5) extends to the east across the area between Independence Fjord and Danmark Fjord where the Zig-Zag Dal Basalt Formation overlies the IFG rocks. The basalts attain a thickness of up to 1350 m and are regarded to be the extrusive equivalent of the Midsommersø Dolerites (Kalsbeek & Jepsen, 1983). They might contribute to the magnetic anomalies.

Anomaly (4). North of Wandel Dal (Fig. 3.16), the positive anomalies remain at the same amplitude level but show longer wavelengths (4). Topography no longer influenc-

Fig. 3.16 (overleaf): Magnetic anomalies along flight lines over North Greenland. Positive anomalies are shaded in light grey, negative anomalies in dark grey. Numbered anomalies are discussed in the text. Geological provinces mentioned in the text are roughly sketched and labelled in Times font. KW: Kap Washington; NVE: Navarana Fjord Escarpment; IFG: Independence Fjord Group; ZZD: Zig-Zag Dal basalts; TLF: Trolle Land Fault. Scale valid at 82°N.

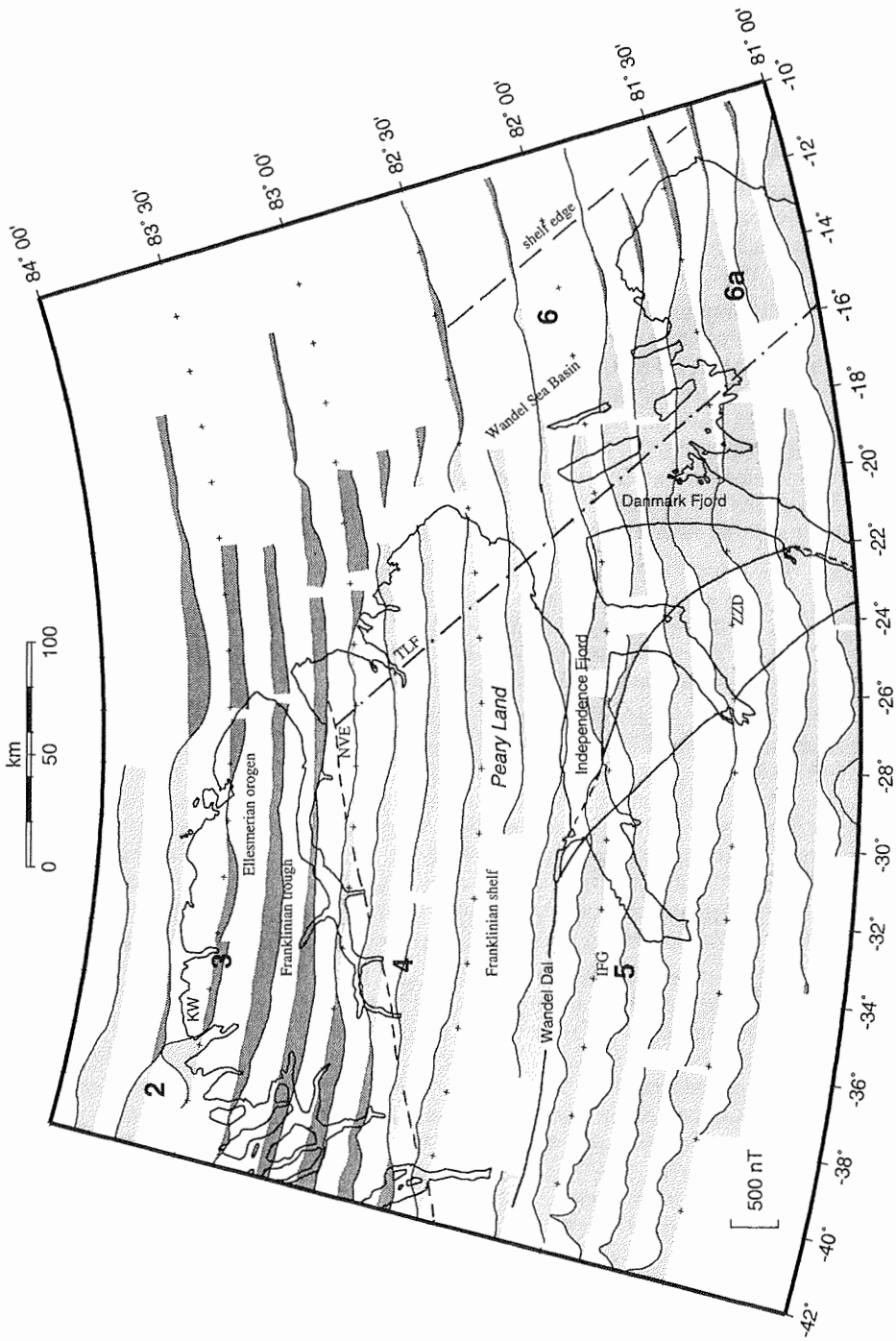
84° 00'
83° 30'
83° 00'
82° 30'
82° 00'
81° 30'
81° 00'
-10°
-12°
-14°
-16°
-18°
-20°
-22°
-24°
-26°
-28°
-30°
-32°
-34°
-36°
-38°
-40°
-42°
km
0
50
100
500 nT
shelf edge
Wandel Sea Basin
Danmark Fjord
Independence Fjord
Peary Land
Franklinian shelf
Wandel Dal
Ellesmerian orogen
Franklinian trough
KW
NVF
TLF
TFG
ZZD
2
3
4
5
6
6a

es the shape of the anomalies. Thus, the magnetic sources probably lie beneath the surface.

At Wandel Dal, the southern boundary of the Lower Palaeozoic Franklinian basin is exposed (Henriksen, 1992). This E-W oriented basin formed during the evolution of a rift perpendicular to the western margin of the Iapetus ocean probably in Latest Precambrian times. It consists of a wide shelf area to the south with mainly carbonate deposits attaining a thickness of 3-4 km increasing towards the north. To the north, a deep trough accumulated up to 8 km of siliciclastic sediments. The border between the deep and shallow basin progressively stepped southwards during the evolution of the basin The today buried steep Navarana Fjord escarpment represents one of these boundaries (Surlyk, 1991; Higgins et al., 1991).

The magnetic anomaly pattern (4) coincides with the shelf region of the Franklinian basin. As the sedimentary infill is unlikely to have significant susceptibilities, the magnetic sources must rather be sought below the basin as is suggested by the long-wavelength character of the anomalies. The magnetic anomalies (4) can be reasonably explained if the basement beneath the shelf part of the Franklinian basin was affected by the volcanic event around 1230 Ma and is also intruded by doleritic sills. Outcrops of IFG including dolerites north-east of the Franklinian shelf (Henriksen, 1992) indicate a large spatial extent of the volcanism. The change in magnetic signature from (5) to (4) is then due to a magnetic layer dipping northward beneath a non-magnetic cover.

Anomaly (3). Although roughly coinciding with the Navarana Fjord escarpment, the transition from the positive magnetic anomalies of (4) to the smooth negative magnetic trough (3) cannot be related to the escarpment, because essentially non-magnetic sedimentary units are exposed on both sides. Two explanations for the negative magnetic anomaly (3) can be brought forward:

Firstly, the anomaly could result from a layer of magnetic material carrying a reversely polarized remanence. A likely carrier of remanence could be a sequence of rift-related volcanics underlying the basin. Surlyk (1991) argues that the rift reached a narrow ocean stage, although no ocean floor volcanics have been observed. Dawes (1990), in contrast, considers the nature of the Kap Washington volcanics as an indication for continental crust underlying the area. Hence, the presence of appropriate magnetic material can be doubted. In addition, the anomaly (3) occupies the area that was affected by the Ellesmerian orogeny (Surlyk, 1991). The orogenic processes might have reworked the volcanic rocks and overprinted or even destroyed an existing remanence.

Alternatively, the negative magnetic anomaly can be interpreted as an edge effect due to a fading out magnetic layer to the south. Forward modelling shows that the amplitude and width of the negative anomaly can be produced by a magnetic layer of reasonable susceptibility at about 8 km depth fading out beneath the deep basin. Transferred to the local geological scenario, this implies that the magnetic basement beneath the Franklinian shelf ends at the transition to the trough. Rifting must have led to considerable crustal thinning and subsidence in the deep basin, eventually even attaining a spreading state (Surlyk, 1991). Even if the basin is underlain by continental crust, normal faulting at the shelf-trough transition (Surlyk, 1991) may have cut off the magnetic basement and displaced it downward. Eventual remnants of the magnetic basement beneath the deep Franklinian basin then became involved in the Ellesmerian orogeny and might have lost their magnetic minerals during metamorphism.

I favour the second interpretation as it does not necessarily require the presence of a carrier of reversed remanent magnetisation and implies a likely geological evolution.

However, a contribution of volcanic rocks with predominantly reversed magnetisation is not excluded. I subscribe to the opinion of Riddihough et al. (1973) and Coles et al. (1976) who consider the transition from magnetic province (4) to (3) as the northern boundary of the stable Precambrian craton.

No geological control is available for the northern and eastern boundary of anomaly (3) as they lie offshore. The original extent of the Franklinian basin towards the north is not known (Surlyk, 1991). The nature of the positive anomalies to the north of (3) and west of (1) thus remains enigmatic. Towards the Wandel Sea, the negative anomaly broadens and fades out. It might also be cut off by geological processes responsible for the formation of the NW-SE trend reflected by anomaly (6).

(6) Wandel Sea basin area (Fig. 3.16)

Magnetic signature (6) marks a prominent NW-SE oriented lineament formed by a gradient in the magnetic field. A striking positive anomaly (6a) parallel to the trend is seen further to the south across Kronprins Christian Land.

Eastern North Greenland was covered by the sedimentary sequences of the Wandel Sea basin from Upper Carboniferous times throughout the Mesozoic. During the Mesozoic, E-W extension formed a NW-SE trending oblique-slip belt with fault-controlled basins (Surlyk, 1991). Magmatic activity is only known from the north-westernmost subbasins (Surlyk, 1991) and is not reflected by the magnetic field. The continental shelf break is parallel to the trend of the mobile belt and probably controlled by faults related to it (Dawes, 1990).

The magnetic gradient is situated roughly halfway between the Trolle Land Fault Zone, marking the western boundary of the Wandel Sea strata (Stemmerik & Håkansson, 1991), and the shelf break (Escher & Pulvertaft, 1995). The sedimentary sequences exposed onshore contain no likely source rocks for the magnetic anomalies. Instead, in eastern Peary Land, the magnetic signature (4) extends eastwards all the way to the gradient. Thus, the dolerite-intruded basement probably underlies the Wandel Sea strata. Downfaulting in the oblique-slip belt, eventually accompanying the formation of the fault-controlled shelf break, may have displaced the magnetic basement considerably downwards. A smooth magnetic gradient over the edge of the magnetic basement would be the result.

Especially conspicuous is the large positive anomaly (6a) crossing Kronprins Christian Land. It cuts off the Caledonian fold belt and its magnetic signature (7). The northward extent of Caledonian fold belt is not known, because it is obscured by the younger structures of the Wandel Sea mobile belt. The northernmost outcrops of Caledonian crystalline basement are seen in Antarctic Bugt (Escher & Pulvertaft, 1995) (Fig. 3.17).

If the Caledonian crystalline complex extended further north and is essentially non-magnetic as to the south, the formation of the large NW-SE magnetic anomaly must post-date Caledonian orogeny. This necessarily implies the introduction of magnetic material to the predominantly non-magnetic crust, preferably during the tectonic regime of the Mesozoic oblique-slip belt. In contrast, the positive anomaly might be caused by older geological units and cut off to the east by the processes forming the gradient. In that case, the positive anomaly must have remained unaffected by the Caledonian orogeny and represent a northern boundary of thick-skinned Caledonian tectonism. It would hence be comparable to the scenario reflected by the contrasting anomaly pattern (7) and (8). Due to the lack of additional geophysical and geological information on

the crustal structure of this area, this crucial question for the understanding of the northern extremity of the Caledonides and its relation to Ellesmerian orogeny, has to remain unsolved.

3.3.2 Caledonian fold belt

The region of the East Greenland Caledonides appears as a predominantly non-magnetic area, which is obvious in the northern part of the fold belt (7). To the south, the magnetic signature of the Caledonides becomes more intricate with isolated strongly positive anomalies (10),(12),(13). Anomalies (8), (9) and (16) - (18) are examples of the magnetic characteristics of the Caledonian foreland or tectonic windows relatively unaffected by the Caledonian orogeny.

(7) Caledonian crystalline complex of northern East Greenland,
(8) Caledonian foreland (Fig. 3.17)

A shallow, non-magnetic trough (7) extends in a N-S direction from about 81°N to 75°N (Fig. 3.15). The magnetic signature (7) seems to be typical for the crystalline core of the Caledonian fold belt which is exposed in the same area. It consists mainly of gneissic rocks in amphibolite facies being a composite product of several metamorphic episodes (Higgins, 1986). Susceptibilities measured on 9 hand specimen representative for the basement lithology (J. D. Friderichsen, pers. comm., 1996) confirmed the non-magnetic character with values below $1 \cdot 10^{-3}$ SI units. To the west, this non-magnetic region is bordered by the positive anomalies (8) and (9) (Fig. 3.15). The transition between (7) and (8) correlates to a major geological boundary. West of this border zone, a sequence of nappes is exposed in the area of (8) containing Proterozoic and Lower Palaeozoic sedimentary units which were thrust westward during the Caledonian orogeny. Deformation and thrusting decreases towards the west (Hurst et al., 1985) and is considered to have affected only higher crustal levels (Henriksen, 1994a).

The aeromagnetic anomaly pattern (8) consists of broad high amplitude anomalies (8b) and partly superimposed short-wavelength patterns (8a) (Fig. 3.17). The short-wavelength anomalies (8a) relate to exposures of IFG rocks including dolerites. In contrast to North Greenland (5) and the western locality (8a), the IFG rocks between Ingolf Fjord and Hekla Sund were involved in the Caledonian orogeny and suffered low- to medium-grade metamorphism. A metadolerite sample from west of Jøkelbugt showed a low susceptibility of $0.7 \cdot 10^{-3}$ SI units. In addition, the outcrops of IFG in Jøkelbugt and in Lambert Land cause no magnetic anomalies. Hence, it can be doubted that the metadolerites produce the anomaly pattern related to the IFG outcrops. S. A. Schack Pedersen et al. (unpublished express report of field season 1995) report from the area between Ingolf Fjord and Hekla Sund the occurrence of laminae of magnetite and haematite within sedimentary layers of the Ingolf Fjord Formation. These rocks could form the explanation for the short-wavelength anomalies in that area, although no ground control by susceptibility measurements exists. The nature of the large positive anomalies (8b) is uncertain. One of them is paired with a small negative anomaly which might point to the existence of a strong remanent magnetisation. None of the anomalies are directly related to surface geology. Their long wavelengths might indicate a deep source.

Several interpretations for the marked contrast between the anomalies (8) and the

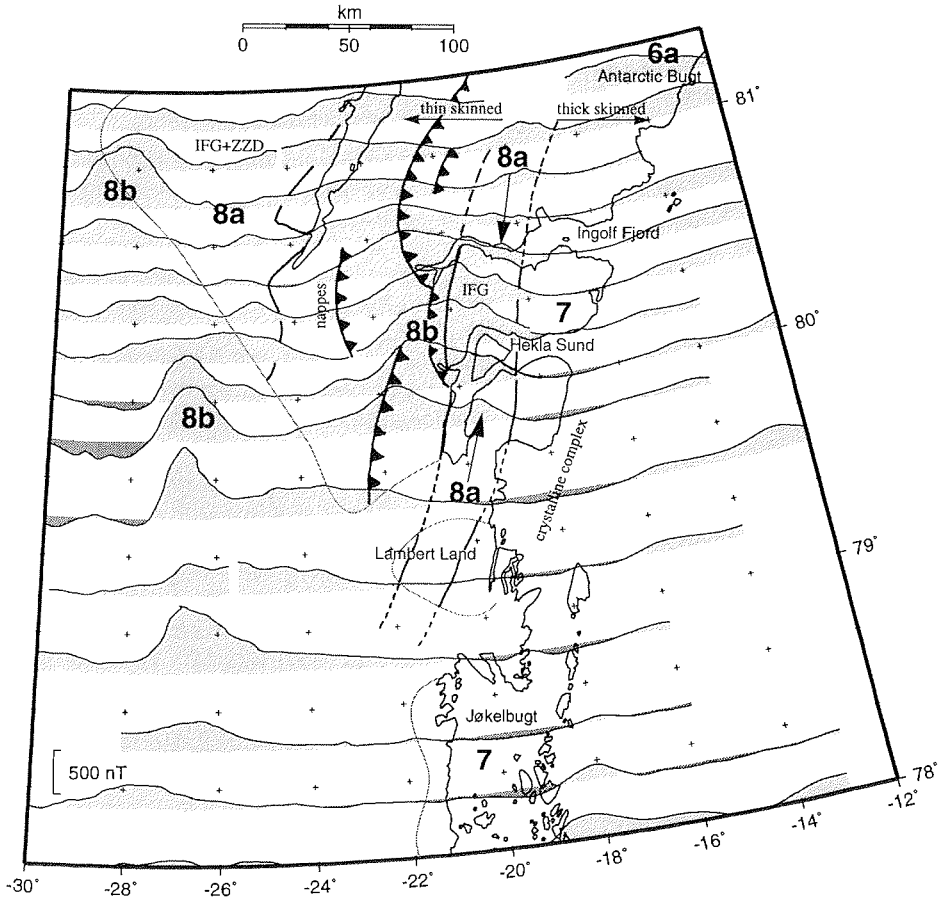

Fig. 3.17: Magnetic anomalies along flight lines over the Caledonides of northern East Greenland. See Fig. 3.16 for map explanation. The grey line marks the boundary of the inland ice. IFG: Independence Fjord Group; ZZD: Zig-Zag Dal basalts. Scale valid at 79°N.

Caledonian crystalline complex devoid of magnetic anomalies (7) are possible involving different conclusions for the regional crustal evolution (Fig. 3.15):

The positive anomalies could be of pre-Caledonian origin and a property of the basement rocks beneath the sedimentary sequences and the Caledonian nappes. For example, one could speculate that their formation is related to the large volcanic event in the Middle Proterozoic and that they represent volcanic centres or feeders rather than the typical dolerite sills and basalt flows of the Zig-Zag Dal region.

In this case two scenarios can be imagined:

Firstly, the magnetic boundary between (7) and (8) existed already in pre-Caledonian times and represents the demarcation line between different kinds of basement. The difference might be that the eastern part was not affected by magmatism. However,

compared to the large spatial extent of the magmatic event, this abrupt eastern end seems unlikely. Another possibility might be a different origin of the basement complexes. Whereas the sedimentary basins of North Greenland are considered to be underlain by Archaean crust (Higgins, 1986), the crystalline complex of the northern Caledonides is assumed to be Early Proterozoic in age (Hurst et al., 1985).

Alternatively, the magnetic boundary between (7) and (8) may have developed in Caledonian times, not necessarily involving pre-existing differences in the basement. It could represent the boundary between thick-skinned and thin-skinned Caledonian tectonism. This means, that the crust remained largely unaffected by Caledonian processes in the western part and retained its earlier acquired magnetic properties. To the east, where the crystalline core of the Caledonian fold belt is exposed, Caledonian reworking was more pervasive affecting larger parts of the crust and destroying an eventually existing magnetisation by metamorphism. However, the extent of Caledonian metamorphism is also in North Greenland much debated (Hurst et al., 1985) and it is not known, whether the amphibolite grade of the exposed gneisses stems from Caledonian metamorphism.

In addition, there are no generally valid rules for the behaviour of magnetite during metamorphism (Shive et al., 1992; Schlinger, 1985) and the involved processes are complex and dependent on initial mineralogy, bulk composition and metamorphic conditions (e.g. prograde/ retrograde, fugacity of water, oxygen). Non-magnetic amphibolite facies rocks have been reported from several areas including West Greenland (Thorning, 1984), East Greenland (Larsen, 1981, see below), the Lofoten (Schlinger, 1985) and Central Norway (Skilbrei et al., 1991). Frost (1988) suggests a reaction consuming magnetite during prograde metamorphism of mafic rocks. Hence, a metamorphic overprint under amphibolite facies conditions during Caledonian times could have destroyed pre-existing magnetite, especially in volcanic rocks included in the basement.

Finally, the positive magnetic anomalies could be attributed to a post-Caledonian event which only affected the region of thin-skinned Caledonian tectonism. However, there is no surface evidence for such an event, making this interpretation highly unlikely.

Considering the overall magnetic characteristics of the Caledonian fold belt, I tend to prefer the second interpretation involving a pervasive Caledonian reworking of the crystalline core destroying existing ferrimagnetic material, but preserving it in the less affected western area. Similar relations between magnetic Caledonian foreland and non-magnetic Caledonian crystalline units are observed at several localities along the western margin of the Caledonides ((9), (17), (18)). It is unlikely, that a contrast in magnetic properties happened to pre-exist exactly along this boundary.

(9) Dronning Louise Land (Fig. 3.18)

The magnetic anomalies over Dronning Louise Land can be divided in three groups, namely an area of high amplitude and short-wavelength anomalies to the west (9a), a narrow non-magnetic trough (9b) and a moderately magnetic area in eastern Dronning Louise Land (9c).

Geologically, the area is also divided in three structural units (Friderichsen et al., 1990) matching grossly the magnetic provinces: The Western Foreland is largely unaffected by Caledonian events. It consists of Late Archaean to Early Proterozoic orthogneissic basement (Strachan et al., 1994) overlain by the sedimentary Trekant series, which

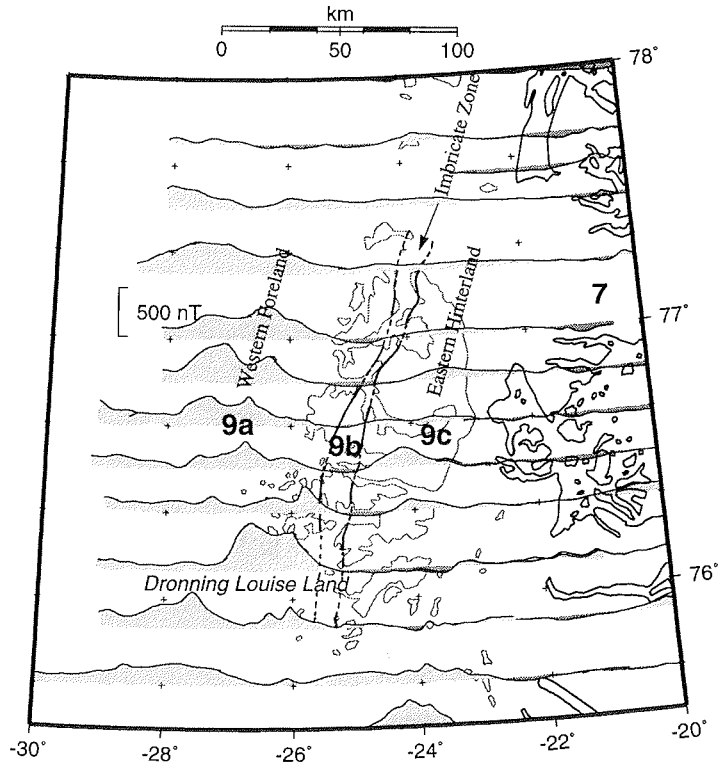

Fig. 3.18: Magnetic anomalies along flight lines over Dronning Louise Land. See Fig. 3.16 for map explanation. Nunataks are outlined by dark grey lines. Scale valid at 77°N.

has been correlated with the IFG to the north. Both are intruded by numerous dolerites comparable to the Midsommersø dolerites. The overlying sedimentary rocks of the Zebra Series are not intruded by the dolerites. Magnetite schists are reported from the basement rocks and magnetite sandstones from the Zebra Series (Friderichsen et al., 1990). However, the volumes seem to be locally insignificant as the area where the latter are described is magnetically quiet.

The magnetic pattern (9a) associated with the Western Foreland closely resembles pattern (5) further north. Accordingly, from the geological and magnetic similarity of these areas, it is inferred that dolerite sills determine the magnetic character.

In north-western Dronning Louise Land, however, the exposed Western Foreland is non-magnetic and the typical positive magnetic anomalies start further west at the edge of the ice cap. Low- to medium-grade Caledonian overprinting was observed in this part of Dronning Louise Land (Henriksen & Higgins, 1976; H.-J. Bengaard, pers. comm., 1997), whereas the south-western part is essentially undisturbed. Frequent low-metamorphic and almost undeformed dolerites (J. D. Friderichsen, pers. comm., 1997) produce the magnetic pattern here. This seems to underline the sensitivity of the magnetic properties of in this case dolerites, to Caledonian metamorphic overprint and yields ad-

ditional support for the above favoured interpretation of anomalies (7) and (8). The positive anomalies cannot be continuously traced northwards to link to the related pattern (8) and (5) (Fig. 3.15). This might be due to a locally less magnetic foreland. On the other hand, the data cover in this area is poor.

In the Imbricate Zone (9b) adjacent to the east, the foreland basement and sedimentary cover sequences suffered Caledonian deformation and NW-ward thrusting accompanied by prograde amphibolite facies metamorphism (Friderichsen et al., 1990), probably destroying the magnetisation of the dolerites. The non-magnetic character of the Imbricate Zone is best observed at the aeromagnetic profile along 76° 30'N where the non-magnetic trough exactly matches the position of the Imbricate Zone. As stated above, the boundary to the positive anomalies deviates to the west into the Western Foreland of north-western Dronning Louise Land delineating the western boundary of Caledonian demagnetisation of the dolerites.

The Eastern Hinterland consists of a high-grade migmatitic basement complex and a medium-grade metasedimentary cover sequence resembling the foreland metasedimentary sequences. Caledonian overprinting has obliterated older structures and only locally a polyphase metamorphic history can be recognized (Friderichsen et al., 1990). Despite the metamorphic overprinting, the area is moderately magnetic, demonstrating that the correlation between magnetic properties and metamorphic grade is intricate. Locally, a correlation between the occurrence of a cover sequence, including magnetite sandstones, and a positive magnetic anomaly can be established (Friderichsen et al., 1990), suggesting that the magnetic sources might be sought in this lithology. However, magnetite-bearing sandstones are also reported from the Imbricate Zone (Friderichsen et al., 1990), where they do not produce anomalies. No information on the volumes and susceptibilities of these rock units exists which could solve this discrepancy.

(10) Payer Land (Fig. 3.15)

North-west Payer Land (74.5°N 24°W) displays a local high amplitude magnetic anomaly attaining more than 750 nT in amplitude. The anomaly has been subject to a detailed aeromagnetic and ground investigation by Larsen (1981). He showed that a high pressure, granulite facies gneiss complex has higher susceptibilities than its amphibolite facies supracrustal surroundings. Larsen (1981) considers the metamorphic development of this area to be due to a single pre-Caledonian event.

The area north-west of anomaly 10 is ice-covered and it is not known whether the same explanation might apply to the positive anomaly north-west of anomaly (10). In addition, no detailed ground studies have been undertaken yet to determine the nature of the positive anomaly to the east of anomaly (10).

(11) Devonian sedimentary basin (Fig. 3.15)

The area (11) shows a slightly increased magnetic field compared to the non-magnetic EBSG and Krummedal (?) supracrustal units exposed in the neighbouring area to the west (Escher & Pulvertaft, 1995). Geologically, the area is characterized by Devonian sedimentary basins. Sporadic volcanism during the sedimentation of the continental basin infill produced some rhyolitic lavas and dolerites (Henriksen & Higgins, 1976). They might be magnetically susceptible and represent the only surface feature which could account for the observed magnetic anomaly.

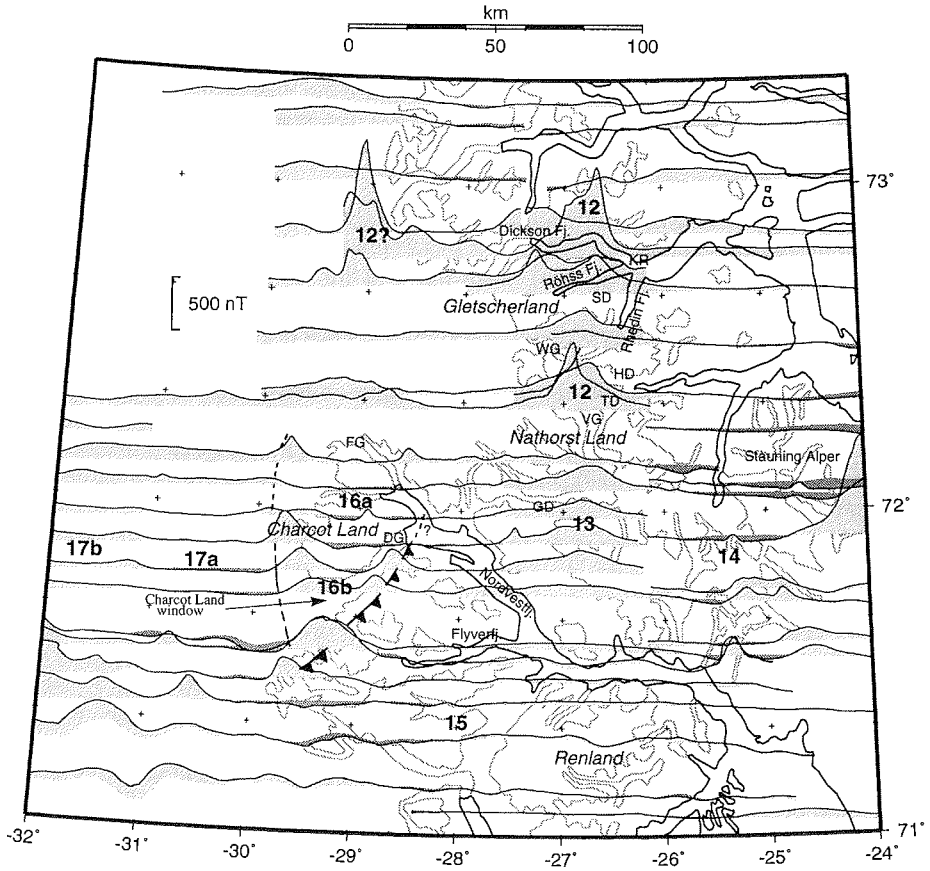

Fig. 3.19: Magnetic anomalies along flight lines over western East Greenland. See Fig. 3.16 for map explanation. Light grey lines delineate borders of ice caps and glaciers. SD: Strømnæsdal; KR: Kap Robert; WG: Wahlenberg Gletscher; VG: Violingletscher; FG: F. Graae Gletscher; DG: Daugaard-Jensen Gletscher; HD: Højdal; TD: Tærskeldal; GD: Grænsedal. Scale valid at 72°N.

(12) Gletscherland complex (Fig. 3.19)

A population of pronounced positive magnetic anomalies (12) is found in the area between Dickson Fjord and the northern part of Violingletscher. It consists of narrow peaks of amplitudes in excess of 850 nT. In addition, broader anomalies are observed. In comparison with the aeromagnetic data of Larsen (1977) between Dickson Fjord and Rhedin Fjord a detailed internal structure became obvious with a series of small anomalies aligned along E-W lineaments. No additional information is available for the anomalies south of Rhedin Fjord. In situ susceptibility measurements have focused on the narrow high amplitude anomalies. In addition, the magnetic properties of basement rocks were studied in Tærskeldal, Strømnæsdal and at Kap Hedlund (chapter 3.2).

A magnetite-bearing granitic gneiss of homogeneously high susceptibility is connected with the high amplitude anomalies at the north side of Röhss Fjord and south of Violingletscher. A similar rock is reported from the south side of Dickson Fjord (Rex & Gledhill, 1981). Simple 2-D forward modelling showed that the amplitude of the magnetic anomalies can be produced by a body of about 1 km length and 300 m thickness. The outcrops were estimated to be of this size. This observation has several geological implications:

The occurrence of these high amplitude anomalies seems to be confined to the Gletscherland infracrustal complex, although its extent towards the south is controversially defined varying between Wahlenberg Gletscher and the north shore of Nordvestfjord (Higgins et al., 1981; Escher & Pulvertaft, 1995; Henriksen & Higgins, 1976). The degree of Caledonian overprint and deformation of the Gletscherland complex is difficult to assess due to the polyphase reworking of the rocks. Haller (1971) attributed the majority of the structures to Caledonian tectonics, whereas Henriksen & Higgins (1976) and Higgins et al. (1981) favour a pre-Caledonian origin. They consider the Late Archaean to Early Proterozoic complex as being largely intact and having experienced only minor Caledonian overprinting. The current re-investigation of the area might shed some light on this question.

In addition, the aeromagnetic data might yield some constraints on the geological evolution of the area. Whereas the Caledonian orogen as a whole appears to be largely devoid of increased concentrations of magnetic minerals, magnetite is present in large quantities in these granitic gneisses. The uniform distribution of magnetite in these rocks at all studied localities suggests that magnetite is a primary ingredient rather than produced locally for example during metamorphism at favourable P-T and compositional conditions. Age determination on this granitic gneiss yielded no conclusive results (Rex & Gledhill, 1981). However, the rock cross-cuts older structures at Violingletscher and at Kap Robert (Rex & Gledhill, 1981), but is itself foliated due to a single metamorphic event, which might be Caledonian or Late Proterozoic (?). Thus, the magnetite must have survived at least Caledonian orogeny, producing the foliation (if not acquired earlier) but retaining the magnetite. Either the special lithology of this rock could preserve magnetite during metamorphism, implying that the occurrence of this rock type is a property of the Gletscherland complex, or metamorphic conditions in Gletscherland must have been such that magnetite was not consumed (e.g. low-grade). A combination of both factors might be most likely.

Susceptibility measurements on the basement rocks of Gletscherland yielded generally non-magnetic gneisses with one exception from Strømnæsdal. This local occurrence of magnetically susceptible rocks might add to the smaller more flat magnetic anomaly south of Röhss Fjord. In Tærskeldal, the sequence of ultramafic bodies contributes at least several tens of nT to the increased level of the magnetic field. However, more of the magnetite-bearing granitic gneiss might be present at depth or concealed beneath icecaps in the area between Violingletscher and Dickson Fjord. A pegmatite dyke of comparable composition with large sheared augen of magnetite exposed in Højdal (Th. Rasmussen, pers. comm., 1997) could be a hint, especially as the aeromagnetic profile ending west of Højdal indicates an increased magnetic field. Finally, metasedimentary rock sequences have not been studied at enough localities to exclude magnetic varieties in this part of Gletscherland.

The narrow high amplitude magnetic anomaly west of the Dickson Fjord area (Fig. 3.19) closely resembles the anomaly over Röhss Fjord which could be attributed to

magnetite-bearing granitic gneisses. The anomaly to the west lies over ice-covered terrain, so no ground control is available to check if the same explanation applies here.

(13) Grænsedal - Jomfrudal metasedimentary sequences (Fig. 3.19)
Flat magnetic anomalies about 40-50 km wide and less than 250 nT in amplitude are centred around 26° 30'W in Nathorst Land. It is uncertain whether this region is part of the Gletscherland infracrustal complex (see above). However, magnetically it can be distinguished from the area immediately to the north by the lack of high amplitude anomalies (12) and from the area to the south by the presence of moderate long-wavelength anomalies (15).

Probable sources might be the metasedimentary sequences encountered frequently in this area as prominent flat lying bands of up to 100 m thickness. Amphibolitic rocks occurring in association with marbles and other metasedimentary rocks exhibit considerable susceptibilities although this is not necessarily the case. An average susceptibility of about $18 \cdot 10^{-3}$ SI units, as measured for the metasedimentary sequence at locality 76 (chapter 3.4) on an extensive 100 m thick band, is sufficient to account for the observed anomalies. The magnetically susceptible rocks from this area show in part a retrograde alteration. The distribution of ferrimagnetic minerals is very heterogeneous suggesting that they might have been produced locally at favourable conditions during retrogression (M. Sergeyev, pers. comm., 1996). Again, this process can be attributed to a combination of favourable lithology and special metamorphic conditions characterizing the region.

(14) Gåsefjord-Stauning Alper migmatite zone (Fig. 3.19)
East of anomaly (13) lies an essentially non-magnetic area. It extends from the Stauning Alper, where the magnetic field has slightly negative values, southwards to Fønfjord (Fig. 3.20). Geologically, the area is dominated by the Gåsefjord-Stauning Alper migmatite and granite zone (Henriksen & Higgins, 1976). Susceptibility measurements were made along the shores of Furesø on migmatized Krummedal metasedimentary rocks (chapter 3.2). They yielded uniformly low susceptibility values of about $0.3 \cdot 10^{-3}$ SI units. At one locality, a porphyritic granite intrusion in the migmatites was studied which could resemble the granite intrusions of the nearby Stauning Alper. It had a susceptibility of only $0.1 \cdot 10^{-3}$ SI units indicating a possible reason for the reduced magnetic field over Stauning Alper compared to the migmatite zone.

(15) Flyverfjord infracrustal complex (Fig. 3.19)
The area between Renland and Charcot Land shows a slightly reduced magnetic field compared to the eastern adjacent province (14) (Fig. 3.15). It belongs to the Vestfjord-Hinks Land gneiss and schist zone (Henriksen & Higgins, 1976). The southern part of this zone is magnetically indistinguishable from (14). It consists of Krummedal metasedimentary rocks folded together with the basement. In the northern part, coinciding with the magnetic low, basement gneisses predominate. They are known as Flyverfjord infracrustal complex and are probably of Archaean age (Henriksen & Higgins, 1976). The transition to the Gletscherland (?) infracrustal complex across Nordvestfjord into Nathorst Land is gradual which is also observed from the slowly northwards increasing magnetic field towards (13).

(16) Charcot Land window (Fig. 3.19)

The Charcot Land window shows a central non-magnetic area (16a) which is surrounded by a ring of moderately positive anomalies (16b) (Fig. 3.19). Detailed susceptibility measurements were undertaken in this area (see chapter 3.2) and suggest a close link between surface geology and aeromagnetic anomalies. The central non-magnetic area (16a) results from the low susceptibilities of the Charcot Land muscovite-granite intrusion and its roof zone where the also predominantly non-magnetic gneisses are invaded by pegmatite dykes. The metasedimentary rocks of the Charcot Land supracrustal series are not associated with magnetic anomalies. This is supported by low susceptibilities. The volume of the strongly magnetic garnet-mica-schist at locality 96 (chapter 3.4) seems to be too small to have any magnetic effect at 3700 m survey altitude.

The ring of positive anomalies (16b) coincides with exposures of weakly metamorphosed basic extrusives and intrusives belonging to the Charcot Land supracrustal sequence (Higgins, 1982). Ground measurements confirmed high susceptibilities for weakly overprinted rocks. However, sheared, foliated and amphibolite facies varieties of these rocks were observed to have lost their ferrimagnetic minerals. This observation yields supporting evidence for the decomposition of magnetite in mafic rocks during prograde metamorphism (Frost, 1988).

The southern, eastern and western boundary of the Charcot Land window is nicely defined by the aeromagnetic data. It coincides with the geological boundary, where it is exposed, for example along the bordering thrust east of Daugaard-Jensen Gletscher. The aeromagnetic data can be used to infer a rough boundary in the ice-covered area to the west. The northern boundary is geologically and magnetically ambiguous due to the higher metamorphic grade of the Charcot Land supracrustals making a distinction from the surrounding Caledonian crystalline complexes difficult. Nordvestfjord and F. Graae Gletscher have previously been assumed to represent the boundary (Higgins, 1982). New field observations, however, suggest a more northern position (J. D. Friderichsen, pers. comm., 1997). The aeromagnetic data tend to yield additional support for this theory, although the nature of the small anomaly east of F. Graae Gletscher is not known.

(17) Caledonian foreland (Fig. 3.19)

West of the Charcot Land window lies a magnetically quiet area (17a) very similar to the Flyverfjord area (15). A single nunatak was visited and low susceptibilities were measured on a Krummedal metasedimentary rock. From the magnetic properties and geological arguments this largely ice-covered region is inferred to belong to the Vestfjord-Hinks Land gneiss and schist zone. Between about 72°N and 71° 30'N, a distinct magnetic boundary delineates the western margin of this zone. Short-wavelength positive anomalies (17b) dominate the magnetic signature of the area to the west. I suggest that this change in magnetic pattern might mark the border to the Caledonian foreland and hence might define the otherwise unknown westward extent of the Caledonian fold belt in this area. Similar magnetic relations between Caledonian orogen and the undisturbed foreland have been observed further north in Dronning Louise Land and Kronprins Christian Land. In addition, the occurrence of tectonic windows (Charcot Land and Paul Stern Land), exposing autochthonous or para-autochthonous foreland beneath Caledonian thrusts (Henriksen & Higgins, 1976), could be regarded as a hint to shallow Caledonian structures which probably fade out towards the west. One could speculate that the magnetic character of the inferred Caledonian foreland

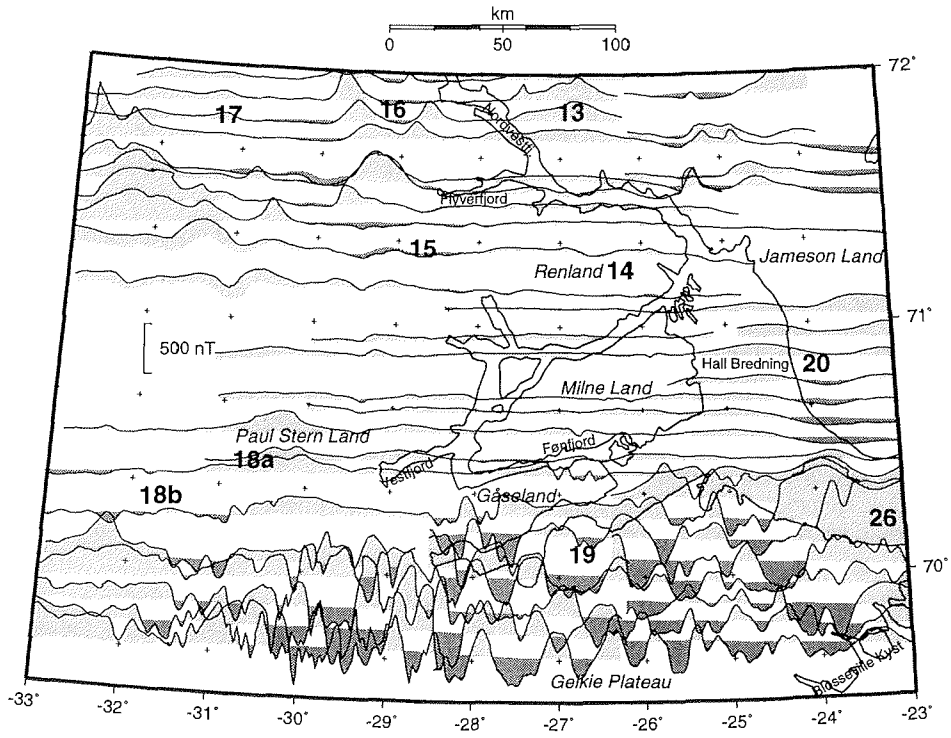

Fig. 3.20: Magnetic anomalies along flight lines over the Scoresby Sund area. See Fig. 3.16 for map explanation. Scale valid at 71°N.

stems from basic intrusives and extrusives as seen in the Charcot Land foreland window. However, due to the ice-cover the nature of the foreland remains unknown. Further north and south, there is no magnetic contrast which could give further evidence on the position of the boundary to the foreland.

(18) Paul Stern Land (Fig. 3.20)

Another tectonic window, the Gåseland window, exposes Caledonian foreland in westernmost Gåseland and Paul Stern Land (Fig. 3.20). The window shows basement rocks in amphibolite facies and a supracrustal metasedimentary sequence (Henriksen & Higgins, 1976). As this lithology is in terms of magnetic properties rather similar to the adjacent Vestfjord - Hinks Land gneiss and schist zone, no pronounced magnetic contrast can be expected. However, a slight increase in the magnetic field (18a) is observed in this area which could be attributed to the foreland window.

West of this moderately positive anomaly, especially in the southern part, there are weakly negative anomalies of very short wavelengths (18b). They seem to be a low amplitude equivalent of the anomaly over the Geikie Plateau (19) and might indicate minor occurrences of flood basalts at the westernmost margin of the Geikie Plateau flood basalt province described below.

3.3.3 Tertiary volcanism

The south-eastern part of the aeromagnetic anomaly map is dominated by magnetic anomalies produced during the episodes of rifting and hotspot related volcanism which started about 64 Ma ago and lasted until about 30 Ma. The volcanic province has been subject to a variety of petrological and geophysical studies and a wealth of information exists complementing the aeromagnetic data and facilitating the interpretation.

(19) Geikie Plateau flood basalts (Fig. 3.20)
The most striking feature of the southern part of the magnetic anomaly map is the quickly and strongly varying magnetic field over the Geikie Plateau (19).

The area is made up by a pile of flood basalts which extruded subaerially in 3 episodes during magnetic chron 26R, 25R or 24R (Saunders et al., 1997). The flood basalts attain a thickness of about 2000 m along the Blosseville Kyst and about 300-500 m inland on Gåseland and Milne Land. The lavas are tholeiitic basalts. Apart from the last episode, which is represented only locally at Kap Brewster by the Igtertivâ Formation, all the basalts carry a reversed remanent magnetisation (Larsen & Watt, 1985). Topographically, the Geikie Plateau consists of plateau-like ice-covered mountains which are deeply incised by numerous valleys. The combined effect of topography and the reversed magnetisation of the basalts produces the characteristic magnetic signature (19).

To the west of the Geikie Plateau beneath the inland ice is an area of strong positive anomalies. The short-wavelength character indicates a shallow source. It is not known whether this anomaly is related to Tertiary volcanism or might be an expression of the Caledonian foreland which could be expected in this area.

(20) Jameson Land basin (Fig. 3.20)
Jameson Land and the adjacent Hall Bredning are marked by broad smooth magnetic anomalies of both weakly positive and negative amplitudes (Fig. 3.15).

Jameson Land hosts a deep Mesozoic sedimentary basin which is heavily intruded by Tertiary dykes and sills. The dykes are generally of metre size whereas sills attain thicknesses of several tens of metres. Seismic reflection data show evidence for sills at several levels deeper in the sedimentary basin (Larsen & Marcussen, 1992). The origin of the intrusions has been related to the volcanic event producing the flood basalts of Geikie plateau. The intrusives seem to carry a remanent magnetisation of reversed polarity. However, this remanence is largely balanced by an induced magnetisation (Larsen & Marcussen, 1992), such that the net effect might be close to zero. Both the magnetic properties and the limited volume of the intrusives may be responsible for the low amplitude of the magnetic anomalies over Jameson Land and the Hall Bredning. At 3700 m survey altitude, the dykes and sills cannot be resolved and in combination with deep seated sills smooth and broad anomalies are caused. The existence of both positive and negative anomalies might reflect varying Q ratios (ratio between remanent and induced magnetisation), however, varying amounts of intrusives or possibly existing normal polarities could produce the same effect.

(21) Northern flood basalt province (Fig. 3.21)
A pronounced negative magnetic anomaly extends from Kong Oscar Fjord across Traill Ø north-north-eastwards to south of Shannon.

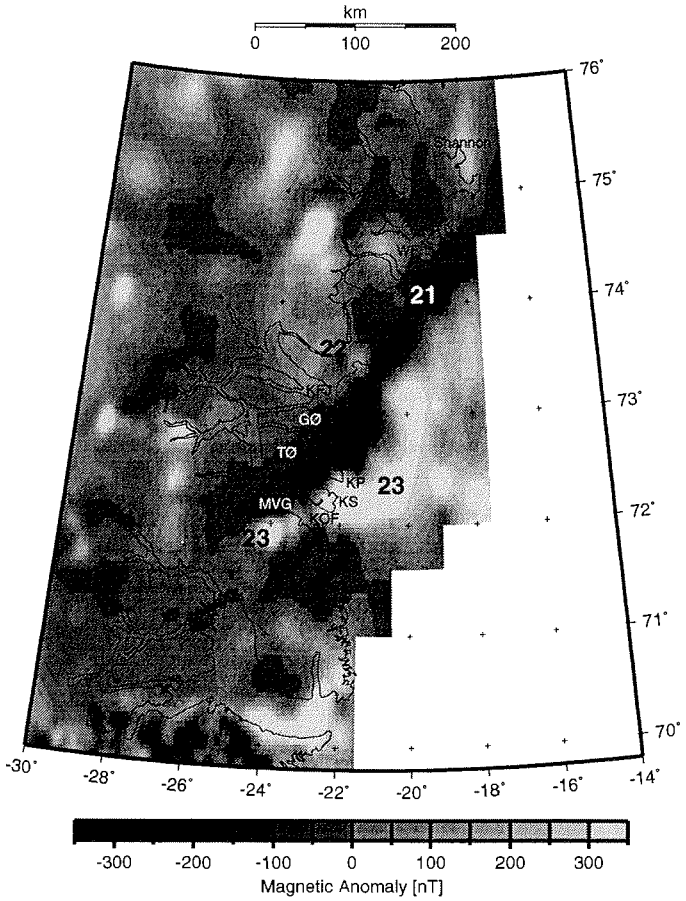

Fig. 3.21: Magnetic anomalies caused by Tertiary volcanism. WF: Wollaston Forland, KFJ: Kejser Franz Joseph Fjord, GØ: Geographical Society Ø, TØ: Traill Ø, KP: Kap Parry, KS: Kap Simpson, KOF: Kong Oscar Fjord, MVG: Mestersvig. Scale valid at 72°N.

Geologically, it comprises the area of the Mesozoic sedimentary basins exposed along the coast from Traill Ø to Wollaston Forland (Fig. 3.21). In addition, north of Kejser Franz Joseph Fjord, the sedimentary units are partly covered by scattered outcrops of tholeiitic basalts, which attain a maximum thickness of about 800 m (Upton et al., 1995). Two volcanic episodes have been defined, and both took place during a period of reversed polarity of the Earth's magnetic field. However, the latest stages of the second episode may have witnessed a polarity change (Upton et al.,1980; Watt, 1994). An age between 60 Ma and 55 Ma is proposed for the eruption of the northern flood basalts. They have been tentatively correlated chronologically with the second phase of volcanism on Geikie Plateau (Larsen & Watt, 1985). The magnetic properties of the northern flood basalts have been studied by Abrahamsen & Nordgerd (1994). They determined an average susceptibility of $10 \cdot 10^{-3}$ SI units and an average Q ratio of 2.8.

As all their samples carried a reversed polarity remanence, the net magnetisation is somewhat less than the remanence.

Upton et al. (1995) argue that the source of the northern basalts must have lain further east and that the outcrops along the coast represent the westernmost manifestation of this volcanic event. The presence of reversely magnetized basalts along the coast and presumably also offshore could therefore explain the magnetic anomaly. However, no outcrops of basalts are found to account for the southern part of the anomaly where it crosses the Mesozoic sedimentary basins of Traill Ø and Geographical Society Ø. The basins are intruded by dykes and sills with a maximum combined thickness of 300 m. Both normal and reversed polarities of magnetisation have been measured (Hald, 1996). The intrusives are related to the sills and dykes of the Scoresby Sund area, although a closer relationship seems to exist to the northern flood basalts. Their magnetic properties and the comparison with the heavily intruded but non-magnetic Jameson Land basin suggests that the intrusives are probably not responsible for the pronounced negative anomaly over Traill Ø and Geographical Society Ø. I therefore conclude, that the negative magnetic anomaly (21) as a whole must have an additional source which is not exposed.

The seismic refraction studies (chapter 4) have revealed the existence of a seismic high velocity layer in the lower crust between about 16 km and 22 km depth. The occurrence of this high velocity layer is correlated with the negative magnetic anomaly. I propose a magmatic origin for the high velocity layer. Forward modelling shows that the magnetic anomaly can be produced if the magmatic underplate carries a magnetisation of reversed polarity.

(22) Myggbukta complex (Fig. 3.15, Fig. 3.21)

A small positive magnetic anomaly at the western margin of the negative anomaly (21) coincides with the so-called Myggbukta complex (Upton et al. 1980, 1995). The Myggbukta complex represents a volcanic centre whose origin has been related to the northern flood basalts. Upton et al. (1995) consider it to be a very late termination of the basaltic volcanism in this area, postdating its onset by about 25 Ma. From the positive magnetic anomaly it can be inferred that the magma extruded either during a normal polarity epoch of the Earth's magnetic field or at least that no significant reversed remanence was acquired.

(23) Late alkaline magmatism (Fig. 3.15, Fig. 3.21)

Large positive magnetic anomalies are situated SW of Mestersvig and on Kap Simpson and Kap Parry from where they seem to extend eastwards onto the shelf (Fig. 3.21). A few additional centres are apparent north of this region forming the eastern boundary of anomaly (21).

Tertiary alkaline magmatic complexes are described from all these localities (Nielsen, 1987) and are inferred to be present offshore as well (Larsen, 1990). An age of about 30 Ma was determined for the volcanic and intrusive centres SW of Mestersvig whereas the magmatic complexes on Traill Ø seem to be about 38 Ma old. Off the coast of Traill Ø, the east-trending continuation of the magnetic anomaly has been interpreted to be due to contemporaneous magmatism concentrating along the Jan Mayen Fracture Zone (Larsen, 1990).

(24) Flank volcanism (Fig. 3.15)
A population of local positive magnetic anomalies occurs at the western nunataks at about 74°N 29°W and the adjacent ice-covered region. From the locality of the middle one of the three marked anomalies in Fig. 3.15, exposures of Tertiary alkaline mafic lavas are reported (Brooks et al., 1979). Upton et al. (1984) present a model for the genesis of these volcanics. They interpret them as due to flank volcanism related to the emplacement of the northern Tertiary flood basalts. In the same region as the Tertiary volcanics, Katz (1952) recorded slightly metamorphosed volcanic rocks of Upper Proterozoic age.

The similarity of the other two magnetic anomalies in this area invites to speculate on a similar Tertiary volcanic origin. The southern of the three anomalies lies close to newly discovered areas of Tertiary basalts which cap the highest summits of the nunataks and are up to 50 m thick (A. K. Higgins, pers. comm., 1997), but the anomaly extends beyond the present area of outcrop of the basalts.

Another manifestation of Tertiary flank magmatism in the western part of the Caledonian fold belt are the doleritic dykes in Charcot Land (see chapter 3.4). Although magnetically susceptible, they are too few to leave traces on the magnetic anomaly map.

3.3.4 Unexplained anomalies

(25) Store Koldewey anomaly (Fig. 3.15)
A marked positive magnetic anomaly characterizes the coastal range between 75°N and 78°N. The anomaly trends roughly N-S parallel to the Store Koldewey Island (76.5°N 18°W) and varies along strike in width and amplitude.

The continental shelf in this area broadens offshore north of 75°N. Larsen (1990) interpreted the magnetic anomaly as a basement high in a series of horst- and graben-like coast parallel structures which probably evolved contemporaneously with the Palaeozoic to Mesozoic sedimentary basins further south. Indications for comparable basins are found in places onshore. However, the geology onshore is dominated by Caledonian crystalline rocks. Eclogite occurrences north of Danmarkshavn suggest an intensive involvement of the crust in Caledonian orogeny (Gilotti, 1993,1994). Therefore, I would expect the crust in this area to be demagnetized during Caledonian metamorphism. Horst-graben structures in a non-magnetic basement cannot produce a pronounced magnetic anomaly such as (25). Hence, the interpretation requires the introduction of magnetic minerals to the crust at a later stage, preferably during the tectonic regime, which formed the horst-graben structures. However, none of the basement areas further south shows a comparable magnetic signature.

(26) Mouth of Scoresby Sund (Fig. 3.15, Fig. 3.20)
A T-shaped positive magnetic anomaly is situated in the mouth of Scoresby Sund. Whereas the E-W branch of the anomaly follows the coast of Geikie Plateau, the NE-SW trend parallels the Blosseville Kyst and anomaly (21). It continues into Liverpool Land.

The origin of this anomaly remains enigmatic. Surface geology yields no obvious explanation. The position of the E-W anomaly along the coast of Geikie Plateau and its positive polarity suggest an edge effect as possible explanation. Although Fig. 3.20

clearly shows a very steep gradient in the magnetic field over the edge of Geikie Plateau, the broad, smooth part of the anomaly over the Scoresby Sund must have a different source. Another hypothesis could attribute the anomaly to Quaternary debris of the flood basalts which accumulated off the shores of Geikie Plateau. Such debris would be unsorted and any remanent magnetisation would be compensated, leaving only an induced magnetisation which necessarily results in a positive anomaly. However, this interpretation implies that the debris has not been eroded by advancing glaciers during the last glaciation. This is in contrast to the findings of Uenzelmann-Neben et al. (1991) who from seismic reflection measurements could show that only a very thin cover of young deposits remains in the Scoresby Sund. In addition, one would expect a similar magnetic signature off the mouth of Scoresby Sund where a fan of sediments has been deposited.

The NE-SW part of the anomaly reflects the trend of the Tertiary break-up tectonics. A dense swarm of feeder dykes intruded the Blosseville Kyst during anomaly 24n times, contemporaneously with the extrusion of the Igtertivâ Formation which carries a normal polarity remanence (Larsen & Watt, 1985). Exposures of the dyke swarm occur around 69°N along the coast. They might not be reflected in the magnetic field as the reversely magnetized flood basalts dominate the outcrops. In contrast, north of Kap Brewster, where the basalts are absent, the dyke swarm might contribute to the magnetic field. However, no surface exposures of the dyke swarm are seen here. In addition, the sills and dykes in the Mesozoic basins failed to produce any significant magnetic anomaly. Hence, a considerable volume of intrusives would have to be postulated in order to explain the magnetic anomaly in the mouth of Scoresby Sund.

4 Seismic and potential field study of East Greenland

4.1 Gravity data

4.1.1 Gravity data base

Land and marine gravity data covering East Greenland were provided by the KMS. The KMS continuously improves the coverage of East Greenland with gravity data on land (Forsberg & Keller, 1997). This study uses the KMS gravity data in processed form as available in May 1997 (Forsberg (1986), Forsberg (1991), Forsberg & Keller (1997)).

From this data base, only gravity stations with information on elevation or water depth, respectively, were selected. Gravity stations on the ice cap generally lack reliable estimates of the ice thickness and were therefore not included. In addition, marine gravity data from three cruises of RV Polarstern were incorporated. The data were processed and checked for consistency with the KMS data by Mandler (1995). Fig. 4.1 shows the distribution of the gravity data.

4.1.2 Accuracy of the gravity data

The determination of land gravity station elevation was undertaken using differential GPS with a resulting accuracy of about 2 m (Forsberg & Keller, 1997). For the older gravity data, elevation was measured with precision altimeters. An estimated accuracy of 5-10 m was achieved, except for stations close to sea level, where the elevation could be estimated within 1 m (Forsberg, 1986). Gravity was measured with Lacoste Romberg instruments. The data were calibrated, corrected for drift and Earth's tides and tied to reference gravity values. The resulting error of a single gravity reading is about 0.05 mgal ($0.05 \cdot 10^{-5}$ m/s^2) (Forsberg & Keller, 1997).

Free-air anomalies were calculated by subtracting the normal gravity according to the GRS80 system (e.g. Torge, 1989). A Bouguer reduction was then performed with a reduction density of $2.67 \cdot 10^3$ kg/m^3 (Forsberg, 1991). An error in the determination of heights of 10 m consequently results in errors of 3 mgal and 2 mgal for the free-air and Bouguer anomalies, respectively. As terrain corrections exist only for about half of the gravity stations (Forsberg & Keller, 1997), the effect of the terrain was not accounted for in this study. The rugged topography of the survey area can produce terrain effects as large as 30-40 mgal. The lacking terrain correction generally yields too low Bouguer values, in particular at elevated locations or close to cliffs (Forsberg, 1991).

Compared to the errors inherent in the gravity readings and the height determination, the error due to the terrain effect is one order of magnitude larger and limits the accuracy of the resulting Bouguer anomaly map. No information is available on the error in water depth and hence the marine gravity data. However, in fjords with marine data adjacent to land gravity data at sea level, the gravity values fit within the range of typical terrain effects.

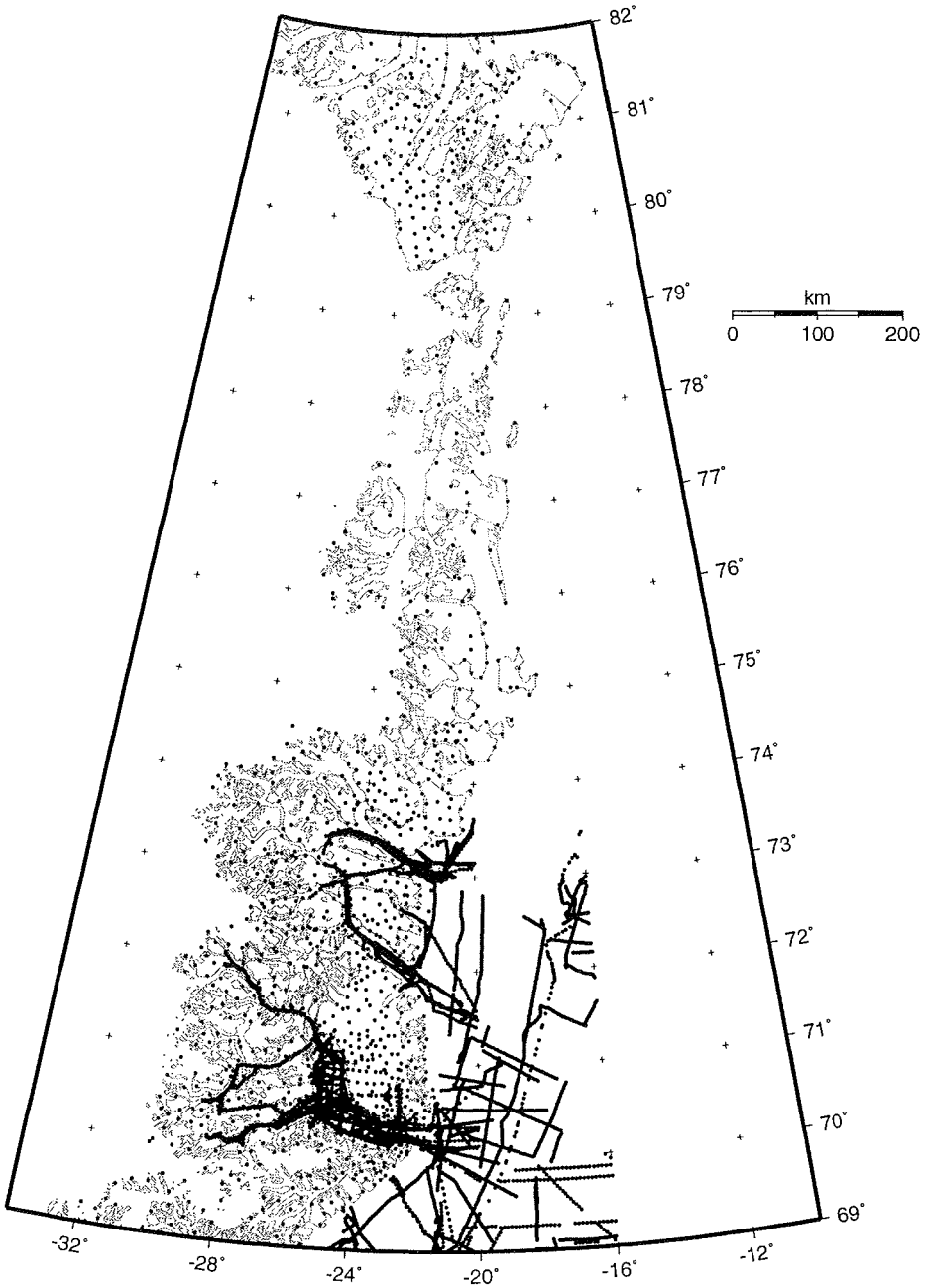

Fig. 4.1: Distribution of gravity data used for the compilation of the Bouguer anomaly map in Fig. 4.2. Scale valid at 75°N.

Fig. 4.2 (overleaf): Bouguer anomaly map of East Greenland. Contour interval 20 mgal. Scale valid at 75°N.

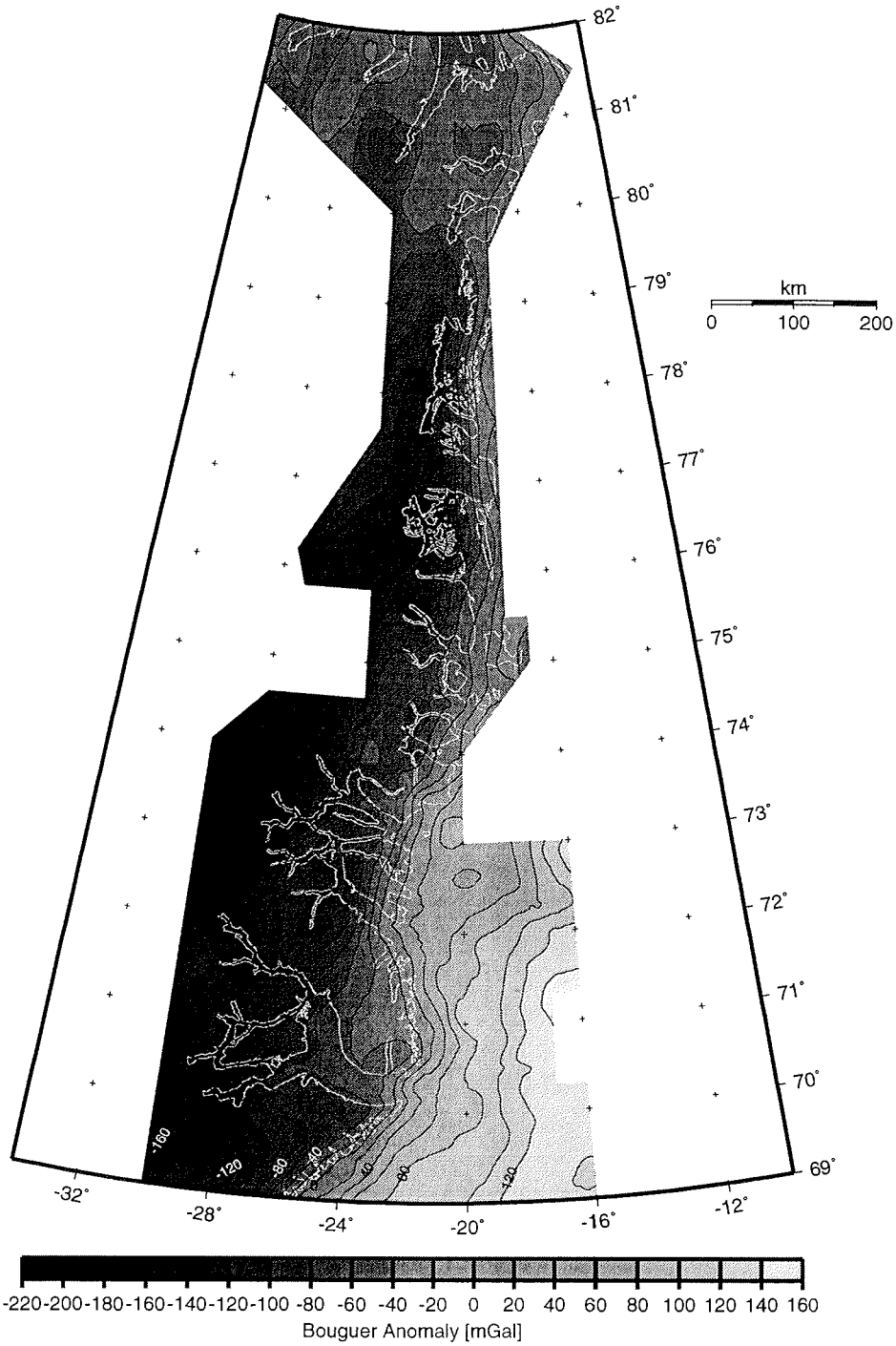
82°
81°
80°
79°
78°
77°
76°
75°
74°
73°
72°
71°
70°
69°
km
0 100 200
-32°
-28°
-24°
-20°
-16°
-12°
-220-200-180-160-140-120-100 -80 -60 -40 -20 0 20 40 60 80 100 120 140 160
Bouguer Anomaly [mGal]

4.1.3 Bouguer anomaly map

The spacing between the gravity data strongly varies in the study area. Whereas gravity measurements in the fjord region and in the Scoresby Sund area are typically 15 km apart, a spacing of about 30 km characterizes the data set between 75°N and 79°N. In contrast, the shipborne data are densely spaced along the shiptracks. They were resampled to one value per 2 km. For map display, the Bouguer gravity data were gridded in the same way as the magnetic data (chapter 3.1.3). A grid cell size of 0.1° longitude and 0.05° latitude was chosen equalling a cell size of about 3 km x 5.5 km at latitude 75°N. The grid was filtered in the space domain with a cosine-type filter of 20 km width (Wessel & Smith, 1995) in order to produce smooth contour lines.

The resulting Bouguer anomaly map is shown in Fig. 4.2. Contour intervals and grey levels of 20 mgal seemed appropriate with respect to the accuracy of the gravity data

4.1.4 Key results

A Bouguer anomaly map was compiled from the gravity data set of the KMS. A terrain correction could not be applied, resulting in a maximum error of the order of 30-40 mgal. However, the Bouguer anomalies span a range of +160 mgal to -220 mgal, which is one order of magnitude larger than the maximum errors. Therefore the regional features of the Bouguer anomaly map can be considered as geologically significant.

The northern part of the survey area north of about 80°N shows an essentially flat Bouguer anomaly. South of 80°N, the Bouguer anomaly map is dominated by a pronounced coast-parallel gradient. Gravity decreases from the coast westwards underneath the Caledonian mountain belt. At about 75°N, this gradient splits up into two branches.

The eastern branch follows the coast southwards. It abruptly changes its direction at about 72°N. Between 72°N and 70°N, the coastal gradient is less pronounced, south of 70°N, however, it even steepens. The western branch of the gradient is seen further inland. It is particularly prominent at about 73°N where it crosses the heads of the large fjords of the fjord region. West of this gradient, the minimum of the Bouguer anomalies is reached in the area of the highest peaks of the Caledonides. The two distinct gradients of the Bouguer gravity in the fjord region of East Greenland are separated by a plateau which is clearly visible around 73°N 25°W. A local minimum is seen at 72°N 25°W at the head of the roughly north-south trending Alpefjord. This minimum coincides with the granite complex of Stauning Alper.

4.2 Seismic refraction data

4.2.1 Data acquisition

During the cruise Arktis X/2 of RV Polarstern in summer 1994, eight seismic refraction profiles were shot in East Greenland. Three profiles extended former wide-angle profiles in the Scoresby Sund area which were acquired during Arktis VII/3 in 1990 (Jokat et al., 1996; Jokat et al., 1995). Only one of the latter profiles was used in this study, which focuses on the seismic refraction data acquired in the large fjords between 72°N and 74°N (Fig. 4.3).

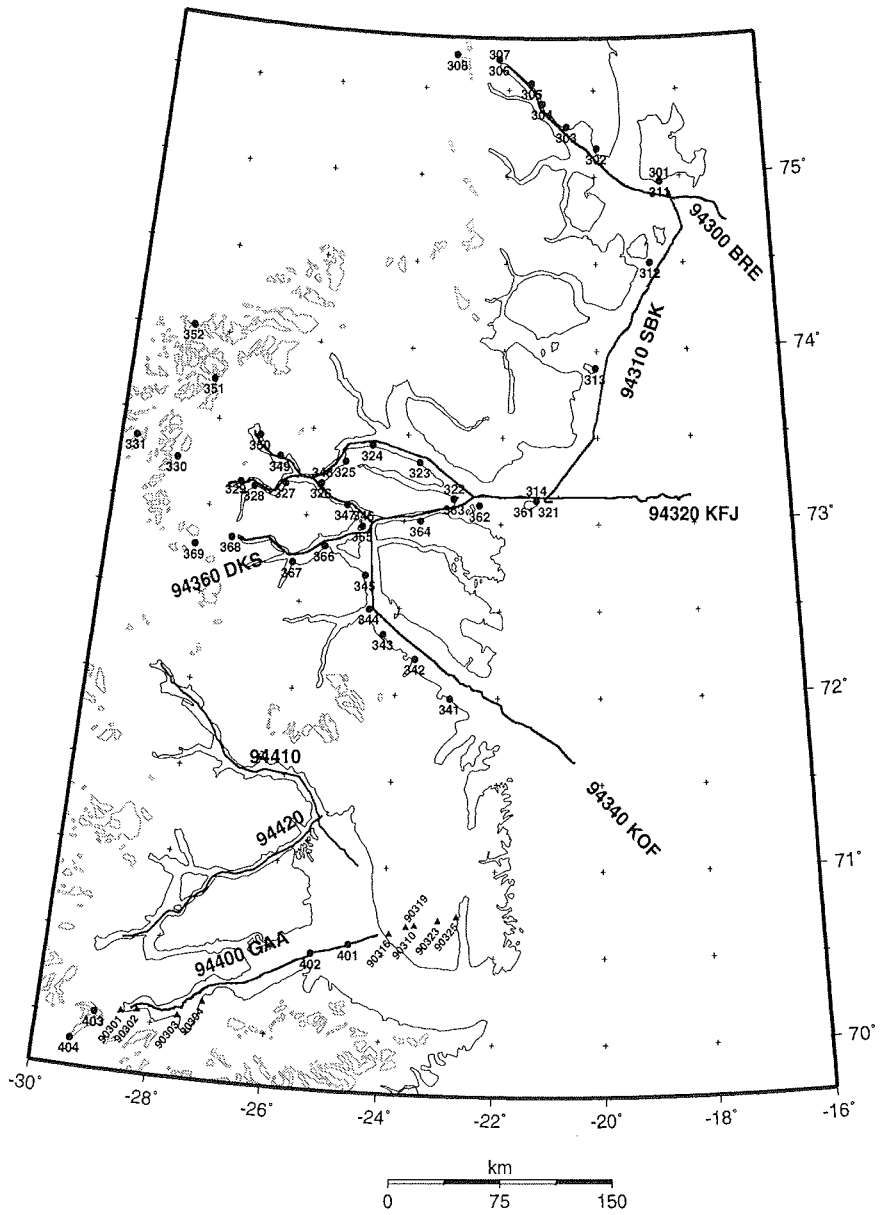

Fig. 4.3: Location of seismic refraction profiles in East Greenland. Grey lines outline nunataks. The solid lines show the airgun shots, the dots represent receiver locations. The profile numbers and names are indicated. The receivers are numbered accordingly, e.g. receivers 341-352 recorded profile 94340. Profiles 94410 and 94420 are not used in this study. Triangles mark receivers used on profile GAA in 1990. BRE: Bredefjord; SBK: Shannon-Bontekoe Ø; KFJ: Kejser Franz Joseph Fjord; KOF: Kong Oscar Fjord; DKS: Dickson Fjord; GAA: Gåsefjord. Scale valid at 73°N.

The seismic survey was designed as a combined land-sea seismic experiment (Jokat et al., 1995). Seismic energy was generated by two 32 l Bolt airguns towed behind RV Polarstern. Shots were fired every 60 s at a cruising speed of 5 kts, resulting in an average shot spacing of about 150 m. Generally, the profiles were shot starting at the head of the fjords, following the fjord eastward until sea-ice in the East Greenland current offshore prevented further progress (Fig. 4.3). As the experiment depends on the fjords as natural sea-ways through the survey area, no straight line profile geometry is possible.

The seismic signals were recorded on land by up to 11 receivers. For details on recording parameters and instrumentation see Appendix 2 and Jokat et al. (1995). The recording equipment was deployed on land at appropriate locations (Fig. 4.3; Appendix 2). Seismic stations on nunataks form the western end of the profiles. Along the fjords, reasonably flat outcrops of bedrock were sought for seismometer sites. These points are often marked by anomalous geology. For example, station 306 is situated on a flat exposure of a granite intrusion surrounded by steep walls made up of Proterozoic sedimentary rocks. Due to the difficult terrain conditions this complication could not be avoided.

All positions were determined by GPS. GPS and DCF signals served as time reference. The water depth in the fjords was measured with the HYDROSWEEP system of RV Polarstern (Monk et al., 1995).

4.2.2 Data processing

The seismic data were available in demultiplexed form. They are sorted station-wise such that each seismic trace represents one shot recorded by a specific receiver. The seismic sections are also organized in this way. In order to avoid introducing artefacts, the further processing was reduced to a minimum and results were carefully checked against the raw data.

Standard processing

- **Editing**
  In one Reftek data logger, named AWI01, the internal quartz clock worked inaccurately. If no GPS time signal was received, discrepancies in time between the internal and external clock built up. The Reftek corrected the error by adjusting the internal clock as soon as it received the GPS time signal again. For example, at station 323, AWI01 did not receive a GPS signal for a period of 57 h and a time difference of 650 ms accumulated, corresponding to an average drift rate of the internal clock of 0.2 ms/min.

  This timing error was corrected for assuming a constant drift rate. It is not possible to check for the validity of this assumption. However, comparable average drift rates were observed while AWI01 was deployed at stations 314 and 349, supporting to some extent this correction. All recordings of AWI01 were checked for the occurrence of timing errors and corrected if necessary.

  The seismic signals recorded at stations 304, 307, 313, 341, 352, 402 and 403 could not be used for the interpretation. The pre-amplification of the data-logger was too low at stations 304, 307 and 313. Station 341 suffered from malfunction of the geophone, whereas noise obscured all arrivals at station 352. Severe discontinuities in time prevented demultiplexing of station 403. The ocean bottom hydrophone at sta-

tion 402 shows a conspicuous offset of the travel time curves by 500 ms towards later arrival times which could not be explained. No attempt was made to recover these recordings.

- **Stacking**
  For an improvement of the signal to noise ratio, the data of several channels at each site were stacked. Only data from vertical component receivers were used. Channels with a considerably higher noise level than the other channels at a station were not included.

  The geophones were distributed over an area of typically 500 m $\times$ 200 m. For constructive interference of two seismic waves arriving at two receivers, the distance between the receivers must be less than $\lambda_a/2$, λ_a being the apparent wavelength of the incident seismic waves. A seismic wave travelling at 6 km/s with a typical frequency of 6 Hz (see below) has a wavelength λ of 1 km. At an incident angle α of typically 45° or less, $\lambda_a = \lambda/\sin\alpha$ is larger than 1.4 km. Hence, the maximum dimension of the array of receivers is considerably smaller than $\lambda_a/2$, justifying a simple summing up of the seismic channels.

- **Plotting**
  Prior to plotting a band-pass filter was applied to suppress high frequency noise. Fechner (1994) studied amplitude spectra of the seismic signals produced by the Bolt airguns and recorded by several types of receivers. The signal energy concentrated always between 4 Hz and 10 Hz with a maximum between 6 Hz and 7 Hz. A band-pass filter passing frequencies from 3 Hz to 17 Hz was applied to the data.

  For plotting, the signals were scaled by automatic gain control within a window of 2000 ms. A reduced travel time versus offset display was chosen with a reduction velocity of 8 km/s enhancing Pn phases as horizontal travel time curves.

Special processing

- **Correction for water depth**
  For determining apparent seismic velocities and intercept times from the seismic sections, it was convenient to remove the water column by calculation. The fjords have a pronounced bottom topography with water depth varying from about 900 m to 100 m. These differences can considerably distort the slope of the travel time curves and lead to errors in the estimation of apparent seismic velocities.

- **Removal of "time signals"**
  Seismic data recorded by 6 of the Refteks and to a lesser extent by the PCMs suffered from cross-talk of the time signal channel. At intervals of 1 s, a signal with strong amplitude is visible on each trace. The waveform of this time signal is variable from station to station and with time. The amplitude of the time signals can exceed the amplitude of the seismic arrivals. All channels were affected.

  The time signal could be suppressed by a combination of predictive deconvolution and a frequency-wave number filter. The predictive deconvolution (Yilmaz, 1987) with an operator length of 1 s and a prediction lag of 840 ms reduced the amplitude of all time signals following the first signal on each trace. Subsequent f-k-filtering uses the fact that the time signal "travels" with infinite velocity across the seismic section, as the time signal appears for each offset at the same time. In the f-k domain the time signal plots along the $k = 0$ axis. A seismic signal travelling at 6 km/s with a typical signal frequency of 6 Hz plots in the f-k domain at $f = 6$ Hz, $k = 1$ km^{-1}. The

f-k filter was designed to suppress wave numbers smaller than 0.45 km^{-1}. The efficiency of this processing scheme was increased if it was preceded by amplitude scaling with an AGC of 2000 ms window length.

The time signal can be successfully removed by this method. It was applied to all disturbed seismic sections. However, only in one case, could a Pn arrival be identified which was previously concealed by the time signal. As this processing method also affects the seismic signals and distorts the waveforms, the arrivals were generally picked from the standard seismic sections. However, the corrected sections helped to correlate the phases.

- **Reverberations**
  Generation of seismic energy by airguns in water often results in seismic signals accompanied by a wave train of reverberations. These reverberations may conceal later arrivals. If strong reverberations were present, a predictive deconvolution with a prediction lag of 100 ms and an operator length of 800 ms, as tested for this purpose by Mandler (1995), was applied. However, no additional later arrivals were detected.

Phase picking

This study uses first and later P-wave arrivals. The P-waves comprise refracted waves through the upper crust (Pg), the lower crust (Pc) and the uppermost mantle (Pn), and reflected arrivals from upper (PcP1) and lower (PcP2) crustal reflectors and the Moho (PmP). S-waves were not studied.

P-wave arrivals were picked from seismic sections at intervals of 1-2 km after standard processing. An error was assigned to each pick, depending on the noise level and the reliability of the phase identification. For example, Pn phases often consisted of an easy-to-correlate relatively strong arrival which was at some places preceded by a weak but clearly visible phase. Hence, the first arrival of the Pn wave may well be earlier than the correlated arrival and an error large enough to include the earlier phase was assigned to the picks (typically ± 150 ms to ± 250 ms). In some seismic sections, reflected arrivals or Pn phases only appeared as a distinct band of seismic energy but no arrivals could be correlated. The main energy was picked with an error including the width of the whole band (± 300 ms to ± 500 ms). However, these picks were only later incorporated in the models and did not constrain the modelling. The majority of the arrivals, in particular the Pg arrivals, were well determined and the error reflects the noise level, which increases with increasing offset. Typical errors ranged from ± 25 ms to ± 150 ms.

In addition, apparent seismic velocities were calculated from the slope of the travel time curves in seismic sections which had been corrected for water depth. Simple estimates of the depth to seismic interfaces were made using intercept times, crossover distances of Pn or wide-angle reflections (Gebrande & Miller, 1985). All these methods assume a homogeneous, horizontally layered subsurface.

The velocity and depth information helped to identify the nature of the phases and their provenance. All picks were classified accordingly. If the character of a phase remained unclear, the picks were marked as unidentified.

Amplitudes

The amplitudes of the seismic waves were only qualitatively incorporated in the models. The large amplitudes of the time signal which affects the majority of the recordings dominate true amplitude plots of the seismic sections such that a visual

comparison with synthetic data is not possible. However, removing the time signal by the method described above affects the amplitudes of the seismic signal. Picking amplitudes and comparing observed and synthetic amplitudes versus offset curves (e.g. Zelt & Forsyth, 1994) encounters the same difficulties. In addition, small-scale heterogeneities in the upper crust as well as the inherent 3-D effects make a quantitative amplitude modelling fraught with uncertainties.

Instead, the relative amplitudes of subsequent arrivals were analysed. AGC windows of 5000 ms were then used for plotting. Especially the amplitudes of reflected arrivals helped to constrain the impedance contrast across the reflector. For example, the amplitudes of the PcP2 reflection at station 361 (Fig. 4.12) are considerably larger than the amplitude of the preceding PcP1 and Pg phases. Accordingly, a larger velocity contrast was attributed to the PcP2 reflector (0.6 km/s) than to the PcP1 reflector (0.2 km/s).

4.2.3 Method of seismic modelling

The experimental design of the seismic survey makes several processing steps necessary before ray tracing methods can be used to derive a model for the P-wave velocity structure of the crust. This processing accounts for the curved geometry of the profiles and the combined land-sea seismic technique with receivers onshore and airgun shots just below the sea surface.

- **Profile projection into a plane**
  Prior to modelling a 2-D approximation had to be made to the 3-D problem. A straight line was fitted through the curved line of the shots applying a least-squares-algorithm (Wessel & Smith, 1995). The receiver locations were then projected into this plane. However, the true shot-receiver distances, i.e. the offsets of the observed P-wave arrivals, remained unchanged. Fig. 4.4 shows the projected profiles and receivers.

  For a laterally inhomogeneous sub-surface, this 2-D approximation involves errors. Due to the curved geometry of the profile, the seismic rays do not travel in a single plane. For example, seismic waves from a shot close to station 321 to receiver 324 pass through a different area than to receiver 326 (Fig. 4.3). Although these seismic waves contain information on the velocity structure along different paths, they need to be modelled in a 2-D approximation as travelling through the same crustal block. Hence, the 2-D model is laterally averaged.

  In addition, an averaging along the profile direction takes place. This is most obvious from the N-S trending part of profile KOF between receivers 346 and 344 (Fig. 4.3), which are 53 km apart. However, in the 2-D model (Fig. 4.4), their distance is 42 km. As the true shot-receiver distances remain unchanged, a ray which travels between receivers 346 and 344 arrives in the 2-D model 11 km east of the projected receiver 344. There, the upper crustal structure might be different and should be defined, for example, by rays travelling between stations 343 and 344 rather than by rays travelling between 346 and 344. Hence, the crustal structure is also averaged in profile direction.

  These two examples represent extreme cases where the error of the 2-D approximation is largest, provided the crustal structure is inhomogeneous. For most parts of the profiles, the deviations of the real profile geometry from the 2-D approximation are small. A straight line geometry is almost realized for profiles BRE, SBK and DKS.

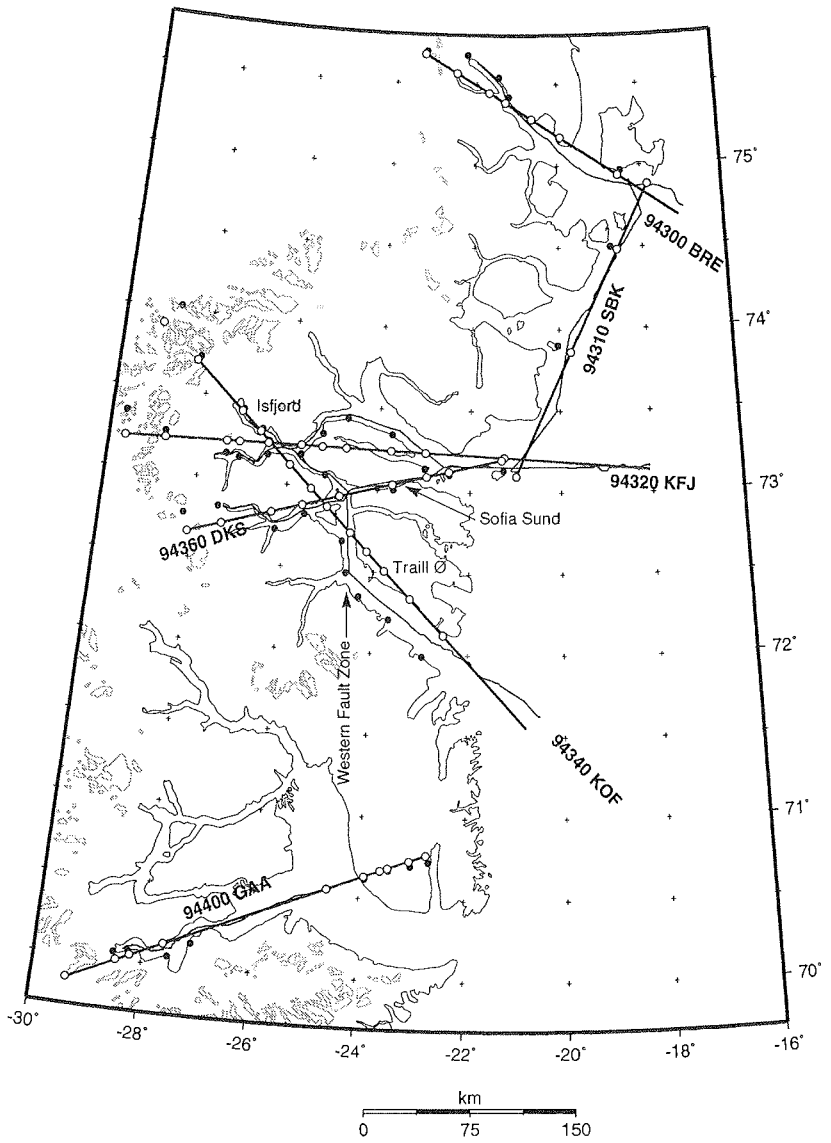

Fig. 4.4: Location of seismic refraction 2-D models in East Greenland. Grey lines outline nunataks. The thin lines show the airgun shots, the dots represent receiver locations. Open circles mark the projected receiver locations. The bold lines show the profile planes for 2-D modelling. Abbreviations as in Fig. 4.3. Scale valid at 73°N.

- **Correction for receiver elevation**
  The projection of shots and receivers into a 2-D model involves further difficulties. Where receivers were deployed along the shores of the fjord, shot and receiver locations coincide in the projected profile. A layer of water needs to be modelled beneath the shots and a layer of bedrock beneath the receivers, but both conditions cannot be implemented simultaneously in the model. Therefore, the receiver locations were projected down to the fjord bottom and the travel times to each receiver were reduced accordingly. A correction velocity was assumed. From the slope of the Pg travel time curves, velocities between 4 km/s to 6 km/s were determined for the uppermost crust depending on local geology. A correction velocity of 5.5 km/s was used throughout as most of the receivers were deployed on crystalline rock. Fig. 4.5 gives an impression of the error due to an incorrect velocity assumption. The differences between the time shifts calculated for various reduction velocities are generally smaller than the typical pick uncertainties.

  The time shift to be applied to the seismic data was calculated by adding the water depth at the projected location of the receiver to the receiver elevation and dividing by the chosen reduction velocity. This is only true for vertical ray incidence. Accounting for varying incidence angles and different ray paths requires modelling. This was not attempted here, as errors inherent in the 2-D approach are estimated to be significantly larger than errors involved in the assumption of vertical ray incidence. Fig. 4.5 lists the time shifts applied to the travel times to the receivers of profile KFJ, where the largest corrections were necessary. Receiver locations beyond the fjord, i.e. the shots, were incorporated in the model at their original elevation with solid rock beneath (KFJ: stations 331, 330; Fig. 4.5).

Station	Elevation [m]	Water depth [m]	Elevation - water depth [m]	Time shift [ms] for 5.5 km/s	Time shift [ms] for 6.0 km/s	Time shift [ms] for 4.0 km/s
331	- 2343	-	-	-	-	-
330	- 1798	-	-	-	-	-
329	- 76	658	- 734	- 133	- 122	- 184
328	- 518	732	- 1250	- 227	- 208	- 312
327	- 335	776	- 1111	- 202	- 185	- 278
326	- 198	746	- 944	- 172	- 157	- 236
325	- 49	450	- 499	- 91	- 83	- 125
324	-115	330	- 445	- 81	- 74	- 111
323	- 25	400	- 425	- 77	- 71	- 106
322	- 198	245	- 443	- 81	- 74	- 111
321	- 244	283	- 527	- 96	- 88	- 132

Fig. 4.5: Correction of the receiver elevation to the fjord bottom for profile KFJ. Heights are positive downwards. Elevation is the true receiver elevation, water depth is at the projected receiver location. The time shifts to be applied to the seismic data are given for different reduction velocities which cover the range of observed P-wave velocities in the uppermost crust. A correction velocity of 5.5 km/s was used throughout.

- **Ray tracing**

  For modelling of the observed travel times, the program by Zelt & Smith (1992) was used. Although this program is designed for inverting the observations for the velocity structure of the sub-surface, it was employed here mainly for forward modelling. The roles of receivers and shots were reversed and rays were traced from each receiver to the shot locations. Modelling was performed layer-wise starting from the top. Velocities and layer boundaries of the upper layers were held fixed when the next deeper layer was modelled. Inversion was only performed to refine the model, especially the geometry of reflectors.

  The program is based on a damped least squares inversion algorithm minimizing the root-mean-square (rms) travel time residual. The rms residual could also be used to assess the quality of the models. However, for this parameter to be meaningful, it is necessary that the errors assigned to each pick represent only uncertainties due to noise. If the error bars define a range of travel times where, depending upon phase identification, any arrival time is equally likely, the rms travel time residual alone no longer represents a measure for the quality of the fit. The problem is demonstrated in a synthetic example in Fig. 4.6. Fig. 4.6a represents an acceptable fit, as the slope could be modelled within the range of the possible arrival times. The rms travel time residual is smaller in Fig. 4.6b, but the slope of the observed travel time curve is not reflected by the model. Fig. 4.6c shows an example where the error bars reflect noise-related uncertainties of well defined phases. Here, minimizing the rms residual yields the best-fitting solution. As the majority of the errors, especially for the Pg phases, belong to this third type, the rms travel time residual gave a rough estimate of the quality of the models.

  An equally important criterion was, that rays could be traced to all observations. The program provides the possibility of two-point ray tracing, selecting only those rays that actually travel between shots and receiver. Due to the inherent 3-D effects and the complex sub-surface structure it was not possible to reach all observation points. However, in the final models rays could be traced to more than 90% of the picks.

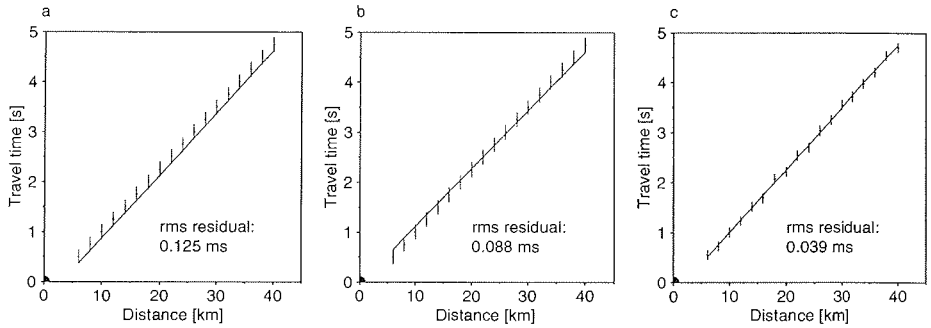

Fig. 4.6: Synthetic examples for the rms travel time residual as measure for the quality of the fit. The error bars in a and b define a range of subparallel phases. No preference could be given to one of the phases. In c the error bars represent noise-related uncertainties of clearly defined phase arrivals. The solid lines show the modelled travel time curve. The meaning of the rms residual is discussed in the text.

In addition, the fit of each solution was visually assessed. More emphasis was put on matching the slope of the observed travel time curves than minimizing the travel time residual. Finally, the simplicity of the solution was an important criterion. No unnecessary details were included in the models. Additional velocity nodes or boundary topography were only implemented if a homogeneous structure could not produce a satisfactory fit. For example, it was not attempted to account for less prominent reflections seen only on single seismic sections.

- **Resolution and uncertainties of the models**
  Prior to geological interpretation of seismic models, it is essential to assess the significance of the model in order to avoid over-interpretation. However, estimating the resolution and the uncertainty of seismic refraction models is difficult as modelling and the assessment of errors involve the subjectivity of the interpreter.

  The program by Zelt & Smith (1992) provides a method to quantitatively estimate the resolution of the parameters which specify the final velocity model. The resolution is a measure for the relative number of rays that determine a parameter. Contoured plots of the resolution of velocity models are shown by various authors (e.g. Barton & White, 1997; Staples et al., 1997). However, the resolution strongly depends upon the parameterization of the model.

  In this study, due to the inherent 3-D effects described above, the upper crust for example was deliberately under-parametrized to allow for the average nature of the model. Consequently, the parameters are much better resolved than in deeper layers with comparable ray coverage, where parameterization was more detailed as the 3-D effects are reduced. Therefore, I preferred to explicitly show the ray coverage for each layer in order to give a more transparent qualitative estimate of the model resolution.

  The absolute uncertainties of the boundary and velocity nodes are estimated following Barton & White (1997). The position of a specific interface node is increasingly perturbed until the travel time fit of the perturbed model clearly deviates from that of the unperturbed model. The maximum perturbation that allows a comparable fit is a measure of the absolute uncertainty (Zelt & Smith, 1992). The equivalent procedure was applied to determine uncertainties of the velocity nodes, while holding the velocity gradient within the layer fixed. The process is time consuming, so only a few representative nodes per layer were tested. Although this method yields a quantitative estimate of absolute errors, it is subjectively assessed whether the perturbed model still yields an acceptable fit of the travel time data. Therefore, the absolute uncertainties have to be considered as rough order-of-magnitude estimates.

4.2.4 Seismic models for the continental crust of East Greenland

The study concentrates on the 3 intersecting profiles through the major fjords in the fjord region of East Greenland, namely the KFJ, DKS and KOF profiles. Initially, the seismic profiles KFJ, DKS and KOF were modelled separately. Subsequently, the seismic models were compared and the intersections analysed. Layer velocities and boundary depths were adjusted to fit within the respective uncertainties. Poorly constrained velocities, e.g. in the lower crust, were standardized on all profiles using the best defined value. The models for each profile were then refined holding the adjusted parameters fixed. The resulting seismic models show very similar characteristics. Therefore, as an example, the model for the profile KFJ will be described in detail be-

low. The results of the DKS and KOF data will be compared with the KFJ profile. The seismic models of all 3 profiles were analysed jointly with gravity and magnetic data available along these profiles (chapter 4).

In addition, the profiles SBK, BRE and GAA were modelled. The results mainly served for comparison of the crustal structure of the principal area of interest with the adjacent areas. The profiles SBK, BRE and GAA are therefore only briefly described below. No integrated analysis of these profiles was undertaken.

I deliberately did not reproduce a large number of seismic sections. For display, the seismic traces have to be bundled in 450 m bins. In addition, the reduction in size and the density display of the amplitudes drastically reduce the quality of the seismic sections such that the onsets of weak phases are no longer discernible. Therefore, only one or two examples per profile are shown. Instead, all picked phases and the modelled travel time curves are shown as well as the ray tracing for all phases.

Profile KFJ (94320)

Profile KFJ was shot along Kejser Franz Joseph Fjord in a W-E direction (Fig. 4.3, Fig. 4.4). The total length of the projected profile is 375 km. Eleven receivers were deployed and recorded high quality seismic signals. The profile is not reversed between km 0 and 63 and between km 270 and 375.

An example of a seismic section is shown in Fig. 4.7. A total of 1442 arrivals were picked, 90% of which could be modelled. Fig. 4.8 shows the picks for each station together with the calculated travel times. The parameterization of the resulting model is shown in Fig. 4.9. Layers 1 to 5 in the following description of the model refer to the grey-shaded units of the model in Fig. 4.9. Fig. 4.10 shows an interpolated model of crustal P-wave velocities. The ray tracing through all layers (Fig. 4.11) gives an impression of how well different regions of the model are constrained by rays.

Layer 1: Pg phases were identified on all record sections. They could be observed up to a maximum offset of 170 km. In the western part of the profile, velocities in the uppermost 2-3 km of the crust rapidly increase from about 5.7 km/s to 6.0 km/s, typical for crystalline rocks. At km 158, Pg phases may be distorted or interrupted (e.g. 322) The profile crosses here the Western Fault Zone which separates the Caledonian orogenic belt from the Devonian sedimentary basin (Escher & Pulvertaft, 1995). Velocities in the Devonian basin vary between 5.3 km/s and 5.7 km/s. East of km 210 they further decrease. Mesozoic sedimentary rocks are exposed here. The seismic velocities at the surface vary strongly in the profile direction from values of about 4.0 km/s to 5.1 km/s. Station 322 for example shows clearly different slopes for the eastern and western branch of the Pg phase. In addition, abrupt changes to significantly higher velocities occur (for example at km 320 on station 321). They are attributed to Tertiary basaltic rocks included in the Mesozoic basin. However, due to the large station spacing and the lack of a reversed profile east of km 270, this small-scale heterogeneity is poorly resolved (c.f. ray tracing in Fig. 4.11). The uncertainty of seismic velocities in the sedimentary basins is about ± 0.2 km/s, whereas velocities in the crystalline rocks could be determined to within ± 0.1 km/s.

Velocities of about 6 km/s are reached in 2 km ± 0.5 km depth in the western part of the profile, whereas to the east a maximum thickness of 6 km ± 1.5 km is modelled for the sedimentary basins. The Mesozoic sedimentary basin was represented by two layers to account for a change in the velocity gradient. Whereas velocity increases rapidly with depth in the surface layer, a moderate increase was modelled for the layer be-

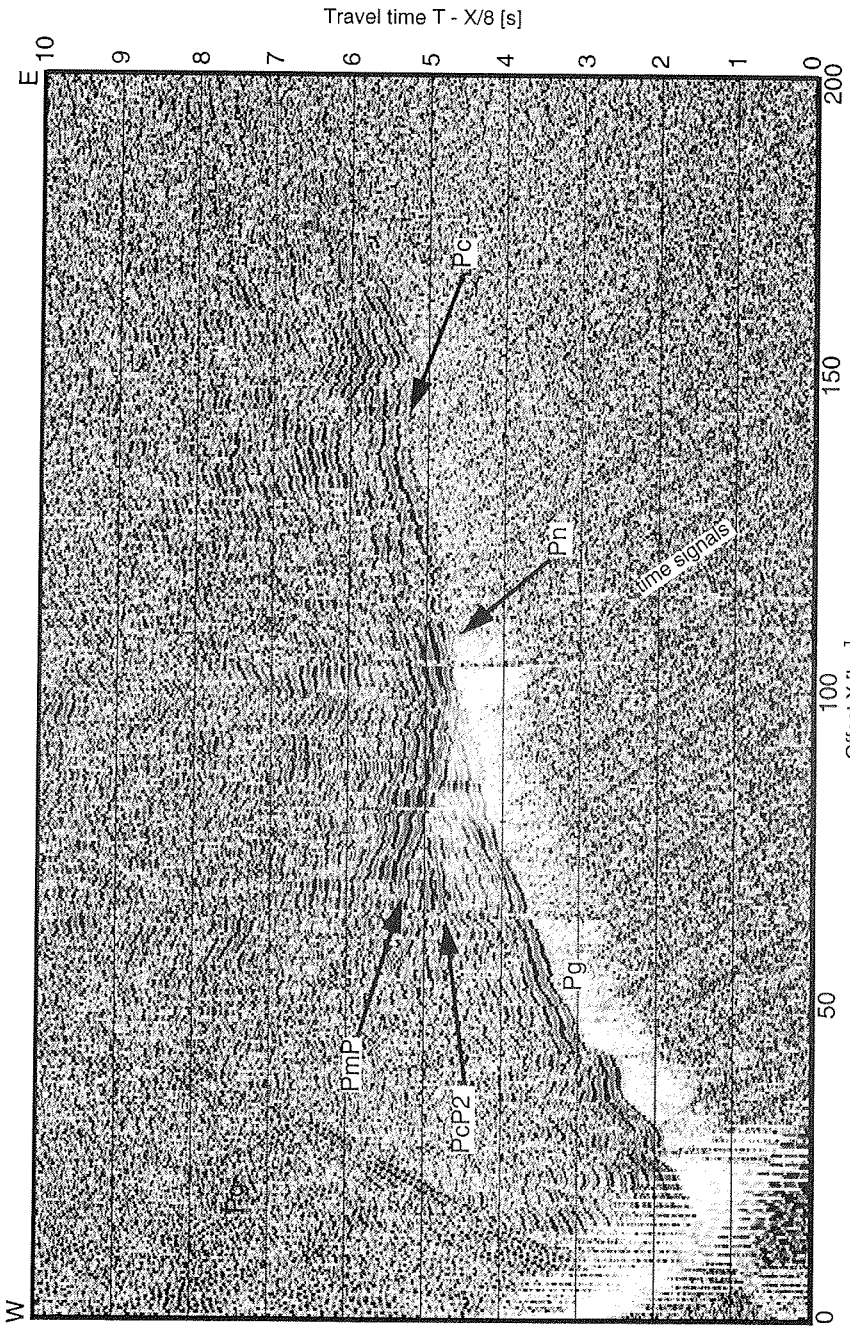

Fig. 4.7: E part of the seismic section recorded by station 323 on profile KFJ. The observed phases are labelled. Note the delay of the Pc phase at its eastern end.

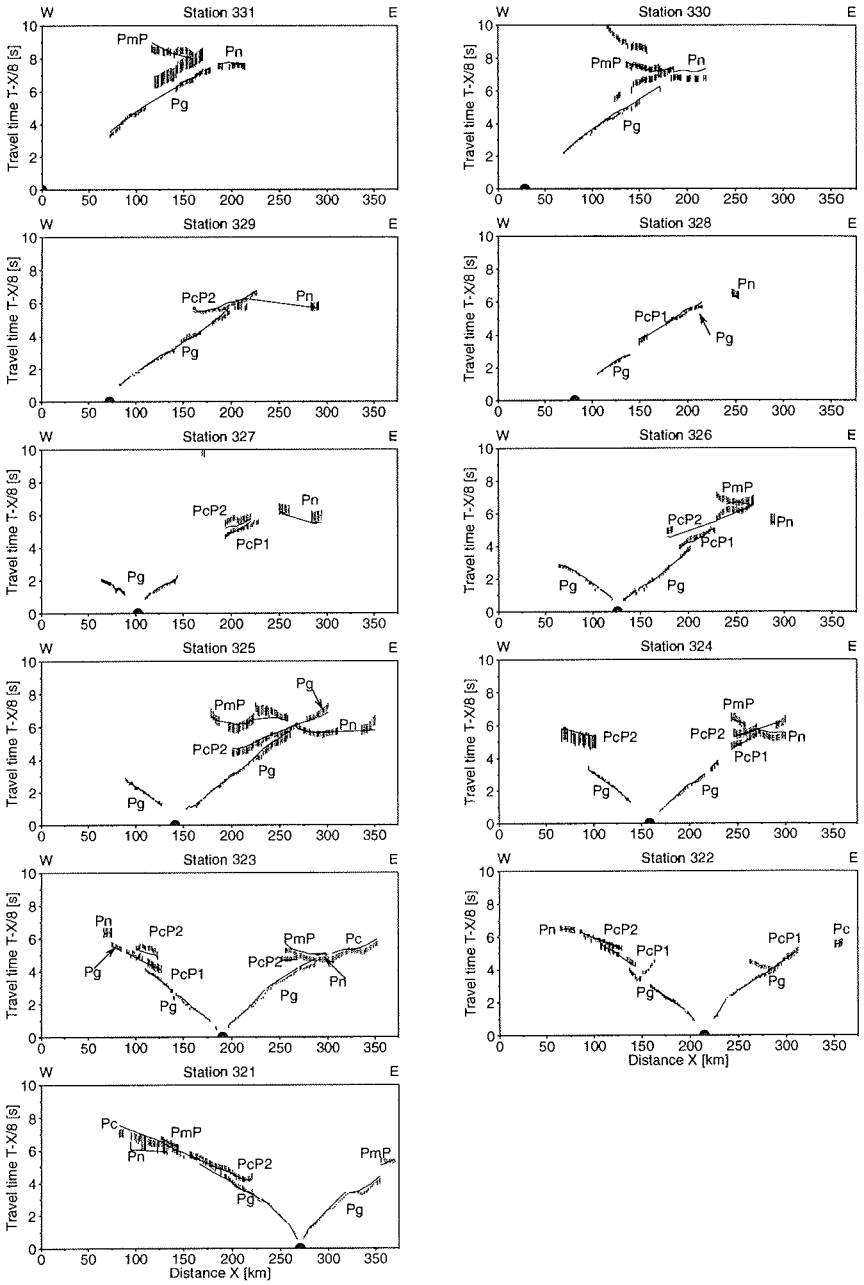

Fig. 4.8: Observed and calculated P-wave arrivals for profile KFJ. Dots show the station location. The observed arrivals are represented by the vertical error bars, the picked arrival time is at the centre, respectively. The lines show the calculated arrivals. Arrivals belonging to one phase were connected and are labelled.

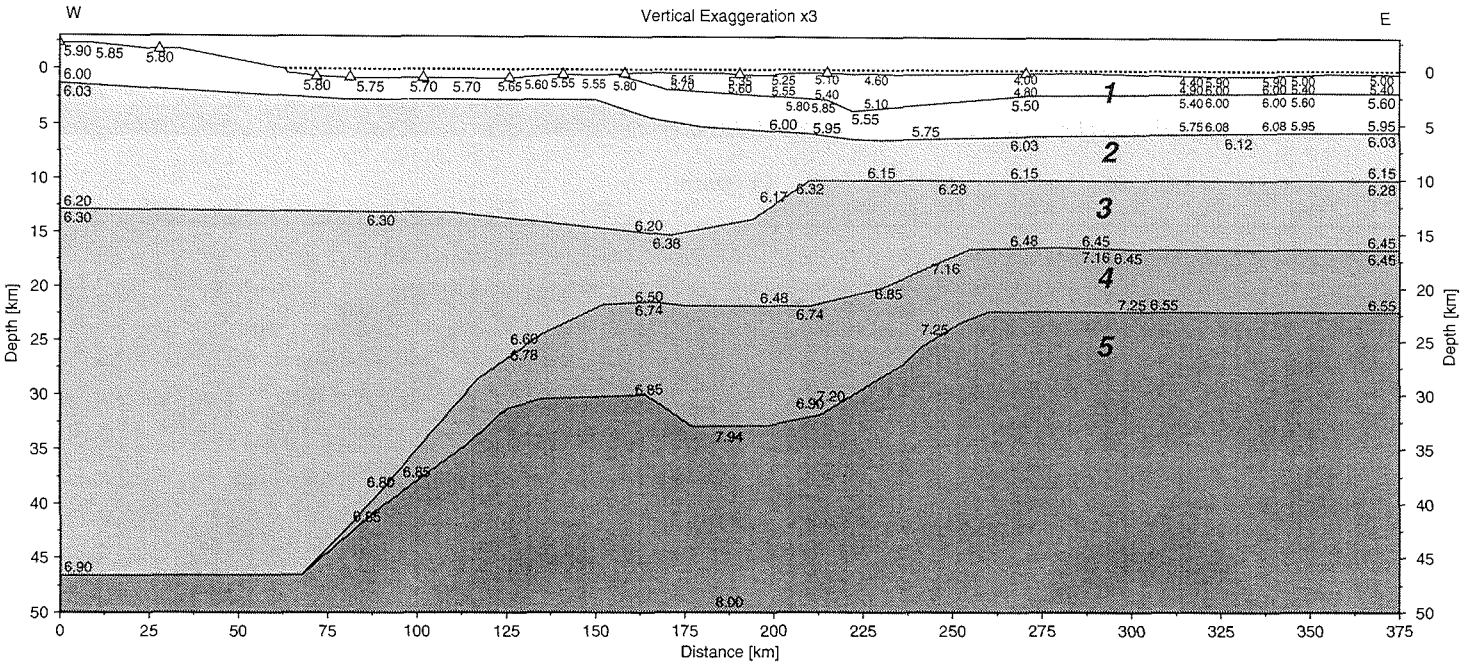

Fig. 4.9: Parameterization of the P-wave velocity model for profile KFJ. Numbers show velocity nodes and their value. Lines represent layer boundaries. The triangles indicate projected receiver locations calculated down to the fjord bottom. The dotted line shows the projected shots. The layer-wise description of the model refers to the grey-shaded units 1-5 of the model.

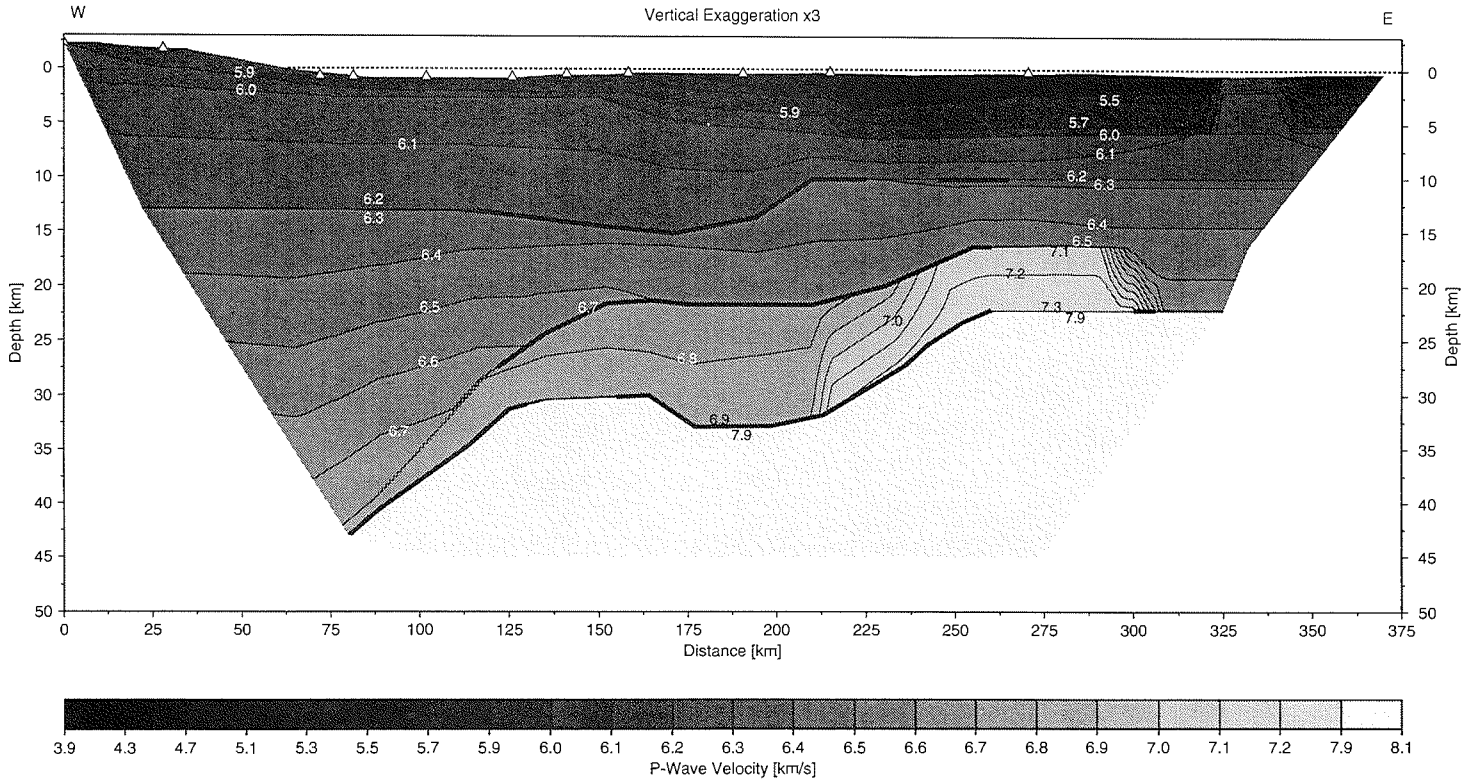

Fig. 4.10: Interpolated P-wave velocity model for profile KFJ. The model is only shown where it is constrained by rays. Thin lines represent contour lines corresponding to the labelled intervals of the scale. Note, that the scale is not equidistant. Bold lines show where rays are reflected off a boundary.

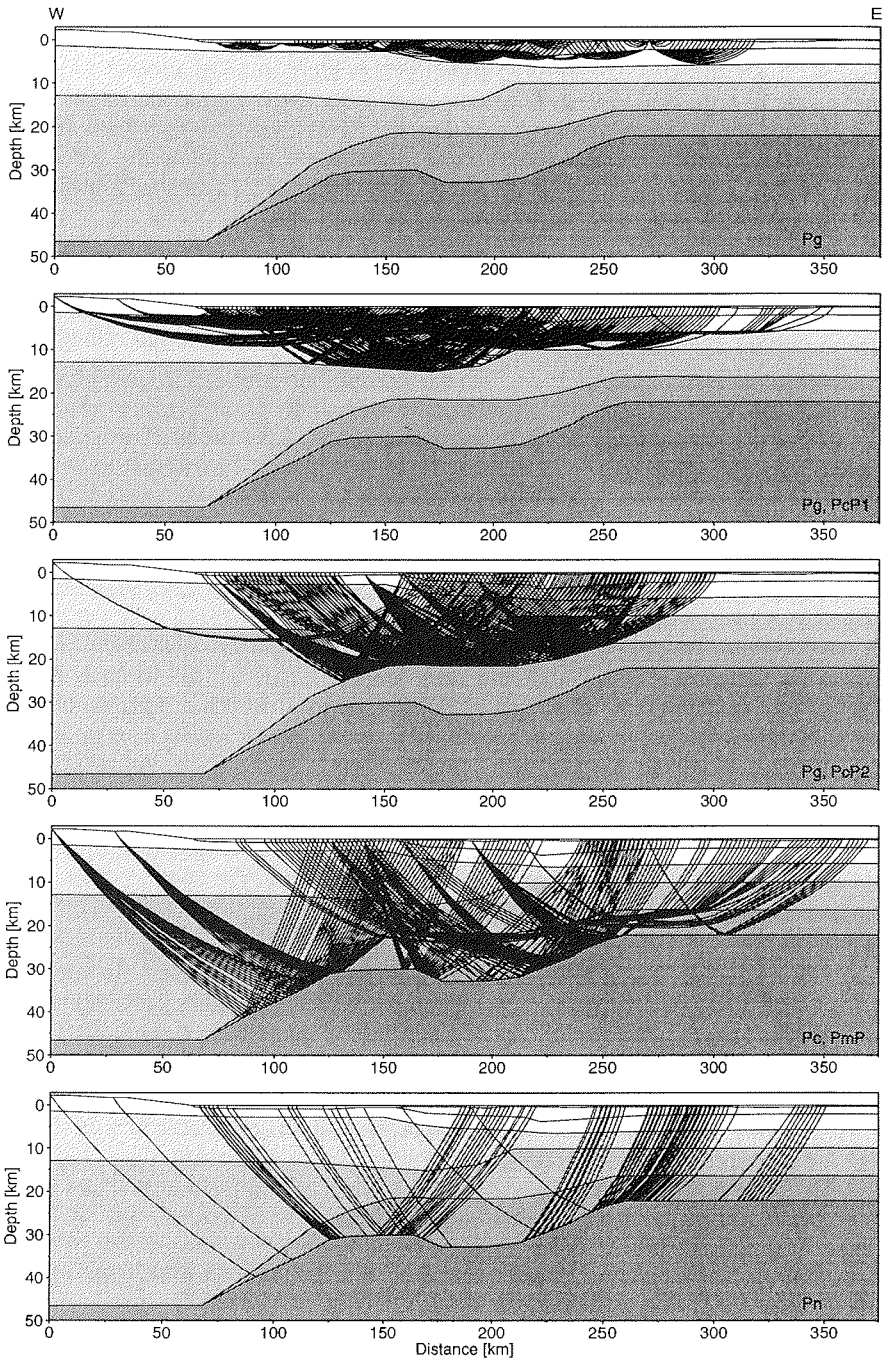

Fig. 4.11: Ray tracing for profile KFJ. Rays through layers 1-5 (c.f. Fig. 4.9) are shown from top to bottom. The respective phases are indicated. Vertical exaggeration x2.

neath without assigning a velocity contrast to the boundary.

Layer 2: In the layer from 2-6 km to 10-14 km depth, seismic velocities increase slowly with depth. The travel time curves have an almost constant slope of about 6.1 km/s (for example station 329). This velocity is constrained to ± 0.1 km/s due to the large number of rays with turning points within this layer (Fig. 4.11). Its lower boundary is marked by a reflector. Six reflected phases (PcP1) could be observed and define the topography of the reflecting boundary (Fig. 4.9). An uncertainty of about ± 1.5 km was assigned to this boundary for the well resolved middle part of the profile.

Layer 3: Only a few diving waves have their turning points beneath in this layer, such that the maximum depth penetration of the Pg phase is about 15 km (Fig. 4.11). Velocities are about 6.3 km/s ± 0.15 km/s. Crustal velocities beneath 15 km depth are not directly observed, but were modelled to fit a large number of wide-angle reflections.

The westernmost part of the profile within the Caledonian range is devoid of any significant reflected phases from the middle and lower crust. Therefore, velocities were assumed to increase continuously with depth from about 6.3 km/s at 15 km depth to a maximum velocity of 6.9 km/s ± 0.2 km/s at the base of the crust at about 43 km depth. These values are within the range of a global average of crustal velocities in orogenic belts (Christensen & Mooney, 1995).

In the middle part of the profile, a prominent west dipping reflector could be defined from 10 PcP2 reflections of high quality. An excellent coverage with rays from both sides allowed the topography of the reflector to be determined to within ± 2 km (Fig. 4.11). The reflector starts at a depth of about 16 km in the eastern part of the profile. In this area, the reflected phase PcP2 has large amplitudes compared to other phases. On station 321 and 361, the amplitude of PcP2 is larger than the amplitude of the Pg phase even at offsets of less than 100 km (Fig. 4.12). No reflected energy from the Moho was discernible following the PcP2 phase in this area. This was verified by a predictive deconvolution to suppress reverberations. Hence, most of the seismic energy is probably reflected by this boundary which must therefore represent a marked contrast in acoustic impedance. Further to the west, Moho phases are visible after the PcP2 phase which loses its dominant character. The reflector dips from 16 km to about 22 km and is observed further to a maximum depth of 27 km. West of about km 220, a considerably lower impedance contrast is assigned to the layer.

Layer 4: Three phases have been identified as refracted rays through the lower crust (Pc). However, they are difficult to distinguish from wide-angle Moho reflections, which follow a similar raypath. On station 321, a distinction of these two phases was conceivable suggesting this phase identification.

From station 323, lower crustal velocities of about 7.2 km/s are derived for the eastern part of the profile. The maximum perturbation producing an acceptable fit was -0.1 km/s to +0.3 km/s confirming the high velocity character. The eastern end of this high velocity layer is poorly constrained as only a few rays travel through this area. However, the easternmost Pn arrivals of station 325 and the easternmost Pc arrivals of station 323 are delayed, suggesting that these rays encounter lower velocities. To the west of the high velocity layer, velocities decrease to 6.8 km/s ± 0.2 km/s as evidenced by the Pc phase of station 321 and a large number of PmP and Pn arrivals.

The topography of the Moho is fairly complex. Two steep slopes separated by a plateau with little undulations were modelled. The Moho dips westward from about 22 km depth beneath the high velocity area, which has hence a thickness of about 6 km, to 30 km

at the plateau. The maximum depth is observed at the western end of the profile at 43 km. The ray coverage by PmP and Pn phases is good allowing constraint of the Moho depth to ± 3 km.

Due to the pronounced Moho topography, the PmP phases may be very curved as for example for station 325. In addition, 3-D effects cause difficulties. If the profile direction is not perpendicular to the strike of the Moho slopes, out-of-plane rays will hit the slope at different offsets. Therefore an average position had to be modelled which does not satisfy all observed PmP or Pn phases within the error limits (e.g. station 323, only the shape is matched here).

Layer 5: The Moho topography produces shadow areas where no diving rays with turning points in the uppermost mantle can reach the surface without assuming unreasonably high velocity gradients in the mantle. However, Pn arrivals were observed at all stations over a wide range of the profile. The Pn waves were therefore assumed to be critically refracted and to travel as head waves along the Moho. The seismic velocity in the uppermost mantle was assumed to be laterally homogeneous. A velocity of 7.94 km/s ± 0.1 km/s fit the Pn arrivals on all profiles best.

Profile DKS (94360)

Profile DKS (Fig. 4.3, Fig. 4.4) follows Dickson Fjord from west to east, crosses Kong Oscar Fjord and joins the profile KFJ at the east end of Sofia Sund. The profile ends at 230 km projected length. Nine receivers were installed along the profile such that only the westernmost 30 km are not reversed. Signal quality was very good. Examples of seismic sections are shown in Fig. 4.12 and Fig. 4.13.

Observed and calculated P-wave arrivals are displayed in Fig. 4.14. Rays could be traced to 1040 of 1079 picks. The 3-D effects are less pronounced than for profile KFJ producing a better fit. The resulting seismic model (Fig. 4.15, Fig. 4.16) is very similar to the model for KFJ. The ray coverage is shown in Fig. 4.17.

Layer 1: Pg rays penetrate to a maximum depth of about 10 km, defining the velocity structure in the upper crust. At the surface the P-wave velocities decrease from about 5.8 km/s in the Caledonian mountain range to 5.3 km/s in the Devonian sedimentary basins east of the Western Fault Zone at km 118. East of about km 170, the Mesozoic sedimentary rocks show velocities of 3.9-4.7 km/s. Velocities increase with depth reaching about 6 km/s at 2 km depth in the western part of the profile and in about 6 km depth beneath the sedimentary basins. The ray coverage and the resolution of velocity and boundary nodes are comparable to profile KFJ.

Layer 2: Corresponding to profile KFJ, layer 2 has a small velocity gradient with a mean velocity of 6.1 km/s ± 0.1 km/s. The lower end of the layer is marked by reflected arrivals PcP1. However, in contrast to profile KFJ, the reflecting boundary is more or less flat-lying at 10-13 km ± 1 km depth. The ray coverage is different from KFJ with some reflected energy stemming from the Caledonian range.

Layer 3: Reflectivity in the lower part of the Caledonian crust is low as for KFJ. Velocities were chosen correspondingly to increase from 6.3 km/s continuously to 6.9 km/s at the base of the crust. To the east, the prominent west dipping reflector causing PcP2 arrivals is clearly visible. It is substantiated by phase arrivals on 7 stations down to a depth of about 25 km where it almost joins the Moho. The character of the PcP2 reflection in the easternmost part of the profile at 16 km depth is identical to profile KFJ. Station 361 nicely demonstrates the large relative amplitude of the PcP2 arrival in contrast

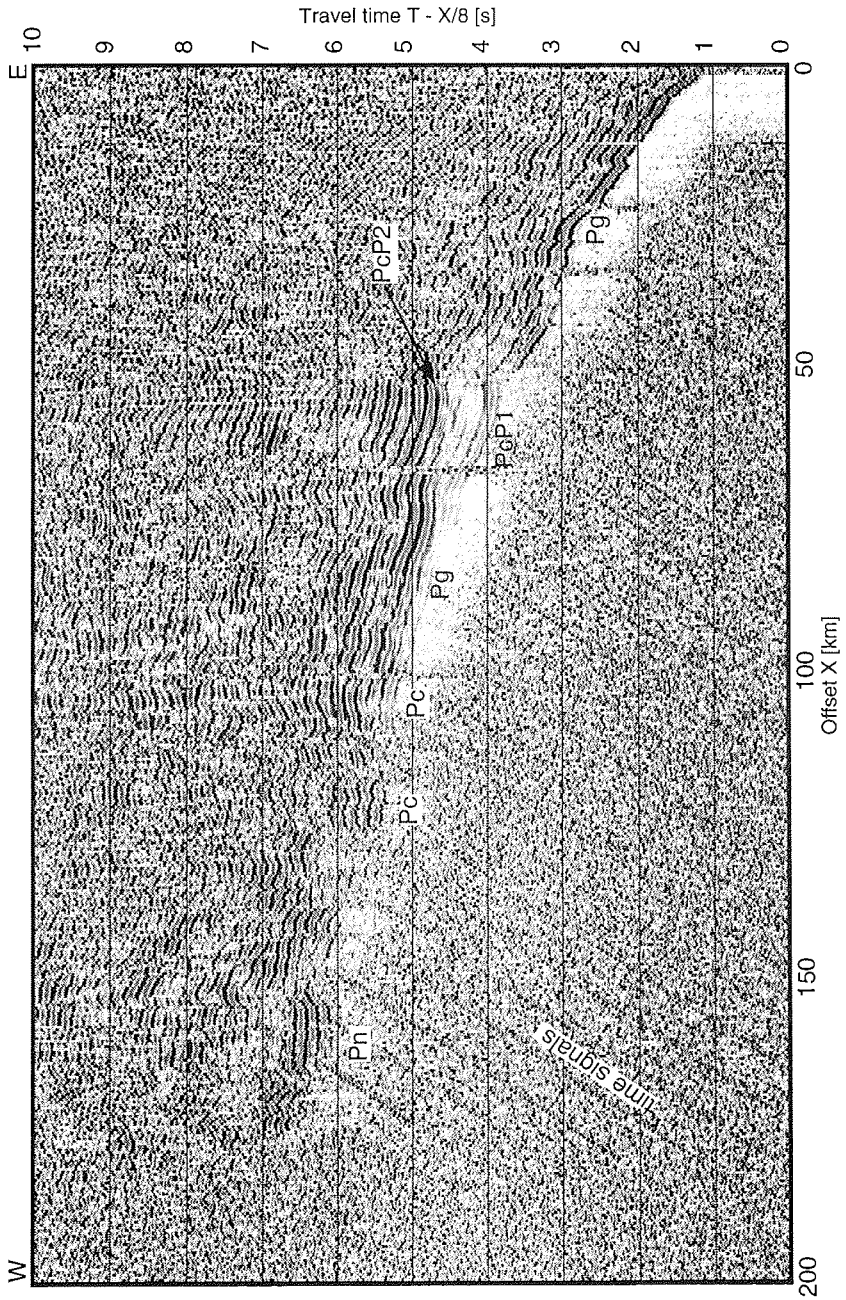

Fig. 4.12: Seismic section recorded by station 361 on profile DKS. The observed phases are labelled. Note the large amplitude of PcP2 compared to PcP1 and Pc.

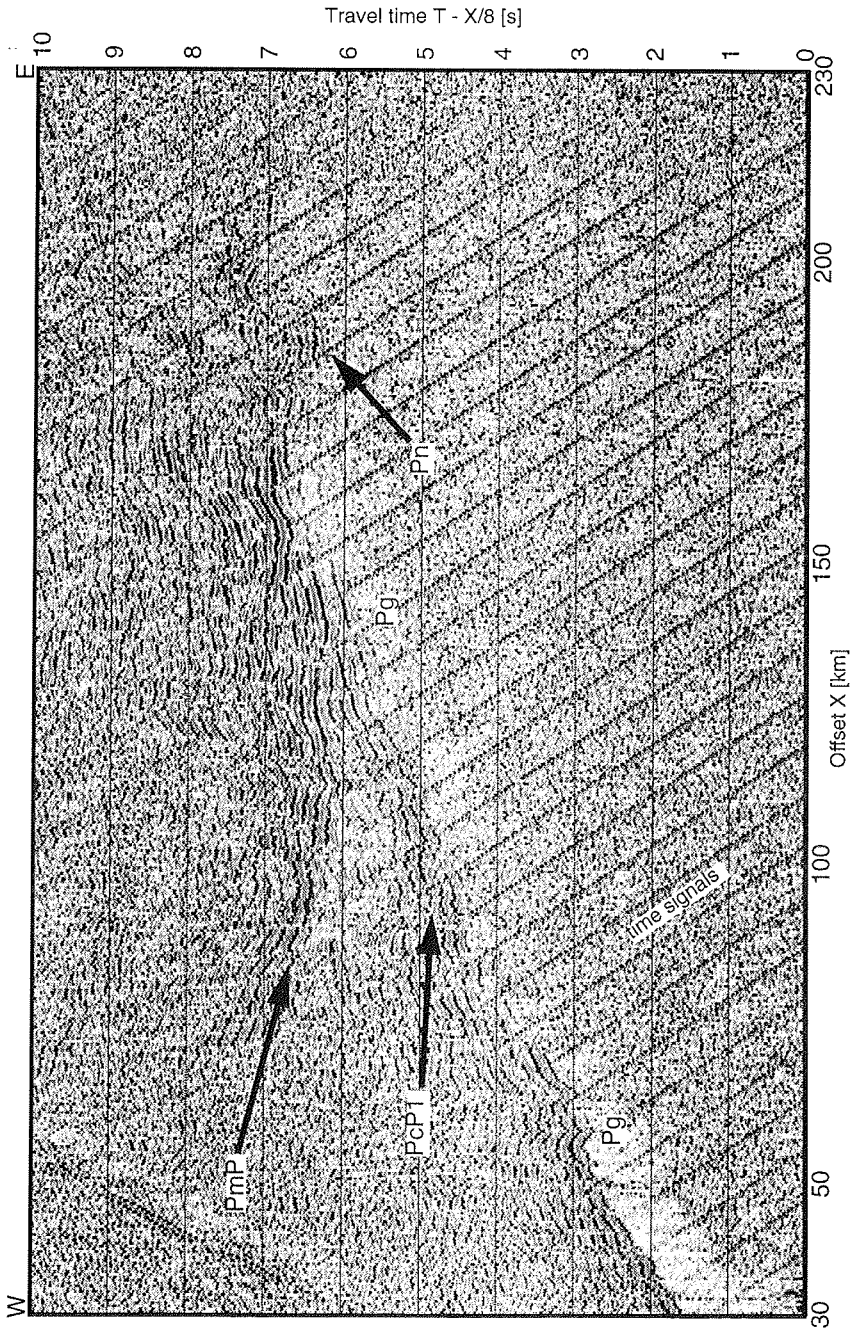

Fig. 4.13: Seismic section recorded by station 369 on profile DKS. The observed phases are labelled. Note the pronounced PmP phase.

to the Pg phase (Fig. 4.12).

Layer 4: Three relatively short Pc phases yield evidence for the high seismic velocity just beneath this reflector. Velocities were similar to those observed on profile KFJ. As the ray coverage was better on profile KFJ, the lower crustal velocities of profile KFJ

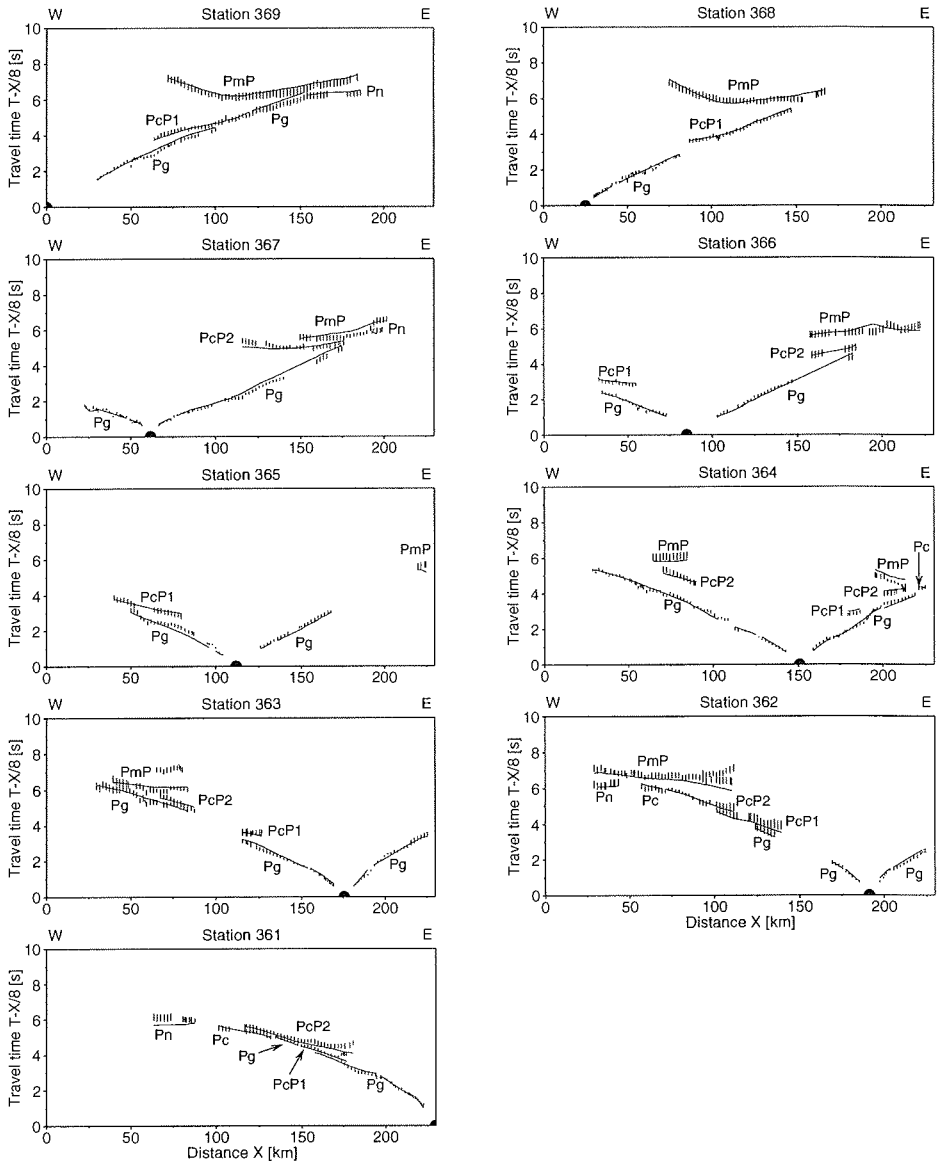

Fig. 4.14: Observed and calculated P-wave arrivals for profile DKS. For explanation of symbols see Fig. 4.8.

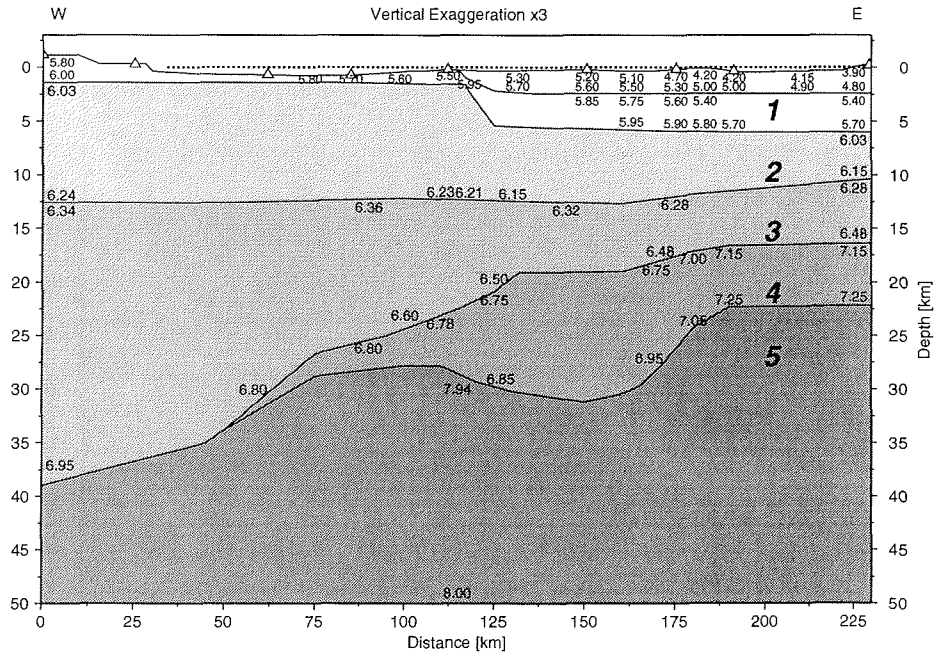

Fig. 4.15: Parameterization of the P-wave velocity model for profile DKS. For legend see Fig. 4.9.

were transferred to this profile. This is justified in particular between stations 363 and 361, where the profiles coincide.

Many PmP and Pn arrivals (Fig. 4.17) could be modelled using the lower crustal velocities from profile KFJ. The Moho also dips westward in two distinct slopes separated by a plateau at 30 km depth. Stations 369 (Fig. 4.13) and 368 show prominent PmP arrivals over an offset range of more than 100 km, defining Moho topography very well (± 2 km). The Moho could only be followed down to 35 km depth due to the limited westward extent of the profile.

Layer 5: The same procedure as for profile KFJ was applied to model the relatively few Pn arrivals.

Profile KOF (94340)

Profile KOF (Fig. 4.3, Fig. 4.4) begins at the head of Isfjord, crosses Kejser Franz Joseph Fjord to follow Kong Oscar Fjord. The profile ends offshore with a total projected length of 350 km. Two major changes in profile direction occur. As a result, the direction of the projected profile differs clearly from the direction of the shiptrack. 3-D effects are most pronounced on this profile.

Twelve receivers were deployed. Stations 341 and 352 did not record usable seismic signals, such that the profile is only reversed between km 48 and km 224. The signal quality was generally poorer than on profiles DKS and KFJ except from station 342

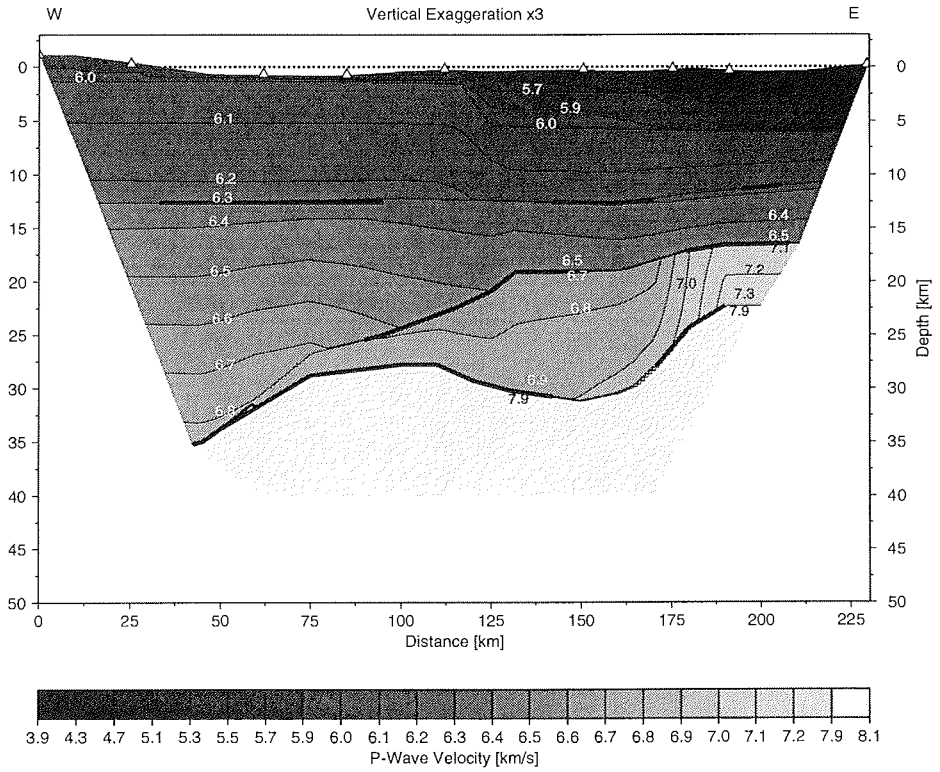

Fig. 4.16: Interpolated P-wave velocity model for profile DKS. For legend see Fig. 4.10

(Fig. 4.18). A total of 915 arrivals were picked, 843 could be modelled (Fig. 4.19). The resulting seismic model is shown in Fig. 4.20 and Fig. 4.21 and its ray cover in Fig. 4.22.

Layer 1: Pg phases were observed on all stations over a maximum offset range varying between 20 km (348) and 190 km (342). Rays penetrate down to 10 km depth. Seismic velocities in the north-western part of the profile at 5.8 km/s resemble those of the other profiles.

Velocities of about 5.5 km/s assigned to the Devonian sedimentary rocks were not observed here. The profile trends parallel to the Western Fault Zone along the N-S oriented branch of the Kong Oscar Fjord. The receivers are deployed to the west of the fault zone, suggesting that the observed velocities belong to Caledonian rocks. Hence, although the projected profile crosses the Devonian basin on Traill Ø (Fig. 4.4), the seismic model does not include any evidence for the Devonian basin. At about km 180, close to station 344, the profile crosses the Western Fault Zone, along which in this area Caledonian rocks are juxtaposed against post-Devonian sedimentary rocks (Escher & Pulvertaft, 1995). Upper crustal velocities decrease from 5.8 km/s to 4.4 km/s - 4.9 km/s across the fault zone. This marked contrast is reflected in the travel

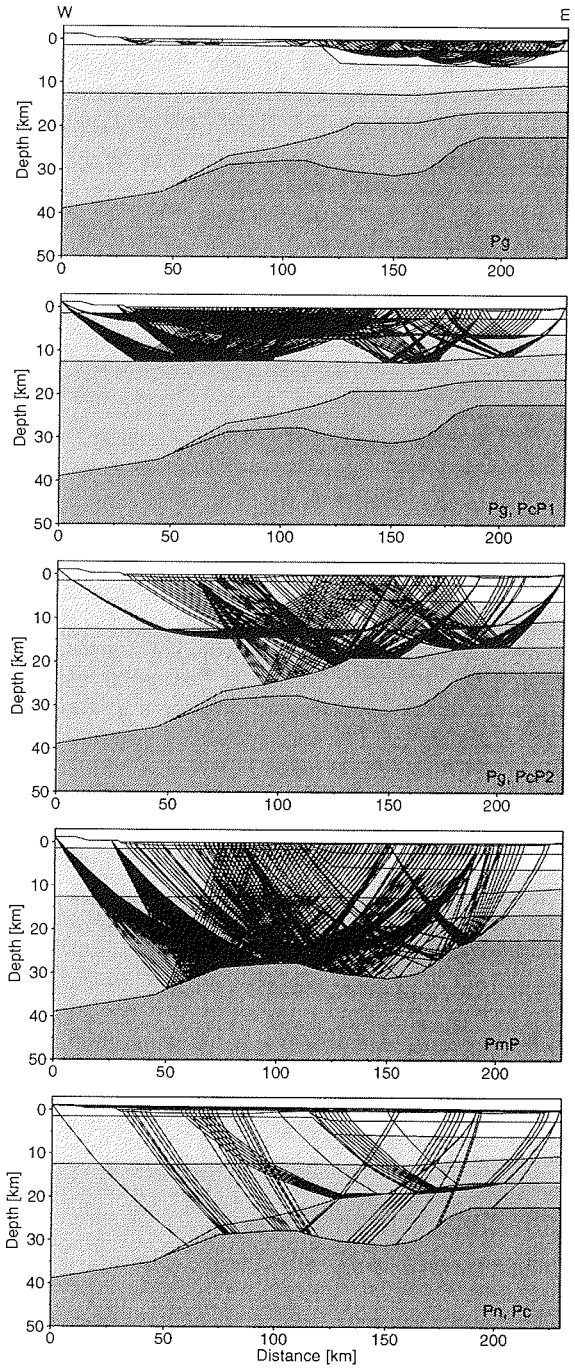

Fig. 4.17: Ray tracing for profile DKS. Rays through layers 1-5 (c.f. Fig. 4.15) are shown from top to bottom. The respective phases are indicated. For clarity, the Pc phase through layer 4 is shown with the Pn phase. Vertical exaggeration x2.

time curves. For example the western Pg branch of station 342 and the eastern Pg branch of station 345 are deflected at km 180 (Fig. 4.18, Fig. 4.19).

Between km 270 and 300, the Pg branch of station 342 shows a convex form with early Pg arrivals. The area coincides with outcrops of Tertiary volcanic rocks (Escher & Pulvertaft, 1995). Increased seismic velocities of about 5.6 km/s at the surface have been modelled to account for the presence of volcanic rocks in the sedimentary basin.

As on profiles DKS and KFJ, velocities of about 6.0 km/s are reached at about 2 km depth in the Caledonian range and at about 5 km depth in the eastern part of the profile, defining the thickness of the sedimentary basin. Ray coverage and errors for the uppermost crust are comparable to profiles KFJ and DKS.

Layer 2: This layer is characterized by slowly increasing seismic velocities of 6.1 km/s ± 0.1 km/s as on profiles DKS and KFJ. Its lower boundary at 12 km ± 2 km is less well defined here. PcP1 phases from only 3 stations were observed which are restricted to the eastern part of the profile. They yield no evidence for topography of the boundary layer.

Layer 3: No direct observations of lower crustal seismic velocities are available here. In analogy to the intersecting profiles DKS and KFJ, velocities were chosen to increase from about 6.3 km/s to 6.5 km/s at the top of the westward dipping reflector. PcP2 arrivals from 5 stations define the topography of this layer, which dips from about 18 km to 22 km depth and approaches the Moho at 30 km depth (Fig. 4.22).

Layer 4: In the eastern part of the profile, the PcP2 phase marks the lower boundary of a band of high reflectivity within which the Moho reflection at the upper end is difficult to detect. To the west, the Moho becomes a prominent reflector which is clearly distinguishable from the PcP2 phase (see seismic section in Fig. 4.18). 7 stations recorded reflected arrivals from the Moho in this area as opposed to one reflection from the eastern part (Fig. 4.22). This change in the character of the Moho reflection suggests that, in analogy to profiles KFJ and DKS, a high velocity layer with high reflectivity may be assumed beneath the lower crustal reflector in the eastern part of the profile. No Pc phases are observed yielding direct evidence for the seismic velocity. Lower crustal velocities on profile KOF were therefore chosen to match the velocities of profiles DKS and KFJ.

The PmP arrivals could be modelled using these velocities and adapting the position of the Moho. The resulting Moho topography is similar to that of profiles KFJ and DKS. Especially the slopes and the flat plateau of the Moho at about 30 km ± 3 km depth are well defined on this profile (Fig. 4.22).

Layer 5: Several Pn phases travel through the high velocity layer (Fig. 4.22). They could be accounted for using 7.94 km/s for the P-wave velocity in the uppermost mantle. Hence, although the velocity structure of the lower crust is not directly observed, the PmP and Pn phases indirectly yield supporting evidence.

Unexplained phases

Several phases could not be identified and accounted for by the models. On all three profiles, reflected phases occur which are delayed in the near-offset range compared to the theoretical arrival times. Typical examples are the PmP and PcP2 phases on station 342, PcP1 and PcP2 on station 361, PmP on station 362 and PcP1 on station 322. In the latter case, the effect is very pronounced, such that the correlation with PcP1 is

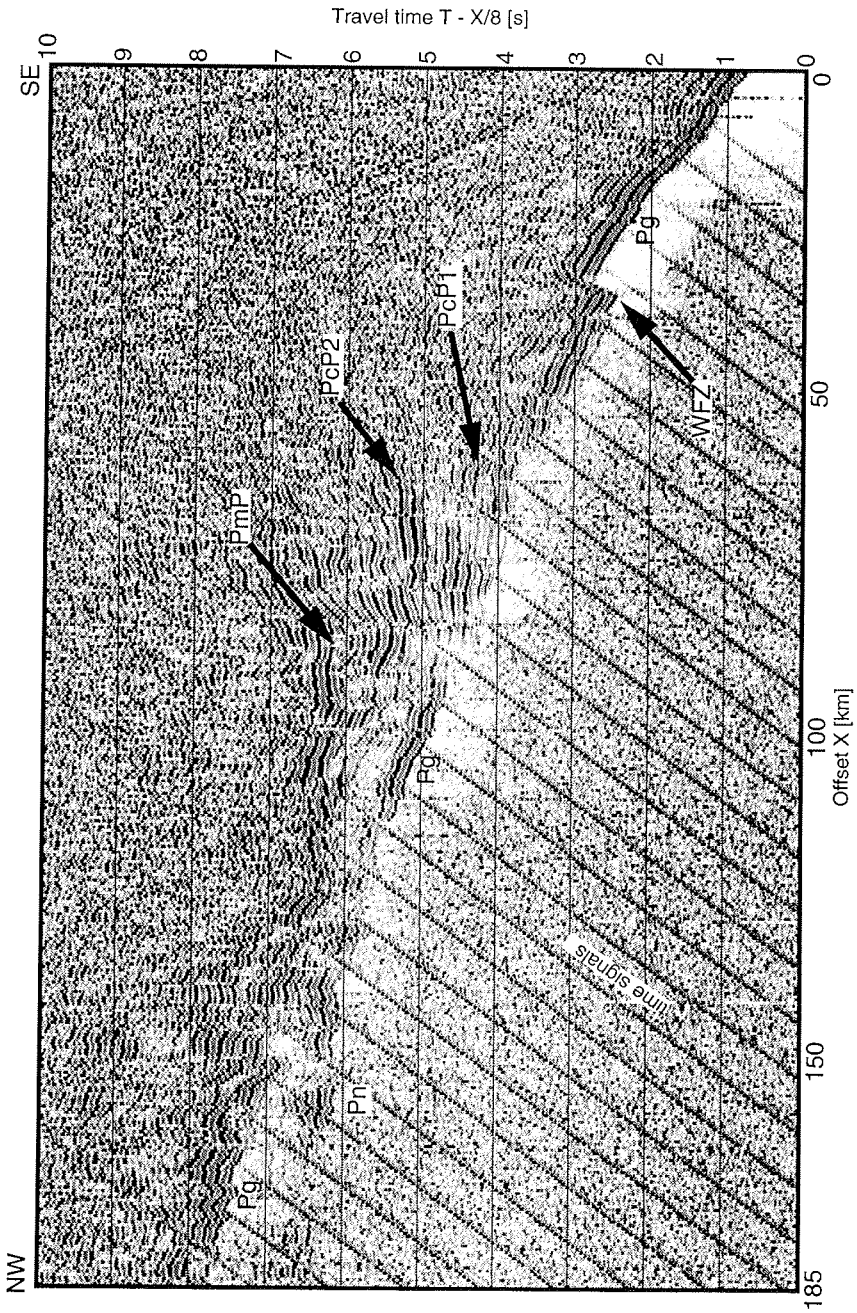

Fig. 4.18: NW part of the seismic section recorded by station 342 on profile KOF. The observed phases are labelled. Note the deflection of Pg at the Western Fault Zone (WFZ).

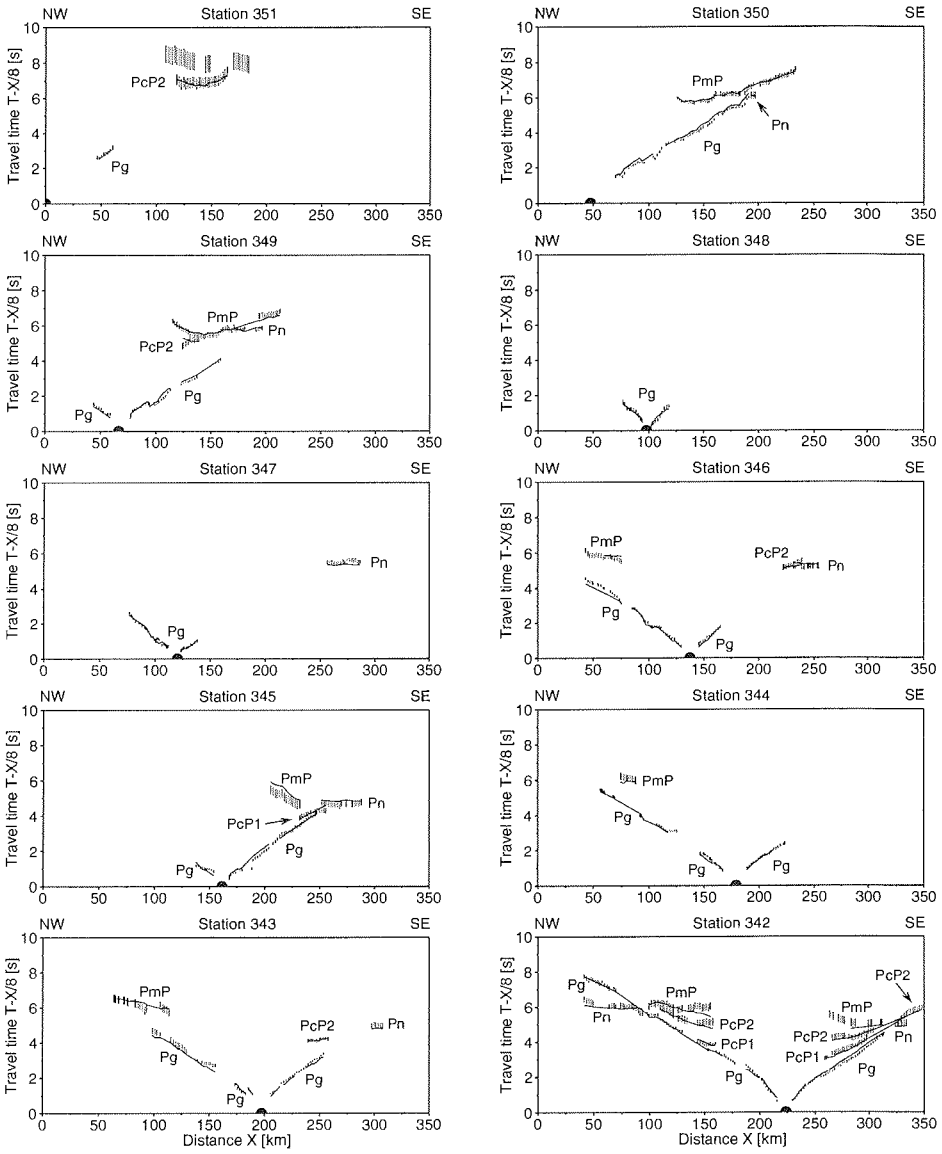

Fig. 4.19: Observed and calculated P-wave arrivals for profile KOF. For explanation of symbols see Fig. 4.8.

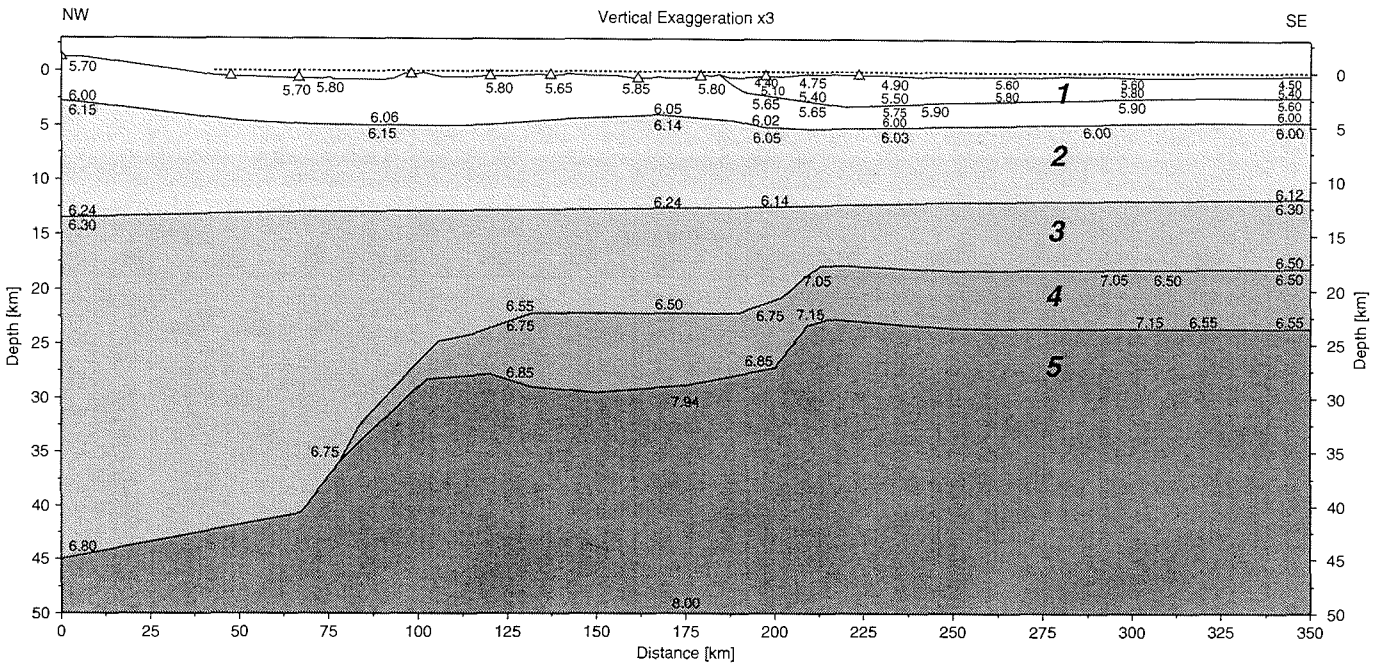

Fig. 4.20: Parameterization of the P-wave velocity model for profile KOF. For legend see Fig. 4.9.

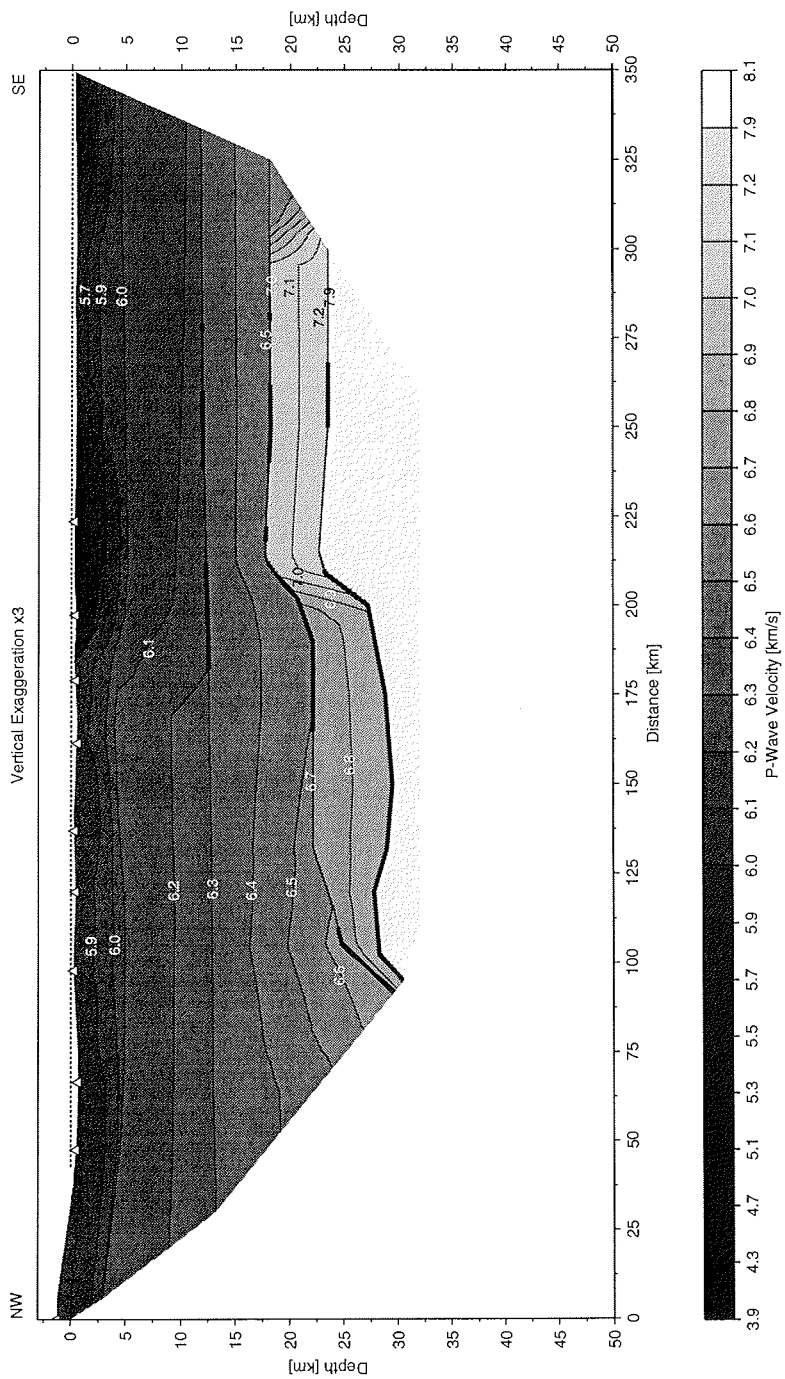

Fig. 4.21: Interpolated P-wave velocity model for profile KOF. For legend see Fig. 4.10

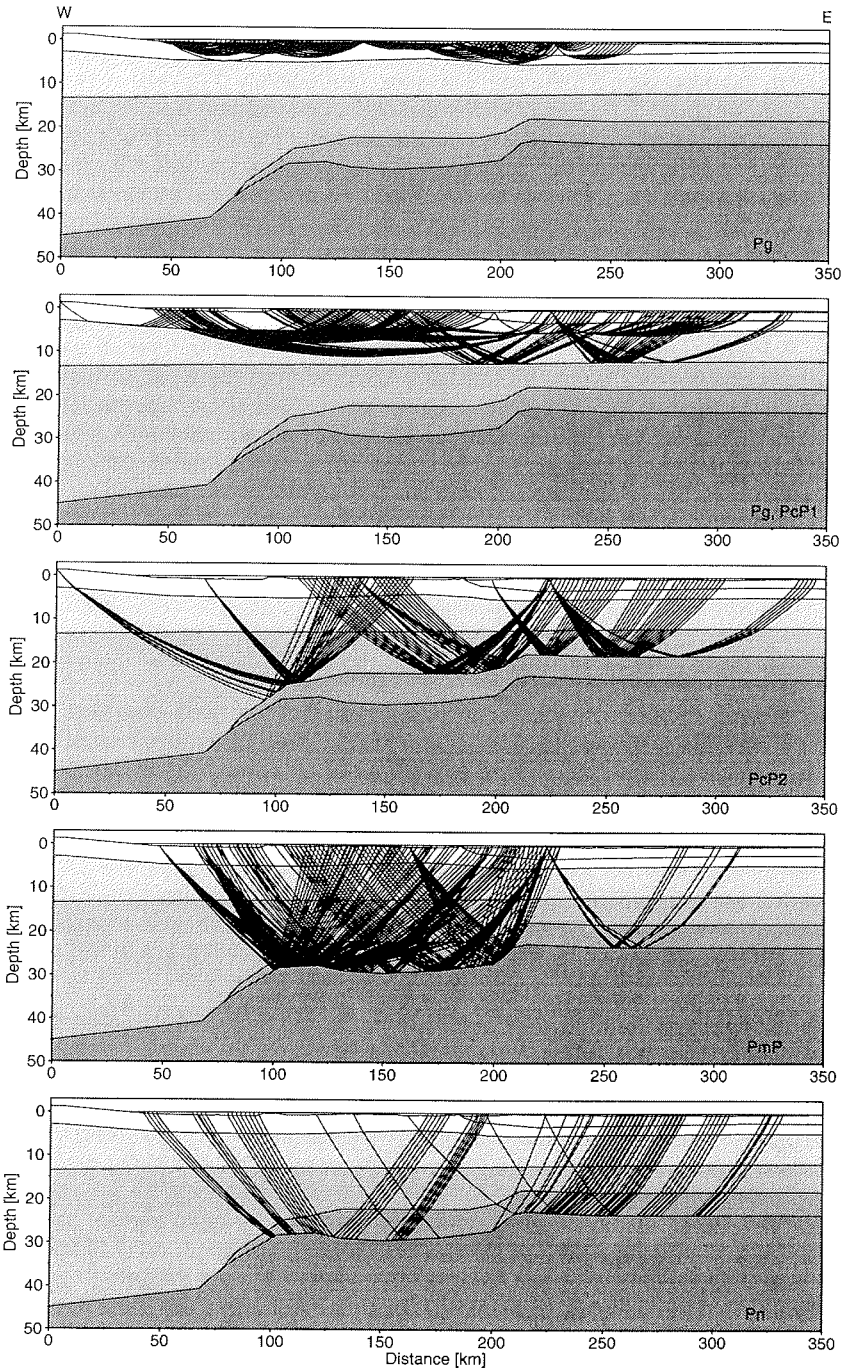

Fig. 4.22: Ray tracing for profile KOF. Rays through layers 1-5 (c.f. Fig. 4.20) are shown from top to bottom. The respective phases are indicated. Vertical exaggeration x2.

vague. Sub-vertical reflectors might account for these phases.

The nunatak stations 331 and 330 on profile KFJ show 3 conspicuous phases, which are parallel to the preceding PmP and Pg phases, respectively (Fig. 4.8). The constant time difference of about 1.1 s between the phases might indicate a multiple reflection beneath the receiver site. As the time shift is the same for Pg and PmP phases, a multiple reflection would have to occur in a near-surface layer with low velocities, such that, despite different incidence angles of the PmP and Pg phases, the multiple reflections follow sub-vertical raypaths. A multiple reflection in the watercolumn beneath the shots is unlikely to produce a constant shift in the travel time curve as the water depth in the offset range of these late phases is highly variable.

The late arrival on the nunatak station 351 has probably the same character. However, PmP and PcP2 phases are very curved and arrive within the time interval defined by the error bars of the PcP2 phase as they are reflected from the western Moho slope where both reflectors merge. Theoretical travel time curves show that the late phase has the same shape as the PmP, but is offset towards later arrival times. It is remarkable, that the observation of this type of phases is restricted to nunatak stations inviting speculations about the role of the surrounding ice sheet for the generation of these phases. However, one exception was found: a similar phase, parallel to the PmP but 1 s later, is also observed on station 363 although this station is not situated on a nunatak.

Profiles SBK (94310), BRE (94300) and GAA (94400)

The most striking features of crustal structure found in the fjord area are the pronounced topography of the Moho and a high velocity layer in the lower crust beneath the Mesozoic basins. Modelling of profiles SBK, BRE and GAA was undertaken in order to check for the existence and extent of these features towards the north and south.

Profile SBK (94310)

Along the 222 km long profile SBK (Fig. 4.3, Fig. 4.4) only 4 receivers were deployed. One of the receivers (station 313) did not record interpretable seismic signals. Therefore, the station spacing was 50 km in the northern part and 172 km in the southern part.

Geologically, exposures of Mesozoic sedimentary rocks and Tertiary basalts alternate along the profile. This results in considerable variations in the seismic velocity of the uppermost crust. The different slopes of the travel time curves (Fig. 4.23) of the Pg phase of station 312 compared to 314, for example, illustrate the regional differences in seismic velocity. In addition, station 314 shows a Pg branch of high velocity preceding a slower Pg phase. However, the large station spacing did not allow resolution of this heterogeneity of the upper crust. Fig. 4.24 shows the ray tracing through the upper crust of a preliminary model. The ray coverage of the upper crust is poor and no reversed configuration is attained. Preliminary modelling using as an additional constraint the models for the profiles BRE and KFJ, which intersect the profile SBK at its ends, showed that the observed arrivals might agree with the existence of a high velocity layer in the lower crust of the southern part of the profile. However, due to the uncertainties of the velocity structure in the upper crust, conclusions on the lower crustal structure are ambiguous. The profile SBK could therefore not be used as supporting evidence for a high velocity layer in the lower crust.

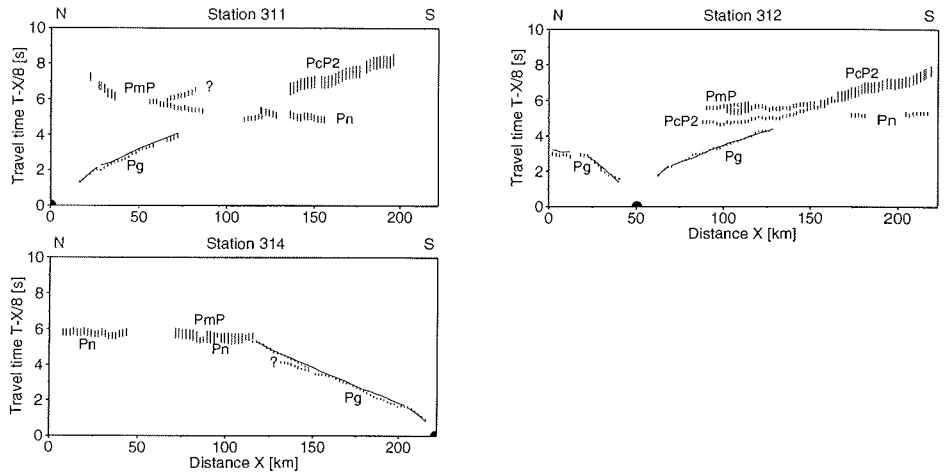

Fig. 4.23: Observed P-wave arrivals for profile SBK. The calculated arrivals of the Pg phase for a preliminary model are marked. For explanation of symbols see Fig. 4.8.

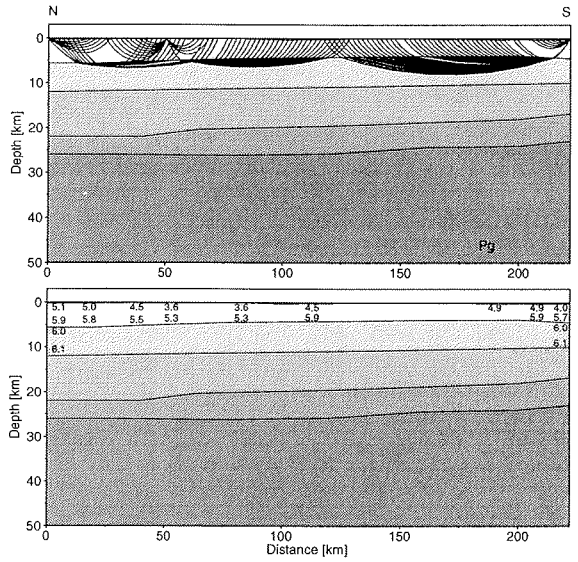

Fig. 4.24: Ray tracing through the uppermost crust of the preliminary model for profile SBK. The parameterization of the uppermost crust is shown below. Note the regional variations in P-wave velocity and the poor constraint by rays. Vertical exaggeration x2.

Profile BRE (94300)

Profile BRE follows Bredefjord from west to east for 210 km. Eight receivers were deployed, the data of 6 of them could be used (Fig. 4.25). The resulting interpolated model is shown in Fig. 4.26.

Seismic velocities in the upper crust are slightly reduced compared to the southern profiles. Values of 5.1 km/s to 5.6 km/s at the surface increasing to 6 km/s at 4 km depth are connected with the thick pile of Eleonore Bay Supergroup sedimentary rocks in Bredefjord (Escher & Pulvertaft, 1995). To the east, velocities of about 4.2 km/s indicate the edge of Mesozoic sedimentary cover. The deflection in all travel time curves at about km 170 is probably due to Tertiary basalts. Velocities of 5.6 km/s to 5.9 km/s account for this structure.

There is little constraint on middle crustal reflectors on this profile. Hence, velocities were modelled to increase to about 6.5 km/s in 20 to 25 km depth, where PcP2 phases recorded by 4 stations yield evidence for a reflector. No observations of lower crustal velocities are available. PmP and Pn phases could be accounted for by assuming velocities to increase from 6.6 km/s to 6.8 km/s at the base of the crust. The Moho dips westwards from 25 km to 35 km depth. The two slopes and a plateau at 30 km depth are still visible but less pronounced than further south. In contrast to the southern profiles, the PcP2 reflector does not merge with the Moho at its western slope.

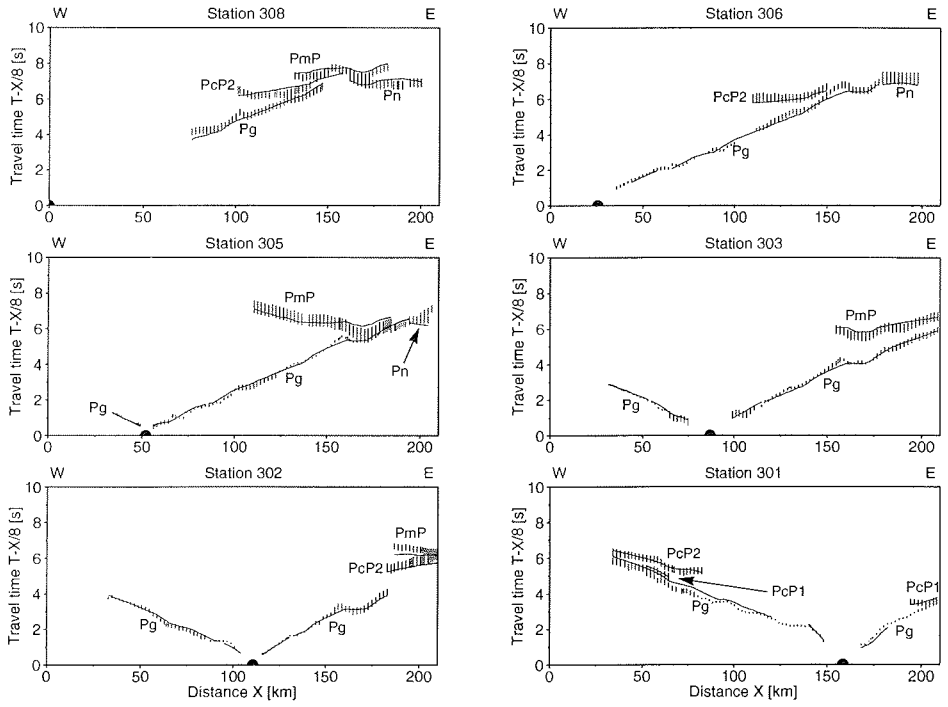

Fig. 4.25: Observed and calculated P-wave arrivals for profile BRE. For explanation of symbols see Fig. 4.8.

Profile GAA (94400)

The seismic refraction data of profile 90300 through Gåsefjord, shot during summer 1990, were modelled by Mandler (1995). The resulting seismic model shows unusually high velocities already at shallow depths. The value of 6.6 km/s at 12 km depth is exceptionally high compared to the global average for orogens of 6.06 ± 0.39 km/s at 10 km depth (Christensen & Mooney, 1995). A value of 7.1 km/s was modelled for the lower crust. As a consequence of the high seismic velocities, a large crustal thickness of at least 48 km had to be introduced in order to account for PmP and Pn phases. In addition, at 3 stations a second PmP phase with slightly different apparent velocity is seen in the western part of the profile over a maximum of 40 km offset range. Mandler (1995) interpreted this as indicating layering of the Moho and he introduced a seismic high velocity layer with 7.3 km/s at the Moho slope at about 40 km depth. Its maximum thickness reaches 3 km, although, the usual thickness is about 1-2 km, which corresponds to 1-2 wavelengths of the PmP wave and is hence at the limit of resolution.

As these results considerably differ from the observations in the fjord region, the profile 90300, which was re-shot and extended in 1994 as profile GAA (94400), was re-interpreted incorporating new data from stations 404 and 401. The observed and calculated arrivals are shown in Fig. 4.27, the resulting interpolated velocity model in Fig. 4.28.

A surface layer with velocities increasing from 5.6 km/s to about 6.1 km/s in 2 km depth was modelled in the south-west part of the profile. The Mesozoic Jameson Land Basin was studied in detail by Fechner & Jokat (1996) and their results were used for the seis-

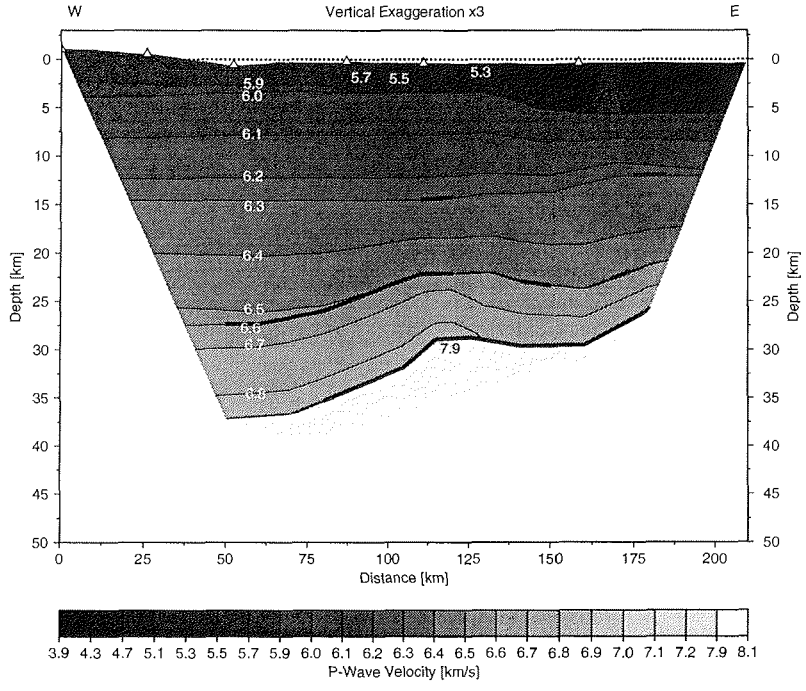

Fig. 4.26: Interpolated P-wave velocity model for profile BRE. For legend see Fig. 4.10

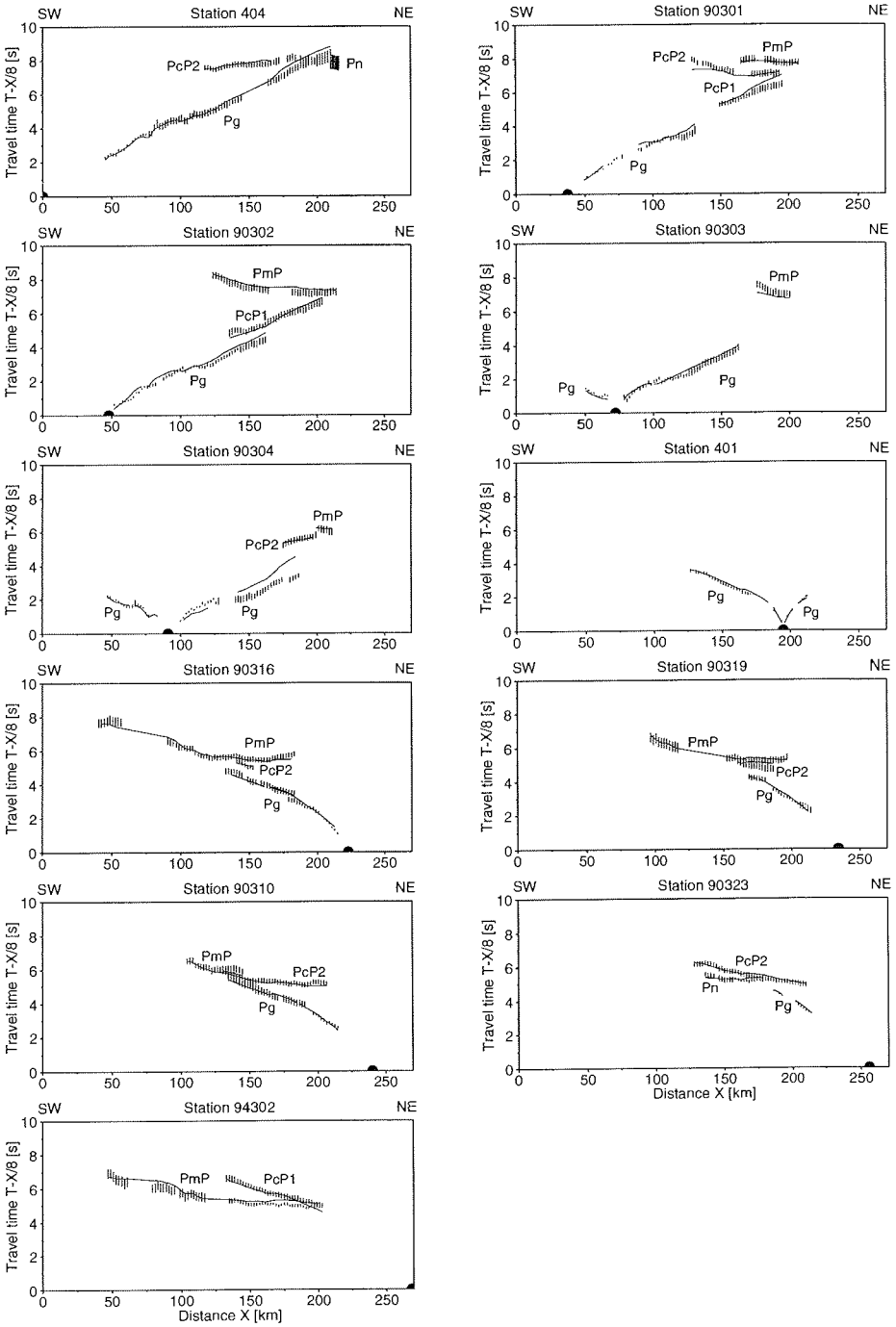

Fig. 4.27: Observed and calculated P-wave arrivals for profile GAA. For explanation of symbols see Fig. 4.8.

mic structure of the north-east part of the profile. Below the surface layer, the fairly constant slope of the Pg branches of about 6.2 km/s rather supports a small velocity gradient than an increase from 6.1 km/s to 6.6 km/s at 2 to 12 km depth. However, regional occurrences of higher velocities than 6.2 km/s in the upper crust cannot be excluded. For example, the western Pg branch of station 304 suggests between km 130 and 180 higher velocities than the other stations. As it is the only exception and all other arrivals were satisfactorily explained by the model, the Pg branch of 304 was considered to indicate a small-scale heterogeneity which was not modelled.

No direct evidence for P-wave velocities exists beneath 12 km depth. Reflections from two infracrustal reflectors were observed. The seismic velocity between these reflectors was assumed to increase continuously from 6.35 km/s to a maximum of 6.7 km/s at 34 km depth. Seismic velocities of 6.8 km/s to 7.0 km/s were modelled for the lowermost crust. These values are in agreement with both observations from the fjord region and global average values for orogens (Christensen & Mooney, 1995). The t^2x^2 - method used by Mandler (1995) to infer lower crustal mean velocities from PmP phases yielded inconclusive results. The limited offset range of the observed PmP hyperbolas does not make it possible to detect and account for the effects of inhomogeneity in the upper crust and the incline of the Moho.

The PcP2 reflector and the Moho show a prominent slope. Moho depth increases continuously from about 22 km beneath the sedimentary basin to about 40 km depth beneath the Caledonian orogen corresponding to the observations in the fjord region. However, no Moho plateau at 30 km depth was seen here.

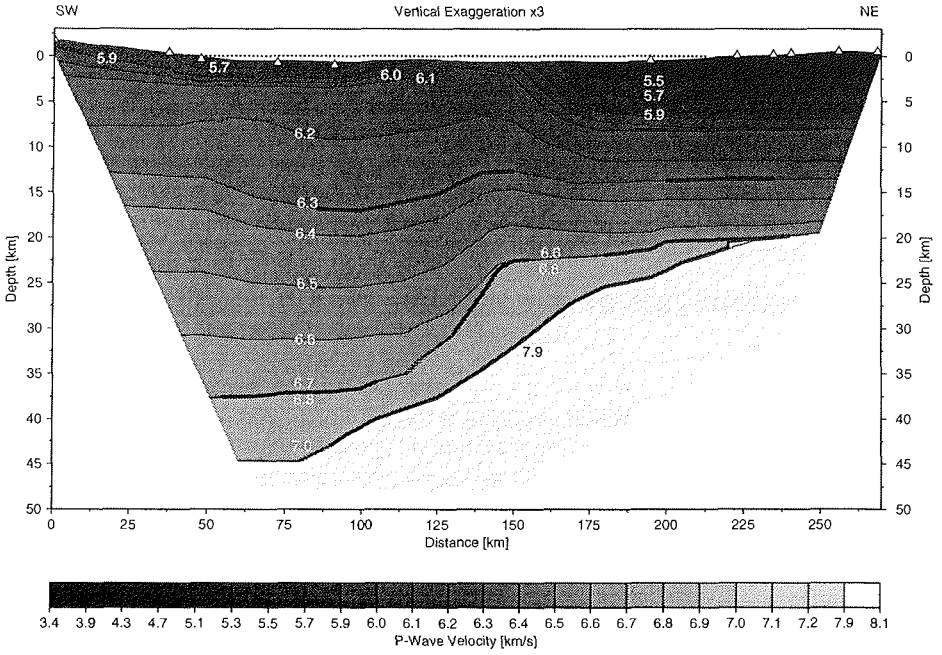

Fig. 4.28: Interpolated P-wave velocity model for profile GAA. For legend see Fig. 4.10.

A high velocity layer, accounting for the second PmP phase, was deliberately not included in this model. The reflected energy originates from the Moho slope. If the profile is not perpendicular to the strike of the slope, side-reflections might cause a comparable signature of the Moho. In addition, the available data do not constrain the lower crust and the Moho in enough detail to yield convincing evidence for the existence or absence of a high velocity layer. Mandler (1995) estimates the uncertainty of the Moho depth to ± 4 km, hence a 0-3 km thick high velocity layer at the Moho is below the resolution of the model. The character of the PmP reflection will therefore rather considered qualitatively as a possible indication of a complex structure of the base of the crust.

4.2.5 Key results

Forward modelling of 6 seismic refraction profiles by ray tracing yielded a first insight in the crustal structure of the fjord region of East Greenland and the neighbouring areas to the north and south.

The crust beneath the Caledonian mountain range is fairly homogeneous without marked reflectivity. Its thickness exceeds 43 km. The Moho rises eastwards and forms a plateau in about 30 km depth beneath the Devonian basins in the fjord region of East Greenland. This plateau is only weakly developed in the Bredefjord area to the north and is absent in the Scoresby Sund area. Here, the Moho rises continuously to about 22 km depth. On all profiles, a pronounced westward dipping reflector in the lower crust runs parallel to the Moho.

A striking feature of the crustal architecture is encountered only in the fjord region of East Greenland (profiles KFJ, DKS and KOF). From the plateau in about 30 km depth the Moho rises in a second slope to about 22 km beneath the Mesozoic sedimentary basins. In this area, a high velocity layer is situated in the lowermost crust. It is about 6 km thick and has P-wave velocities in excess of 7.1 km/s. Its top at about 16 km depth is connected with a large contrast in acoustic impedance resulting in prominent reflections. The northward extent of this high velocity layer could not be determined as the data cover on profile SBK is too poor. The high velocity layer at the Moho slope in the Scoresby Sund area as proposed by Mandler (1995) could not be confirmed.

4.3 Joint analysis of geophysical data

4.3.1 Method

The seismic models of the crustal structure in the fjord region formed the basis for joint modelling of seismic, gravity and magnetic data. The gravity data were extracted from the gridded Bouguer anomaly map along the projected seismic profiles, i.e. the model planes. Low-level aeromagnetic survey data flown along the shiptracks of KFJ, KOF and DKS were projected into the respective model planes.

The geometry of the seismic models was expressed in polygons. A representative P-wave velocity was assigned to each polygon. These velocities were converted to densities using an experimental, depth-dependent, nonlinear relationship between density and P-wave velocity derived by Christensen & Mooney (1995) for continental crust (Appendix 3a). As the relationship is not valid for sedimentary rocks, densities determined

from the Nafe-Drake curve (Nafe & Drake, 1957) served as starting values which were adjusted during modelling. To account for the observed Bouguer gravity, the Moho was modelled in areas were it was not constrained previously by seismic data.

Joint analysis of magnetic data, seismic data and geological information allowed identification of magnetized parts of the crust. Preliminary forward modelling served to test if the sources can explain the magnetic anomalies without geologically unreasonable assumptions for the geometry or magnetic properties of the source.

Gravity and magnetic anomalies were modelled using the commercial software package LCT. The gravity and magnetic effect of the 2-D model is calculated based on the Talwani-type polygon parameterization of the model (Talwani et al., 1959; Talwani, 1965).

4.3.2 Combined models for the crustal structure of the fjord region of East Greenland

The resulting models for seismic and potential field data will be illustrated in detail using profile KFJ as an example followed by a discussion of similarities and differences of profiles DKS and KOF.

Profile KFJ

Gravity: Fig. 4.29 shows the polygon parameterization of profile KFJ. Changes with respect to the layers 1-5 of the seismic model (Fig. 4.9) were made in the upper crust and lower crust. Layer 1 was subdivided into 3 polygons accounting for the different seismic velocities. The upper part of the Mesozoic sedimentary basin forms one polygon with 4.2 km/s typical P-wave velocity. The lower part of the basin and the Devonian sedimentary rocks were assigned a representative velocity of 5.55 km/s and the third polygon represents the Caledonian rocks with roughly 5.85 km/s. The western part of layer 3 comprising the middle and lower Caledonian crust was subdivided on the basis of the velocity-depth profile into an upper part with 6.4 km/s and a lower part with typically 6.7 km/s. This reflects the compositional change from a silica-rich upper and middle crust to a mafic lower crust. An approximate depth of 27 km for this transition agrees well with the global average crustal model of Christensen & Mooney (1995). Layer 4 consists of a polygon with lower crustal velocities of about 6.75 km/s to the west. The high velocity layer was assigned a velocity of 7.2 km/s. East of the high velocity layer, velocities were poorly constrained. Velocities comparable to layer 3 were assumed. Appendix 3b shows the depth-dependent conversion of velocities to densities.

The subsequent modelling held the geometry of the model as well as the above determined densities fixed. The only parameters to be varied were the Moho depth in the east and west end of the profile where it was not defined by seismic data and the densities of the sedimentary rocks in the upper crust. With this approach the long-wavelength component of the observed Bouguer gravity could satisfactorily be modelled.

The residues have short-wavelength character. Their maximum amplitude is 28 mgal at km 287 whereas the average absolute residuum is about 6 mgal. It has not been attempted to account for these remaining short-wavelength anomalies as their origin is unclear and their size might reflect the accuracy of the gravity data set.

Modelling resulted in a density of $2.30 \cdot 10^3$ kg/m^3 for the upper part of the sedimentary basin which is consistent with the density of the Jurassic sedimentary rocks of the Jameson Land Basin derived from gravimetric studies by Forsberg (1986). A density of

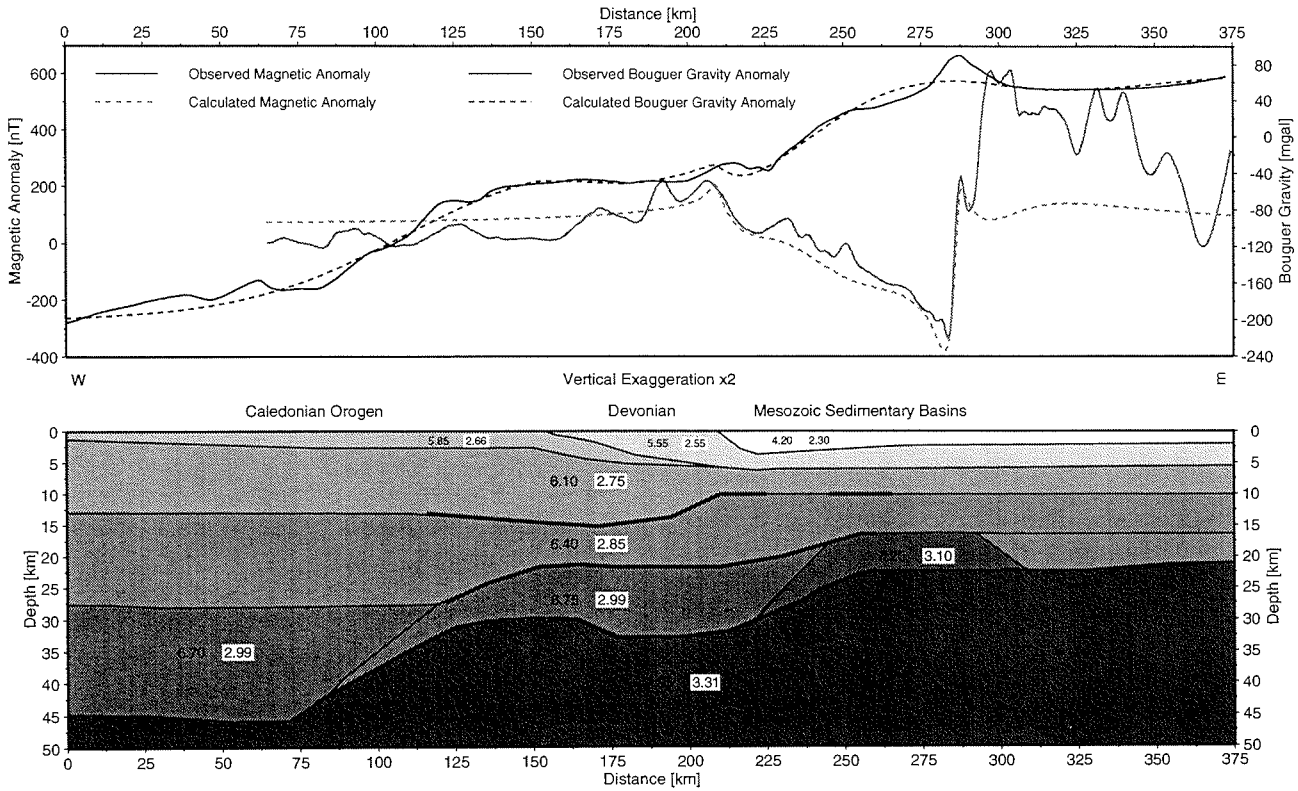

Fig. 4.29: Modelling of potential field data along profile KFJ. The seismic model is expressed as polygons of constant velocity (black numbers). Converted densities are highlighted in white. Bold lines mark reflectors (c.f. Fig. 4.10). Observed and calculated potential field data are shown above. Magnetic source bodies are discussed in the text.

$2.55 \cdot 10^3$ kg/m^3 for the Devonian sedimentary rocks is close to the value predicted by the Nafe-Drake curve (Nafe & Drake, 1957) for P-wave velocities of about 5.55 km/s. Moho depth was adjusted to a maximum depth of 45 km beneath the Caledonian orogen. At the east end of the profile the Moho further rises to about 20 km depth.

Magnetics: The magnetic field along the profile (Fig. 4.29) is dominated by a prominent negative magnetic anomaly (anomaly (21) in Fig. 3.15). Modelling and interpretation of this anomaly is based on the following geophysical and geological observations:

- *Geologic setting.* The magnetic anomaly is situated along the onshore short-cut between two rift segments A and B of the initial break-up the North Atlantic (Fig. 4.30). The strike direction of the anomaly is parallel to the rift. The anomaly coincides with exposures of the Mesozoic sedimentary basins onshore. The basins are intruded by Tertiary dykes and sills and partly overlain by Tertiary tholeiitic basalts (see chapter 3.3.3). As discussed in chapter 3.3.3 the magnetic anomaly is clearly related to the Tertiary volcanic activity but cannot be explained by the exposed Tertiary volcanics alone.
- *Magnetic signature.* The shape of the magnetic anomaly gives additional hints as to the location of possible source bodies. Short-wavelength anomalies correlating with exposures of basalts are superimposed on a long-wavelength trend of the anomaly forming the prominent slope from km 200 to 275. This magnetic signature is even

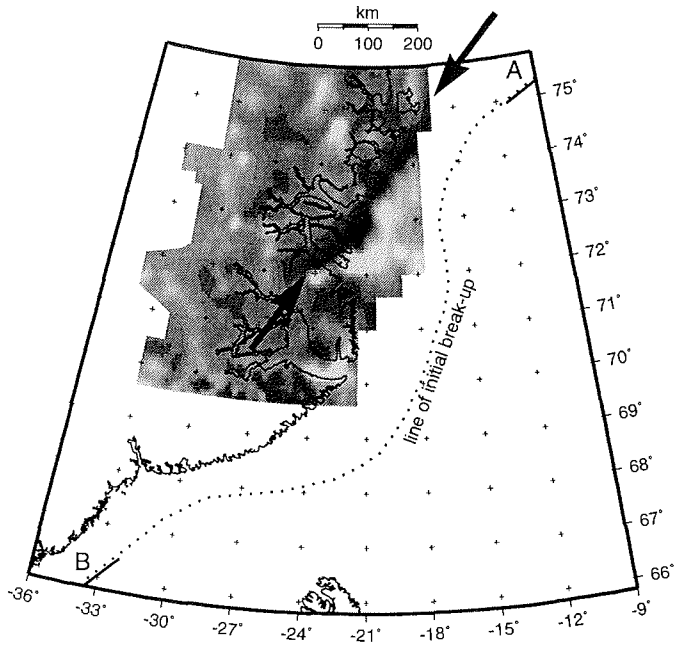

Fig. 4.30: Position of negative magnetic anomaly (arrows) with respect to the line of initial break-up of the North Atlantic (dotted line; after Larsen & Watt, 1985) and the oldest marine magnetic anomalies 24 B (bold line; after Escher & Pulvertaft, 1995) defining the rift segments A and B. For grey-scale refer to Fig. 4.31. Scale valid at 72°N.

more obvious from the detailed aeromagnetic data set of Larsen (1977). A composite source consisting of the exposed sources and a deep-seated source producing the long-wavelength anomaly can most easily account for the observed anomalies without requiring a special source geometry.

In addition, the long-wavelength part of the anomaly cannot be explained as an edge effect of, for example, the positive anomaly to the east. Its edge produces the steep flank and the minimum of the negative anomaly. The negative anomaly therefore requires a source body which carries a remanent magnetisation acquired during a reversed polarity epoch of the Earth's magnetic field.

- *Seismic evidence.* On all three seismic profiles through the fjord region the negative magnetic anomaly coincides with the position of the seismic high velocity layer. This is illustrated in Fig. 4.31.

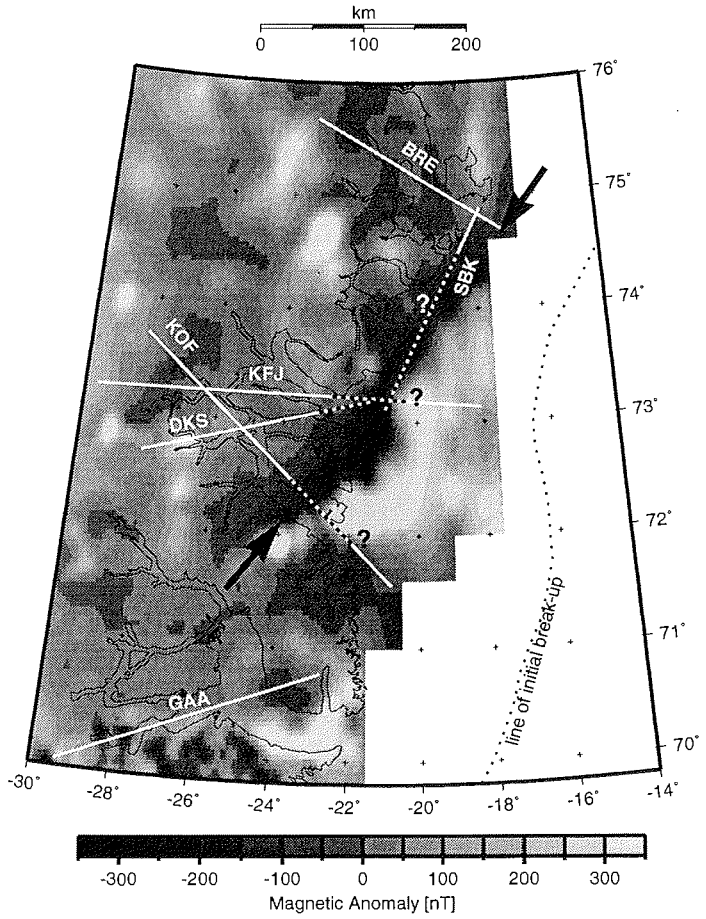

Fig. 4.31: Position of seismic high velocity layer (dashed line) on each seismic profile (white lines) as compared to the prominent negative magnetic anomaly (arrows). The eastward extent of the high velocity layer and its existence along profile SBK are speculative. Scale valid at 72°N.

The geologic setting and the characteristics of the magnetic anomaly favour a deep-seated source of magmatic origin produced during the Tertiary volcanic event. The correlation between magnetic anomaly and seismic high velocity layer suggests an interpretation of the high velocity layer as a magmatic underplate carrying a reversed remanent magnetisation.

To test this interpretation, a primitive forward modelling of the magnetic anomaly was undertaken. The seismic high velocity layer was given a remanent and induced magnetisation, which in this case have opposite direction. The net magnetisation necessary to account for the slope of the negative magnetic anomaly was about 0.22 A/m. This relatively weak magnetisation of the magmatic underplate might indicate that only parts of it actually exhibit magnetic properties.

In addition, tests were made to incorporate the basalts at the surface and account for the steep flank of the anomaly at km 285. The positive anomaly (see chapter Fig. 3.3.3, anomaly 23) is assumed to be produced by a layer of younger (normal polarity) volcanics overlying a thin sheet of older (reversed polarity) basalts. Using published average susceptibility and Q data for both extrusives ($10 \cdot 10^{-3}$ SI units; Q = 2.8; Abrahamsen & Nordgerd, 1994) a normal polarity volcanic layer of about 20 m thickness extending at the surface from km 285 towards the east can produce the observed steep flank (Fig. 4.29). The short-wavelength positive anomalies east of this flank are considered to result from topography or interruptions of this layer. However, this modelling only shows that no unreasonable assumptions have to be made. An infinity of other solutions are conceivable if the distribution and topography of the basalts and their magnetic properties are not known in detail.

Profile DKS

Gravity: The same parameters for the P-wave velocity-density conversion were used as for profile KFJ (Appendix 3b). The observed gravity could be fitted apart from the significant discrepancy between km 37 and 97. Here, the misfit reaches 57 mgal, which is beyond the error inherent in the data. Data coverage is relatively poor in this area. A single unreliable measurement might therefore have a significant effect. However, the poorly fitting part of the profile is too extended to result from a single outlier in the data set. Therefore, an explanation in terms of geology must be sought. The area roughly coincides with the Gletscherland infracrustal complex (Higgins et al., 1981). The Gletscherland complex represents a magnetically outstanding feature, as in contrast to the surrounding geological units it may host high amplitude magnetic anomalies (see chapter 3.3.2). It may therefore also have anomalous densities. However, on the Bouguer anomaly map (Fig. 4.2), a regional correlation between the positive anomaly and the Gletscherland complex is not obvious. In addition, seismic data yield no hints of increased seismic velocities, but high-density bodies in the mountains above the seismic receiver elevation or off the profile cannot be detected and might affect the gravity data. The origin of the large positive gravity residuum therefore has to remain unexplained.

Magnetics: Fig. 4.32 shows the observed magnetic anomalies. Apart from the high amplitude anomalies over the Gletscherland complex, the negative magnetic anomaly associated with Tertiary igneous activity is cut at the east end of the profile. The composite character of the anomaly, consisting of short-wavelength anomalies produced at shallow depth superimposed on a long-wavelength negative anomaly originating from a deep source, is very evident. The anomaly could be accounted for using the same modelling parameters as for profile KFJ.

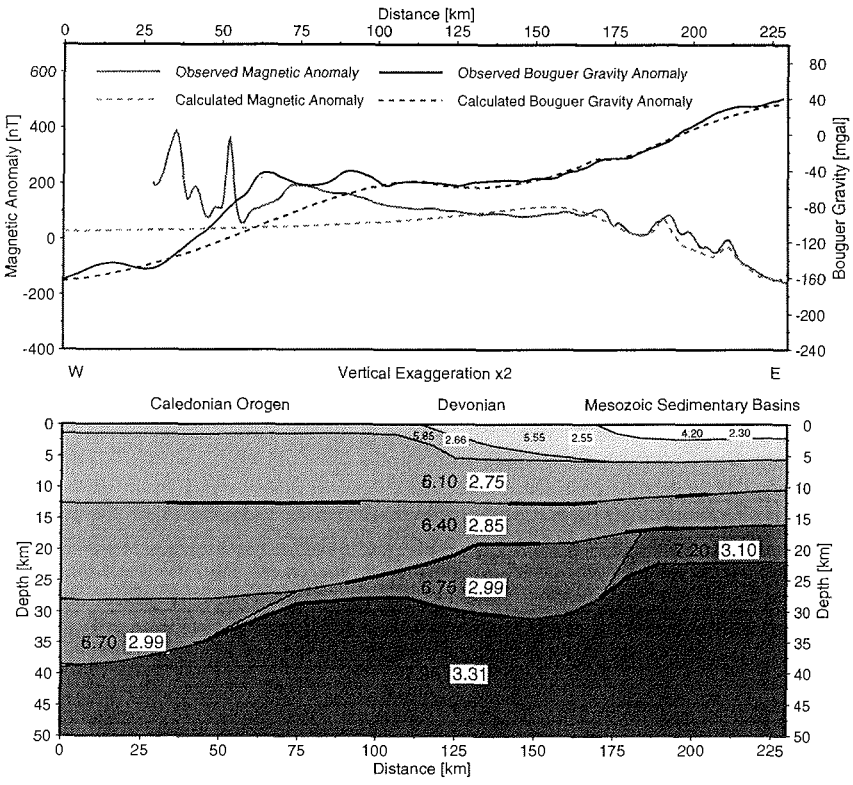

Fig. 4.32: Modelling of potential field data along profile DKS. The seismic model is expressed as polygons of constant velocity (black numbers). Converted densities are highlighted in white. Bold lines mark reflectors (c.f. Fig. 4.16). Observed and calculated potential field data are shown above.

Profile KOF

Gravity: Due to the pronounced non-straight geometry of the profile KOF difficulties were encountered in modelling. The profile is oriented oblique rather than perpendicular to the strike of the geological structures (Fig. 4.31). In particular, Pg rays do not travel in the model plane and therefore sample different structures than the gravity data.

The same velocity-density conversion as for profile KFJ was used, except for the high velocity layer, which is here better characterized by a velocity of 7.1 km/s (Appendix 3b). The Moho was adjusted to fit the long-wavelength trend in the gravity data. The Moho rises to about 19 km depth at the east end of the profile. A maximum depth of about 44 km is reached beneath the Caledonian range. The middle part of the model above the Moho plateau was difficult to model. The plateau is about 100 km wide as on the other profiles. However, gravity shows a local minimum here, which could not be accounted for using the seismically defined geometry of the sedimentary basins. The contact between Devonian and post-Devonian sedimentary rocks is located at

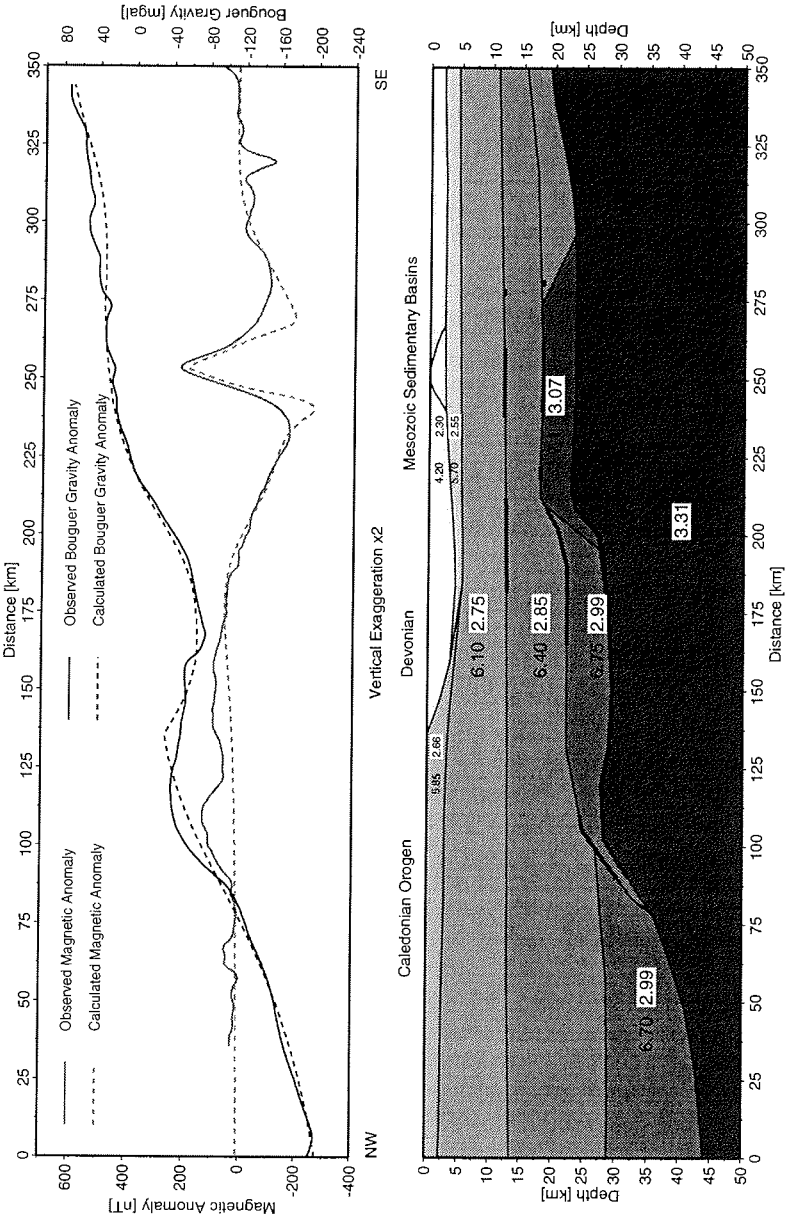

Fig. 4.33: Modelling of potential field data along profile KOF. The seismic model is expressed as polygons of constant velocity (black numbers). Converted densities are highlighted in white. Bold lines mark reflectors (c.f. Fig. 4.21). Observed and calculated potential field data are shown above. Magnetic source bodies are discussed in the text.

about km 184. The typical P-wave velocities of the Devonian basin west of km 184 are not observed, as P-waves probably travel on the west side of the Western Fault Zone in Caledonian rocks. Nevertheless, gravity is affected by the low-density Devonian sedimentary rocks. Therefore, as on the other profiles a density of $2.55 \cdot 10^3$ kg/m^3 was modelled between the km 184 and the Western Fault Zone at km 158. However, large residues still remained and the low-density body was extended to km 137 across Ella Ø where Devonian outcrops are present. In addition, the density needed to be reduced to $2.30 \cdot 10^3$ kg/m^3 as in the post-Devonian sedimentary rocks. No geological explanation could be found for these regional differences in the density of the Devonian rocks. In addition, it is not possible to estimate to what extent the unfavourable profile direction and inherent errors in the data influence this misfit. For example, the gravity slope at km 158 could be produced by a discontinuity in the data set due to the transition from land to marine data as the fjord is crossed. On the other hand, a downthrow of the Devonian block east of the Western Fault Zone of about 3 km, as proposed by Larsen & Bengaard (1991), might cause the local gravity minimum.

Magnetics: The negative magnetic anomaly on this profile is superimposed by a prominent positive anomaly (Fig. 4.33). It is produced by alkaline magmatism about 30 Ma ago (see chapter 3.3.3, anomaly 23). Modelling showed, that the shape of the magnetic anomaly can be reproduced by introducing in addition to the magmatic underplate a magnetically susceptible body at shallow depth. As both geometry and magnetic properties of the source cannot be determined, the modelled source has to be considered as representing one of an infinity of possible solutions.

4.3.3 Discussion

Is a magmatic underplate likely ...

... to carry a remanent magnetisation?

The magmatic underplate extends over a depth from 16 - 22 km. It can only exhibit magnetic properties, if the Curie temperature is not exceeded. If magnetite is the dominant magnetic mineral, the Curie temperature roughly coincides with the 600° C isotherm (Shive et al., 1992). For a standard geotherm, 600° C is reached at about 40 km depth (e.g. Fowler & Nisbet, 1982). However, depending on the geothermal conditions, Curie depths for magnetite range from 20 km in the Basin and Range province to 74 km for the Sierra Nevada (Shive et al., 1992). Hence, at least the upper part of the magmatic underplate can be assumed to carry a magnetisation and produce the observed anomaly.

As the observed magnetic effect of the magmatic underplate is relatively weak (c.f. net magnetisation), it could be possible that a part of the underplate is situated beneath the Curie depth, that the high velocity layer represents a layered intrusion consisting only partially of intrusive material or that strong induced and remanent magnetisations almost cancel each other (Q~1). As nothing is known about the geothermal conditions in this area and the magnetic properties of the intrusives, no conclusions can be made.

Evolved mafic magma at the base of the crust is considered a likely source of sizable magnetic anomalies (Wasilewski & Mayhew, 1982). McSwiggin et al. (1987) interpreted the magnetic anomalies associated with the Middle Proterozoic mid-continental rift of America as due to volcanics and intrusive rocks occurring in the centre of the rift down to a depth of 20 km.

... to be positioned at the Moho?

As the density of the melts is between the density of the lower crust and the Moho, the melts tend to pond at the crust-mantle boundary (e.g. White, 1992).

... to exist in this geological setting?

The magmatic underplate is situated in a rift environment beneath Mesozoic sedimentary basins. At about 64 Ma, the Iceland hotspot impinges on the lithosphere of Greenland (White & McKenzie, 1989, Hill, 1991). Beneath the thinned continental crust, the thermal anomaly of the hotspot leads to the production of large volumes of melt (White & McKenzie, 1989). During a reversed polarity epoch, probably 26r, 25r, or 24r (Saunders et al., 1997), vast amounts of flood basalts extruded to form the Geikie Plateau south of Scoresby Sund whereas only minor volumes of flood basalts are found north of Kong Oscar Fjord in the area of the magmatic underplate. Upton et al. (1995) examined the petrology of these northern flood basalts and proposed that a large part of the melts from which the basalts derived may have been retained at depth in a magmatic underplate.

Hence, there are geological and petrological arguments to support the interpretation that the magmatic underplate formed in association with the emplacement of the Tertiary flood basalts in East Greenland during a reversed polarity epoch.

... to have the observed dimensions?

The seismic data suggest a thickness of about 6 km for the magmatic underplate. The Tertiary magmatic event which accompanied the break-up of the North Atlantic also underplated the continental margins of the North Atlantic. Although the underplate here is not situated at a continental margin, a comparison with underplates at the continental margins helps to assess the results. Skogseid et al. (1992) modelled a thickness of about 5 km for the underplating of the conjugate Vøring margin.

The western and southern margin of the magmatic underplate in the fjord region of East Greenland are well defined. Magnetic and seismic data control the western margin. The south limit can be inferred from the magnetic anomaly which fades out just south of Kong Oscar Fjord. More difficult to determine is the north extent, as the data cover it only marginally. A change in magnetic signature of the anomaly can be observed just east of Shannon on the magnetic anomaly map of Thorning (1988). The east extent of the magmatic underplate is debatable. The eastern boundary shown in the models has been tentatively inferred from seismic data. However, data coverage in this area is poor. Magnetically, the eastern border is obscured by the strong positive anomaly. On profile KOF, the gentle westward slope just east of the positive anomaly might yield additional support for the modelled geometry. However, both magnetic and seismic data could be reconciled with an underplate stretching out further to the east, possibly as far as the continental margin. Weigel et al. (1995) propose a seismic high velocity layer in about 17-23 km depth off the mouth of Kong Oscar Fjord. However, their data do not constrain the lowermost crust until about 80 km off the coast close to the continental margin. Therefore, no conclusions on a possible continuation of the magmatic underplate towards the continental margin can be made on the basis of this data set.

Assuming a north-south extent from Kong Oscar Fjord to Shannon (about 350 km) and an east-west extent of about 60 km from profile KFJ, the total volume of the 6 km thick magmatic underplate amounts to roughly 126 000 km^3. Not taking possible magmatic material beneath the shelf and the continental margin into account, this volumes has

to be considered in relation to the volume of magmatic products of the Geikie plateau flood basalt province. Larsen et al. (1989) estimate a total production along the 200 km between 69°N and Scoresby Sund of about 120 000 km^3. Nielsen & Brooks (1981) give a figure of 190 000 km^3 for the extrusives south of 70°N. In contrast, the northern flood basalt province produced roughly 24 000 km^3 of basalts (Upton et al., 1984). Adding this value to the volume of the magmatic underplate situated beneath this area, a total melt production of about 150 000 km^3 results. Large uncertainties are involved in this estimate, in particular concerning the east extent of the underplate and potential underplating beneath the Geikie Plateau. However, it demonstrates that the dimensions of the modelled magmatic underplate are not unrealistic in terms of melt production along the onshore short-cut between the rift segments of the nascent North Atlantic rift.

4.3.4 Key results

From a combination of magnetic, seismic and geological observations, the existence of an about 6 km thick magmatic underplate beneath the Mesozoic basins north of Kong Oscar Fjord can be shown. It formed during the emplacement of the onshore flood basalt provinces of East Greenland. Its dimensions probably reflect melt productivity along the Tertiary rift, although, there is uncertainty as to the east extent of the underplate.

Using a P-wave velocity to density conversion and adjusting the Moho topography in seismically unconstrained areas, the crustal model derived from seismic data can account for the long wavelength trend of the Bouguer anomaly. Local residues could partially be explained in terms of geology. The combined gravimetric effects of the Moho topography and the associated sedimentary basins at the surface results in a Bouguer anomaly which reflects the topography of the Moho remarkably well. Fig. 4.34 shows the horizontal derivative of the Bouguer anomaly map. It is calculated along west direction. Hence, the westward directed gradients in the Bouguer map appear as positive anomalies. This map can be used to infer the location and regional trends of the Moho slopes, which are of particular interest for further interpretation. However, care has to be taken when interpreting the gravity gradients as Moho slopes. For example, the extension of the eastern Bouguer gradient across Kong Oscar Fjord beyond 72°N 24°W is due to the local gravity minimum caused by the Stauning Alper granites rather than to Moho topography.

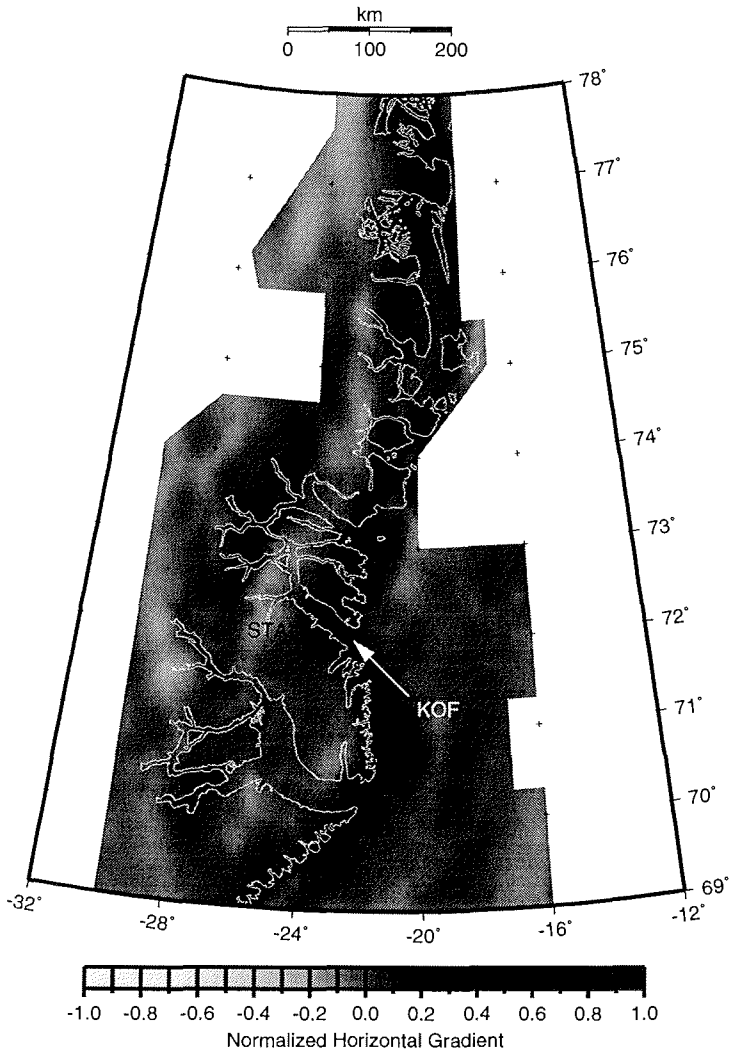

Fig. 4.34: Horizontal gradient along 270° of the Bouguer anomaly map in Fig. 4.2. Dark colours represent westward gradients of the Bouguer anomaly. They coincide with slopes in the Moho apart from the area south of Kong Oscar Fjord (KOF) close to the Stauning Alper (STA) (see text). Scale valid at 72°N.

5 Post-Caledonian evolution of East Greenland

5.1 Model for the crustal evolution of East Greenland

The joint analysis of the geophysical data sets yielded models for the architecture of the continental crust of East Greenland between Gåsefjord (69°N) and Bredefjord (75°N). These results are now considered and interpreted in a regional geological framework. A model for the crustal evolution of East Greenland following the Caledonian orogeny is derived and discussed below. The model is based on a reconnaissance type data set, and is therefore very simplistic and intended to explain prominent regional-scale structures. It does not claim to account for all aspects of the complex real evolution.

5.1.1 Crustal structure of the East Greenland Caledonides

The closure of the Iapetus ocean and the subsequent continental collision between Laurentia (North America) and Baltica (Europe) led to the formation of the Caledonian fold belt in Silurian times (e.g. Ziegler, 1989; Soper et al., 1992). The Precambrian crust of East Greenland underwent deformation and metamorphism of varying intensity. Geophysical data characterize its present structure. Seismic and gravity data constrain the maximum thickness of the crust beneath the Caledonian mountains to about 45 km. The only indications on the original thickness of the Caledonian crust at the time of orogeny stem from Caledonian eclogites found in a zone north of Danmarkshavn (77°N, Fig. 5.2) (Gilotti, 1993; Brueckner & Gilotti, 1993). They formed at pressures in excess of 15 kbar (Gilotti, 1994) indicating a crustal thickness of more than 55 km.

In the seismic refraction data, the Caledonian crustal block appears as seismically relatively transparent and void of marked reflectors. The internal structure of the Caledonian orogen is best revealed from its magnetic characteristics. The northern part of the Caledonides shows a fairly homogeneous magnetic pattern. Areas which were involved in thick-skinned Caledonian tectonics were demagnetized during orogeny. South of about 76°N, the orogen is more heterogeneous. The results of ground and airborne magnetic studies might place constraints on regional variations in the degree and intensity of Caledonian deformation and metamorphism.

5.1.2 Devonian extensional collapse of the East Greenland Caledonides

After the compressional tectonics had ceased, the overthickened Caledonian crustal wedge collapsed (e.g. McClay et al., 1986). Extensional collapse along regional-scale extensional faults is a common phenomenon widely observed in orogens (e.g. Basin and Range (Coney & Harms, 1984), Himalayas (Burchfield & Royden, 1985)). Displacement along extensional faults provides an effective mechanism for the thinning of overthickened lithosphere to a pre-orogenic thickness (Dewey, 1988) and generally follows about 20-30 Ma after the crustal thickening.

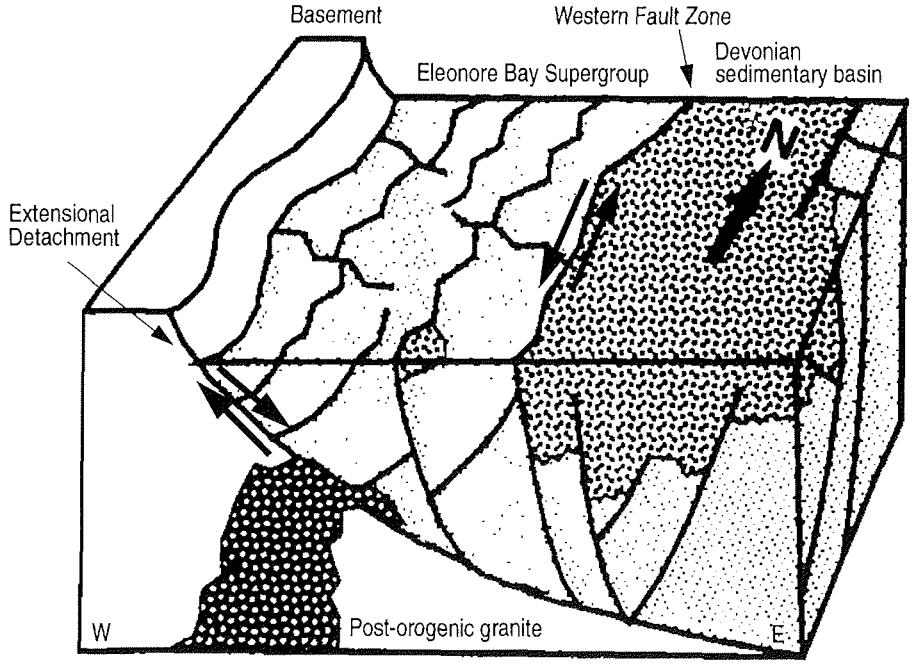

Fig. 5.1: Model for the extensional detachment in Kejser Franz Joseph Fjord (after Hartz & Andresen, 1995).

A variety of surface structures testify to Late Silurian to Early Devonian extensional tectonics in East Greenland.

- Fault-controlled Devonian intra-montane basins formed in Norway, Britain and East Greenland (McClay et al., 1986). The spectacular examples exposed in the fjord region of East Greenland accumulated up to 8 km of continental sediments (Haller, 1971). The Devonian basins eventually extended further south into the Scoresby Sund area as shown by outcrops along the margins of the Jameson Land Basin (Escher & Pulvertaft, 1995) (Fig. 5.1, Fig. 5.2).
- Reactivation of former compressional structures as extensional fault zones has been recognized in Central and North-East Greenland (Hartz & Andresen, 1995; Strachan, 1994). Eleonore Bay Supergroup sedimentary rocks in the hanging wall of faults are displaced towards the east along an east-dipping extensional detachment. According to Hartz & Andresen (1995), this detachment may have crustal dimensions with the fault-bounded Devonian basins forming in the hanging wall of the detachment (Fig. 5.1).
- The extension was accompanied by sinistral strike-slip motion along major fault zones, for example, the Great Glen fault in Scotland, the Walls Boundary Fault in the Shetlands (McClay et al., 1986) and the Western Fault Zone in East Greenland (Larsen & Bengaard, 1991) (Fig. 5.1, Fig. 5.7).
- Syn- and post-orogenic granites mainly intruded the area between the Eleonore Bay Supergroup rocks and the adjacent Caledonian metamorphic complexes (Henrik-

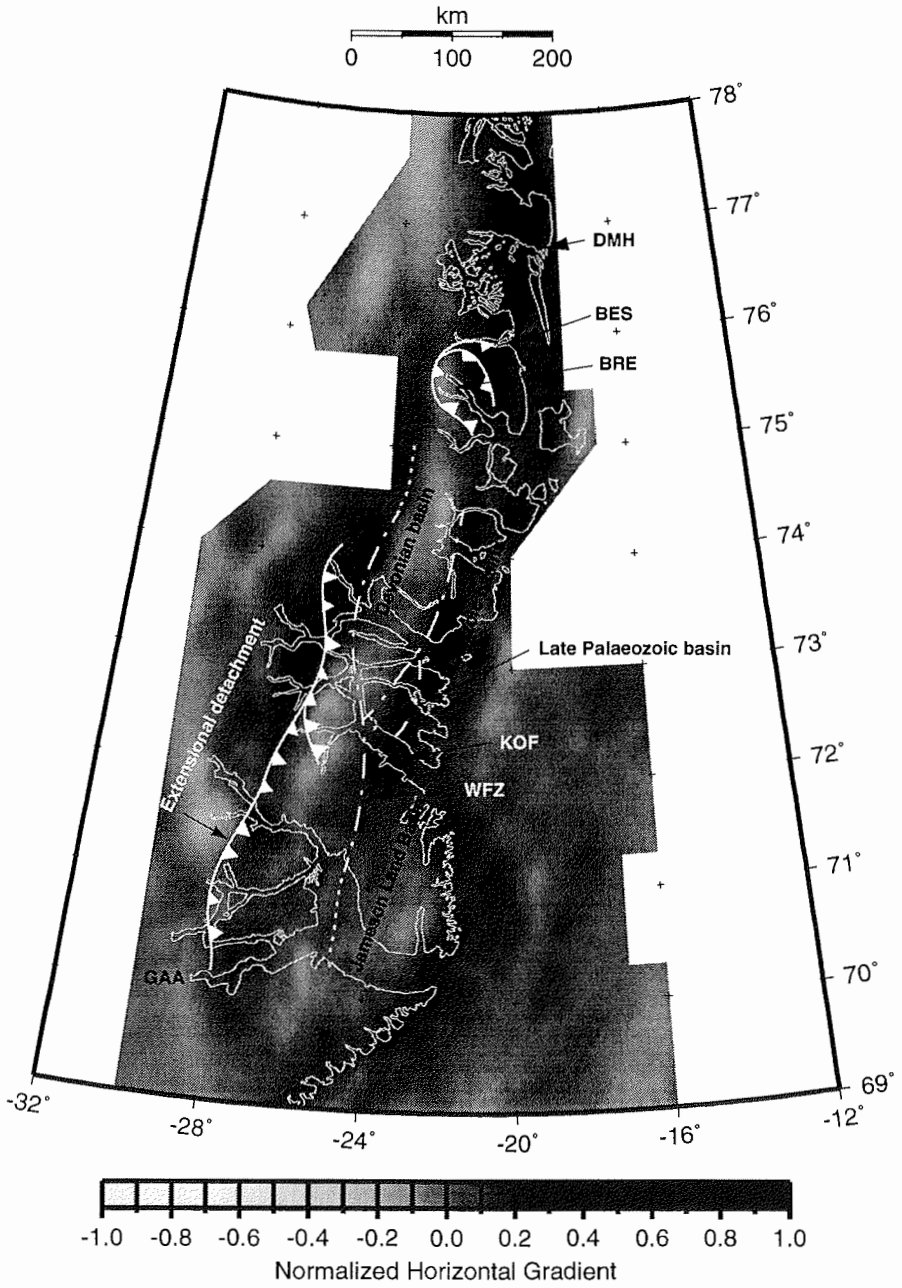

Fig. 5.2: Surface structures active during Devonian extensional collapse in relation to the Moho topography represented by the horizontal gradient along 270° of the Bouguer anomaly map (c.f. Fig. 4.34). GAA: Gåsefjord, WFZ: Western Fault Zone, KOF: Kong Oscar Fjord, BRE: Bredefjord, BES: Bessel Fjord, DMH: Danmarkshavn. Scale valid at 72°N.

sen, 1985). These intrusions partly formed as decompression melts during extension (Hartz & Andresen, 1995; Strachan, 1994). Minor volcanic activity accompanied the sedimentation in the Devonian basins (Henriksen, 1985).

These surface manifestations of the Devonian extensional tectonics are considered in relation to the deep crustal structures, in particular the Moho topography represented by the horizontal gradient of the Bouguer anomaly map (Fig. 5.2). The position of the Devonian basin in the fjord region is exactly mirrored by the plateau of the Moho. Interestingly, the extensional detachment fault more or less follows the western Moho slope. I conclude from these observations that the western Moho slope and the Moho plateau formed during Devonian extensional collapse.

Wernicke (1985) proposed a simple shear model for crustal extension which is derived from very similar surface and deep crustal structures in the Basin and Range Province (Fig. 5.3). Extension is accommodated along a low-angle shear zone envisaged as extending deep into the lithospheric mantle. Discrete shear between two sheets is observed at the surface, where brittle deformation produces a set of related normal faults in the hanging wall of the detachment. Fault bounded sedimentary basins form and fill with coarse clastic sediments. The distal margin of significant upper crustal extension is situated where the shear zone cuts into the mantle. A Moho slope forms in this area. The differences in the relative amounts of thinning of the crust and lithospheric mantle result in a variable subsidence history along the rift. Subsidence is expected where the crust is thinned but not the lithospheric mantle. In Wernicke's model this applies to the proximal side of the area where the shear zone cuts the crust-mantle boundary. Finally, the simple shear model implies that extension is accommodated by asthenospheric convection rather than stretching of the lithosphere as in a pure shear model (McKenzie, 1978).

I propose an analogous model for the Devonian crustal extension in East Greenland based on the surface and deep crustal structures active in Devonian times (Fig. 5.4): The crust failed along a major west-dipping shear zone. The prominent lower crustal

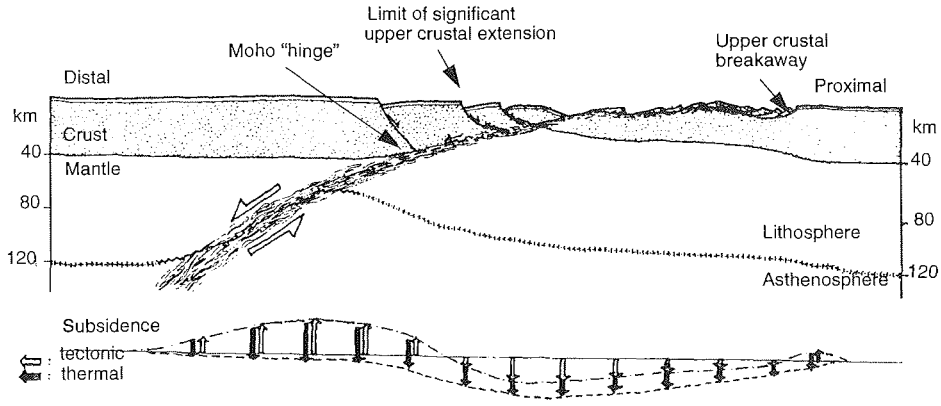

Fig. 5.3: Hypothetic simple shear model for lithospheric extension after Wernicke (1985). Theoretical subsidence curves are shown below. "Proximal" and "distal" refer to the position of rift elements with respect to the upper crustal breakaway.

reflector observed on all seismic profiles might delineate this shear zone. As in the model by Wernicke (1985), a prominent Moho slope formed in the area where the shear zone reaches the base of the crust. This is nicely reflected in the seismic models by the lower crustal reflector merging with the western Moho slope. In the footwall of the shear zone, the displacement brought lower crustal material up to higher crustal levels. The increased seismic velocities between the shear zone and the Moho plateau might testify to this process. In the hanging wall of the shear zone, brittle faulting is observed at surface levels. Pre-existing fault zones were reactivated as extensional faults. As predicted by Wernicke's model, the western limit of upper crustal extensional structures is roughly defined by the shear zone cutting into the mantle. This explains the position of the east-dipping detachment with respect to the Moho slope. Subsidence will occur in the thinned crustal block east of the Moho slope which is underlain by largely unaffected lithospheric mantle. In this area, fault-controlled sedimentary basins formed above the elevated Moho and accumulated up to 8 km of clastic sediments. Relatively weak magmatic activity accompanied the Devonian sedimentation. Wernicke (1985) attributes the origin of these melts to decompression melting after the unloading of the footwall of the shear zone.

Devonian surface and deep crustal structures observed in the fjord region fit well into the concept of Wernicke's simple shear model. In this area, the extensional structures at the surface and in the lower crust are best preserved. However, from the north-south extent of the western Moho slope (Fig. 5.2), I suggest that the proposed mechanism for the Devonian extensional collapse affected the whole area between Gåsefjord and Bredefjord. In the Gåsefjord area (see seismic section in Fig. 4.28), subsequent tectonic events obscured these structures (see below). The Moho gradient changes its characteristics close to the Bredefjord area (Fig. 5.2) and might mark a northern boundary of the simple shear mechanism extensional collapse (see discussion in chapter 5.2.2).

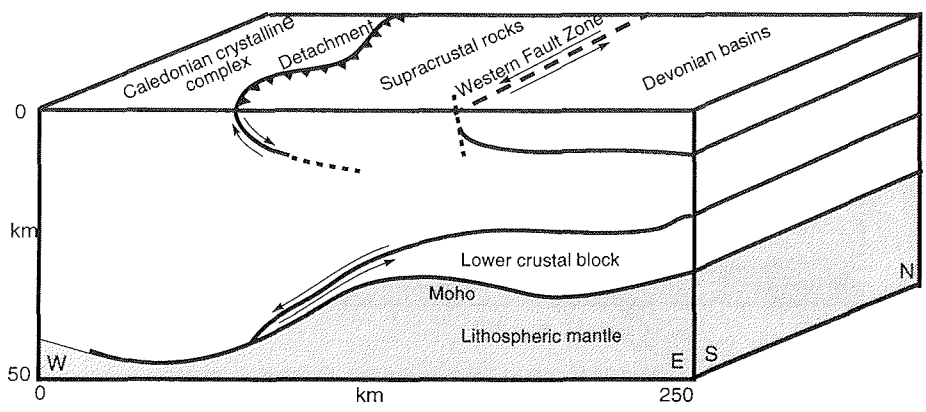

Fig. 5.4: Model of crustal structures active during Devonian crustal extension in East Greenland. Deep crustal structures are inferred from the seismic profile KFJ. Scales are approximate.

5.1.3 Post-Devonian extension

The sedimentary record of the Late Palaeozoic to Mesozoic basins of East Greenland allows reconstruction of the post-Devonian extensional history (Surlyk, 1990). Rifting initiated by the Devonian extensional collapse gradually died out in mid-Permian times. The Late Permian saw the beginning of a long phase of thermal subsidence. Minor

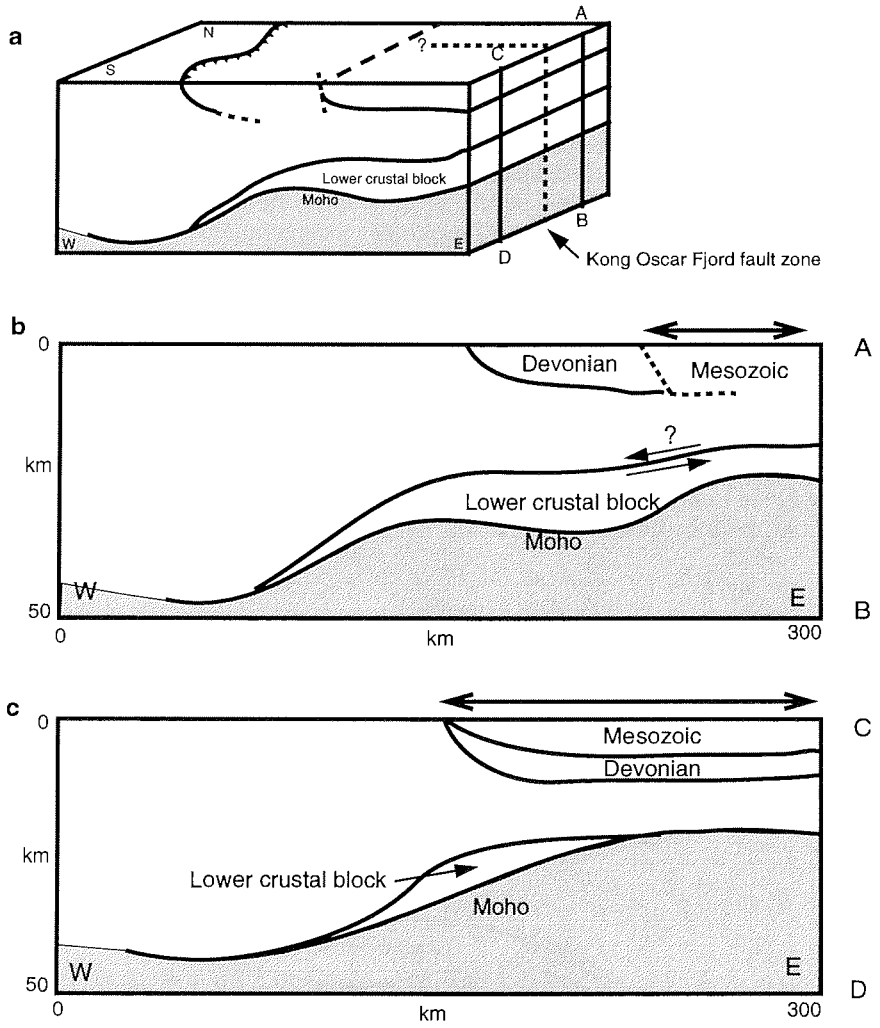

Fig. 5.5: Model for post-Devonian extension in East Greenland. **a)** Situation after Devonian extensional collapse. The position of the crustal sections AB and CD relative to the Kong Oscar Fjord fault zone is indicated. **b)** Post-Devonian extension north of Kong Oscar Fjord. Deep crustal structures are inferred from seismic profile KFJ. Extension shifted to the east relative to the Devonian structures. **c)** Post-Devonian extension south of Kong Oscar Fjord. Deep crustal structures are inferred from seismic profile GAA. Extension affects the same crustal block as Devonian extension.

faulting occurred, for example along a cross-fault following the NW-SE trending branch of Kong Oscar Fjord. In Late Jurassic to Early Cretaceous times, however, a major rifting event began, the most important since the Devonian extensional collapse. North of Kong Oscar Fjord, syn-rift sedimentary rocks deposited in tilted, fault-controlled half-grabens testify to significant tectonic activity. In contrast, south of Kong Oscar Fjord there is little evidence for fault activity and the Jameson Land Basin subsided regularly.

Fig. 5.2 relates the position of the Late Palaeozoic to Mesozoic sedimentary basins to the Moho topography. North of Kong Oscar Fjord, the Mesozoic basin is in fault contact with the neighbouring Devonian sedimentary rocks to the west. This fault contact is matched by a prominent second westward slope of the Moho along which the Moho dips from 22 km beneath the Mesozoic basin to 30 km depth beneath the Devonian basin. However, this Moho gradient stops at Kong Oscar Fjord. South of Kong Oscar Fjord, the Late Palaeozoic to Mesozoic sedimentary sequences were deposited on top of the Devonian sedimentary rocks (Surlyk, 1990; Larsen & Marcussen, 1992). No second Moho slope is visible apart from the gradient along the coast of Liverpool Land (chapter 5.2.5) and the Moho rises steadily from 45 km depth beneath the Caledonian orogen to culminate at about 22 km depth beneath the Jameson Land Basin (Larsen & Marcussen, 1992; Fechner & Jokat,1996).

From these observations, I derive the following model for the post-Devonian extension (Fig. 5.5): After mainly thermal subsidence since the mid-Permian, the Late Jurassic to Early Cretaceous rifting represents a major event in crustal evolution.

- North of Kong Oscar Fjord (Fig. 5.5b), new rift structures developed and the Devonian extensional structures to the west, including the shear zone and the Moho slope and plateau, were preserved. A new Moho slope formed, matched at the surface by the fault contact between Devonian and Mesozoic strata. However, due to Tertiary magmatic overprinting of the Mesozoic basins, no evidence for the mechanism of crustal thinning is visible. A renewed simple shear rifting (Wernicke, 1985) might be just as likely as pure shear extension (McKenzie, 1978), to mention the two extreme theories. In any case, the extension was accompanied by significant brittle faulting at the surface.
- In contrast, south of Kong Oscar Fjord (Fig. 5.5c) the Late Jurassic to Early Cretaceous extension did not shift to the east relative to the Devonian structures but affected the crustal block hosting the Devonian sedimentary basin. The crust beneath the Devonian basins was further thinned destroying the probably existing Devonian Moho plateau at 30 km depth. The extension may have reactivated the prominent Devonian shear zone. However, the relatively undisturbed sedimentation probably points to a continuous stretching of the crust. The crustal thinning finally led to the smooth and continuous Moho slope rising from the Caledonian orogen to the Jameson Land Basin, where the Devonian sedimentary sequence is buried beneath Mesozoic deposits.
- A lineament following Kong Oscar Fjord represents a major fault zone which accommodated the differential movement of the two crustal blocks. Its post-Devonian activity is well documented in the sedimentary record (Surlyk, 1990).

5.1.4 Tertiary magmatism

At about 64 Ma, the Iceland hotspot impinged on the continental crust of East Greenland. Its centre was probably situated in the area of Kangerlussuaq (68°N), but its ef-

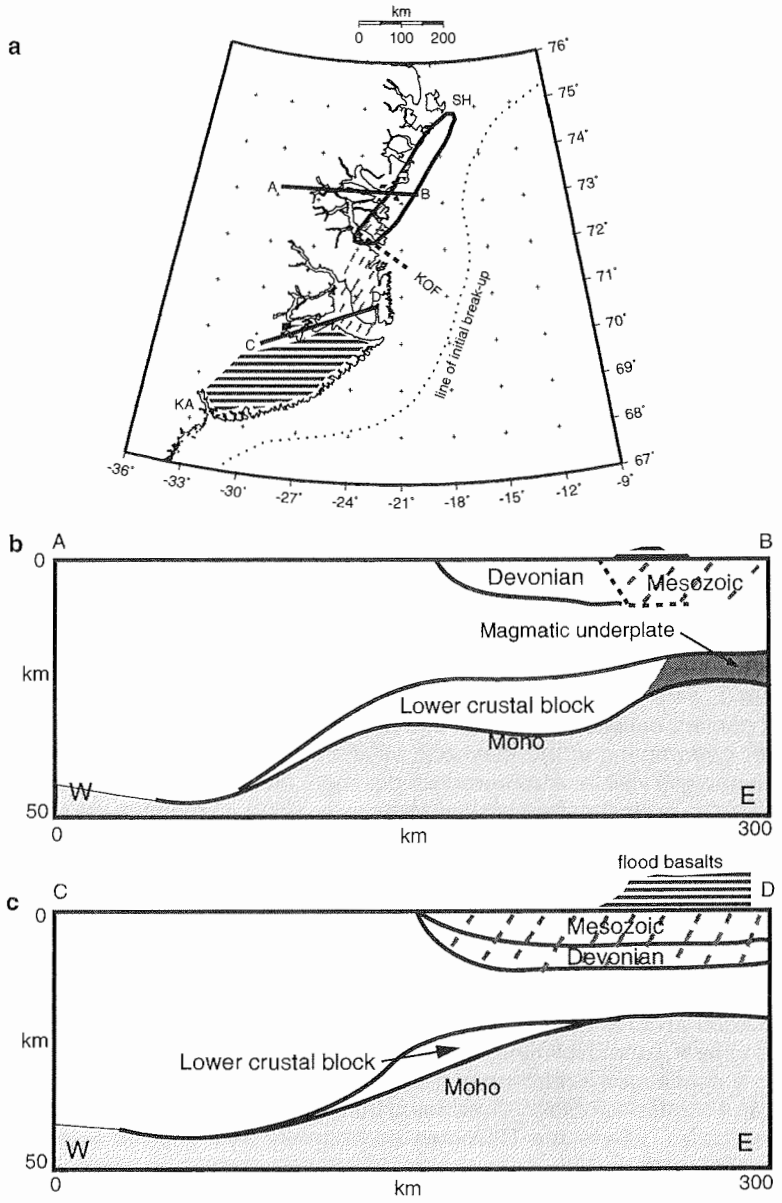

Fig. 5.6: Model for Tertiary magmatism in East Greenland. **a)** Distribution of magmatic activity. Ruled: flood basalts; grey-hatched: intrusives in Mesozoic basins; dashed line, KOF: Kong Oscar Fjord fault zone; bold oval: underplating. KA: Kangerlussuaq, SH: Shannon. Scale valid at 72°N. **b)** Model of underplated crust north of Kong Oscar Fjord. Structures are derived from seismic profile KFJ. **c)** Model of non-underplated crust south of Kong Oscar Fjord. Extrusive activity predominates. Structures are derived from seismic profile GAA.

fects reach as far north as 75°N (White & McKenzie, 1989). Mesozoic rifting had thinned the crust to a thickness of about 22 km. At these "thinspots" large volumes of melts were generated. Extrusive and intrusive magmatism took place probably during one of the epochs 26r, 25r or 24 r (Saunders et al., 1997). A marked contrast exists in the volume of flood basalts across Kong Oscar Fjord (c.f. chapter 4.3.3). South of Kong Oscar Fjord, a volume of 120 000 km^3 - 190 000 km^3 is estimated, excluding the basalts which once covered the heavily dyke-intruded Jameson Land area (Larsen & Marcussen, 1992; Saunders et al., 1997). North of Kong Oscar Fjord only some 24 000 km^3 of basalts was extruded.

The integrated analysis of geophysical data revealed another contrast across Kong Oscar Fjord. Whereas magmatism significantly underplated the northern area, no evidence for a comparable process is found south of Kong Oscar Fjord.

Fig. 5.6 illustrates the hypothesis which explains these observations. Influenced by the Iceland hotspot, melts formed beneath the thinned continental crust along a line from at least Kangerlussuaq (68°N) to Shannon (75°N) (Fig. 5.6a). South of Kong Oscar Fjord, the melts could ascend through the crust and large volumes of melts erupted as flood basalts (Fig. 5.6c). North of Kong Oscar Fjord, in contrast, the majority of the molten material became trapped at the crust-mantle boundary to crystallize as a magmatic underplate (Fig. 5.6b). The abrupt change of the character of Tertiary magmatism across Kong Oscar Fjord is unlikely to result from differences in the structure of the plume. Pressure and temperature conditions at the base of the crust are unlikely to vary significantly over a distance of a few tens of kilometres, in particular if a comparable crustal thickness can be expected. I therefore suggest that the pre-existing lithospheric structure critically controlled the magmatic activity. A differential development of the areas south and north of Kong Oscar Fjord was shown to start after Devonian extensional collapse. In particular during Late Jurassic to Early Cretaceous rifting, the crust north and south of Kong Oscar Fjord evolved in different ways. Hence, there is reason to assume that this evolution resulted in a marked difference of crustal properties north and south of Kong Oscar Fjord which finally determined the behaviour of the crust towards the Tertiary melts. Rifting along the line from Kangerlussuaq to Shannon was not successful and continental break-up took place further to the east (Fig. 5.6a). Therefore the Tertiary magmatic history is preserved in a continental setting.

The reconnaissance character of the data set does not allow resolution of the crustal structure north of Kong Oscar Fjord in enough detail to detect significant differences from the better known area south of Kong Oscar Fjord (Larsen & Marcussen, 1992; Weigel et al., 1995; Fechner & Jokat, 1996). Probable differences are discussed below.

5.1.5 Key results

The Caledonian orogen collapsed in Devonian times along a major west dipping shear zone. By simple shear mechanism extension, the crustal thickness was reduced from originally more than 55 km to a more stable 40 to 30 km. At least the area between 69°N and 75°N experienced this type of extensional collapse. Post-Devonian extension divides the area into two differently developing parts. A marked contrast exists in the Late Jurassic - Early Cretaceous rifting north and south of Kong Oscar Fjord. In the northern area, considerable tectonic activity accompanied the formation of new extensional structures east of the Devonian structures. South of Kong Oscar Fjord, the same crustal block was continuously further thinned without evoking much tectonic activity at the surface. These differences in crustal evolution critically governed Tertiary magmatism.

Under the influence of the Iceland hotspot, melts formed beneath the entire rift. The crust north of Kong Oscar Fjord trapped these melts at its base, whereas south of Kong Oscar Fjord, the melts easily reached the surface and erupted.

5.2 Discussion

The architecture and evolution of the continental crust of Central East Greenland is considered in a regional framework. The following discussion sheds some light on the question as to whether the proposed model for crustal evolution can also be applied to the northern part of the East Greenland Caledonides. In addition, the model is assessed in comparison with the crustal structure of the conjugate Norwegian Caledonides and the Caledonides of northern Britain (Fig. 5.7).

5.2.1 Crustal structure of the Caledonian orogen

The present crustal structure of the East Greenland Caledonides differs in some aspects from the structure of the British and Scandinavian Caledonides. Whereas in East Greenland the crust thickens beneath the Caledonian orogen to about 45 km, mountain

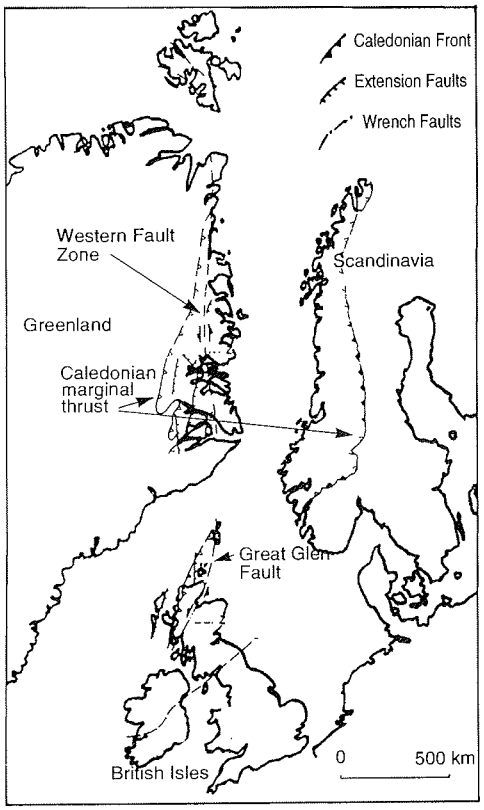

Fig. 5.7: Pre-drift reconstruction of the North Atlantic showing the Caledonian orogen and the main structures active in Devonian times (after Larsen & Bengaard, 1991).

roots are absent both in Norway and Scotland (Meissner, 1986; Dyrelius, 1985). Beneath the Grampian Mountains of Scotland, the P-wave velocity increases with depth in a very similar way to that in East Greenland. Starting with slowly increasing velocities around 6.1 km/s, 6.4 km/s is reached at 20 km depth. Beneath a reflector at that depth, the lower crust shows velocities ranging from 6.6 km/s to 7.0 km/s at the base of the crust at about 30 km depth (Barton, 1992). In contrast to the Caledonides of East Greenland, the Moho is fairly shallow and flat-lying beneath Scotland. Beneath Scandinavia, the Moho plunges continuously eastward from about 30 km depth at the west coast to about 50 km beneath the Fennoscandian shield (Kinck et al., 1991; Meissner, 1986). Moho depths correlate poorly with the mountain range, and the continuous increase in crustal thickness from the continental margin to the shield seems to be unaffected by the Caledonian orogen (Bannister et al., 1991). This has been interpreted as indicating lacking orogenic roots (Meissner, 1986; Bannister, 1991; Dyrelius, 1985), and Meissner (1979) suggested that the mountain roots were "scraped off" by asthenospheric creep processes caused by the opening of the Norwegian-Greenland Sea. However, a pronounced negative Bouguer anomaly is connected with the Scandinavian Caledonides. This negative anomaly cannot entirely be explained by the crustal structure and some mass deficiency must be located in the lithospheric mantle (Dyrelius, 1985). Bannister et al. (1991) delineated a zone of anomalously low sub-Moho seismic velocities beneath the Caledonian range of Norway from tomographic studies which yields additional support for this interpretation.

Compared to the Scandinavian Caledonides, the crustal structure of the East Greenland Caledonides shows the expected characteristics of a mountain range. The wide-angle seismic data can be satisfactorily explained by a standard velocity-depth function for orogens (Christensen & Mooney, 1995). The Moho depth reflects the regional relief of the orogen. The highest peaks of the Caledonides coincide with both gravity minima and the thickest crust. Bouguer gravity in North-East Greenland seems to increase again west of the mountain range. Hence, although the Bouguer gravity data of Central East Greenland do not extend beyond the minimum beneath the highest parts of the mountain range, an increase in Bouguer gravity towards the ice-covered Caledonian foreland might be speculated. I therefore consider the thickened crust beneath the Caledonides as an orogenic root. In addition, the density distribution in the crust as derived from seismic data can fully account for the negative Bouguer anomaly. A low density upper mantle is neither necessary in the models nor obvious from the data set.

The question arises as to whether these structural differences between the East Greenland and Scandinavian Caledonides formed during Caledonian orogeny, or if they witness to differences in the post-Caledonian evolution.

Surface geology clearly indicates, that the East Greenland and Scandinavian Caledonian orogens did not evolve symmetrically. Westerly directed subduction of the Iapetus ocean beneath Laurentia preceded the continent-continent collision (e.g. Soper et al., 1992). Ophiolite complexes derived from the Iapetus ocean were accreted to Baltica. The collision of Baltica and Laurentia led to eastward directed thrusting in Baltica. A thick pile of thrust nappes depressed the underlying crystalline crust down to depths of 60-100 km resulting in high pressure metamorphism of the basement (e.g. Dallmeyer et al., 1994). The Caledonides of East Greenland record the westward imbrication of Baltica. However, nappe stacking of comparable intensity involving allochthonous gneisses has so far not been described in East Greenland, neither are ophiolite sequences.

In addition, there is much uncertainty about the palaeo-position of Greenland with respect to Norway (Fig. 5.7). Sinistral transpression accompanied the closure of the Iapetus ocean (Soper et al., 1992; Ziegler, 1989). More orthogonal motion between Laurentia and Baltica is inferred for the time of continental collision. However, sinistral transtensional tectonics accompanied Devonian extension (Larsen & Bengaard, 1991; Ziegler, 1989; McClay et al., 1986). The amount of sinistral strike-slip motion is debated (Hartz & Andresen, 1995; Larsen & Bengaard, 1991), and it is not certain if Norway and Greenland were juxtaposed prior to Late Devonian times (e.g. Dallmeyer et al., 1994).

Considering the complexity of the Caledonian evolution, the time range of the tectonic events in East Greenland can be expected to be akin to Scandinavia (Dallmeyer et al., 1994), but due to the structural anisotropy, a symmetric architecture of the continental crust of Norway and East Greenland already at the time of orogeny would be surprising.

5.2.2 Extensional collapse of the Caledonian orogen

Extensional collapse in East Greenland: east or west-dipping detachment?

Evidence for the Devonian extensional collapse of the East Greenland Caledonides previously came mainly from surface geological observations. Strachan (1994) and Hartz & Andresen (1995) recognized shear sense indicators suggesting a generally top-to-the-east displacement along east dipping shear zones. Hartz & Andresen (1995) proposed that this listric detachment may have crustal dimensions (Fig. 5.1). They based this speculation on an interpretation of seismic reflection data from Jameson Land Basin by Larsen & Marcussen (1992) (Fig. 5.8). However, there is only weak indication for a lower crustal east-dipping reflector in the data (H. C. Larsen, pers. comm., 1997). As the crust in Jameson Land was heavily intruded by dykes and sills in Tertiary times, it might be difficult to distinguish between a shear zone and a sheet-like intrusion, and an unambiguous interpretation is not possible.

However, the existence of a lower crustal west-dipping reflector is well documented by the presented seismic refraction data of the fjord region. It might be a relic structure from orogenic processes (westerly subduction of Iapetus?) but its relation to the Dev-

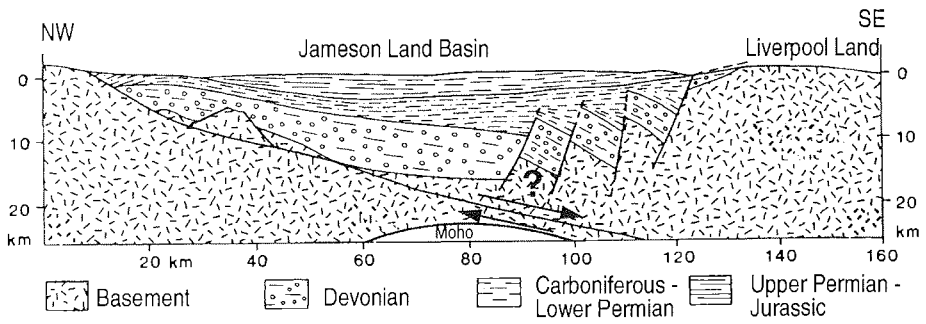

Fig. 5.8: Generalized basin structure of the Jameson Land Basin based on the interpretation of seismic reflection data by Larsen & Marcussen (1992). The east-dipping intra-crustal reflector was considered to represent a Devonian shear zone. After Larsen & Marcussen (1992).

onian surface structures suggests Devonian activity along the inferred shear zone. Hence, a crustal-scale east-dipping detachment cannot be supported by this data set. On the other hand, no conclusions on the depth extent of this east-dipping detachment can be made. The Eleonore Bay Supergroup rocks have comparable seismic velocities to the Caledonian crystalline basement and the detachment is therefore not visible in the wide-angle data. It is possible that the east-dipping detachment is rooted at the shear zone as in the model by Wernicke (1985). However, the flat-lying upper crustal reflector at about 12 km depth (see Fig. 4.29) could possibly represent a lower boundary of the detachment.

Considerable doubt exists about the timing and relative importance of the extensional structures at the surface and the sinistral strike-slip motion along the Western Fault Zone. Larsen & Bengaard (1991) attribute a dominant role to the Western Fault Zone and propose a significant displacement along the fault, whereas Hartz & Andresen (1995) consider the Western Fault Zone as one large fault among a series of other faults in the hanging wall of the detachment (Fig. 5.1). As the wide-angle data are unable to image this sub-vertical fault zone, no light can be shed on this question which has far-reaching implications, e.g. on the relative positions of Norway and Greenland at the time of the collapse of the Caledonian orogen.

Simple shear extensional collapse in the northern part of the East Greenland Caledonides?

No seismic data across the Caledonian fold belt exist north of 76°N. Therefore the validity of the model for the extensional collapse derived for the fjord region must be assessed on the basis of potential field data and surface geology.

Gravity. The Bouguer anomaly map shows a change in character north of about 75°N (Fig. 5.2, Fig. 4.2). The two gradients merge to form a single one which follows the coast towards the north. Note that on the seismic profile BRE, the two Moho gradients can still be distinguished, but they are no longer separated by a Moho plateau. In addition, the amplitude of the negative Bouguer anomaly decreases indicating that the Moho shallows northward.

Magnetics: The aeromagnetic signature of the Caledonides changes in the area around 76°N from a heterogeneous, complex structure in the south to a smooth non-magnetic appearance in the north (see chapter 5.1.1).

Geochemistry: Steenfelt (1990) studied geochemical patterns in Greenland and could distinguish with this method tectono-stratigraphic provinces in Precambrian provinces which might otherwise be difficult to recognize. One of these geochemically inferred boundaries is located in East Greenland at Bessel Fjord (76°N, Fig. 5.2) (A. Steenfelt, pers. comm., 1997).

Extensional structures: Caledonian thrusts reactivated as extensional faults are found as far north as Bessel Fjord (76°N). North of 76°N, however, no prominent detachments are found onshore. Exposures of small basins filled with sedimentary rocks of probably Carboniferous age exist, for example west of Danmarkshavn in Dove Bugt. Offshore, the continental shelf broadens significantly north of 76°N. Larsen (1990) infers horst-and-graben structures from aeromagnetic data for this otherwise unexplored region. Hinz et al. (1991,1993) found deep sediment-filled rift basins on a seismic profile north of 79°N which they interpret to be Carboniferous to Permian. Hence, extensional structures might be found offshore; their age, however, is ambiguous such that the rift structures need not necessarily be Devonian. Another striking observation is, that

Caledonian syn-kinematic granite intrusions are entirely absent north of Bessel Fjord (Escher & Pulvertaft, 1995). South of 76°N, these granites are particularly common in areas where sedimentary material is available for melting, i.e. Krummedal-type or Eleonore Bay Supergroup sedimentary rocks. The absence of Caledonian granites north of 76°N might therefore reflect the absence of such sedimentary material in the northern area. However, an alternative explanation might be that decompression melting during Devonian extension did not play a major role in this region.

Exhumation of eclogites: The exposure of lower crustal rocks in the probably Caledonian (Brueckner & Gilotti, 1993) eclogite province near Danmarkshavn places constraints on the Caledonian and post-Caledonian tectonic evolution of the area. The eclogites may have been brought to the surface already during Caledonian compressional tectonics. Duchêne et al. (1997) propose a model, where eclogites are brought to the surface in an accretionary prism during convergent plate motion. Alternatively, substantial post-Caledonian crustal thinning may have exhumed the eclogites as in the models proposed for the extensional collapse of the Norwegian Caledonides (see below and Fig. 5.9). However, the simple shear mechanism extensional collapse in the fjord region of East Greenland cannot be expected to bring lower crustal material to the surface in the area of the present Caledonian fold belt. As it is hosted in the hanging wall of the west-dipping shear zone, an exhumation of deeply buried parts of the crust is unlikely. This may explain the absence of eclogites in the fjord region. A different extensional mechanism must therefore have affected the northern area if the eclogites were exhumed during an extensional tectonic regime.
Hence, the absence of eclogites in the Caledonian crystalline complexes of the fjord region of East Greenland and their presence north of 76°N may reflect different Caledonian or post-Caledonian tectonic histories along the East Greenland fold belt. For further conclusions, however, it is crucial to know the relative timing of the exhumation of the eclogites and the transition from compressional to extensional tectonics.

Pre-Caledonian history: Prior to the Caledonian orogeny, structural differences along the present coast of Greenland must already have existed. South of about 76°N, the crystalline complexes witness probably to at least three orogenic events (e.g. Henriksen, 1985), whereas present knowledge indicates only two pre-Caledonian orogenies affecting the northern area (e.g. Henriksen, 1994a; Escher & Pulvertaft, 1995).

All these geophysical and geological data indicate that the present Caledonian orogen of East Greenland can structurally be divided into a northern and southern part. The boundary between the two areas is roughly situated at 76°N. Differences between both areas already existed at the time of the Caledonian orogeny which, in addition, affected the region in different ways. Indications on different behaviour during the post-orogenic collapse may be the absence of granitic intrusions, the presence of eclogites and lacking extensional structures onshore in the northern area. I therefore conclude that the extensional collapse as described for the fjord region probably only affected the area south of about 76°N.

Comparison with the extensional collapse of the Scandinavian Caledonides

Extensional structures are well exposed and have been extensively studied in the Caledonian fold belt of Norway (e.g. Andersen & Jamtveit, 1990; Andersen et al., 1991; Fossen & Rykkelid, 1992; Séguret et al., 1989). In particular, the exposure of lower crustal material in the eclogite province (Griffin et al., 1985) of the Western Gneiss Region of south-western Norway (Fig. 5.9) allows the study of processes responsible for exhu-

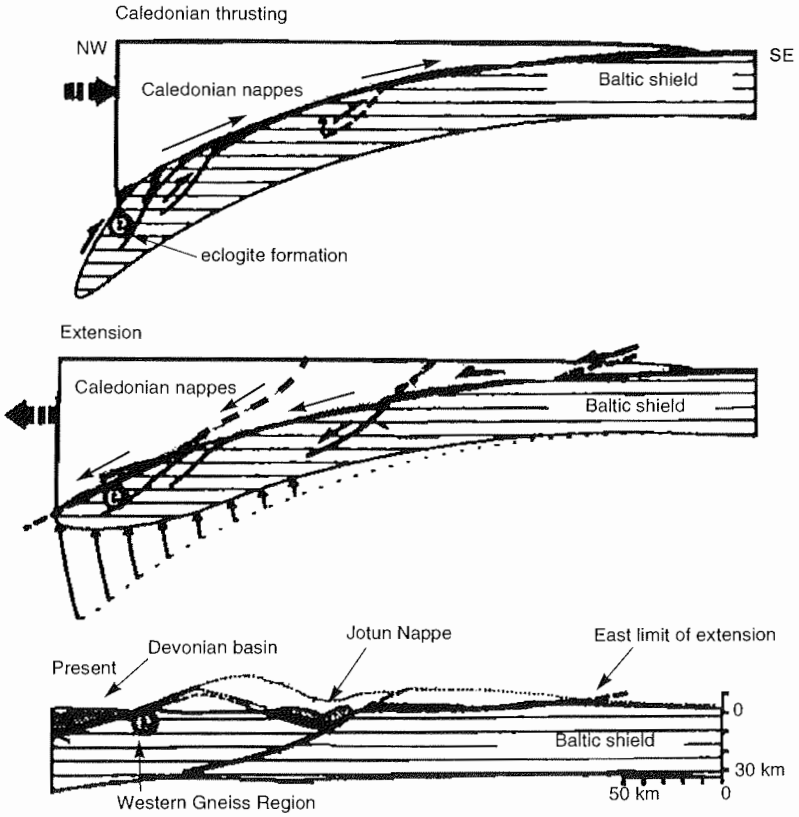

Fig. 5.9: Cross-section through the Caledonian orogen of Norway during contraction, extension and at present day (after Fossen & Rykkelid, 1992). During extension, two major west-dipping shear zones form after back-sliding of the Caledonian nappes has almost ceased. Note the exhumation of eclogites in the Western Gneiss Region in the footwall of the western detachment.

mation of these parts of the crust (e.g. Andersen & Jamtveit, 1990). A number of different models (e.g. Andersen & Jamtveit, 1990; Andersen et al., 1991; Fossen & Rykkelid, 1992; Séguret et al., 1989) have been proposed to account for the observed manifestations of extensional tectonics, in particular the back-sliding of the Caledonian nappes, the exhumation of eclogites, the activation of west-dipping extensional shear zones and the formation of fault-bounded Devonian sedimentary basins close to the Norwegian coast. Although these models differ in some aspects, the main idea of the Devonian extensional collapse can be summarized as follows (e.g. Fossen & Rykkelid, 1992) (Fig. 5.9): The subduction of Baltica beneath Laurentia deeply buried the Baltic crust and led to high-pressure metamorphism and eclogite formation. Compression was rapidly followed by extension and back-sliding of the Caledonian nappe pile and therefore unloading and uplift of the Baltic crust. Partly subsequently, partly simultaneously, west-dipping shear zones were reactivated as extensional faults. Extension

along these shear zones prevailed and exhumed the footwall of the detachment which hosts the eclogites. In the hanging wall of the shear zone, the prolonged extension produced subsidence and formation of fault-controlled Devonian basins. The west-dipping shear zones surface in the Caledonides of Norway. Hurich & Kristoffersen (1988) found indications in marine seismic data that these shear zones are of crustal scale and to be found at lower crustal levels offshore southern Norway. Most authors agree that a modified Wernicke (1985) simple shear model can explain the extensional collapse. Variations in the intensity of the Devonian extension are observed along the Norwegian Caledonides, and Fossen & Rykkelid (1992) suggest that extension in northern Norway never reached the magnitude of extension in southern Norway.

The model for extensional collapse of the East Greenland Caledonides fits well into the concept of a simple shear extensional collapse of the Caledonian fold belt as a whole. The inherent structural anisotropy produced by westward subduction of the Iapetus ocean favoured a simple shear mechanism extension which takes advantage of pre-existing structures. In contrast to Norway, where footwall rocks of the shear zone are exposed, the East Greenland Caledonides are essentially situated in the hanging wall of a lower crustal shear zone and therefore exhibit different characteristics. Subsidence and basin formation seem to have played a more important role in Greenland, whereas the rapid exhumation of lower crustal rocks is not observed in the fjord region of East Greenland. It is tempting to speculate that the lower crustal shear zone in East Greenland might be a westward continuation of the west-dipping shear zones surfacing in western Norway. However, Devonian extension was complex and a whole set of shear zones may have developed as in Norway (Fig. 5.9). In addition, the amount of sinistral strike-slip displacement during Devonian extension is not known. Finally, Mesozoic rifting and the opening of the North Atlantic obscured relic structures of Devonian extension along the continental margins. Therefore, the affinity of extensional structures in Norway and Greenland can clearly be stated, but a correlation of structures is not possible.

5.2.3 The Kong Oscar Fjord fault zone - a long-lived structure

The activity of the Kong Oscar Fjord fault zone is documented in the sedimentary record of the Lower Palaeozoic to Mesozoic basins. Surlyk (1990) found evidence for its existence as early as Late Permian. However, structural differences across the Kong Oscar Fjord may have evolved much earlier and the differential Mesozoic rifting may just be a later consequence. One striking observation is that exposures of the Late Proterozoic Eleonore Bay Supergroup sedimentary rocks are restricted exactly to the area between Kong Oscar Fjord and 76°N. This northern boundary was discussed as representing a major structural boundary already in pre-Caledonian times. A similar nature of the Kong Oscar Fjord area may therefore be likely.

The activity of the Kong Oscar Fjord boundary during Tertiary break-up is easier to document as it forms the southern limit of magmatic underplating. However, the Kong Oscar Fjord area continued to act as a structural boundary. The initial break-up of the North Atlantic left the continental sliver of the Jan Mayen Ridge at the coast of Central East Greenland south of the Proto-Jan Mayen Fracture Zone offshore Kong Oscar Fjord (e.g. Eldholm et al., 1990) (Fig. 5.10). At about marine magnetic anomaly 6 time, rifting between Jan Mayen and Greenland was successful and Jan Mayen separated along the Jan Mayen Fracture Zone. Its landward projection ends just north of Kong Oscar Fjord. The late alkaline volcanism in this area which produced the magnetic

anomaly numbered 23 in Fig. 3.15 (chapter 3.3.3) reflects magmatic activity along the Jan Mayen Fracture Zone (Larsen, 1990).

Hence, the Kong Oscar Fjord area may be considered as a long-lived zone of weakness of the crust which became repeatedly reactivated during geological history.

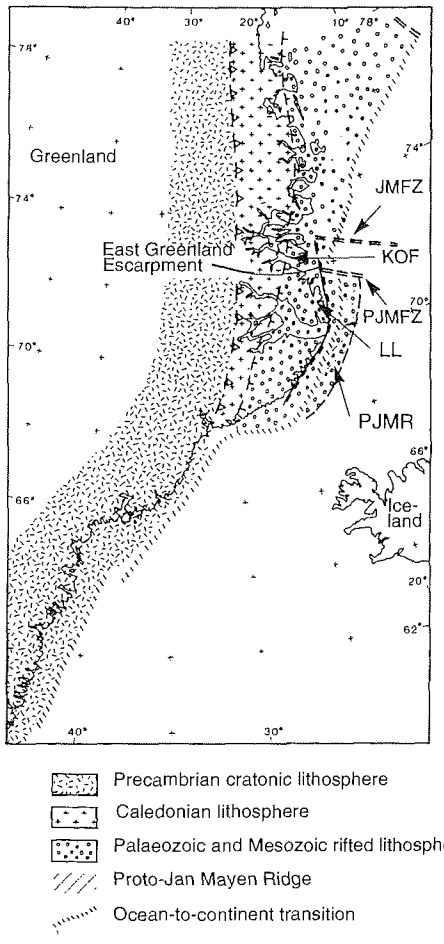

Fig. 5.10: Position of the Proto-Jan Mayen Ridge (PJMR), the Proto-Jan Mayen Fracture zone (PJMFZ) and the Proto-Jan Mayen Fracture Zone with respect to Kong Oscar Fjord (KOF) and Liverpool Land (LL) (after Larsen, 1990).

5.2.4 Lithospheric control of Tertiary magmatic underplating

Differential crustal evolution north and south of Kong Oscar Fjord exerted influence on Tertiary magmatic underplating. What are the critical parameters controlling the behaviour of the crust towards the Tertiary melts?

The Jameson Land Basin has been geophysically well studied in the course of hydrocarbon exploration and due to its relatively easy accessibility (e.g. Larsen & Marcussen, 1992; Weigel et al., 1995; Fechner & Jokat, 1996). Data of comparable density

and quality are lacking north of Kong Oscar Fjord, and a comparison of the details of crustal structure remains speculative. Some differences in crustal structure, however, may be inferred from the contrasting evolution of the two areas.

Thickness of the sedimentary basins. North of Kong Oscar Fjord, the Mesozoic sedimentary basins evolved east of the Devonian basins due to the eastward shift of Mesozoic rifting with respect to the Devonian rifting. In the Jameson Land Basin, however, the Mesozoic sequences were deposited on top of the Devonian. Hence, assuming similar sedimentation rates, a significant difference in the thickness of the sedimentary basins should result. Reconnaissance type wide-angle seismic data are not well suited to find the base of the sedimentary basins. An approximate thickness of about 6 km was modelled for the Mesozoic basins north of Kong Oscar Fjord. Fechner & Jokat (1996) derived a thickness of 6-8 km for the Jameson Land Basin. Vertical incidence seismic data, however, give a better constraint on the thickness of this basin by reflections from the bottom of the basin. Larsen & Marcussen (1992) obtained a thickness of 12-15 km for the Jameson Land Basin (Fig. 5.8). In the southern part of Jameson Land Basin, the bottom of the sedimentary basin is difficult to infer from seismic data as indicated by the different interpretation of Fechner & Jokat (1996). In northern Jameson Land Basin, however, seismic reflections from basement rocks in about 12-15 km depth can clearly be identified (H. C. Larsen, pers. comm., 1997). If the crust in both areas was comparably thick prior to Tertiary magmatism, then the different thicknesses of the sedimentary basins also imply different thicknesses of the underlying crystalline basement. Beneath the Jameson Land Basin, the crystalline crust was probably reduced to a few kilometres (Fig. 5.8), whereas some 16 km of crystalline crust may have been present beneath the northern area. Hence, the melts generated beneath the thinned crust might penetrate through the crystalline basement and ascend to the surface much easier south than north of Kong Oscar Fjord.

Lithospheric thinning. A critical parameter, which might determine the lithospheric influence on melts, is the amount of preceding lithospheric thinning (β-value of lithospheric stretching, McKenzie, 1978; White & McKenzie, 1989). This β-value varies for example along a simple shear rift (Wernicke, 1985), whereas it is constant across a pure shear rift (McKenzie, 1978). Therefore, it is important to know by which mechanism the lithosphere was thinned. The strength of the thinned lithosphere might also govern the behaviour of the crust towards melts at its base.

In East Greenland, Late Jurassic - Early Cretaceous rifting thinned the lithosphere in different ways north and south of Kong Oscar Fjord, but the mechanisms of lithospheric thinning could not be determined on the basis of the available data set. However, an indication of considerable differences is given by the varying thickness of crystalline crust beneath the sedimentary basins. In addition, the persistent thinning of the same crustal block south of Kong Oscar Fjord since Devonian times may have weakened the structure of the crust more than north of Kong Oscar Fjord where rifting shifted eastwards.

Liverpool Land. The fragment of Caledonian crust of Liverpool Land and the eastward adjacent Jan Mayen Ridge may have played a governing role in the development of the Late Jurassic - Early Cretaceous rift. Eventually torn off by Devonian extension, this block of Caledonian crystalline crust may have focused Mesozoic crustal thinning to the rift between the present day Caledonides and Liverpool Land and prevented an eastward shift of the rift. Later, an escarpment formed east of Liverpool Land during and after the separation of the Jan Mayen Ridge (Larsen, 1990). It can be traced as the

East Greenland escarpment further south marking the area where the Jan Mayen Ridge was once situated (Fig. 5.10). A gradient in the Bouguer anomaly follows this escarpment (Fig. 5.2). In the area of Liverpool Land it indicates the thickening of the crust to about 30 km beneath the Caledonian Liverpool Land block (Fig. 5.8).

5.2.5 Post-drift Tertiary evolution of East Greenland

The question arises as to what extent the crustal structure has been changed by events post-dating the magmatic underplating and the onset of sea floor spreading.

An obvious consequence of the ceasing magmatism are vertical movements of the crust. During rifting, especially when accompanied by hotspot thermal anomalies of the mantle, uplift is expected dependent on the amount of preceding lithospheric thinning (White & McKenzie, 1989). This uplift is supported dynamically by convective flow from the hotspot and isostatically due to the anomalously light, hot upper mantle material. After the onset of spreading, the newly formed continental margins subside due to thermal contraction of the lithosphere. Subsidence curves of the East Greenland volcanic continental margin witness to this process (e.g. Larsen, 1990). Onshore, however, considerable Tertiary uplift has taken place in order to bring the flood basalts, which extruded at sea-level, to their present position up to 2 km above sea-level (e.g. Larsen, 1990). Little is known about vertical movements of the underplated area north of Kong Oscar Fjord, although Larsen (1990) also suggests uplift for this area. These processes are unlikely to alter the crustal structure significantly apart from surface erosion and normal faulting along the coast which needs to take up the differential movements of the shelf and the onshore area.

The tectonism which accompanied the splitting of the Jan Mayen Ridge from East Greenland is more likely to overprint the crustal structure. Volcanism along the landward projection of the Jan Mayen Fracture Zone affected the shelf off Kong Oscar Fjord and scattered locations inland. Striking differences in crustal structure with less affected areas, for example Kejser Franz Joseph Fjord, could not be found.

Hence, I conclude that the present architecture of the crust onshore in the fjord region of East Greenland has not been drastically changed since Tertiary magmatic underplating.

6 Summary and outlook

6.1 Conclusions

This study is based on a large reconnaissance-type set of geophysical data covering East Greenland on a regional scale. The difficult conditions for fieldwork prevented an ideal use of geophysical techniques. Hence, the data set is fraught with uncertainties arising, for example, from 3-D effects in the seismic data, lacking terrain corrections of the Bouguer gravity data and incomplete removal of the vigorous transient variations of the polar external magnetic field of the Earth. However, the accuracy of the data set is sufficient to resolve the prominent large-scale structures which dominate the architecture of the continental crust of East Greenland.

The effective combination of all available data sets and their integrated interpretation allowed conclusions far beyond the implications of a single method. The combined analysis of geoscientific data proved a powerful tool for imaging the crustal structure and for reconstructing its evolution. In particular, the intensive integration of geological information was vital for this study. In this way, contributions to some outstanding geological problems of East Greenland could be made:

- The western margin of the Caledonian fold belt south of Dronning Louise Land (77°N) is concealed by the inland ice. The magnetic signature of this western margin was examined in Dronning Louise Land by comparing aeromagnetic data and surface geology. A similar pattern was recognized in the ice-covered region west of the Charcot Land window (72°N) and is interpreted to define the western boundary of the Caledonian orogen. The northern termination of the Caledonides cannot be inferred from the aeromagnetic data, although constraints on the tectonic processes at the intersection between the Caledonian fold belt and the Wandel Sea strike-slip belt could be made.
- The survival or generation of magnetite during metamorphic events can help to constrain the pressure-temperature conditions of metamorphism. Aeromagnetic data therefore provide valuable additional information, especially in areas where polyphase metamorphism has obscured the individual evolution of different regions. On the basis of the regional aeromagnetic map, the Caledonian fold belt could be subdivided into two parts. In the northern part, thick-skinned Caledonian tectonics demagnetized the crust, whereas the Caledonian foreland and the part of the orogen, which experienced thin-skinned Caledonian tectonics, retained their magnetic characteristics. In the southern part, aeromagnetic data and ground susceptibility measurements help to distinguish Caledonian crystalline complexes with different petromagnetic evolution. The Gletscherland complex, for example, hosts a characteristic magnetite-bearing granitic gneiss which did not loose its high susceptibility during the Caledonian orogeny. The effect of varying degree of metamorphism on the magnetic properties could also be studied in the Charcot Land window.
- Seismic and gravity data revealed the hardly known architecture of the Caledonian crust of East Greenland. The mountain belt has a root reaching down to 45 km beneath the highest topographic elevations. The observed distribution of seismic ve-

locities with depth and the crustal thickness are in agreement with global averages for continental crust in orogenic belts. In this context, the crustal structure of the Scandinavian Caledonides has to be considered as anomalous. However, due to the structural anisotropy inherent in the Caledonian orogeny, a symmetric crustal structure in Scandinavia and East Greenland cannot be expected.

- A significant contribution could be made to the problem of Devonian extensional collapse of the East Greenland Caledonides. It most likely occurred along a west-dipping shear zone which is situated in the lower crust beneath the Caledonides. By analogy with Norway, a simple shear model for lithospheric thinning can explain the observed surface and deep crustal structures. This type of extensional collapse probably affected East Greenland between about 70° and 76°N. The Caledonian eclogites at about 77°N cannot be exhumed by the proposed mechanism. In addition, significant structural differences, both pre- and post-Caledonian in origin, between the areas north and south of 76°N suggest that the simple shear model can probably not be extrapolated to the northern area.
- Differences in the evolution of the Mesozoic sedimentary basins of East Greenland, inferred from the sedimentary record of the basins, could be substantiated by geophysical data. In Mesozoic times, extension shifted eastwards with respect to Devonian extension and preserved the Devonian collapse structures in the fjord region. South of Kong Oscar Fjord, however, Mesozoic extension affected the same crustal block as Devonian extension. In contrast to the northern area, no significant tectonic activity at the surface accompanied the extension. Different mechanisms of rifting are therefore likely to have thinned the crust north and south of Kong Oscar Fjord. Kong Oscar Fjord represents a zone of weakness in the crust which was reactivated several times throughout the geological history of the area. It accommodated the differential Mesozoic evolution of the crust on each side.
- The striking contrast in volumes of Tertiary flood basalts between the northern flood basalt province and the Geikie Plateau could be plausibly explained. The combination of aeromagnetic and seismic data revealed a Tertiary magmatic underplate beneath the Mesozoic basins north of Kong Oscar Fjord. In contrast to the Scoresby Sund area, the Tertiary melts, produced under the influence of the Iceland hotspot, did not extrude in large volumes but became trapped at the crust-mantle boundary. The abrupt change between non-underplated and underplated crust at Kong Oscar Fjord suggests that the underplating was controlled by the lithospheric setting. The differential evolution of the crust south and north of Kong Oscar Fjord since Mesozoic times probably resulted in contrasting crustal properties which critically determined the behaviour of the crust towards melts. However, on the basis of the available data set, these differences have to remain speculative.

6.2 Suggestions for further work

This study not only shed some light on geological problems but also raised new questions. Several problems remained unanswered, while others require further work.

- The enormous size of the data set, which was processed, compiled and interpreted in this study, prevented examining every detail of the individual data sets. Only the most striking features were incorporated in the interpretation. The seismic data in particular contain additional information. S-waves have not yet been considered. Al-

though considerably less S-phases than P-phases were observed, it should be possible to construct a rough shear wave velocity model. This might then allow an overview over v_p/v_s ratios as supplementary parameters to describe the properties of the crust.

- The seismic refraction profiles 94410 and 94420 in the Scoresby Sund area have not yet been incorporated in this study. The profile 94410 along Nordvestfjord was shot in 1990 and extended in 1994. Preliminary modelling showed that the new data do not comply with the model presented by Mandler (1995) which includes, as in the case of profile GAA, too high seismic velocities at mid-crustal depths. A re-interpretation of the profile and a modelling of profile 94420 should be envisaged. Although these profiles do not extend far into the Mesozoic Jameson Land Basin, they might show more relic structures of the Devonian extensional collapse and the Late Jurassic - Early Cretaceous rifting. It may be possible to better constrain the processes active during these events and reveal the critical differences to the northern area. The profile along Nordvestfjord is situated at the northern margin of the Scoresby Sund area close to the Kong Oscar Fjord structural boundary. It might therefore represent a key profile in constraining the differences in crustal structure north and south of Kong Oscar Fjord.
- A very useful and easy-to-get by-product of any kind of land-based field work in East Greenland are ordinary density measurements of surface rocks. In particular, densities of the sedimentary rocks were difficult to determine from seismic velocities. With this additional information, the gravity models of the fjord region could be improved. In addition, information on the thickness of the sedimentary basins from commercial seismic reflection data would be very valuable for detailed gravity modelling. A 3-D gravity model of the fjord region could then be envisaged, which would allow to constrain the topography of the Moho in more detail and, for example, to obtain hints on the east extent of the magmatic underplate in terms of gravity data.
- Additional research is needed in the field of petromagnetism. Too little is known about the behaviour of magnetite during metamorphism. As the boundary conditions of metamorphism vary widely from one case to another and a general theory is still lacking, detailed studies of the crystalline complexes in East Greenland are needed. The magnetic studies should be combined with analyses of the pressure-temperature histories of metamorphism and with age determinations. Recognizing correlations between the magnetic properties of a rock and its metamorphic history allows full use of the potential of the aeromagnetic data for mapping crystalline complexes of the Caledonides, even in inaccessible terrain. As the reconnaissance-type aeromagnetic data tends to blur details of magnetic signatures, high resolution aeromagnetic data in regions of special interest are desirable for combined studies of geology and magnetic properties.
- Geophysical data, in particular seismic data, are urgently needed north of 76°N in order to understand the structure and evolution of the Caledonian orogen. The formation and exhumation of eclogites in this area represents a key problem in the understanding of the Caledonian orogeny and the subsequent extensional collapse. This study could shed some light on the processes which affected the area south of 76°N. It was concluded that different processes may have been active north of 76°N, but their nature remained unclear. In order to investigate this problem, it is necessary to look for relic structures of extensional tectonics. These structures may be situated offshore on the East Greenland shelf which is heavily obstructed by sea-ice all year

round. Other indications on both orogenic and collapse structures should be found in the area of the Caledonian fold belt itself. The lack of extensive E-W oriented fjords and the fact that the inland ice reaches almost to the coast make a seismic transect through the Caledonian orogen north of 76°N a very difficult if not impossible task.

- The most promising research target to pursue is undoubtedly the influence of lithospheric setting on magmatic underplating. Magmatic underplating plays an important role in the evolution of volcanic continental margins. The physical properties of the rifting lithosphere may critically govern the formation and the size of a magmatic underplate. However, along the continental margins, where continental rifting successfully reached the stage of sea-floor spreading, the crustal structures which once determined underplating, are obscured by the formation of large wedges of subaerially extruded volcanics ("seaward dipping reflectors", Hinz, 1981) and by later subsidence and sedimentation along the margin (e.g. White & McKenzie, 1989). In addition, as the margins are submerged and bar geological field observations, marine geophysical techniques are required for their investigation.

  East Greenland, in contrast, provides an excellent natural laboratory to study the lithospheric influence on magmatic underplating. Rifting was not successful in this area. Therefore, the magmatic underplate is preserved in a continental setting and is largely unaffected by later processes. Hence, magmatic underplating can be examined as an isolated process in this area. The presented geophysical and geological data form the framework for further work on this subject. Underplated and non-underplated regions could be identified and related to the contrasting evolution of the lithosphere. Further research should aim at determining the physical properties of the lithosphere which governed the underplating. Detailed geophysical data sets are necessary for this purpose. Whereas the area south of Kong Oscar Fjord is reasonably well investigated, comparable data are lacking for the area north of Kong Oscar Fjord. The seismic refraction survey in 1994 had reconnaissance character and was not designed to focus on this problem. I therefore propose a renewed detailed seismic experiment in the mouth of Kejser Franz Joseph Fjord aiming especially at the question of crustal architecture and magmatic underplating. The poorly constrained thickness of the sedimentary basins and the deep crustal structure could be determined by combining seismic reflection and refraction techniques. In addition, information on the structure and extent of the magmatic underplate and its possible connection to the continental margin is crucial for the understanding of the underplating process. A survey setup needs to be designed which focuses on imaging the magmatic underplate. The use of ocean-bottom-hydrophones might be necessary. Furthermore, the north-south trending seismic profile between Shannon and the mouth of Kejser Franz Joseph Fjord should be re-shot and considerably more than 4 receivers should be deployed. This profile can detect structural changes along the strike of the underplate and their possible relation to the overlying crust. Finally, all available geoscience data should be incorporated in the seismic study in order to describe the physical properties of the crust north and south of Kong Oscar Fjord as completely as possible. A comparison between both regions might then reveal the differences in crustal structure which controlled Tertiary magmatic underplating.

7 Acknowledgements

I am greatly indebted to my thesis advisor Prof. Dr. H. Miller for giving me the unique possibility to work on this large and valuable data set including data from 6 seasons of field work. Whereas 4 expeditions had been planned and partly accomplished before the start of my thesis, Prof. Dr. H. Miller supported my wishes to further complete the data set and made two additional seasons of fieldwork possible. I greatly benefited from his guidance and constant openness to my scientific results, ideas and problems.

Dr. W. Jokat and Dr. U. Meyer are thanked for initiating the seismic refraction and aeromagnetic projects, respectively. They acquired parts of the data and were involved in the early stages of data processing. Both provided advice throughout my thesis. I gratefully acknowledge the assistance of my colleagues and fellow Ph.D. students at the Department of Marine Geophysics and Glaciology, in particular M. Studinger, F. Nitsche, Dr. N. Fechner and Dr. G. Uenzelmann-Neben. They helped to overcome the problems arising during daily work. H. Nübold modelled the seismic profile GAA during his practical training at AWI. Prof. Dr. U. Bleil is thanked for serving as co-referee.

A major part of this thesis involved geological interpretation of geophysical data which required an intimate knowledge of East Greenland's geology. The geologists of the Department for Geological Mapping at GEUS, in particular Dr. N. Henriksen, Dr. J. Friderichsen and Dr. A. Higgins, helped me to acquire this knowledge by providing me with literature, geological maps, recent research results and a collection of representative rock samples from North-East Greenland for susceptibility measurements. I greatly profited from my visits to Copenhagen where I was given the chance to present my work and discuss it with the constantly interested geologists. I am greatly indebted to Dr. N. Henriksen for making a participation in the geological fieldwork of summer 1997 possible and for effectively integrating me and my geophysical work into the project. In addition, discussions of my thesis with Prof. Dr. B. Upton, Dr. L. Larsen, Dr. E. Hartz, and Dr. J. Gilotti, proved very fruitful. Dr. A. Higgins, Dr. J. Friderichsen and Dr. W. Jokat kindly reviewed the manuscript of this thesis. I am especially grateful to Dr. A. Higgins for eliminating english errors, improving the style of the thesis and for his thorough revision of all geological topics.

The KMS, in particular Dr. R. Forsberg, is thanked for providing the gravity data set. I also received the digital data sets of coastlines and topography of Greenland from KMS. The Danish Meteorological Institute gave me access to registrations of transient variations of the Earth's magnetic field at Danmarkshavn. Data from the Leirvogur observatory were provided by the Science Institute, University of Iceland.

Fieldwork in East Greenland would not have been possible without external support. The crew of Polar2 and the engineers of Aerodata are thanked for their excellent collaboration during the AEROMAG campaigns. I gratefully acknowledge the logistic help of Dr. H. Andersson, Danish Polar Centre (DPC). DPC operated a basestation magnetometer at Zackenberg during AEROMAG96. Efficient logistic support was also supplied by Flugfélag Íslands. The Institute for Geophysics of the University of Munich kindly provided a kappameter for my fieldwork in 1997, for which I am indebted to Dr. J. Pohl.

My fieldpartners during summer 1997, namely Dr. J. Friderichsen, K. Thrane, Dr. S. Elvevold and Dr. J. Gilotti, deserve my warmest thanks. They taught me a lot of geology, patiently answered my numerous geological questions and contributed to the success of my geophysical fieldwork.

I derived much of my motivation and energy for working on this thesis from the vivid memory of fascinating flights, walks and rubberboat trips in East Greenland with Dr. J. Friderichsen, S. Seydel, J. Skirnisson and M. Zikesch, who shared my enthusiasm for East Greenland and for the stunning beauty of its landscape.

8 References

Abrahamsen, N., and P. Nordgerd, Rock magnetism of Tertiary volcanics from North-East Greenland, *Rapp. Grønlands geol. Unders., 162*, 195-200, 1994.

Andersen, T. B., B. Jamtveit, J. F. Dewey and E. Swensson, Subduction and eduction of continental crust: major mechanisms during continent-continent collision and orogenic extensional collapse, a model based on the south Norwegian Caledonides, *Terra Nova, 3,* 303-310, 1991.

Andersen, T. B., and B. Jamtveit, Uplift of deep crust during orogenic extensional collapse: a model based on field studies in the Sogn-Sunnfjord region of western Norway, *Tectonics, 9,* 1097-1111, 1990.

Bannister, S. C., B O. Ruud and E. S. Husebye, Tomographic estimates of sub-Moho seismic velocities in Fennoscandia and structural implications, *Tectonophysics, 189,* 37-53, 1991.

Barton, A. J., and R. S. White, Crustal structure of the Edoras Bank continental margin and mantle thermal anomalies beneath the North Atlantic, *J. Geophys. Res., 102, B2,* 3109-3129, 1997.

Barton, C. E., What is the Earth's "Normal" Magnetic Field, *EOS Trans. AGU, 76,* p. 13, 1995.

Barton, P. J., LISPB revisited: a new look under the Caledonides of northern Britain, *Geophys. J. Int., 110,* 371-391, 1992.

Blakely, R. J., *Potential theory in gravity and magnetic applications,* 441 pp., Cambridge University Press, Cambridge, 1995.

Blakely, R. J., and G. G. Connard, Crustal studies using magnetic data, in L. C. Parkiser and W. D. Mooney (eds.), *Geophysical framework of the continental United States*, Geological Society of America Memoir 172, 45-60, Boulder, Colorado, 1989.

Boyd, L. A., The fiord region of East Greenland, *American Geographical Society, Special Publication No. 18*, 1935.

Brooks, C. K., A. K. Pedersen and D. C. Rex, The petrology and age of alkaline mafic lavas from the nunatak zone of central East Greenland, *Bull. Grønlands geol. Unders., 133*, 1-28, 1979.

Burchfield, B. C., and L. H. Royden, North-south extension within the convergent Himalayan region, *Geology, 13,* 679-682, 1985.

Brueckner, H. K., and J. A. Gilotti, Preliminary age constraints on the timing of eclogite facies metamorphism, North-East Greenland, *Geol. Soc. Am. Abstracts with programs, 25,* 340, 1993.

Christensen, N. I., and W. D. Mooney, Seismic velocity structure and composition of the continental crust: A global view, *J. Geophys. Res., 100, B7,* 9761-9788, 1995.

Coles, R. L., G. V. Haines and W. Hannaford, Large scale magnetic anomalies over western Canada and the Arctic; a discussion, *Can. J. Earth Sci., 13,* 790-802, 1976.

Coney, P. J., and T. A. Harms, Cordilleran metamorphic core complexes: Cenozoic extensional relics of Mesozoic compression, *Geology, 12,* 550-554, 1984.

Dallmeyer, R. D., R. A. Strachan and N. Henriksen, $^{40}Ar/^{39}Ar$ mineral age record in NE Greenland: implications for tectonic evolution of the North Atlantic Caledonides, *J. geol. Soc. London, 151,* 615-628, 1994.

Dawes, P. R., The North Greenland continental margin, in A. Grantz, L. Johnson and J. F. Sweeney (eds.), The Arctic Ocean region, Geological Society of America, *The Geology of North America, vol. L,* 211-226, Boulder, Colorado, 1990.

Dewey, J. F., Extensional collapse of orogens, *Tectonics, 7,* 1123-1139, 1988.

Duchêne, S., J.-M. Lardeaux and F. Albarède, Exhumation of eclogites: insights from depth-time path analysis, *Tectonophysics, 280,* 125-140, 1997.

Dyrelius, D., A geophysical perspective of the Scandinavian Caledonides, in D. G. Gee and B. A. Sturt (eds.), *The Caledonide Orogen - Scandinavia and related areas*,185-194, J. Wiley & Sons Ltd, London, 1985.

Eldholm, O., J. Skogseid, E. Sundvor and A. M. Myhre, The Norwegian-Greenland Sea, in A. Grantz, L. Johnson and J. F. Sweeney (eds.), The Arctic Ocean region, Geological Society of America, *The Geology of North America, vol. L,* 351-364, Boulder, Colorado, 1990.

Escher, J. C., and T. C. R. Pulvertaft, Geological map of Greenland, 1: 2 500 000, Geological Survey of Denmark and Greenland, Copenhagen, 1995.

Fechner, N., Detailed refraction seismic investigations in the inner Scoresby Sund, East Greenland (in German), *Reports on Polar Research, 143,* Alfred Wegener Institute for Polar and Marine Research, Bremerhaven, 1994.

Fechner, N., and W. Jokat, Seismic refraction investigations on the crustal structure of the western Jameson Land Basin, East Greenland, *J. Geophys. Res., 101, B7,* 15867-15881, 1996.

Forsberg, R., Gravity measurements in Jameson Land and neighbouring parts of East Greenland, *Meddelelser om Grønland, Geoscience, 15,* 24 pp., 1986.

Forsberg, R., Gravity measurements in East Greenland 1986-88, *Technical report, 4,* 32 pp., National Survey and Cadastre, Copenhagen, 1991.

Forsberg, R., and K. Keller, Gravity and GPS measurements in Greenland 1996, unpublished survey and processing report, 39 pp., National Survey and Cadastre, Copenhagen, 1997.

Fossen, H., and E. Rykkelid, Postcollisional extension of the Caledonide orogen in Scandinavia: Structural expressions and tectonic significance, *Geology, 20,* 737-740, 1992.

Fowler, C. M. R., and E. G. Nisbet, The thermal background to metamorphism II. Simple two-dimensional conductive models, *Geoscience Canada, 9,* 208-214, 1982.

Friderichsen, J. D., R. E. Holdsworth, H. F. Jepsen and R. A. Strachan, Caledonian and pre-Caledonian geology of Dronning Louise Land, North-East Greenland, *Rapp. Grønlands geol. Unders., 148,* 133-141, 1990.

Frost, B. R., A review of graphite-sulfide-oxide-silicate equilibria in metamorphic rocks, *Recond. Soc. Ital. Miner. Petrol., 43,* 25-40, 1988.

Gebrande, H., and H. Miller, Refraktionsseismik (in German), in F. Bender (ed.), *Angewandte Geowissenschaften, vol. 2,* 226-260, Ferdinand Enke Verlag, Stuttgart, 1985.

Gilotti, J. A., Discovery of a medium-temperature eclogite province in the Caledonides of North-East Greenland, *Geology, 21,* 523-526, 1993.

Gilotti, J. A., Eclogites and related high-pressure rocks from North-East Greenland, *Rapp. Grønlands geol. Unders., 162,* 77-90, 1994.

Griffin, W. L., H. Austrheim, K. Brastad, I. Brynhi, A. G. Krill, E. J. Krogh, M. B. E. Mørk, H. Qvale and B. Tørudbakken, High-pressure metamorphism in the Scandinavian Caledonides, in D. G. Gee and B. A. Sturt (eds.), *The Caledonide Orogen - Scandinavia and related areas*, 127-130, J. Wiley & Sons Ltd, London, 1985.

Hald, N., Early Tertiary lavas and sills on Traill Ø and Geographical Society Ø, northern East Greenland: petrography and geochemistry, *Bull. Grønlands geol. Unders., 171,* 29-34, 1996.

Haller, J., *Geology of the East Greenland Caledonides,* 413 pp., Interscience Publishers, New York, 1971.

Hansen, B. T., R. H. Steiger and A. K. Higgins, Isotopic evidence for a Precambrian metamorphic event within the Charcot Land window, East Greenland Caledonian fold belt, *Bull. geol. soc. Denmark, 29,* 151-160, 1981.

Hansen, R. O., and Y. Miyazaki, Continuation of potential fields between arbitrary surfaces, *Geophysics, 49*, 787-795, 1984.

Hartz, E., and A. Andresen, Caledonian sole thrust of central East Greenland: a crustal-scale Devonian extensional detachment?, *Geology, 23*, 637-640, 1995.

Henkel, H., Petrophysical properties (density and magnetization) of rocks from the northern part of the Baltic Shield, *Tectonophysics, 192*, 1-19, 1991.

Henriksen, N., The Caledonides of central East Greenland 70°-76°N, in D. G. Gee and B. A. Sturt (eds.), *The Caledonide Orogen - Scandinavia and related areas*, 1095-1113, J. Wiley & Sons Ltd, London, 1985.

Henriksen, N., Descriptive text to the geological map of Greenland, 1: 500 000, sheet 7, Nyeboe Land, and sheet 8, Peary Land, 40 pp., Geological Survey of Greenland, Copenhagen, 1992.

Henriksen, N., Geology of North-East Greenland (75°-78°N) - the 1988-90 mapping project, *Rapp. Grønlands geol. Unders., 162*, 5-16, 1994a.

Henriksen, N., Eastern North Greenland 1993-1995 - a new 1: 500 000 mapping project, *Rapp. Grønlands geol. Unders., 160*, 47-51, 1994b.

Henriksen, N., and A. K. Higgins, East Greenland Caledonian fold belt, in A. Escher and W. S. Watt (eds.), *Geology of Greenland,* 182-246, Geological Survey of Greenland, Copenhagen, 1976.

Henriksen, N., and A. K. Higgins, The North Greenland Project, *Bull. Grønlands geol. Unders., 160*, 9-24, 1991.

Higgins, A. K., Descriptive text to the geological map of Greenland,1: 100 000, sheets Charcot Land 71 Ø.4N and Krummedal 71 Ø.4S, 26 pp., Geological Survey of Greenland, Copenhagen, 1982.

Higgins, A. K., Geology of central and eastern North Greenland, *Rapp. Grønlands geol. Unders., 128*, 37-54, 1986.

Higgins, A. K., J. D. Friderichsen and T. Thyrsted, Precambrian metamorphic complexes in the East Greenland Caledonides (72°-74°N) - their relationships to the Eleonore Bay Group, and Caledonian orogenesis, *Rapp. Grønlands geol. Unders., 104*, 5-46, 1981.

Higgins, A. K., J. R. Ineson, J. S. Peel, F. Surlyk and M. Sønderholm, Lower Paleozoic Franklinian Basin of North Greenland, *Bull. Grønlands geol. Unders., 160*, 71-139, 1991.

Hill, R. I., Starting plumes and continental break-up, *Earth and Planetary Science Letters, 104,* 398-416, 1991.

Hinz, K., A hypothesis of terrestrial catastrophes - wedges of very thick oceanward dipping layers beneath passive margins - their origin and paleoenvironmental significance, *Geol. Jahrbuch, E22,* 3-28, 1981.

Hinz, K., H. Meyer and H. Miller, North-East Greenland Shelf north of 79°N: results of a reflection seismic experiment in sea ice, *Marine and Petroleum Geology, 8,* 461-467, 1991.

Hinz, K., O. Eldholm, M. Block and J. Skogseid, Evolution of North Atlantic volcanic continental margins, in J. R. Parker (ed.), *Petroleum Geology of Northwest Europe: Proceedings of the 4th Conference,* 901-913, The Geological Society, London, 1993.

Hochstetter, F. von, O. Lenz, F. Toula, A. Bauer and O. Heer, Geologie, in K. Koldewey (ed.), *Die Zweite Deutsche Polarfahrt in den Jahren 1869 und 1870 unter Führung von Kapitän Karl Koldewey, Band II, Wissenschaftliche Ergebnisse,* 471-517, F. A. Brockhaus, Leipzig, 1874.

Hurich, C. A., and Y. Kristoffersen, Deep structure of the Caledonian orogen in southern Norway: New evidence from marine seismic reflection profiling, *Norges Geologiske undersøkelse Special Publication, 3,* 96-101, 1988.

Hurst, J. M., H. F. Jepsen, F. Kalsbeek, W. S. McKerrow and J. S. Peel, The geology of the northern extremity of the East Greenland Caledonides, in D. G. Gee and B. A. Sturt (eds.), *The Caledonide Orogen - Scandinavia and related areas,*1046-1069, J. Wiley & Sons Ltd, London, 1985.

IAGA Division V Working Group 8, R. A. Langel, chairman, International Geomagnetic Reference Field, 1991 revision, *J. Geomagn. Geoelectr., 43*, 1007, 1991.

Jokat, W., P. Alberts, H. Gödde, N. Fechner, H. Fischbeck, C. Kopsch, B. Kunsch, N. Lensch, H. Martens, K. Moorfeld, V. Schlindwein, M. Studinger and D. Sylvester, Seismic refraction, in H.-W. Hubberten (ed.), The expedition ARKTIS-X/2 of RV "Polarstern" in 1994, *Reports on Polar Research, 174,* Alfred Wegener Institute for Polar and Marine Research, Bremerhaven, 1995.

Jokat, W., A. Eckstaller, B. Hesemann, W. van Heuwerswyn, H. Miller, N. Lensch, S. Missiean, G. Uenzelmann-Neben, N. Fechner, A. Rosenberger and K. Vanneste, Marine Geophysik (in German), in H. Miller and H. Grobe, The expedition ARKTIS-VII/3 of RV "Polarstern" in 1990, *Reports on Polar Research, 189,* Alfred Wegener Institute for Polar and Marine Research, Bremerhaven, 1996.

Kalsbeek, F., and H. F. Jepsen, The Midsommersø Dolerites and associated intrusions in the Proterozoic platform of eastern North Greenland - a study of the interaction between intrusive basic magma and sialic crust, *J. Petrol., 24,* 605-634, 1983.

Kalsbeek, F., A. P. Nutman and P. N. Taylor, Palaeoproterozoic basement province in the Caledonian fold belt of North-East Greenland, *Precambrian Res., 63,* 163-178, 1993.

Kamide, Y., and S. Kokubun, Two-component auroral electrojet: Importance for substorm studies, *J. Geophys. Res., 101, A6,* 13027-13046, 1996.

Katz, H. R., Ein Querschnitt durch die Nunatakzone Ostgrönlands (ca. 74° n. Br.), *Meddelelser om Grønland, 144,* 65pp., 1952.

Kertz, W., *Einführung in die Geophysik II,* 440 pp., Bibliographisches Institut, Mannheim, 1989.

Kinck, J. J., E. S. Husebye and C.-E. Lund, The south Scandinavian crust: structural complexities from seismic reflection and refraction profiling, *Tectonophysics, 189,* 117-133, 1991.

Koch, L., and J. Haller, Geological map of East Greenland 72°-76°N (1: 250 000), *Meddelelser om Grønland, 183,* 26pp., 1971.

Larsen, H. C., Aeromagnetiske undersøgelse i Østgrønland 1974, unpublished internal report in open GGU-file, 124 pp., 1977.

Larsen, H. C., A high-pressure granulite facies complex in north-west Payers Land, East Greenland fold belt, *Bull. geol. Soc. Denmark, 29,* 161-174, 1981.

Larsen, H. C. , The East Greenland Shelf, in A. Grantz, L. Johnson and J. F. Sweeney (eds.), The Arctic Ocean region, Geological Society of America, *The Geology of North America, vol. L,* 185-210, Boulder, Colorado, 1990.

Larsen, H. C., and C. Marcussen, Sill-intrusion, flood basalt emplacement and deep crustal structure of the Scoresby Sund region, East Greenland, in B. C. Storey, T. Alabaster and R. J. Pankhurst (eds.), Magmatism and the causes for continental break-up, *Geological Society Special Publication, 68,* 365-386, 1992.

Larsen, L. M., and W. S. Watt, Episodic volcanism during break-up of the North Atlantic: evidence from the East Greenland plateau basalts, *Earth and Planetary Science Letters, 73,* 105-116, 1985.

Larsen, L. M., W. S. Watt and M. Watt, Geology and petrology of the Lower Tertiary plateau basalts of the Scoresby Sund region, East Greenland, *Bull. Grønlands geol. Unders.,157,* 1-164, 1989.

Larsen, P.-H., and H.-J. Bengaard, Devonian basin initiation in East Greenland: a result of sinistral wrench faulting and Caledonian extensional collapse, *J. geol. Soc. London, 148,* 355-368, 1991.

Leliak, P., Identification and evaluation of magnetic field sources of magnetic airborne detector equipped aircraft, *IRE Transactions on Aerospace and Navigational Electronics, 8,* 95-105, 1961.

Mandler, H., The crustal structure of the Scoresby Sund area, East Greenland: Results from refraction seismic and gravity measurements (in German), *Reports on Polar Research, 172,* Alfred Wegener Institute for Polar and Marine Research, Bremerhaven, 1995.

McClay, K. R., M. G. Norton, P. Coney and G. H. Davis, Collapse of the Caledonian orogen and the Old Red Sandstone, *Nature, 323,* 147-149, 1986.

McKenzie, D., Some remarks on the development of sedimentary basins, *Earth and Planetary Science Letters, 40,* 25-32, 1978.

McSwiggin, P. L., G. B. Morey, and V. W. Chandler, New model of the midcontinent rift in eastern Minnesota and western Wisconsin, *Tectonics, 6,* 677-685, 1987.

Meissner, R., Fennoscandia - a short outline of its geodynamical development, *Geojournal, 3.3,* 227-233, 1979.

Meissner, R., *The continental crust - a geophysical approach,* International Geophysics Series, 34, 426 pp., Academic Press, London, 1986.

Mertikas, S. P., A study on the performance of covariance matrix estimators, *Marine Geodesy, 16,* 259-276, 1993.

Monk, J., C. Schreyer and R. Seitz, Bathymetrical surveying using the HYDROSWEEP system, in H.-W. Hubberten (ed.), The expedition ARKTIS-X/2 of RV "Polarstern" in 1994, *Reports on Polar Research, 174,* Alfred Wegener Institute for Polar and Marine Research, Bremerhaven, 1995.

Nafe, J. E., and C. L. Drake, Variation with depth in shallow and deep water marine sediments of porosity, density and the velocity of compressional and shear waves, *Geophysics, 22,* 523-552, 1957.

Nielsen, T. F. D., Tertiary alkaline magmatism in East Greenland: a review, in J. G. Fitton and B. G. J. Upton (eds.), Alkaline igneous rocks, *Geological Society Special Publication, 30,* 489-515, 1987.

Nielsen, T. F. D., and C. K. Brooks, The E Greenland rifted continental margin: an examination of the coastal flexure, *J. geol. Soc. London, 138,* 559-568, 1981.

Ostenso, N. A., and R. J. Wold, Aeromagnetic survey of the Arctic Ocean; Techniques and interpretations, *Marine Geophysical Research, 1,* 178-219, 1971.

Rex, D. C., and A. R. Gledhill, Isotopic studies in the East Greenland Caledonides (72°-74°N) - Precambrian and Caledonian ages, *Rapp. Grønlands geol. Unders., 104,* 47-72, 1981.

Riddihough, R. P., G. V. Haines and W. Hannaford, Regional magnetic anomalies of the Canadian Arctic, *Can. J. Earth Sci., 10,* 157-163, 1973.

Saunders, A. D., J. G. Fitton, A. C. Kerr, M. J. Norry and R. W. Kent, The North Atlantic igneous province, in J. J. Mahoney and M. F. Coffin (eds.), Large Igneous Provinces, *AGU Monograph,* in press, 1997.

Schlinger, C. M., Magnetization of lower crust and interpretation of regional magnetic anomalies: example from Lofoten and Vesterålen, Norway, *J. Geophys. Res., 90, B13,* 11484-11504, 1985.

Séguret, M., M. Séranne, A. Chauvet and M. Brunel, Collapse basin: A new type of extensional sedimentary basin from the Devonian of Norway, *Geology, 17,* 127-130, 1989.

Shive, P. N., R. J. Blakely, B. R. Frost and D. M. Fountain, Magnetic properties of the lower continental crust, in D. M. Fountain, R. Arculus and R. W. Kay (eds.), Continental lower crust, *Developments in Geotectonics, 23,*145-177, Elsevier, Amsterdam, 1992.

Skilbrei, J. R., T. Skyseth and O. Olesen, Petrophysical data and opaque mineralogy of high-grade and retrogressed lithologies: implications for the interpretation of aeromagnetic anomalies in Northern Vestranden, Central Norway, *Tectonophysics, 192,* 21-31, 1991.

Skogseid, J., T. Pedersen, O. Eldholm and B. T. Larsen, Tectonism and magmatism during NE Atlantic continental break-up: the Vøring Margin, in B. C. Storey, T. Alabaster and R. J. Pankhurst (eds.), Magmatism and the causes for continental break-up, *Geological Society Special Publication, 68,* 305-320, 1992.

Smith, W. H. F, and P. Wessel, Gridding with continuous curvature splines in tension, *Geophysics, 55,* 293-305, 1990.

Soper, N. J., R. A. Strachan, R. E. Holdsworth, R. A. Gayer and R. O. Greiling, Sinistral transpression and the Silurian closure of Iapetus, *J. geol. Soc. London, 149,* 871-880, 1992.

Sønderholm, M., and H. F. Jepsen, Proterozoic Basins of North Greenland, *Bull. Grønlands geol. Unders., 160*, 49-69, 1991.

Sønderholm, M., and H. Tirsgaard, Lithostratigraphic framework of the Upper Proterozoic Eleonore Bay Supergroup of East and North-East Greenland, *Bull. Grønlands geol. Unders., 167*, 39 pp., 1993.

Staples, R. K., R. S. White, B. Brandsdóttir, W. Menke, P. K. H. Maguire and J. H. McBride, Färoe-Iceland Ridge Experiment: 1. Crustal structure of northeastern Iceland, *J. Geophys. Res., 102, B4*, 7849-7866, 1997.

Steenfelt, A., Geochemical patterns related to major tectono-stratigraphic units in the Precambrian of northern Scandinavia and Greenland, in A. G. Darnley and R. G. Garrett (eds.), International geochemical mapping, *J. Geochem. Explor., 39,* 35-48, 1990.

Stemmerik, L., and E. Håkansson, Carboniferous and Permian history of the Wandel Sea Basin, North Greenland, *Bull. Grønlands geol. Unders., 160,* 141-151, 1991.

Strachan, R. A., Evidence in North-East Greenland for Late Silurian-Early Devonian regional extension during the Caledonian orogeny, *Geology, 22,* 913-916, 1994.

Strachan, R. A., J. D. Friderichsen, R. E. Holdsworth and H. F. Jepsen, Regional geology and Caledonian structure, Dronning Louise Land, North-East Greenland, *Rapp. Grønlands geol. Unders., 162*, 71-76,1994.

Surlyk, F., Timing, style and sedimentary evolution of Late Palaeozoic - Mesozoic extensional basins of East Greenland, in R. F. P. Hardman and J. Brooks (eds.), Tectonic events responsible for Britain's oil and gas reserves, *Geological Society Special Publication, 55,* 107-125, 1990.

Surlyk, F., Tectonostratigraphy of North Greenland, *Bull. Grønlands geol. Unders., 160*, 25-47, 1991.

Talwani, M., Computation with the help of a digital computer of magnetic anomalies caused by bodies of arbitrary shape, *Geophysics, 30,* 797-817, 1965.

Talwani, M., J. L. Worzel and M. Landisman, Rapid gravity computations for two-dimensional bodies with application to the Mendocino submarine fracture zone, *J. Geophys. Res., 64,* 59-69, 1959.

Thorning, L., Aeromagnetic maps of parts of southern and central West Greenland: acquisition, compilation and general analysis of data, *Rapp. Grønlands geol. Unders., 122*, 1-36, 1984.

Thorning, L., Aeromagnetic anomaly map of Greenland, Sheet 5 (69°30'-76°00'N, 12°-24°W), 1: 1 000 000, Geological Survey of Greenland, Copenhagen, 1988.

Torge, W., *Gravimetry,* 465 pp., Walter de Gruyter, Berlin, 1989.

Uenzelmann-Neben, G., W. Jokat and K. Vanneste, Quaternary sediments in Scoresby Sund, East Greenland: their distribution as revealed by reflection seismic data, in P. Möller, C. Hjort and Ó. Ingólfsson (eds.), The last interglacial-glacial cycle: preliminary report on the PONAM field work in Jameson Land and Scoresby Sund, East Greenland, *Lundqua report, 33,* 139-148, 1991.

Upton, B. G. J., C. H. Emeleus and N. Hald, Tertiary volcanism in northern East Greenland: Gauss Halvø and Hold with Hope, *J. geol. Soc. London, 137,* 491-508, 1980.

Upton, B. G. J., C. H. Emeleus and R. D. Beckinsale, Petrology of the Northern East Greenland Tertiary Flood Basalts: Evidence from Hold with Hope and Wollaston Foreland, *J. Petrol., 25,* 151-184, 1984.

Upton, B. G. J., C. H. Emeleus, D. C. Rex and M. F. Thirlwall, Early Tertiary magmatism in North-East Greenland, *J. geol. Soc. London, 152,* 959-964, 1995.

Wasilewski, P. J., and M. A. Mayhew, Crustal xenoliths magnetic properties and long wavelength anomaly source requirements, *Geophys. Res. Lett., 9,* 329-332, 1982.

Watt, S. W., Stratigraphy and correlation of the Tertiary plateau basalts in North-East Greenland, *Rapp. Grønlands geol. Unders., 162*, 195-200, 1994.

Weigel, W., E. R. Flüh, H. Miller, A. Butzke, G. A. Dehgani, V. Gebhardt, I. Harder, J. Hepper, W. Jokat, D. Kläschen, S. Kreymann, S. Schüßler and Z. Zhao - GROEKORT Study Group, Investigations

of the East Greenland continental margin between 70° and 72°N by deep seismic sounding and gravity studies, *Marine Geophysical Researches, 17,* 167-199, 1995.

Wernicke, B., Uniform-sense normal simple shear of the continental lithosphere, *Can. J. Earth Sci., 22,* 108-125, 1985.

Wessel, P., and W. H. F. Smith, Free software helps map and display data, *EOS Trans. AGU, 72,* p. 441, 1991.

Wessel, P., and W. H. F. Smith, New version of the Generic Mapping Tools released, *EOS Trans. AGU, 76,* p. 329, 1995.

White, R. S., Magmatism during and after continental break-up, in B. C. Storey, T. Alabaster and R. J. Pankhurst (eds.), Magmatism and the causes for continental break-up, *Geological Society Special Publication, 68,* 1-16, 1992.

White, R. S., and D. P. McKenzie, Magmatism at rift zones: the generation of volcanic continental margins and flood basalts, *J. Geophys. Res., 94, B6,* 7685-7729, 1989.

Wright, J. K., The exploration of the fiord region of East Greenland: a historical outline, in L. A. Boyd, The fiord region of East Greenland, *American Geographical Society, Special Publication No. 18,* 317-357, 1935.

Yilmaz, Ö, Seismic data processing, *Investigations in geophysics, 2,* 526 pp., Society of exploration geophysicists, Tulsa, 1987.

Zelt, C. A., and R. B. Smith, Seismic traveltime inversion for 2-D crustal velocity structure, *Geophys. J. Int., 108,* 16-34, 1992.

Zelt, C. A., and D. A. Forsyth, Modeling wide-angle seismic data for crustal structure: Southeastern Grenville Province, *J. Geophys. Res., 99, B6,* 11687-11704, 1994.

Ziegler, P. A., Late Caledonian framework of western and central Europe, in D. G. Gee and B. A. Sturt (eds.), *The Caledonide Orogen - Scandinavia and related areas*, 3-18, J. Wiley & Sons Ltd, London, 1985.

9 Appendix

Appendix 1

Susceptibility data acquired in East Greenland

Locality	Latitude [degree N]	Longitude [degree W]	Number of measurements	Site mean susceptibility [10^{-3} SI units]	ROCKTYPE
1	72.6395	27.1085	61	0.20	METASEDK
2	72.6377	27.0882	30	0.32	METASEDK
3	72.6355	27.0862	50	12.0	BASGNEIS
4	72.6348	27.0865	70	0.26	BASGNEIS
5	72.6355	27.0807	33	8.94	BASGNEIS
6	72.6390	27.1150	30	0.12	METASEDK
7	72.6400	27.1402	60	1.47	METASEDK
8	72.9750	29.1462	29	0.35	METASEDE
9	72.9805	28.7473	20	0.06	METASEDE
10	72.5452	27.6472	20	0.72	BASAMPHI
11	72.5452	27.6472	20	0.31	BASGNEIS
12	72.6763	27.3447	40	3.82	BASGNEIS
13	72.7137	26.1562	21	0.70	BASAMPHI
14	72.7123	26.1467	30	0.58	BASGNEIS
15	72.6727	27.2900	80	34.1	BASGNGRA
16	72.7675	26.5893	21	63.1	BASGNGRA
17	72.3448	26.3967	30	2.54	BASGNEIS
18	72.3448	26.3967	10	1.20	BASAMPHI
19	72.3450	26.4457	21	68.9	BASPERID
20	72.3548	26.4142	40	2.40	BASGNEIS
21	72.3563	26.4193	31	32.0	BASPERID
22	72.3563	26.4193	20	0.87	BASAMPHI
23	72.3563	26.4193	30	1.04	BASGNEIS
24	72.3283	26.6620	20	0.33	BASGNEIS
25	72.3320	26.7468	10	59.4	BASPERID
26	72.3300	26.7393	40	2.35	BASGNEIS
27	72.3263	25.9540	30	0.16	METASEDK
28	72.3107	25.8507	20	0.11	METASEDE
29	72.3252	25.9020	30	0.13	METASEDE
30	72.2872	25.9558	20	0.24	METASMIK
31	72.3578	26.3115	31	0.26	METASMIK
32	72.3683	26.4288	20	2.06	BASAMPHI
33	72.3077	26.9525	31	34.9	BASGNGRA
34	72.3413	26.5625	20	3.19	BASGNEIS

Locality	Latitude [degree N]	Longitude [degree W]	Number of measurements	Site mean susceptibility [10^{-3} SI units]	ROCKTYPE
35	72.3355	26.5077	10	10.6	BASPERID
36	72.3407	26.6180	30	2.94	BASGNEIS
37	72.3425	26.6155	30	0.28	BASGNEIS
38	72.3348	26.6052	40	0.34	BASGNEIS
39	72.3348	26.6052	30	0.21	METASEDK
40	72.3295	26.5797	41	7.72	BASGNEIS
41	72.3287	26.5748	30	2.50	BASGNEIS
42	72.0647	26.3403	60	0.87	BASGNEIS
43	72.0503	26.3162	40	1.09	BASGNEIS
44	72.0440	26.2975	21	0.19	METASEDK
45	72.0392	26.2357	20	0.08	METASPEK
46	72.0408	26.1515	31	0.17	METASMIK
47	72.1133	26.4192	20	0.30	METASEDK
48	72.1250	26.3523	20	0.41	METASEDK
49	72.1853	26.5847	19	0.41	METASEDK
50	71.9203	26.3385	20	0.28	BASGNEIS
51	72.0225	26.5725	30	0.66	BASGNEIS
52	72.0232	25.9845	40	0.35	METASMIK
53	72.0183	25.8898	20	0.17	METASMIK
54	72.0147	25.8417	20	0.14	METASPEK
55	71.9975	25.9307	40	0.24	METASMIK
56	72.0000	25.9785	20	0.21	METASMIK
57	72.0000	26.0060	10	0.01	METASMIK
58	72.0050	26.0583	20	0.12	METASMIK
59	72.0115	26.1032	10	0.10	METASMIK
60	72.0123	26.1588	10	0.21	METASMIK
61	72.0110	26.3123	40	0.34	BASGNEIS
62	72.0205	26.4237	60	1.26	BASGNEIS
63	72.1200	26.6688	31	4.67	BASGNEIS
64	72.0833	26.7863	41	1.44	BASGNEIS
65	72.1002	27.0978	19	27.8	BASGNEIS
66	72.1045	27.3460	20	0.32	BASGNEIS
67	72.0282	27.0728	40	17.2	MARAMPHI
68	72.0030	27.1960	20	1.04	MARAMPHI
69	72.0262	27.6537	100	3.37	BASGNEIS
70	72.0288	27.7072	80	1.64	BASGNEIS
71	72.0222	27.7830	60	0.44	BASGNEIS
72	72.0222	27.7830	20	1.13	BASAMPHI
73	72.0222	27.7830	20	1.86	METASEDK
74	72.0222	27.7830	40	17.6	MARAMPHI
75	72.032	27.6610	30	1.26	MARAMPHI
76	72.0392	27.6935	170	17.9	MARAMPHI
77	72.0965	28.8800	90	0.24	CBASGNEI

Locality	Latitude [degree N]	Longitude [degree W]	Number of measurements	Site mean susceptibility [10^{-3} SI units]	ROCKTYPE
78	72.0902	28.8943	20	0.20	CBASGNEI
79	72.0793	28.8873	50	0.26	CBASGRAN
80	72.0892	28.8533	30	0.26	CBASGNEI
81	72.0938	28.8513	40	19.6	CTERTDOL
82	72.0938	28.8513	20	0.26	CSUPRAMS
83	72.0938	28.8513	20	0.83	CSUPRAAM
84	71.8035	28.7112	50	24.7	CSUPRAAI
85	71.8035	28.7112	20	24.6	BASPERID
86	71.7858	29.1337	30	1.15	CSUPRAAI
87	71.8042	29.4985	30	27.6	CSUPRAAI
88	72.0238	30.0038	30	0.62	METASEDK
89	72.0208	29.3785	20	0.75	CSUPRAMS
90	72.1105	29.1697	20	14.6	CTERTDOL
91	72.1105	29.1697	30	0.38	CBASGRAN
92	72.2112	28.9280	20	0.59	CSUPRAMS
93	72.1722	28.7173	20	0.56	CSUPRAMS
94	72.1722	28.7173	20	27.8	CSUPRAAI
95	72.0278	28.9460	30	0.71	CBASGRAN
96	72.0202	28.6400	30	0.30	CBASGNEI
97	71.9965	28.4733	19	138	CSUPRAMS
98	71.9965	28.4733	10	7.06	CSUPRAAM
99	72.0618	27.9713	30	3.83	MARAMPHI
100	72.0618	27.9713	10	0.48	BASGNEIS
101	72.0688	28.0602	20	0.73	CSUPRAMS
102	72.2027	28.6622	20	0.61	CSUPRAMS

Abbreviations:

BASGNEIS	basement gneiss
BASAMPHI	basement amphibolites
BASPERID	ultramafic rocks
BASGNGRA	magnetite-bearing granitic gneiss
METASEDK	Krummedal (?) metasedimentary rocks
METASMIK	migmatized Krummedal metasedimentary rocks
METASPEK	pegmatite dyke in Krummedal metasedimentary rocks
MARAMPHI	amphibolitic rocks associated with marbles
METASEDE	Eleonore Bay Supergroup or equivalent metasedimentary rocks
CBASGRAN	Charcot Land window basement granites
CBASGNEI	Charcot Land window basement gneisses
CSUPRAMS	Charcot Land window metasedimentary rocks
CSUPRAAM	Charcot Land window amphibolites
CSUPRAAI	Charcot Land window gabbros and greenschists
CTERTDOL	Charcot Land window Tertiary dolerite dyke

Appendix 2

Location and recording parameters of receiver stations used for the acquisition of the seismic refraction profiles 94300, 94310, 94320, 94340, 94360 and 94400.

Station	Profile	Latitude [degree N]	Longitude [degree W]	Elevation [m]	Instruments	No. of channels	AWI archive cartridge no.
301	94300	74.970	18.467	18	3Z, 3K, REF	6	C05118
302	94300	75.165	19.948	381	4Z, PCM	4	C05050
303	94300	75.289	20.633	33	3Z, REF	3	C05069
304	94300	75.423	21.208	52	3Z, REF	3	C05119
305	94300	75.542	21.462	43	3Z, REF	3	C05068
306	94300	75.676	22.253	579	4Z, PCM	4	C05051
307	94300	75.676	22.253	579	3K LIP, REF	3	C05120
308	94300	75.698	23.275	1097	2Z, REF	2	C05067
311	94310	74.970	18.467	34	3Z, 3K, REF	6	C05114
312	94310	74.505	18.766	12	4Z, REF	4	C05115
313	94310	73.902	20.035	216	3Z, REF	3	C05116
314	94310	73.139	21.273	244	3Z, 3K, REF	6	C05117
321	94320	73.139	21.273	244	3Z, 3K, REF	6	C05124-25
322	94320	73.141	22.991	198	4Z, PCM	4	C05153
323	94320	73.344	23.730	25	3Z, 3K, REF	6	C05126-27
324	94320	73.429	24.734	115	3Z, 3K, REF	6	C05128
325	94320	73.325	25.278	49	3Z, REF	3	C05129
326	94320	73.191	25.740	198	4Z, PCM	4	C05160
327	94320	73.172	26.481	335	3K LIP, REF	3	C05132
328	94320	73.139	27.114	518	2Z, REF	2	C05130
329	94320	73.157	27.405	76	2Z, REF	2	C05131
330	94320	73.251	28.789	1798	3Z, REF	3	C05133
331	94320	73.346	29.690	2343	3Z, REF	3	C05134
341	94340	71.991	22.935	116	3K LIP, REF	3	C05164
342	94340	72.213	23.645	18	4Z, REF	4	C05332
343	94340	72.347	24.295	12	3Z, REF	3	C05163
344	94340	72.487	24.601	18	3K, REF	3	C05162
345	94340	72.678	24.719	76	3Z, REF	3	C05156
346	94340	72.959	24.837	61	4Z, PCM	4	C05273
347	94340	73.076	25.175	30	3K LIP, REF	3	C05158
348	94340	73.191	25.740	198	4Z, PCM	4	C05274

Station	Profile	Latitude [degree N]	Longitude [degree W]	Elevation [m]	Instruments	No. of channels	AWI archive cartridge no.
349	94340	73.325	26.637	30	3Z, 3K, REF	6	C05159
350	94340	73.435	27.093	36	3Z, REF	3	C05157
351	94340	73.728	28.194	1277	3Z, REF	3	C05154
352	94340	74.021	28.784	1992	3Z, REF	3	C05155
361	94360	73.139	21.273	244	3Z, 3K, REF	6	C05298
362	94360	73.106	22.454	24	3Z, REF	3	C05299
363	94360	73.141	22.988	218	4Z, PCM	4	C05272
364	94360	73.008	23.658	204	3Z, REF	3	C05300
365	94360	72.959	24.837	61	4Z, PCM	4	C05297
366	94360	72.830	25.572	80	3K LIP, REF	3	C05176
367	94360	72.723	26.198	80	3Z,3K REF	6	C05175
368	94360	72.831	27.472	335	3Z, REF	3	C05185
369	94360	72.768	28.202	1189	3Z, REF	3	C05174
401	94400	70.550	24.620	-401	OBH	2	C05324
402	94400	70.484	25.277	-517	OBH	1	C05325
403	94400	70.026	28.989	1064	3Z, REF	3	C05326
404	94400	69.858	29.350	1825	3Z, 3K LIP, REF	6	C05327

Abbreviations:

Z: SENSOR vertical component geophones, resonant frequency 4.5 Hz
3K: SENSOR 3-component geophones, resonant frequency 4.5 Hz
K LIP: Lippmann 3-component seismometer, resonant frequency 1 Hz
PCM: Lennartz PCM; sample rate 200 Hz; DCF time signal
REF: Reftek; sample rate 100 Hz; GPS time signal
OBH: ocean bottom hydrophone

Appendix 3a

Nonlinear, depth-dependent relationship between compressional wave velocity and density after Christensen & Mooney (1995).

$$\rho = a + b/v_p$$

Depth [km]	a [10^3 kg m^{-3}]	b [10^3 kg m^{-3}/km s^{-1}]	S(ρ, v_p) [10^3 kg m^{-3}]
10	4.929	-13.294	0.069
20	5.055	-14.094	0.062
30	5.141	-14.539	0.057
40	5.212	-14.863	0.054

Abbreviations:

ρ: Density
v_p: Compressional wave velocity
$S(\rho,v_p)$: Standard error of estimate of ρ on V_p

Appendix 3b

Depth-dependent conversion of average P-wave velocities of the seismic models for profiles KFJ, DKS and KOF to densities using the above relationship.

$\bar{v}_p$ [km s^{-1}]	d [km]	ρ [10^3 kg m^{-3}]	S(ρ, v_p) [10^3 kg m^{-3}]
5.85	10	2.66	0.07
6.10	10	2.75	0.07
6.40	20	2.85	0.06
6.70	40	2.99	0.05
6.75	30	2.99	0.06
7.20 (KFJ, DKS)	20	3.10	0.06
7.10 (KOF)	20	3.07	0.06
7.95	30	3.31	0.06

Abbreviations:

$\bar{v}_p$: Representative layer P-wave velocity
d: Depth
ρ: Resulting density
$S(\rho,v_p)$: Standard error of estimate of ρ

Folgende Hefte der Reihe „Berichte zur Polarforschung" sind bisher erschienen:

* **Sonderheft Nr. 1/1981** – „Die Antarktis und ihr Lebensraum",
Eine Einführung für Besucher – Herausgegeben im Auftrag von SCAR
Heft Nr. 1/1982 – „Die Filchner-Schelfeis-Expedition 1980/81",
zusammengestellt von Heinz Kohnen
* **Heft Nr. 2/1982** – „Deutsche Antarktis-Expedition 1980/81 mit FS 'Meteor'",
First International BIOMASS Experiment (FIBEX) – Liste der Zooplankton- und Mikronektonnetzfänge
zusammengestellt von Norbert Klages
Heft Nr. 3/1982 – „Digitale und analoge Krill-Echolot-Rohdatenerfassung an Bord des Forschungsschiffes 'Meteor'" (im Rahmen von FIBEX 1980/81, Fahrtabschnitt ANT III), von Bodo Morgenstern
Heft Nr. 4/1982 – „Filchner-Schelfeis-Expedition 1980/81",
Liste der Planktonfänge und Lichtstärkemessungen
zusammengestellt von Gerd Hubold und H. Eberhard Drescher
* **Heft Nr. 5/1982** – „Joint Biological Expedition on RRS 'John Biscoe', February 1982",
by G. Hempel and R. B. Heywood
* **Heft Nr. 6/1982** – „Antarktis-Expedition 1981/82 (Unternehmen 'Eiswarte')",
zusammengestellt von Gode Gravenhorst
Heft Nr. 7/1982 – „Marin-Biologisches Begleitprogramm zur Standorterkundung 1979/80 mit MS 'Polarsirkel' (Pre-Site Survey)" – Stationslisten der Mikronekton- und Zooplanktonfänge sowie der Bodenfischerei
zusammengestellt von R. Schneppenheim
Heft Nr. 8/1983 – „The Post-Fibex Data Interpretation Workshop",
by D. L. Cram and J.-C. Freytag with the collaboration of J. W. Schmidt, M. Mall, R. Kresse, T. Schwinghammer
* **Heft Nr. 9/1983** – „Distribution of some groups of zooplankton in the inner Weddell Sea in summer 1979/80",
by I. Hempel, G. Hubold, B. Kaczmaruk, R. Keller, R. Weigmann-Haass
Heft Nr. 10/1983 – „Fluor im antarktischen Ökosystem" – DFG-Symposium November 1982
zusammengestellt von Dieter Adelung
Heft Nr. 11/1983 – „Joint Biological Expedition on RRS 'John Biscoe', February 1982 (II)",
Data of micronecton and zooplankton hauls, by Uwe Piatkowski
Heft Nr. 12/1983 – „Das biologische Programm der ANTARKTIS-I-Expedition 1983 mit FS 'Polarstern'",
Stationslisten der Plankton-, Benthos- und Grundschleppnetzfänge und Liste der Probennahme an Robben und Vögeln, von H. E. Drescher, G. Hubold, U. Piatkowski, J. Plötz und J. Voß
* **Heft Nr. 13/1983** – „Die Antarktis-Expedition von MS 'Polarbjörn' 1982/83" (Sommerkampagne zur Atka-Bucht und zu den Kraul-Bergen), zusammengestellt von Heinz Kohnen
* **Sonderheft Nr. 2/1983** – „Die erste Antarktis-Expedition von FS 'Polarstern' (Kapstadt, 20. Januar 1983 – Rio de Janeiro, 25. März 1983)", Bericht des Fahrtleiters Prof. Dr. Gotthilf Hempel
Sonderheft Nr. 3/1983 – „Sicherheit und Überleben bei Polarexpeditionen",
zusammengestellt von Heinz Kohnen
* **Heft Nr. 14/1983** – „Die erste Antarktis-Expedition (ANTARKTIS I) von FS 'Polarstern' 1982/83",
herausgegeben von Gotthilf Hempel
Sonderheft Nr. 4/1983 – „On the Biology of Krill *Euphausia superba*" – Proceedings of the Seminar and Report of the Krill Ecology Group, Bremerhaven 12.-16. May 1983, edited by S. B. Schnack
Heft Nr. 15/1983 – „German Antarctic Expedition 1980/81 with FRV 'Walther Herwig' and RV 'Meteor'" – First International BIOMASS Experiment (FIBEX) – Data of micronekton and zooplankton hauls
by Uwe Piatkowski and Norbert Klages
Sonderheft Nr. 5/1984 – „The observatories of the Georg von Neumayer Station", by Ernst Augstein
Heft Nr. 16/1984 – „FIBEX cruise zooplankton data",
by U. Piatkowski, I. Hempel and S. Rakusa-Suszczewski
Heft Nr. 17/1984 – „Fahrtbericht (cruise report) der 'Polarstern'-Reise ARKTIS I, 1983",
von E. Augstein, G. Hempel und J. Thiede
Heft Nr. 18/1984 – „Die Expedition ANTARKTIS II mit FS 'Polarstern' 1983/84",
Bericht von den Fahrtabschnitten 1, 2 und 3, herausgegeben von D. Fütterer
Heft Nr. 19/1984 – „Die Expedition ANTARKTIS II mit FS 'Polarstern' 1983/84",
Bericht vom Fahrtabschnitt 4, Punta Arenas-Kapstadt (Ant-II/4), herausgegeben von H. Kohnen
Heft Nr. 20/1984 – „Die Expedition ARKTIS II des FS 'Polarstern' 1984, mit Beiträgen des FS 'Valdivia' und des Forschungsflugzeuges 'Falcon 20' zum Marginal Ice Zone Experiment 1984 (MIZEX)",
von E. Augstein, G. Hempel, J. Schwarz, J. Thiede und W. Weigel
Heft Nr. 21/1985 – „Euphausiid larvae in plankton samples from the vicinity of the Antarctic Peninsula, February 1982", by Sigrid Marschall and Elke Mizdalski

Heft Nr. 22/1985 – „Maps of the geographical distribution of macrozooplankton in the Atlantic sector of the Southern Ocean", by Uwe Piatkowski
Heft Nr. 23/1985 – „Untersuchungen zur Funktionsmorphologie und Nahrungsaufnahme der Larven des Antarktischen Krills *Euphausia superba* Dana", von Hans-Peter Marschall
Heft Nr. 24/1985 – „Untersuchungen zum Periglazial auf der König-Georg-Insel Südshetlandinseln/ Antarktika. Deutsche physiogeographische Forschungen in der Antarktis. – Bericht über die Kampagne 1983/84", von Dietrich Barsch, Wolf-Dieter Blümel, Wolfgang Flügel, Roland Mäusbacher, Gerhard Stäblein, Wolfgang Zick
* **Heft Nr. 25/1985** – „Die Expedition ANTARKTIS III mit FS 'Polarstern' 1984/85", herausgegeben von Gotthilf Hempel
* **Heft Nr. 26/1985** – „The Southern Ocean"; A survey of oceanographic and marine meteorological research work by Hellmer et al.
Heft Nr. 27/1986 – „Spätpleistozäne Sedimentationsprozesse am antarktischen Kontinentalhang vor Kapp Norvegia, östliche Weddell-See", von Hannes Grobe
Heft Nr. 28/1986 – „Die Expedition ARKTIS III mit 'Polarstern' 1985", mit Beiträgen der Fahrtteilnehmer, herausgegeben von Rainer Gersonde
* **Heft Nr. 29/1986** – „5 Jahre Schwerpunktprogramm 'Antarktisforschung' der Deutschen Forschungsgemeinschaft." Rückblick und Ausblick. Zusammengestellt von Gotthilf Hempel, Sprecher des Schwerpunktprogramms
Heft Nr. 30/1986 – „The Meteorological Data of the Georg-von-Neumayer-Station for 1981 and 1982", by Marianne Gube and Friedrich Obleitner
Heft Nr. 31/1986 – „Zur Biologie der Jugendstadien der Notothenioidei (Pisces) an der Antarktischen Halbinsel", von A. Kellermann
Heft Nr. 32/1986 – „Die Expedition ANTARKTIS-IV mit FS 'Polarstern' 1985/86", mit Beiträgen der Fahrtteilnehmer, herausgegeben von Dieter Fütterer
Heft Nr. 33/1987 – „Die Expedition ANTARKTIS-IV mit FS 'Polarstern' 1985/86 – Bericht zu den Fahrtabschnitten ANT-IV/3-4", von Dieter Karl Fütterer
Heft Nr. 34/1987 – „Zoogeographische Untersuchungen und Gemeinschaftsanalysen an antarktischem Makroplankton", von U. Piatkowski
Heft Nr. 35/1987 – „Zur Verbreitung des Meso- und Makrozooplanktons in Oberflächenwasser der Weddell See (Antarktis)", von E. Boysen-Ennen
Heft Nr. 36/1987 – „Zur Nahrungs- und Bewegungsphysiologie von *Salpa thompsoni* und *Salpa fusiformis*", von M. Reinke
Heft Nr. 37/1987 – „The Eastern Weddell Sea Drifting Buoy Data Set of the Winter Weddell Sea Project (WWSP) 1986", by Heinrich Hoeber und Marianne Gube-Lehnhardt
Heft Nr. 38/1987 – „The Meteorological Data of the Georg von Neumayer Station for 1983 and 1984", by M. Gube-Lenhardt
Heft Nr. 39/1987 – „Die Winter-Expedition mit FS 'Polarstern' in die Antarktis (ANT V/1-3)", herausgegeben von Sigrid Schnack-Schiel
Heft Nr. 40/1987 – „Weather and Synoptic Situation during Winter Weddell Sea Project 1986 (ANT V/2) July 16 – September 10, 1986", by Werner Rabe
Heft Nr. 41/1988 – „Zur Verbreitung und Ökologie der Seegurken im Weddellmeer (Antarktis)", von Julian Gutt
Heft Nr. 42/1988 – „The zooplankton community in the deep bathyal and abyssal zones of the eastern North Atlantic", by Werner Beckmann
Heft Nr. 43/1988 – „Scientific cruise report of Arctic Expedition ARK IV/3", Wissenschaftlicher Fahrtbericht der Arktis-Expedition ARK IV/3, compiled by Jörn Thiede
Heft Nr. 44/1988 – „Data Report for FV 'Polarstem' Cruise ARK IV/1, 1987 to the Arctic and Polar Fronts", by Hans-Jürgen Hirche
Heft Nr. 45/1988 – „Zoogeographie und Gemeinschaftsanalyse des Makrozoobenthos des Weddellmeeres (Antarktis)", von Joachim Voß
Heft Nr. 46/1988 – „Meteorological and Oceanographic Data of the Winter-Weddell-Sea Project 1986 (ANT V/3)", by Eberhard Fahrbach
Heft Nr. 47/1988 – „Verteilung und Herkunft glazial-mariner Gerölle am Antarktischen Kontinentalrand des östlichen Weddellmeeres", von Wolfgang Oskierski
Heft Nr. 48/1988 – „Variationen des Erdmagnetfeldes an der GvN-Station", von Arnold Brodscholl
* **Heft Nr. 49/1988** – „Zur Bedeutung der Lipide im antarktischen Zooplankton", von Wilhelm Hagen
Heft Nr. 50/1988 – „Die gezeitenbedingte Dynamik des Ekström-Schelfeises, Antarktis", von Wolfgang Kobarg
Heft Nr. 51/1988 – „Ökomorphologie notothenüder Fische aus dem Weddellmeer, Antarktis", von Werner Ekau
Heft Nr. 52/1988 – „Zusammensetzung der Bodenfauna in der westlichen Fram-Straße", von Dieter Piepenburg
* **Heft Nr. 53/1988** – „Untersuchungen zur Ökologie des Phytoplanktons im südöstichen Weddellmeer (Antarktis) im Jan./Febr. 1985", von Eva-Maria Nöthig

Heft Nr. 54/1988 – „Die Fischfauna des östlichen und südlichen Weddellmeeres: geographische Verbreitung, Nahrung und trophische Stellung der Fischarten", von Wiebke Schwarzbach
Heft Nr. 55/1988 – „Weight and length data of zooplankton in the Weddell Sea in austral spring 1986 (ANT V/3)", by Elke Mizdalski
Heft Nr. 56/1989 – „Scientific cruise report of Arctic expeditions ARK IV/1, 2 & 3", by G. Krause, J. Meincke und J. Thiede
Heft Nr. 57/1989 – „Die Expedition ANTARKTIS V mit FS 'Polarstern' 1986/87", Bericht von den Fahrtabschnitten ANT V/4-5 von H. Miller und H. Oerter
* **Heft Nr. 58/1989** – „Die Expedition ANTARKTIS VI mit FS 'Polarstern' 1987/88", von D. K. Fütterer
Heft Nr. 59/1989 – „Die Expedition ARKTIS V/1a, 1b und 2 mit FS 'Polarstern' 1988", von M. Spindler
Heft Nr. 60/1989 – „Ein zweidimensionales Modell zur thermohalinen Zirkulation unter dem Schelfeis", von H. H. Hellmer
Heft Nr. 61/1989 – „Die Vulkanite im westlichen und mittleren Neuschwabenland, Vestfjella und Ahlmannryggen, Antarktika", von M. Peters
* **Heft-Nr. 62/1989** – „The Expedition ANTARKTIS VII/1 and 2 (EPOS I) of RV 'Polarstern' in 1988/89", by I. Hempel
Heft Nr. 63/1989 – „Die Eisalgenflora des Weddellmeeres (Antarktis): Artenzusammensetzung und Biomasse, sowie Ökophysiologie ausgewählter Arten", von Annette Bartsch
Heft Nr. 64/1989 – „Meteorological Data of the G.-v.-Neumayer-Station (Antarctica)", by L. Helmes
Heft Nr. 65/1989 – „Expedition Antarktis VII/3 in 1988/89", by I. Hempel, P. H. Schalk, V. Smetacek
Heft Nr. 66/1989 – „Geomorphologisch-glaziologische Detailkartierung des arid-hochpolaren Borgmassivet, Neuschwabenland, Antarktika", von Karsten Brunk
Heft-Nr. 67/1990 – „Identification key and catalogue of larval Antarctic fishes", edited by Adolf Kellermann
Heft-Nr. 68/1990 – „The Expediton Antarktis VII/4 (Epos leg 3) and VII/5 of RV 'Polarstern' in 1989", edited by W. Arntz, W. Ernst, I. Hempel
Heft-Nr. 69/1990 – „Abhängigkeiten elastischer und rheologischer Eigenschaften des Meereises vom Eisgefüge", von Harald Hellmann
Heft-Nr. 70/1990 – „Die beschalten benthischen Mollusken (Gastropoda und Bivalvia) des Weddellmeeres, Antarktis", von Stefan Hain
Heft-Nr. 71/1990 – „Sedimentologie und Paläomagnetik an Sedimenten der Maudkuppe (Nordöstliches Weddellmeer)", von Dieter Cordes
Heft-Nr. 72/1990 – „Distribution and abundance of planktonic copepods (Crustacea) in the Weddell Sea in summer 1980/81", by F. Kurbjeweit and S. Ali-Khan
Heft-Nr. 73/1990 – „Zur Frühdiagenese von organischem Kohlenstoff und Opal in Sedimenten des südlichen und östlichen Weddellmeeres", von M. Schlüter
Heft-Nr. 74/1991 – „Expeditionen ANTARKTIS-VIII/3 und VIII/4 mit FS 'Polarstern' 1989", von Rainer Gersonde und Gotthilf Hempel
Heft-Nr. 75/1991 – „Quartäre Sedimentationsprozesse am Kontinentalhang des Süd-Orkney-Plateaus im nordwestlichen Weddelmeer (Antarktis)", von Sigrun Grünig
Heft-Nr. 76/1991 – „Ergebnisse der faunistischen Arbeiten in Benthal von King George Island (Südshetlandinseln, Antarktis)", Martin Rauschert
Heft-Nr. 77/1991 – „Verteilung von Mikroplankton-Organismen nordwestlich der Antarktischen Halbinsel unter dem Einfluß sich ändernder Umweltbedingungen in Herbst", von Heinz Klöser
Heft-Nr. 78/1991 – „Hochauflösende Magnetostratigraphie spätquartärer Sedimente arktischer Meeresgebiete", von Norbert R. Nowaczyk
Heft-Nr. 79/1991 – „Ökophysiologische Untersuchungen zur Salinitäts- und Temperaturtoleranz antarktischer Grünalgen unter besonderer Berücksichtigung des ß-Dimethylsulfoniumpropionat (DMSP) – Stoffwechsels", von Ulf Karsten
Heft-Nr. 80/1991 – „Die Expedition ARKTIS VII/1 mit FS 'POLARSTERN' 1990", herausgegeben von Jörn Thiede und Gotthilf Hempel
Heft-Nr. 81/1991 – „Paläoglaziologie und Paläozeanographie im Spätquartär am Kontinentalrand des südlichen Weddellmeeres, Antarktis", von Martin Melles
Heft-Nr. 82/1991 – „Quantifizierung von Meereiseigenschaften: Automatische Bildanalyse von Dünnschnitten und Parametrisierung von Chlorophyll- und Salzgehaltsverteilungen", von Hajo Eicken
Heft-Nr. 83/1991 – „Das Fließen von Schelfeisen – numerische Simulationen mit der Methode der finiten Differenzen", von Jürgen Determann
Heft-Nr. 84/1991 – Die Expedition ANTARKTIS VIII/1-2, 1989 mit der Winter Weddell Gyre Study der Forschungsschiffe 'Polarstern' und 'Akademik Fedorov' ", von Ernst Augstein, Nicolai Bagriantsev und Hans Werner Schenke
Heft-Nr. 85/1991 – „Zur Entstehung von Unterwassereis und das Wachstum und die Energiebilanz des Meereises in der Atka Bucht, Antarktis", von Josef Kipfstuhl

Heft-Nr. 86/1991 – „Die Expedition ANTARKTIS-VIII mit FS 'Polarstern' 1989/90. Bericht vom Fahrtabschnitt ANT-VIII/5", herausgegeben von Heinz Miller und Hans Oerter
Heft-Nr. 87/1991 – „Scientific cruise reports of Arctic expeditions ARK-VI/1-4 of RV 'Polarstern' in 1989", edited by G. Krause, J. Meincke & H. J. Schwarz
Heft-Nr. 88/1991 – „Zur Lebensgeschichte dominanter Copepodenarten *(Calanus finmarchicus, C. glacialis, C. hyperboreus, Metridia longa)* in der Framstraße", von Sabine Diel
Heft-Nr. 89/1991 – „Detaillierte seismische Untersuchungen am östlichen Kontinentalrand des Weddell-Meeres vor Kapp Norvegia, Antarktis", von Norbert E. Kaul
Heft-Nr. 90/1991 – „Die Expedition ANTARKTIS VIII mit FS 'Polarstern' 1989/90. Bericht von Fahrtabschnitten ANT VIII/6-7", herausgegeben von Dieter Karl Fütterer und Otto Schrems
Heft-Nr. 91/1991 – „Blood physiology and ecological consequences in Weddell Sea fishes (Antarctica)", by Andreas Kunzmann.
Heft-Nr. 92/1991 – „Zur sommerlichen Verteilung des Mesozooplanktons im Nansen-Becken, Nordpolarmeer", von Nicolai Mumm.
Heft-Nr. 93/1991 – Die Expedition ARKTIS VII mit FS 'Polarstern' 1990. Bericht von Fahrtabschnitten ARK VII/2", herausgegeben vom Gunther Krause.
Heft-Nr. 94/1991 – „Die Entwicklung des Phytoplanktons im östlichen Weddellmeer (Antarktis) beim Übergang vom Spätwinter zum Frühjahr", von Renate Scharek.
Heft-Nr. 95/1991 – „Radioisotopenstratigraphie, Sedimentologie und Geochemie jungquartärer Sedimente des östlichen Arktischen Ozeans", von Horst Bohrmann.
Heft-Nr. 96/1991 – „Holozäne Sedimentationsentwicklung im Scoresby Sund, Ost-Grönland", von Peter Marienfeld
Heft-Nr. 97/1991 – „Strukturelle Entwicklung und Abkühlungsgeschichte der Heimefrontfjella (Westliches Dronning Maud Land / Antarktika)", von Joachim Jacobs
Heft-Nr. 98/1991 – „Zur Besiedlungsgeschichte des antarktischen Schelfes am Beispiel der Isopoda (Crustacea, Malacostraca)", von Angelika Brandt
Heft-Nr. 99/1992 – „The Antarctic ice sheet and environmental change: a three-dimensional modelling study", by Philippe Huybrechts
* **Heft-Nr. 100/1992** – „Die Expeditionen ANTARKTIS IX/1-4 des Forschungsschiffes 'Polarstern' 1990/91", herausgegeben von Ulrich Bathmann, Meinhard Schulz-Baldes, Eberhard Fahrbach, Victor Smetacek und Hans-Wolfgang Hubberten
Heft-Nr. 101/1992 – „Wechselbeziehungen zwischen Spurenmetallkonzentrationen (Cd, Cu, Pb, Zn) im Meerwasser und in Zooplanktonorganismen (Copepoda) der Arktis und des Atlantiks", von Christa Pohl
Heft-Nr. 102/1992 – „Physiologie und Ultrastruktur der antarktischen Grünalge *Prasiola crispa* ssp. *antarctica* unter osmotischem Streß und Austrocknung", von Andreas Jacob
Heft-Nr. 103/1992 – „Zur Ökologie der Fische im Weddellmeer", von Gerd Hubold
Heft-Nr. 104/1992 – „Mehrkanalige adaptive Filter für die Unterdrückung von multiplen Reflexionen in Verbindung mit der freien Oberfläche in marinen Seismogrammen", von Andreas Rosenberger
Heft-Nr. 105/1992 – „Radiation and Eddy Flux Experiment 1991 *(REFLEX I)*", von Jörg Hartmann, Christoph Kottmeier und Christian Wamser
Heft-Nr. 106/1992 – „Ostracoden im Epipelagial vor der Antarktischen Halbinsel - ein Beitrag zur Systematik sowie zur Verbreitung und Populationsstruktur unter Berücksichtigung der Saisonalität", von Rüdiger Kock
Heft-Nr. 107/1992 – „ARCTIC '91: Die Expedition ARK-VIII/3 mit FS 'Polarstern' 1991", herausgegeben von Dieter K. Fütterer
Heft-Nr. 108/1992 – „Dehnungsbeben an einer Störungszone im Ekström-Schelfeis nördlich der Georg-von-Neumayer Station, Antarktis. - Eine Untersuchung mit seismologischen und geodätischen Methoden", von Uwe Nixdorf
Heft-Nr. 109/1992 – „Spätquartäre Sedimentation am Kontinentalrand des südöstlichen Weddellmeeres, Antarktis", von Michael Weber
Heft-Nr. 110/1992 – „Sedimentfazies und Bodenwasserstrom am Kontinentalhang des nordwestlichen Weddellmeeres", von Isa Brehme
Heft-Nr. 111/1992 – „Die Lebensbedingungen in den Solekanälchen des antarktischen Meereises", von Jürgen Weissenberger
Heft-Nr. 112/1992 – „Zur Taxonomie von rezenten benthischen Foraminiferen aus dem Nansen Becken, Arktischer Ozean", von Jutta Wollenburg
Heft-Nr. 113/1992 – „Die Expedition ARKTIS VIII/1 mit FS 'Polarstern' 1991", herausgegeben von Gerhard Kattner
* **Heft-Nr. 114/1992** – „Die Gründungsphase deutscher Polarforschung, 1865-1875", von Reinhard A. Krause
Heft-Nr. 115/1992 – „Scientific Cruise Report of the 1991 Arctic Expedition ARK VIII/2 of RV "Polarstern" (EPOS II)", by Eike Rachor

Heft-Nr. 116/1992 – „The Meteorological Data of the Georg-von-Neumayer-Station (Antarctica) for 1988, 1989, 1990 and 1991", by Gert König-Langlo
Heft-Nr. 117/1992 – „Petrogenese des metamorphen Grundgebirges der zentralen Heimefrontfjella (westliches Dronning Maud Land / Antarktis)", von Peter Schulze
Heft-Nr. 118/1993 – „Die mafischen Gänge der Shackleton Range / Antarktika: Petrographie, Geochemie, Isotopengeochemie und Paläomagnetik", von Rüdiger Hotten
* **Heft-Nr. 119/1993** – „Gefrierschutz bei Fischen der Polarmeere", von Andreas P. A. Wöhrmann
* **Heft-Nr. 120/1993** – „East Siberian Arctic Region Expedition '92: The Laptev Sea – its Significance for Arctic Sea-Ice Formation and Transpolar Sediment Flux", by D. Dethleff, D. Nürnberg, E. Reimnitz, M. Saarso and Y.P. Savchenko. – „Expedition to Novaja Zemlja and Franz Josef Land with RV 'Dalnie Zelentsy' ", by D. Nürnberg and E. Groth
* **Heft-Nr. 121/1993** – „Die Expedition ANTARKTIS X/3 mit FS 'Polarstern' 1992", herausgegeben von Michael Spindler, Gerhard Dieckmann und David Thomas
Heft-Nr. 122/1993 – „Die Beschreibung der Korngestalt mit Hilfe der Fourier-Analyse: Parametrisierung der morphologischen Eigenschaften von Sedimentpartikeln", von Michael Diepenbroek
* **Heft-Nr. 123/1993** – „Zerstörungsfreie hochauflösende Dichteuntersuchungen mariner Sedimente", von Sebastian Gerland
Heft-Nr. 124/1993 – „Umsatz und Verteilung von Lipiden in arktischen marinen Organismen unter besonderer Berücksichtigung unterer trophischer Stufen", von Martin Graeve
Heft-Nr. 125/1993 – „Ökologie und Respiration ausgewählter arktischer Bodenfischarten", von Christian F. von Dorrien
Heft-Nr. 126/1993 – „Quantitative Bestimmung von Paläoumweltparametern des Antarktischen Oberflächenwassers im Spätquartär anhand von Transferfunktionen mit Diatomeen", von Ulrich Zielinski
Heft-Nr. 127/1993 – „Sedimenttransport durch das arktische Meereis: Die rezente lithogene und biogene Materialfracht", von Ingo Wollenburg
Heft-Nr. 128/1993 – „Cruise ANTARKTIS X/3 of RV 'Polarstern': CTD-Report", von Marek Zwierz
Heft-Nr. 129/1993 – „Reproduktion und Lebenszyklen dominanter Copepodenarten aus dem Weddellmeer, Antarktis", von Frank Kurbjeweit
Heft-Nr. 130/1993 – „Untersuchungen zu Temperaturregime und Massenhaushalt des Filchner-Ronne-Schelfeises, Antarktis, unter besonderer Berücksichtigung von Anfrier- und Abschmelzprozessen", von Klaus Grosfeld
Heft-Nr. 131/1993 – „Die Expedition ANTARKTIS X/5 mit FS 'Polarstern' 1992", herausgegeben von Rainer Gersonde
Heft-Nr. 132/1993 – „Bildung und Abgabe kurzkettiger halogenierter Kohlenwasserstoffe durch Makroalgen der Polarregionen", von Frank Laturnus
Heft-Nr. 133/1994 – „Radiation and Eddy Flux Experiment 1993 *(REFLEX II)*", by Christoph Kottmeier, Jörg Hartmann, Christian Wamser, Axel Bochert, Christof Lüpkes, Dietmar Freese and Wolfgang Cohrs
* **Heft-Nr. 134/1994** – „The Expedition ARKTIS-IX/1", edited by Hajo Eicken and Jens Meincke
Heft-Nr. 135/1994 – „Die Expeditionen ANTARKTIS X/6-8", herausgegeben von Ulrich Bathmann, Victor Smetacek, Hein de Baar, Eberhard Fahrbach und Gunter Krause
Heft-Nr. 136/1994 – „Untersuchungen zur Ernährungsökologie von Kaiserpinguinen *(Aptenodytes forsteri)* und Königspinguinen *(Aptenodytes patagonicus)*", von Klemens Pütz
* **Heft-Nr. 137/1994** – „Die känozoische Vereisungsgeschichte der Antarktis", von Werner U. Ehrmann
Heft-Nr. 138/1994 – „Untersuchungen stratosphärischer Aerosole vulkanischen Ursprungs und polarer stratosphärischer Wolken mit einem Mehrwellenlängen-Lidar auf Spitzbergen (79°N, 12°E)", von Georg Beyerle
Heft-Nr. 139/1994 – „Charakterisierung der Isopodenfauna (Crustacea, Malacostraca) des Scotia-Bogens aus biogeographischer Sicht: Ein multivariater Ansatz", von Holger Winkler
Heft-Nr. 140/1994 – „Die Expedition ANTARKTIS X/4 mit FS 'Polarstern' 1992", herausgegeben von Peter Lemke
Heft-Nr. 141/1994 – „Satellitenaltimetrie über Eis – Anwendung des GEOSAT-Altimeters über dem Ekströmisen, Antarktis", von Klemens Heidland
Heft-Nr. 142/1994 – „The 1993 Northeast Water Expedition. Scientific cruise report of RV 'Polarstern' Arctic cruises ARK IX/2 and 3, USCG 'Polar Bear' cruise NEWP and the NEWLand expedition", edited by Hans-Jürgen Hirche and Gerhard Kattner
Heft-Nr. 143/1994 – „Detaillierte refraktionsseismische Untersuchungen im inneren Scoresby Sund/ Ost Grönland", von Notker Fechner
Heft-Nr. 144/1994 – „Russian-German Cooperation in the Siberian Shelf Seas: Geo-System Laptev Sea", edited by Heidemarie Kassens, Hans-Wolfgang Hubberten, Sergey M. Pryamikov and Rüdiger Stein
* **Heft-Nr. 145/1994** – „The 1993 Northeast Water Expedition. Data Report of RV ‚Polarstern' Arctic Cruises IX/2 and 3", edited by Gerhard Kattner and Hans-Jürgen Hirche
Heft-Nr. 146/1994 – „Radiation Measurements at the German Antarctic Station Neumeyer 1982 – 1992", by Torsten Schmidt and Gert König-Langlo

Heft-Nr. 147/1994 – „Krustenstrukturen und Verlauf des Kontinentalrandes im Weddell Meer/Antarktis", von Christian Hübscher

Heft-Nr. 148/1994 – „The expeditions NORILSK/TAYMYR 1993 and BUNGER OASIS 1993/94 of the AWI Research Unit Potsdam", edited by Martin Melles

Heft-Nr. 149/1994 – „Die Expedition ARCTIC '93. Der Fahrtabschnitt ARK-IX/4 mit FS ‚Polarstern' 1993", herausgegeben von Dieter K. Fütterer

Heft-Nr. 150/1994 – „Der Energiebedarf der Pygoscelis-Pinguine: eine Synopse", von Boris M. Culik

Heft-Nr. 151/1994 – „Russian-German Cooperation: The Transdrift I Expedition to the Laptev Sea", edited by Heidemarie Kassens and Valeriy Y. Karpiy

Heft-Nr. 152/1994 – „Die Expedition ANTARKTIS-X mit FS 'Polarstern' 1992. Bericht von den Fahrtabschnitten ANT X/1a und 2", herausgegeben von Heinz Miller

Heft-Nr. 153/1994 – „Aminosäuren und Huminstoffe im Stickstoffkreislauf polarer Meere", von Ulrike Hubberten

Heft-Nr. 154/1994 – „Regional and seasonal variability in the vertical distribution of mesozooplankton in the Greenland Sea", by Claudio Richter

Heft-Nr. 155/1995 – „Benthos in polaren Gewässern", herausgegeben von Christian Wiencke und Wolf Arntz

Heft-Nr. 156/1995 – „An adjoint model for the determination of the mean oceanic circulation, air-sea fluxes and mixing coefficients", by Reiner Schlitzer

Heft-Nr. 157/1995 – „Biochemische Untersuchungen zum Lipidstoffwechsel antarktischer Copepoden", von Kirsten Fahl

* **Heft-Nr. 158/1995** – „Die deutsche Polarforschung seit der Jahrhundertwende und der Einfluß Erich von Drygalskis", von Cornelia Lüdecke

Heft-Nr. 159/1995 – „The distribution of $\delta\,^{18}O$ in the Arctic Ocean: Implications for the freshwater balance of the halocline and the sources of deep and bottom waters", by Dorothea Bauch

* **Heft-Nr. 160/1995** – „Rekonstruktion der spätquartären Tiefenwasserzirkulation und Produktivität im östlichen Südatlantik anhand von benthischen Foraminiferenvergesellschaftungen", von Gerhard Schmiedl

Heft-Nr. 161/1995 – „Der Einfluß von Salinität und Lichtintensität auf die Osmolytkonzentrationen, die Zellvolumina und die Wachstumsraten der antarktischen Eisdiatomeen *Chaetoceros* sp. und *Navicula* sp. unter besonderer Berücksichtigung der Aminosäure Prolin", von Jürgen Nothnagel

Heft-Nr. 162/1995 – „Meereistransportiertes lithogenes Feinmaterial in spätquartären Tiefseesedimenten des zentralen östlichen Arktischen Ozeans und der Framstraße", von Thomas Letzig

Heft-Nr. 163/1995 – „Die Expedition ANTARKTIS-XI/2 mit FS 'Polarstern' 1993/94", herausgegeben von Rainer Gersonde

Heft-Nr. 164/1995 – „Regionale und altersabhängige Variation gesteinsmagnetischer Parameter in marinen Sedimenten der Arktis", von Thomas Frederichs

Heft-Nr. 165/1995 – „Vorkommen, Verteilung und Umsatz biogener organischer Spurenstoffe: Sterole in antarktischen Gewässern", von Georg Hanke

Heft-Nr. 166/1995 – „Vergleichende Untersuchungen eines optimierten dynamisch-thermodynamischen Meereismodells mit Beobachtungen im Weddellmeer", von Holger Fischer

Heft-Nr. 167/1995 – „Rekonstruktionen von Paläo-Umweltparametern anhand von stabilen Isotopen und Faunen-Vergesellschaftungen planktischer Foraminiferen im Südatlantik", von Hans-Stefan Niebler

Heft-Nr. 168/1995 – „Die Expedition ANTARKTIS XII mit FS 'Polarstern' 1994/95. Bericht von den Fahrtabschnitten ANT XII/1 und 2", herausgegeben von Gerhard Kattner und Dieter Karl Fütterer

Heft-Nr. 169/1995 – „Medizinische Untersuchung zur Circadianrhythmik und zum Verhalten bei Überwinterern auf einer antarktischen Forschungsstation", von Hans Wortmann

Heft-Nr. 170/1995 – DFG-Kolloquium: Terrestrische Geowissenschaften – Geologie und Geophysik der Antarktis

Heft-Nr. 171/1995 – „Strukturentwicklung und Petrogenese des metamorphen Grundgebirges der nördlichen Heimefrontfjella (westliches Dronning Maud Land/Antarktika)", von Wilfried Bauer

Heft-Nr. 172/1995 – „Die Struktur der Erdkruste im Bereich des Scoresby Sund, Ostgrönland: Ergebnisse refraktionsseismischer und gravimetrischer Untersuchungen", von Holger Mandler

Heft-Nr. 173/1995 – „Paläozoische Akkretion am paläopazifischen Kontinentalrand der Antarktis in Nordvictorialand – P-T-D-Geschichte und Deformationsmechanismen im Bowers Terrane", von Stefan Matzer

Heft-Nr. 174/1995 – „The Expediton ARKTIS-X/2 of RV 'Polarstern' in 1994", edited by Hans-W. Hubberten

Heft-Nr. 175/1995 – „Russian-German Cooperation: The Expedition TAYMYR 1994", edited by Christine Siegert and Dmitry Bolshiyanov

Heft-Nr. 176/1995 – „Russian-German Cooperation: Laptev Sea System", edited by Heidemarie Kassens, Dieter Piepenburg, Jörn Thiede, Leonid Timokhov, Hans-Wolfgang Hubberten and Sergey M. Priamikov

Heft-Nr. 177/1995 – „Organischer Kohlenstoff in spätquartären Sedimenten des Arktischen Ozeans: Terrigener Eintrag und marine Produktivität", von Carsten J. Schubert

Heft-Nr. 178/1995 – „Cruise ANTARKTIS XII/4 of RV 'Polarstern' in 1995: CTD-Report", by Jüri Sildam

Heft-Nr. 179/1995 – „Benthische Foraminiferenfaunen als Wassermassen-, Produktions- und Eisdriftanzeiger im Arktischen Ozean", von Jutta Wollenburg

Heft-Nr. 180/1995 – „Biogenopal und biogenes Barium als Indikatoren für spätquartäre Produktivitäts-änderungen am antarktischen Kontinentalhang, atlantischer Sektor", von Wolfgang J. Bonn
Heft-Nr. 181/1995 – „Die Expedition ARKTIS X/1 des Forschungsschiffes 'Polarstern' 1994", herausgegeben von Eberhard Fahrbach
Heft-Nr. 182/1995 – „Laptev Sea System: Expeditions in 1994", edited by Heidemarie Kassens
Heft-Nr. 183/1996 – „Interpretation digitaler Parasound Echolotaufzeichnungen im östlichen Arktischen Ozean auf der Grundlage physikalischer Sedimenteigenschaften", von Uwe Bergmann
Heft-Nr. 184/1996 – „Distribution and dynamics of inorganic nitrogen compounds in the troposphere of continental, coastal, marine and Arctic areas", by María Dolores Andrés Hernández
Heft-Nr. 185/1996 – „Verbreitung und Lebensweise der Aphroditiden und Polynoiden (Polychaeta) im östlichen Weddellmeer und im Lazarevmeer (Antarktis)", von Michael Stiller
Heft-Nr. 186/1996 – „Reconstruction of Late Quaternary environmental conditions applying the natural radionuclides ^{230}Th, ^{10}Be, ^{231}Pa and ^{238}U: A study of deep-sea sediments from the eastern sector of the Antarctic Circumpolar Current System", by Martin Frank
Heft-Nr. 187/1996 – „The Meteorological Data of the Neumayer Station (Antarctica) for 1992, 1993 and 1994", by Gert König-Langlo and Andreas Herber
Heft-Nr. 188/1996 – „Die Expedition ANTARKTIS-XI/3 mit FS 'Polarstern' 1994", herausgegeben von Heinz Miller und Hannes Grobe
Heft-Nr. 189/1996 – „Die Expedition ARKTIS-VII/3 mit FS 'Polarstern' 1990", herausgegeben von Heinz Miller und Hannes Grobe
Heft-Nr. 190/1996 – „Cruise report of the Joint Chilean-German-Italian Magellan 'Victor Hensen' Campaign in 1994", edited by Wolf Arntz and Matthias Gorny
Heft-Nr. 191/1996 – „Leitfähigkeits- und Dichtemessung an Eisbohrkernen", von Frank Wilhelms
Heft-Nr. 192/1996 – „Photosynthese-Charakteristika und Lebensstrategien antarktischer Makroalgen", von Gabriele Weykam
Heft-Nr. 193/1996 – Heterogene Reaktionen von N_2O_5 und HBr und ihr Einfluß auf den Ozonabbau in der polaren Stratosphäre", von Sabine Seisel
Heft-Nr. 194/1996 – „Ökologie und Populationsdynamik antarktischer Ophiuroiden (Echinodermata)", von Corinna Dahm
Heft-Nr. 195/1996 – „Die planktische Foraminifere *Neogloboquadrina pachyderma* (Ehrenberg) im Weddellmeer, Antarktis", von Doris Berberich
Heft-Nr. 196/1996 – „Untersuchungen zum Beitrag chemischer und dynamischer Prozesse zur Variabilität des stratosphärischen Ozons über der Arktis", von Birgit Heese
Heft-Nr. 197/1996 – „The Expedition ARKTIS-XI/2 of RV 'Polarstern' in 1995", edited by Gunther Krause
Heft-Nr. 198/1996 – „Geodynamik des Westantarktischen Riftsystems basierend auf Apatit-Spaltspuranalysen", von Frank Lisker
Heft-Nr. 199/1996 – „The 1993 Northeast Water Expedition. Data Report on CTD Measurements of RV 'Polarstern' Cruises ARKTIS IX/2 and 3", by Gereon Budéus and Wolfgang Schneider
Heft-Nr. 200/1996 – „Stability of the Thermohaline Circulation in analytical and numerical models", by Gerrit Lohmann
Heft-Nr. 201/1996 – „Trophische Beziehungen zwischen Makroalgen und Herbivoren in der Potter Cove (King George-Insel, Antarktis)", von Katrin Iken
Heft-Nr. 202/1996 – „Zur Verbreitung und Respiration ökologisch wichtiger Bodentiere in den Gewässern um Svalbard (Arktis)", von Michael K. Schmid
Heft-Nr. 203/1996 – „Dynamik, Rauhigkeit und Alter des Meereises in der Arktis – Numerische Untersuchungen mit einem großskaligen Modell", von Markus Harder
Heft-Nr. 204/1996 – „Zur Parametrisierung der stabilen atmosphärischen Grenzschicht über einem antarktischen Schelfeis", von Dörthe Handorf
Heft-Nr. 205/1996 – „Textures and fabrics in the GRIP ice core, in relation to climate history and ice deformation", by Thorsteinn Thorsteinsson
Heft-Nr. 206/1996 – „Der Ozean als Teil des gekoppelten Klimasystems: Versuch der Rekonstruktion der glazialen Zirkulation mit verschieden komplexen Atmosphärenkomponenten", von Kerstin Fieg
Heft-Nr. 207/1996 – „Lebensstrategien dominanter antarktischer Oithonidae (Cyclopoida, Copepoda) und Oncaeidae (Poecilostomatoida, Copepoda) im Bellingshausenmeer", von Cornelia Metz
Heft-Nr. 208/1996 – „Atmosphäreneinfluß bei der Fernerkundung von Meereis mit passiven Mikrowellen-radiometern", von Christoph Oelke
Heft-Nr. 209/1996 – „Klassifikation von Radarsatellitendaten zur Meereiserkennung mit Hilfe von Line-Scanner-Messungen", von Axel Bochert
Heft-Nr. 210/1996 – „Die mit ausgewählten Schwämmen (Hexactinellida und Demospongiae) aus dem Weddellmeer, Antarktis, vergesellschaftete Fauna", von Kathrin Kunzmann
Heft-Nr. 211/1996 – „Russian-German Cooperation: The Expedition TAYMYR 1995 and the Expedition KOLYMA 1995", by Dima Yu. Bolshiyanov and Hans-W. Hubberten

Heft-Nr. 212/1996 – „Surface-sediment composition and sedimentary processes in the central Arctic Ocean and along the Eurasian Continental Margin", by Ruediger Stein, Gennadij I. Ivanov, Michael A. Levitan, and Kirsten Fahl
Heft-Nr. 213/1996 – „Gonadenentwicklung und Eiproduktion dreier *Calanus*-Arten (Copepoda): Freilandbeobachtungen, Histologie und Experimente", von Barbara Niehoff
Heft-Nr. 214/1996 – „Numerische Modellierung der Übergangszone zwischen Eisschild und Eisschelf", von Christoph Mayer
Heft-Nr. 215/1996 – „Arbeiten der AWI-Forschungsstelle Potsdam in Antarktika, 1994/95", herausgegeben von Ulrich Wand
Heft-Nr. 216/1996 – „Rekonstruktion quartärer Klimaänderungen im atlantischen Sektor des Südpolarmeeres anhand von Radiolarien", von Uta Brathauer
Heft-Nr. 217/1996 – „Adaptive Semi-Lagrange-Finite-Elemente-Methode zur Lösung der Flachwassergleichungen: Implementierung und Parallelisierung", von Jörn Behrens
Heft-Nr. 218/1997 – „Radiation and Eddy Flux Experiment 1995 *(REFLEX III)*", by Jörg Hartmann, Axel Bochert, Dietmar Freese, Christoph Kottmeier, Dagmar Nagel, and Andreas Reuter
Heft-Nr. 219/1997 – „Die Expedition ANTARKTIS-XII mit FS 'Polarstern' 1995. Bericht vom Fahrtabschnitt ANT-XII/3", herausgegeben von Wilfried Jokat und Hans Oerter
Heft-Nr. 220/1997 – „Ein Beitrag zum Schwerefeld im Bereich des Weddellmeeres, Antarktis. Nutzung von Altimetermessungen des GEOSAT und ERS-1", von Tilo Schöne
Heft-Nr. 221/1997 – „Die Expedition ANTARKTIS-XIII/1-2 des Forschungsschiffes 'Polarstern' 1995/96", herausgegeben von Ulrich Bathmann, Mike Lucas und Victor Smetacek
Heft-Nr. 222/1997 – „Tectonic Structures and Glaciomarine Sedimentation in the South-Eastern Weddell Sea from Seismic Reflection Data", by László Oszkó
Heft-Nr. 223/1997 – „Bestimmung der Meereisdicke mit seismischen und elektromagnetisch-induktiven Verfahren", von Christian Haas
Heft-Nr. 224/1997 – „Troposphärische Ozonvariationen in Polarregionen", von Silke Wessel
Heft-Nr. 225/1997 – „Biologische und ökologische Untersuchungen zur kryopelagischen Amphipodenfauna des arktischen Meereises", von Michael Poltermann
Heft-Nr. 226/1997 – „Scientific Cruise Report of the Arctic Expedition ARK-XI/1 of RV 'Polarstern' in 1995", edited by Eike Rachor
Heft-Nr. 227/1997 – „Der Einfluß kompatibler Substanzen und Kryoprotektoren auf die Enzyme Malatdehydrogenase (MDH) und Glucose-6-phosphat-Dehydrogenase (G6P-DH) aus *Acrosiphonia arcta* (Chlorophyta) der Arktis und Antarktis", von Katharina Kück
Heft-Nr. 228/1997 – „Die Verbreitung epibenthischer Mollusken im chilenischen Beagle-Kanal", von Katrin Linse
Heft-Nr. 229/1997 – „Das Mesozooplankton im Laptevmeer und östlichen Nansen-Becken – Verteilung und Gemeinschaftsstrukturen im Spätsommer", von Hinrich Hanssen
Heft-Nr. 230/1997 – „Modell eines adaptierbaren, rechnergestützten, wissenschaftlichen Arbeitsplatzes am Alfred-Wegener-Institut für Polar- und Meeresforschung", von Lutz-Peter Kurdelski
Heft-Nr. 231/1997 – „Zur Ökologie arktischer und antarktischer Fische: Aktivität, Sinnesleistungen und Verhalten", von Christopher Zimmermann
Heft-Nr. 232/1997 – „Persistente chlororganische Verbindungen in hochantarktischen Fischen", von Stephan Zimmermann
Heft-Nr. 233/1997 – „Zur Ökologie des Dimethylsulfoniumpropionat (DMSP)-Gehaltes temperierter und polarer Phytoplanktongemeinschaften im Vergleich mit Laborkulturen der Coccolithophoride *Emiliania huxleyi* und der antarktischen Diatomee *Nitzschia lecointei*", von Doris Meyerdierks
Heft-Nr. 234/1997 – „Die Expedition ARCTIC '96 des FS 'Polarstern' (ARK XIII) mit der Arctic Climate System Study (ACSYS)", von Ernst Augstein und den Fahrtteilnehmern
Heft-Nr. 235/1997 – „Polonium-210 und Blei-210 im Südpolarmeer: Natürliche Tracer für biologische und hydrographische Prozesse im Oberflächenwasser des Antarktischen Zirkumpolarstroms und des Weddellmeeres", von Jana Friedrich
Heft-Nr. 236/1997 – „Determination of atmospheric trace gas amounts and corresponding natural isotopic ratios by means of ground-based FTIR spectroscopy in the high Arctic", by Arndt Meier
Heft-Nr. 237/1997 – „Russian-German Cooperation: The Expedition TAYMYR / SEVERNAYA ZEMLYA 1996", edited by Martin Melles, Birgit Hagedorn and Dmitri Yu. Bolshiyanov.
Heft-Nr. 238/1997 – „Life strategy and ecophysiology of Antarctic macroalgae", by Iván M. Gómez.
Heft-Nr. 239/1997 – „Die Expedition ANTARKTIS XIII/4-5 des Forschungsschiffes ‚Polarstern' 1996", herausgegeben von Eberhard Fahrbach und Dieter Gerdes.
Heft-Nr. 240/1997 – „Untersuchungen zur Chrom-Speziation in Meerwasser, Meereis und Schnee aus ausgewählten Gebieten der Arktis", von Heide Giese.
Heft-Nr. 241/1997 – „Late Quaternary glacial history and paleoceanographic reconstructions along the East Greenland continental margin: Evidence from high-resolution records of stable isotopes and ice-rafted debris", by Seung-Il Nam.

Heft-Nr. 242/1997 – „Thermal, hydrological and geochemical dynamics of the active layer at a continuous permafrost site, Taymyr Peninsula, Siberia", by Julia Boike.
Heft-Nr. 243/1997 – „Zur Paläoozeanographie hoher Breiten: Stellvertreterdaten aus Foraminiferen", von Andreas Mackensen.
Heft-Nr. 244/1997 – „The Geophysical Observatory at Neumayer Station, Antarctica. Geomagnetic and seismological observations in 1995 and 1996", by Alfons Eckstaller, Thomas Schmidt, Viola Gaw, Christian Müller and Johannes Rogenhagen.
Heft-Nr. 245/1997 – „Temperaturbedarf und Biogeographie mariner Makroalgen – Anpassung mariner Makroalgen an tiefe Temperaturen", von Bettina Bischoff-Bäsmann.
Heft-Nr. 246/1997 – „Ökologische Untersuchungen zur Fauna des arktischen Meereises", von Christine Friedrich.
Heft-Nr. 247/1997 – „Entstehung und modifizierung von marinen gelösten organischen Substanzen", von Berit Kirchhoff.
Heft-Nr. 248/1997 – „Laptev Sea System: Expeditions in 1995", edited by Heidemarie Kassens.
Heft-Nr. 249/1997 – „The Expedition ANTARKTIS XIII/3 (EASIZ I) of RV ‚Polarstern' to the eastern Weddell Sea in 1996", edited by Wolf Arntz and Julian Gutt.
Heft-Nr. 250/1997 – „Vergleichende Untersuchungen zur Ökologie und Biodiversität des Mega-Epibenthos der Arktis und Antarktis", von Andreas Starmans.
Heft-Nr. 251/1997 – „Zeitliche und räumliche Verteilung von Mineralvergesellschaftungen in spätquartären Sedimenten des Arktischen Ozeans und ihre Nützlichkeit als Klimaindikatoren während der Glazial/Interglazial-Wechsel", von Christoph Vogt.
Heft-Nr. 252/1997 – „Solitäre Ascidien in der Potter Cove (King George Island, Antarktis). Ihre ökologische Bedeutung und Populationsdynamik", von Stephan Kühne.
Heft-Nr. 253/1997 – „Distribution and role of microprotozoa in the Southern Ocean", by Christine Klaas.
Heft-Nr. 254/1997 – „Die spätquartäre Klima- und Umweltgeschichte der Bunger-Oase, Ostantarktis", von Thomas Kulbe.
Heft-Nr. 255/1997 – „Scientific Cruise Report of the Arctic Expedition ARK-XIII/2 of RV ‚Polarstern' in 1997", edited by Ruediger Stein and Kirsten Fahl.
Heft-Nr. 256/1998 – „Das Radionuklid Tritium im Ozean: Meßverfahren und Verteilung von Tritium im Südatlantik und im Weddellmeer", von Jürgen Sültenfuß.
Heft-Nr. 257/1998 – „Untersuchungen der Saisonalität von atmosphärischem Dimethylsulfid in der Arktis und Antarktis", von Christoph Kleefeld.
Heft-Nr. 258/1998 – „Bellingshausen- und Amundsenmeer: Entwicklung eines Sedimentationsmodells", von Frank-Oliver Nitsche.
Heft-Nr. 259/1998 – „The Expedition ANTARKTIS-XIV/4 of RV ‚Polarstern' in 1997", by Dieter K. Fütterer.
Heft-Nr. 260/1998 – „Die Diatomeen der Laptevsee (Arktischer Ozean): Taxonomie und biogeographische Verbreitung", von Holger Cremer
Heft-Nr. 261/98 – „Die Krustenstruktur und Sedimentdecke des Eurasischen Beckens, Arktischer Ozean: Resultate aus seismischen und gravimetrischen Untersuchungen", von Estella Weigelt.
Heft-Nr. 262/98 – „The Expedition ARKTIS-XIII/3 of RV 'Polarstern' in 1997", by Gunther Krause.
Heft-Nr. 263/98 – „Thermo-tektonische Entwicklung von Oates Land und der Shackleton Range (Antarktis) basierend auf Spaltspuranalysen", von Thorsten Schäfer.
Heft-Nr. 264/98 – „Messungen der stratosphärischen Spurengase ClO, HCl, O_3, N_2O, H_2O und OH mittels flugzeuggetragener Submillimeterwellen-Radiometrie", von Joachim Urban.
Heft-Nr. 265/98 – „Untersuchungen zu Massenhaushalt und Dynamik des Ronne Ice Shelfs, Antarktis", von Astrid Lambrecht.
Heft-Nr. 266/98 – „Scientific Cruise Report of the Kara Sea Expedition of RV 'Akademik Boris Petrov' in 1997", edited by Jens Matthiessen and Oleg Stepanets.
Heft-Nr. 267/98 – „Die Expedition ANTARKTIS-XIV mit FS 'Polarstern' 1997. Bericht vom Fahrtabschnitt ANT-XIV/3", herausgegeben von Wilfried Jokat und Hans Oerter.
Heft-Nr. 268/98 – „Numerische Modellierung der Wechselwirkung zwischen Atmosphäre und Meereis in der arktischen Eisrandzone", von Gerit Birnbaum.
Heft-Nr. 269/98 – „ Katabatic wind and Boundary Layer Front Experiment around Greenland (KABEG '97)", by Günther Heinemann.
Heft-Nr. 270/98 – „Architecture and evolution of the continental crust of East Greenland from integrated geophysical studies", by Vera Schlindwein.

* vergriffen/out of print
** nur noch beim Autor/only from the author